General Disclaimer

One or more of the Following Statements may affect this Document

- This document has been reproduced from the best copy furnished by the organizational source. It is being released in the interest of making available as much information as possible.

- This document may contain data, which exceeds the sheet parameters. It was furnished in this condition by the organizational source and is the best copy available.

- This document may contain tone-on-tone or color graphs, charts and/or pictures, which have been reproduced in black and white.

- This document is paginated as submitted by the original source.

- Portions of this document are not fully legible due to the historical nature of some of the material. However, it is the best reproduction available from the original submission.

Produced by the NASA Center for Aerospace Information (CASI)

X-4..
PREPRINT

NASA TM X- 65629

A CONCEPTUAL STUDY OF A UHF-VHF HYBRID AERONAUTICAL SATELLITE FOR A DELTA LAUNCH VEHICLE

W. N. REDISCH
A. F. WHITE
G. GOLDBERG

JANUARY 1971

AUG 1971
RECEIVED
NASA STI FACILITY
INPUT BRANCH

GSFC
GODDARD SPACE FLIGHT CENTER
GREENBELT, MARYLAND

FACILITY FORM 602
N71-32175 (ACCESSION NUMBER)
279 (PAGES)
TMX-65629 (NASA CR OR TMX OR AD NUMBER)
G3 (THRU)
(CODE)
31 (CATEGORY)

A CONCEPTUAL STUDY OF A UHF-VHF HYBRID SATELLITE FOR A DELTA LAUNCH VEHICLE

Dr. W. N. Redisch
A. F. White
G. Goldberg

January 1971

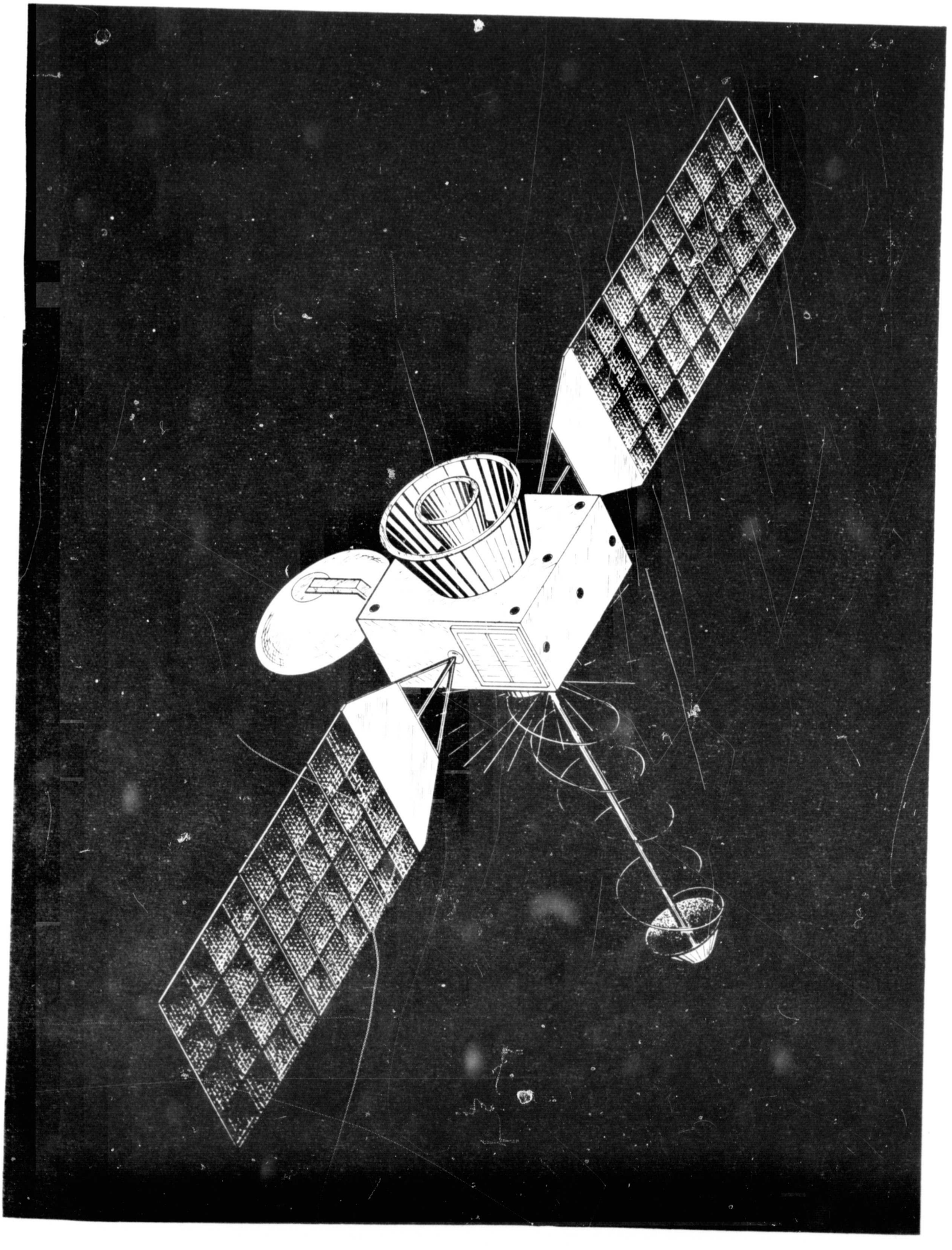


TABLE OF CONTENTS

Paragraph	Title	Page
1.0	INTRODUCTION	1-1
2.0	GUIDELINES AND MISSION SEQUENCE	2-1
3.0	OVERALL SYSTEM DESCRIPTION	3-1
3.1	GENERAL	3-1
3.2	EARTH SEGMENT	3-2
3.3	RADIO DETERMINATION	3-3
3.4	DATA AND VOICE TELE COMMUNICATION	3-6
3.5	SPACE SEGMENT	3-6
4.0	SPACECRAFT DESIGN	4-1
4.1	MECHANICAL DESIGN DESCRIPTION	4-1
4.1.1	Introduction	4-1
4.1.2	Equipment Module	4-1
4.1.3	Solar Array	4-2
4.1.4	VHF Antenna	4-3
4.1.5	L-Band Antenna	4-3
4.1.6	POLANG Antenna	4-4
4.2	STRUCTURAL DESIGN AND ANALYSIS	4-4
4.2.1	Summary	4-4
4.2.2	Solar Arrays	4-4
4.2.3	Module	4-7
4.2.4	Cylinder/Frustum	4-8
4.2.5	VHF Antenna	4-8
4.2.6	Preliminary Structure Dynamics	4-9
4.3	MASS PROPERTIES	4-9
4.4	TEMPERATURE CONTROL SUBSYSTEM	4-20

TABLE OF CONTENTS (Cont'd)

Paragraph	Title	Page
4.4.1	System Description	4-20
4.4.1.1	Thermal Louvers	4-23
4.4.1.2	Thermal Coatings	4-24
4.4.1.3	Multilayer Insulation	4-25
4.4.1.4	Heat Pipes	4-26
4.4.2	Analysis	4-27
4.4.2.1	Thermal Control of Module Equipment	4-27
4.4.2.2	Solar Panels	4-29
4.4.2.3	Heat Pipe Spacing	4-34
4.4.2.4	Temperature and Distortions of Tubular VHF Antenna	4-38
4.5	ATTITUDE AND ORBIT CONTROL	4-40
4.5.1	Mission Sequence, Operation and Requirements Summary for Control	4-40
4.5.2	Apogee Motor	4-50
4.5.3	Attitude Control System (ACS)	4-51
4.5.3.1	ACS Control Modes	4-51
4.5.3.2	Solar Pressure Torque Analyses	4-58
4.5.3.3	Pitch Axis Control Analysis	4-69
4.5.3.4	Sensors	4-74
4.5.3.5	Torquers	4-80
4.5.3.6	Estimated ACS Weight/Power	4-80
4.5.4	Auxiliary Propulsion System (APS)	4-80
4.5.4.1	Selection of a Preferred APS	4-83
4.5.4.2	Thruster Configurations	4-85
4.5.4.3	Impulse Requirements and Propellant Load	4-89
4.5.4.4	APS Configuration/Layout	4-90

TABLE OF CONTENTS (Cont'd)

Paragraph	Title	Page
4.6	COMMUNICATION SUBSYSTEM	4-93
4.6.1	Introduction	4-93
4.6.2	Communications Transponder Description	4-104
4.6.3	Communication Antennas	4-116
4.6.3.1	C-Band Earth-Viewing Horn Antenna	4-116
4.6.3.2	POLANG Antenna Considerations	4-118
4.6.3.3	VHF Antenna Considerations	4-119
4.6.3.4	L-Band Antenna Considerations	4-121
4.7	POWER SYSTEM DESIGN CONSIDERATIONS	4-123
4.7.1	System Configuration	4-123
4.7.2	Battery	4-125
4.7.2.1	Battery Sizing	4-133
4.7.2.2	Battery Conditioner	4-135
4.7.3	Battery Charge Regulator	4-136
4.7.4	Discharge Regulator	4-139
4.7.5	Shunt Regulator	4-141
4.7.6	Solar Array	4-145
4.7.6.1	Solar Panel Drive	4-150
4.7.7	Telemetry Monitors	4-154
4.7.7.1	Overall Functions	4-154
4.7.7.2	Specific Functions	4-154
4.7.8	Commands	4-157
4.7.9	Weight Summary	4-159
4.7.10	Launch Phase	4-159
4.7.11	Conclusion	4-159
4.8	TELEMETRY AND COMMAND SUBSYSTEM	4-161
4.8.1	Introduction	4-161

TABLE OF CONTENTS

Paragraph	Title	Page
4.8.2	Telemetry	4-161
4.8.2.1	Multiplexer	4-161
4.8.2.2	Data Switching Unit	4-169
4.8.2.3	TM Transmitters	4-171
4.8.2.4	T and C Antenna System	4-171
4.8.2.5	T and C Antenna	4-171
4.8.3	Command	4-173
4.8.3.1	Command Receiver	4-173
4.8.3.2	Command Decoder	4-173
Appendix A	Preliminary Structural Analysis	A-1
Appendix B	Solar Torque Calculations - Nominal Case	B-1
Appendix C	Incremental Tolerance and Solar Torque Analysis	C-1

LIST OF FIGURES

Figure No.	Title	Page
3.3-1	System Configuration for Surveillance	3-5
3.5-1	Hybrid Configuration Deployed	3-6A
3.5-2	Hybrid Configuration Stowed	3-13
3.5-3	Reference Orientation	3-14
4.1-1	Earth Oriented Spacecraft Rotating Solar Array	4-1A
4.1-2	Spacecraft Structure	4-1B
4.1-3	Equipment Installation	4-2A
4.1-4	Thermal Control System	4-2B
4.1-5	Solar Array Details	4-2C
4.1-6	Solar Array Restraint and Release System	4-3A
4.1-7	VHF Antenna	4-3B
4.1-8	L-Band Antenna	4-3C
4.2-1	Hybrid Spacecraft Preliminary Design Loads	4-6
4.4-1	Louver Effective Emissivity Vs. Blade Opening Angle	4-28
4.4-2	Orbital Insulation Heat Leakage vs. Average Regions Temperature	4-30
4.4-3	Dissipation - Active Module Temperature	4-31
4.4-4	Dissipation - Passive Module Temperature	4-32
4.4-5	Incident Solar Angle at Solstice	4-33
4.4-6	Solar Cell Temperature and Gradient Across Panel Vs. Emissivity of Back Facesheets	4-35
4.5-1	Hybrid Configuration (Stowed)	4-41
4.5-2	Hybrid Configuration (Deployed)	4-44
4.5-3	Reference Orientation	4-45
4.5-4	Vehicle Centered Orbital and Body Reference Frames	4-46
4.5-5	Attitude Control System Block Diagram (Operational Mode)	4-48
4.5-6	Orbital Geometry for Solar Torque Calculation	4-61

LIST OF FIGURES

Figure No.	Title	Page
4.5-7	Solar Pressure Torques - Nominal Case	4-62
4.5-8	Spacecraft y-Axis Precession	4-68
4.5-9	Limit Cycle Model	4-71
4.5-10	Angular Excursion Vs. Wheel Speed Change	4-72
4.5-11	Time to Null S/C Rate Vs. Wheel Speed Change	4-73
4.5-12	LMSC "NOHS" Scan Geometry	4-77
4.5-13	Alternate Jet Configurations	4-86
4.5-14	Hybrid Configuration - 12 Jet Utilization	4-88
4.5-15	Hybrid Configuration - 12 Jet, 4 Tank Schematic Layout	4-91
4.6-1	Integrated Communications Transponder	4-105
4.6-2	L-Band Power Amplifier Configurations	4-107
4.6-3	1800 MHz Amplifier-Equivalent Circuit Diagram	4-111
4.6-4	Power Amplifier Mechanical Design	4-112
4.6-5	L-Band Power Amplifier Performance	4-113
4,7-1	Direct Energy Transfer System	4-124
4.7-2	Umbra and Penumbra Patterns for a Synchronous Equatorial Orbit	4-128
4.7-3	Shadow Time (Composite of Umbra and Penumbra Times) for a Synchronous Equatorial Orbit	4-129
4.7-4	Battery Wiring Diagram	4-131
4.7-5	Battery Return Disconnect Wiring Diagram	4-132
4.7-6	12 A-H Battery Capacity as a function of Temperature	4-134
4.7-7	Battery Charge Regulator Block Diagram	4-137
4.7-8	Recharge Capacity As a Function of Charge Current	4-138
4.7-9	Boost Converter Simplified Diagram	4-140
4.7-10	Solar Array Partial Shunt Regulator Block Diagram	4-142
4.7-11	Solar Array Unregulated Section Operating Point Prior to End of Life	4-143

LIST OF FIGURES

Figure No.	Title	Page
4.7-12	Solar Array Regulated Section Operating Point Prior to End of Life	4-143
4.7-13	Solar Array Unregulated Section Operating Point at End of Life	4-144
4.7-14	Solar Array Regulated Section Operating Point at End of Life	4-144
4.7-15	Typical I-V Characteristic of Solar Array Upon Exit from Occult (BOL)	4-146
4.7-16	Typical I-V Characteristic of Solar Array (BOL)	4-147
4.7-17	Typical Analog Voltage Monitor Circuit	4-155
4.7-18	Typical Discrete Monitor Circuit	4-155
4.7-19	Typical Temperature Monitor Circuit	4-155
4.8-1	Hybrid T & C System	4-162
4.8-2	T&C Power Interfaces	4-167
4.8-3	Data Multiplexer	4-168
4.8-4	B1-Phase Signal	4-170
4.8-5	Hybrid Feed	4-172
4.8-6	Composite Antenna Gain Chart	4-174
4.8-7	Antenna Model	4-175
4.8-8	Command Decoder Logic Flow	4-176
4.8-9	PCM Command Format	4-177
	APPENDIX B	
B-1	Solar Torque Model (Top View)	B-3
B-2	Solar Torque Model (Side, Back/Front View)	B-4
B-3	Torque Calculation Summary - Equinox Example	B-5
B-4	Torque Calculation Summary - Solstice Example	B-6
	APPENDIX C	
C-1	Bearing Clearances, Solar Array Drive	C-9
C-2	Solar Panel Hinge Pin Clearances	C-10

LIST OF TABLES

Table	Title	Page
3.5-1	Hybrid Spacecraft Weight Summary	3-7
3.5-2	Power System Night/Day/Transfer Orbit	3-10
4.2-1	Structural Subsystem-Design Conditions	4-5
4.3-1	Hybrid Spacecraft Weight Summary	4-11
4.3-2	Power System Weight Summary	4-12
4.3-3	Telemetry and Command Weight Summary	4-13
4.3-4	Communication System Weight Summary	4-14
4.3-5	Stabilization and Control System Weight Summary	4-15
4.3-6	Auxiliary Propulsion System Weight	4-16
4.3-7	Structural System Weight Summary	4-17
4.3-8	Miscellaneous Weight Breakdowns	4-18
4.3-9	Mass Properties Summary	4-19
4.5-1	Solar Pressure Torque Summary - Nominal Cast	4-64
4.5-2	CG-CP Deviation Summary	4-65
4.5-3	Solar Torques Due to Tolerance Effects	4-67
4.5-4	Earth Sensor Candidates	4-75
4.5-5	Sun Sensor Candidates	4-79
4.5-6	Candidate Momentum Wheel Characteristics	4-81
4.5-7	Estimated ACS Weight and Power	4-82
4.5-8	Catalytic Hydrazine Thrusters	4-84
4.5-9	Auxiliary Propulsion System Weight	4-92
4.6-1	Assumptions	4-94
4.6-2	UHF & VHF Link Power Budgets	4-95
4.6-3	UHF Link Power Budget For Four Aircraft Antenna Gains	4-96
4.6-4	UHF Transmitter Power/Aircraft Gain Tradeoff for Down Link	4-97

LIST OF TABLES

Table	Title	Page
4.6-5	VHF Transmitter Power Requirements	4-99
4.6-6	C-Band Link Power Budget	4-101
4.6-7	C-Band Transmitter Power Requirements	4-102
4.6-8	Power Amplifier Requirement Summary	4-103
4.6-9	Comparison of TWTA and Solid State L-Band Power Amplifiers	4-109
4.6-10	Performance of C-Band Earth Viewing Horn Antenna	4-117
4.7-1	Power System Night/Day Transfer Orbit Power Loads	4-126
4.7-2	Candidate Drive Subsystems	4-151
4.7-3	Power System Telemetry Monitor	4-156
4.7-4	Power System Commands	4-158
4.7-5	Power System Weight Summary	4-160
4.8-1	Telemetry Characteristics	4-163
4.8-2	Tentative Command Characteristics	4-164
4.8-3	Power Budget	4-165
4.8-4	Weight Budget	4-166

APPENDIX B

B-1	Solar Torque Data Summary	B-7

FOREWARD

During 1970 GSFC personnel were actively engaged in studies in support of the definition of an aeronautical satellite system for the oceanic region. The conceptual spacecraft design in this report was performed by the Space & Electronics System Division, Fairchild-Hiller Corporation, Germantown, Maryland, on contract NAS5-11822 in support of the studies and under the direction of the authors.

1.0 INTRODUCTION AND SUMMARY

This volume presents the conceptual design and analysis of a geo-synchronous equatorial satellite to be used for aeronautical services. The satellite is referred to as a Hybrid since it will be capable of communication at either VHF or UHF (L-Band) or at both frequency bands simultaneously. The concept studied herein is a momentum wheel stabilized, earth-oriented satellite, with UHF, VHF, and C-Band Earth pointing antennas. The 900-watt satellite is launched on the Advanced Thorad-DELTA launch vehicle and utilizes an apogee engine to achieve synchronous equatorial orbit. The primary purpose of this study is to determine if a Hybrid satellite design which satisfies the assumed stated guidelines is compatible with the DELTA launch vehicle capability.

Since the material presented is the preliminary result of a conceptual design study, the results should therefore not be considered final. As such, some of the conceptual approaches presented are not fully proven and require further investigation. In order to expedite the design study, the trade-off studies in various areas of interest were performed in parallel. Consequently slight differences in assumptions may be found. However, each discipline has been approached in a conservative manner and the impact of these differences on the spacecraft design concept is inconsequential. The design of the mobile and earth segments is not included as a part of this study since the feasibility of the spacecraft is the main objective.

The study guidelines are tabulated in Section 2.0, as well as the mission sequence of operation. Although it is fully realized that the mission guidelines are not firm at this date, the study has shown that the specific guidelines that were chosen for the study can be met, but the margin is not as great as one would

prefer at this stage. Design compatibility with most of the guidelines stated has been verified, and the corresponding data is included in this report. However, due to the sensitivity of the Hybrid design, verification of concurrence with some of the guidelines require more detailed analysis than that normally performed during a conceptual study effort.

Section 3.0 presents the overall system description. This section is included to familiarize the reader with the overall mission description with which the Hybrid satellite system must be compatible. The overall approach to aircraft communication and surveillance is discussed. This section also includes a general description of the spacecraft and its subsystem.

Section 4.0 presents a more detailed conceptual design of the spacecraft. Although several concepts were considered, an earth-viewing satellite with sun tracking solar arrays seemed to be the most practical approach with preference towards housing the VHF electronics with the VHF antenna. Once the VHF electronics were thus housed with the earth-viewing antennas, it seemed advisable to place the L-Band electronics in the same module thereby eliminating any rotation between the L-Band electronics and the L-Band antenna. Since a significant portion of the satellite equipment was thus incorporated in the earth-viewing module, it was most practical to include the remainder of the spacecraft subsystems therein. The design concept presented is a typical example of an earth-oriented synchronous satellite but does not necessarily represent the optimum design at either the system or subsystems level. The concept does utilize existing space proven hardware whenever possible.

Although the spacecraft concept presented appears feasible and compatible with the DELTA launch vehicle, there are several disadvantages associated with it. The concept presented reflects a high risk design (no array/wheel failure modes of operation) and a minimal eclipse capability. A weight growth margin of only nine percent (see Section 4.3 Mass Properties) at this early stage in the program could cause many difficulties in the future. A ten percent margin (see Section 2.1 Guidelines) is usually the minimum acceptable margin, and fifteen percent margin would be preferable for a moment wheel stabilized synchronous satellite design, as opposed to the more conventional spin stabilized design.

An additional weight savings of 35 pounds would be obtained if the satellite were limited to VHF communications alone, rather than utilizing both frequency bands. Of this weight, 5 pounds is allocated to the L-band antenna and 30 pounds to the transponder.

Conversely, an additional weight savings of 55 pounds would be obtained if the satellite were limited to L-band communications alone. Of this weight, 8 pounds is allocated to the VHF antenna, 27 pounds to the transponder, and 20 pounds to solar array and associated spacecraft structure. The 92-inch long VHF helix antenna causes a shadowing problem which requires those portions of the solar arrays closest to the spacecraft body to be void of cells. This penalizes the solar array weight and consequently the spacecraft structure weight by approximately 20 pounds. (A trade-off study considering allowable shadowing of the cells vs. no shadowing of the cells would have to be performed during the detailed design effort to be certain that moving the cell area outboard is indeed the best solution).

A further disadvantage of the power supply system utilized is the number of slip rings required. (The shunted system requires twice the number of power slip rings as the non-shunted system.) The primary advantage of the shunted power supply system, however, is the near constant power profile from start of life to end of life of the spacecraft. Once firmer guidelines are established, a more detailed trade-off analysis would be performed prior to a final decision as to which system is more applicable for this mission.

The thermal control system is burdened by the earth-oriented concept in that every facet of the equipment module is impinged by solar energy at one time or another, as opposed to a sun-oriented satellite which would have approximately 50% of its area always radiating to cold space. In order to maintain the thermal control required in the guidelines, a rather unique thermal control system (see Section 4.4) was devised.

The selection of an earth-oriented spacecraft as the preferred approach for the Hybrid, with a single axis drive for the solar panels to track the sun, has a major impact on the favored attitude and orbit control system and its associated advantages and disadvantages. The 0.5-degree accuracy guideline for 3-axis stabilization to this reference orientation for a projected 3-5 year mission represents the next most important factor affecting the attitude control system. This accuracy requirement could be relaxed if only VHF communications were involved.

A large momentum wheel operating at a high bias speed is used for semi-passive gyroscopic stabilization about the roll/yaw axes in the orbit plane. Onboard, closed-loop nulling of pitch angle errors is effected by limited up-down accelerations of this same wheel.

Ground command of the hydrazine jets for 3-axis torqueing should only be required every 1-2 days for corrective precession of the y axis, and to keep the wheel running near its nominal bias speed. The varying solar aspect of the earth-tracking satellite causes significant variations in the dominant solar pressure torques, however, and makes them difficult to predict.

The proposed jet configuration provides a fully redundant 3-axis torqueing capability. Because of the earth-oriented attitude of the satellite, additional flexibility is provided by the body-mounted thrusters for precession of the pitch axis in a given inertial direction. This could permit elimination of some of the thrusters while still retaining redundant torqueing capabilities for reliability purposes.

Several of the same thrusters are ground commanded for spin axis precession and orbit control in the initial spin-stabilized mode used for attitude control during coasting in the transfer orbit, and during injection into synchronous orbit and initial correction thereof. Translation thrusters on the $\pm x$ sides of the satellite can be ground commanded for East-West station keeping and station relocation at any time in synchronous orbit.

The Hybrid has been designed with a very favorable, high spin-to-transverse axis inertia ratio while the panels are stowed for the spinning phase. Hence, passive spin stabilization can be employed for the spin-stable satellite for long term control in this mode, with no need for active nutation damping.

During the operational mode in synchronous orbit, use of a 2-axis earth sensor aligned with the satellite's + z axis, which is caused to track the local vertical, provides continuous roll (North-South) and pitch (East-West) angle information. These are the angles of greatest concern from a mission standpoint.

Standby and/or functional redundancy have been provided for the sensors and thrusters for reliable long life operation of the attitude and orbit control systems during the initial spin and the final operational modes. The on-board control functions have been minimized to improve weight/power and reliability, while still placing reasonable command/control requirements upon the ground station for a preoperational system. However, no truly effective back up operational mode has been defined should the large momentum wheel fail. One possible approach is to use two small wheels instead of one large one. In this way a reasonable mission capability could be realized with reduced attitude control accuracy or more frequent ground corrective commands should one wheel fail. This approach would probably involve more weight and complexity in the wheel system, however.

Several additional disadvantages for the earth-oriented Hybrid are that a fairly involved ground command/control operation must be performed to acquire the reference orientation, and that failure of either one of the solar array drives would probably cause loss of attitude control.

2.0 GUIDELINES AND MISSION SEQUENCE

2.1 GUIDELINES

2.1.1 ORBIT

(a) Synchronous equatorial

(b) Two spacecraft in orbit

(c) Maximum shadow = 72 minutes

2.1.2 LAUNCH VEHICLE

(a) DELTA + 9 CASTOR II + TE-M-364-4

(b) Fairing - proposed Canadian Telesat fairing

(c) One spacecraft per launch

(d) Vehicle will inject 1355 lb. spacecraft into a 100 x 19, 323 N.M. transfer orbit inclined at 28.5 degrees

(e) Standard adapter - 53 lbs.

2.1.3 TECHNOLOGY

(a) Use available technology, space qualified when possible

(b) Five year desirable life time, 3 year minimum

2.1.4 COVERAGE AREA

The coverage area is the "NETCOS Polygon" (Section 3.0) for both communications and surveillance. (However future trade-offs between smaller voice communication coverage and/or larger surveillance coverage areas could be optimized)

2.1.5 SPACECRAFT CRITERIA

The spacecraft shall be momentum wheel stabilized earth oriented in its operational mode with solar panels that are single axis driven to track the sun. The spacecraft design shall be capable of longterm survival in the spinning mode with a spin axis orientation that is favorable for solar power generation. During this mode,

no surveillance and communication need be performed and the primary VHF and L-band antennas need not be operative or deployed.

2.1.5.1 Stabilization

The spacecraft shall be passivly spin stabilized during the transfer orbit and momentum wheel stabilized in synchronous orbit. A backup stabilization mode is desired in the event of failure of the control system or solar array drive.

2.1.5.2 Power

(a) 900 watt, beginning of life raw power solar array

(b) Use lightweight rigid solar arrays and rechargeable nickel cadmium batteries.

(c) Design solar array and battery for the following loads:

(1) 130 watts operational capability in shadow (85 for housekeeping, 45 for surveillance). Note: If coverage area is varied eclipse performance and battery weight will change accordingly.

(2) 60 watts operational capability during the transfer orbit.

2.1.5.3 Communications

(a) Use a combination of L band, C band, and VHF

(b) Use parabolic reflector with at least 22 db gain on the axis and a 9.5^{o} by 12.2^{o} half power beam width for L-band communications.

(c) Use an 11 db gain helical antenna with a half power-beam width of 50^{o} for VHF communications.

(d) Provide a C-Band antenna which gives a 11.6 db gain in the direction of the ground stations.

(e) Provide a C-Band POLANG antenna.

(f) Provide VHF capability for spacecraft telemetry and command during launch and transfer orbit.

2.1.5.4 Structure

Lightweight design utilizing standard spacecraft construction.

2.1.5.5 Propulsion and Controls

(a) Use a solid propellant motor on the spacecraft for circularizing the transfer orbit and removing its inclination

(b) Use hydrazine liquid propulsion subsystem for injection error correction, orbital trim and attitude control. Velocity impulse for orbit control shall be 360 f. p. s.

(c) No N-S station keeping

(d) 1/2 degree accuracy about all three axes.

2.1.5.6 Thermal

(a) Maintain hydrazine at 5^{o}C or above.

(b) Maintain battery between 0^{o}C and 10^{o}C.

2.1.5.7 Attitude Determination

(a) Earth Sensing

(b) Sun Sensing

(c) POLANG

2.1.5.8 Weight

(a) Maximum injection weight into transfer orbit (including adapter) 1355 lbs.

(b) Provide weight contingency = 10% of the maximum possible spacecraft weight after apogee motor firing.

2.1.5.9 Inertia

The spacecraft configuration shall have a favorable ratio of spin-to-transverse inertias of 1.1 or greater for passive spin stability in the stowed configuration.

2.2 MISSION SEQUENCE

(a) Liftoff.

(b) Third stage spin-up to approximately 75 rpm.

(c) Third stage ignition.

(d) Third stage burnout.

(e) Spacecraft injection into 100 x 19,323 N. M., 28.5 - degree inclined transfer orbit at the equator.

(f) Spacecraft Separation. (Spacecraft spin axis in plane of transfer orbit.)

(g) Partial despin of spacecraft to approximately 45 rpm

(h) Ground tracking of spacecraft to determine transfer orbit injection errors.

(i) Reorientation of spacecraft spin axis to proper attitude for apogee motor firing. Verification that spacecraft attitude is correct for apogee motor firing.

(j) Ground station will determine attitude using telemetry data from the spacecraft attitude sensors and POLANG.

(k) Apogee motor firing (approximately 36 seconds).

(l) Ground tracking of spacecraft to determine spacecraft orbit.

(m) Initial correction of in-plane orbit errors using hydrazine system.

(n) Despin spacecraft.

(o) Deploy solar array panels.

(p) Acquire reference earth-oriented attitude.

(q) Uncage solar panels and activate drive motor to track sun.

(r) Final correction of synchronous orbit errors.

(s) Activate communications and initiate spacecraft operation.

3.0 OVERALL SYSTEM DESCRIPTION

3.1 GENERAL

The Aeronautical Satellite System is composed of three primary system segments, connected by a communication line. They are:

(1) the space segment

(2) the mobile segment, and

(3) the earth segment

The space segment consists of the launch vehicles and two spacecraft which would be placed by the launch vehicles into a synchronous geostationary orbit located at approximately 20°W and 60°W longitude for North Atlantic Coverage.

The mobile segment consists of the aircraft (or possibly other mobile user such as marine vessels).

The earth segment consists of the air traffic earth terminals, the Air Traffic Control Centers, satellite control centers and required tracking and calibration stations.

The system complex is designed to meet particular requirements in fullfilling its role as an Aeronautical Satellite System.

For purposes of this study, the system provides surveillance and communication in an area defined by the following six (6) points which circumscribe a spherical polygon in the North Atlantic.

	Longitude	Latitude
1	0°	15°N
2	0°	50°N
3	20°W	65°N
4	60°W	65°N
5	80°W	50°N
6	80°W	15°N

In a final design, separate surveillance and communication coverage areas would be traded off with system capabilities.

3.2 EARTH SEGMENT

The Earth Segment consists of Air Traffic Earth Terminals (ATET), Air Traffic Control Centers (ATCC), Satellite Control Centers (SCC), and Calibration and Tracking Stations (CTS).

3.2.1 AIR TRAFFIC EARTH TERMINALS

There is to be at least one ATET on each side of the Atlantic Ocean and all ATET's will be essentially identical. Either ATET may act as a primary while the other acts as a secondary and all functions are interchangeable. Either ATET is capable of being the sole terminal for operating the system.

Basically, the ATET is the link that, via the satellites, connects the Air Traffic Controllers with the Mobiles. It transmits and receives all signals related to Air Traffic Control (surveillance, voice and data). It processes all incoming data (such as computing mobile locations) and does the appropriate routing of all signals to and from the mobiles and disseminates processed data (such as mobile locations). It also provides the overall system control, maintains timing, power and frequency control, and directs any emergency operations.

The main facilities of an ATET consist of a ground station complex with approximately a 10-footantenna, computers and software, signal routing equipment, and all necessary interconnect lines.

3.2.2 AIR TRAFFIC CONTROL CENTERS

Initially there will be many ATCC's as is presently the situation. There may or may not be an ATCC physically co-located with either or both ATET's. For a preoperational system, not all aircraft will be outfitted with the necessary mobile equipment to be part of the ATC system. Hence, a preoperational demonstration must be coordinated and phased in with existing ATC facilities and procedures. Eventually, for an operational system, it is envisioned that the ATCC's will be centralized and located at the ATET's if the system economics so dictate.

The main functions of an ATCC is to display all information to an air traffic controller and he, computer aided, will make the ATC decisions and communicate with all the aircraft in his jurisdiction under control of the system via

the ATET's (and through the satellites). The ATCC originates and terminates all ATC messages. It interfaces with all the appropriate Air Traffic Service (ATS) organizations.

Certain ATC operations will be possible on a simultaneous and independent basis from either ATET without regard to which is acting as primary. For example, any ATC Center can derive surveillance information by either ATET having direct reception from the satellites. Development of operational procedures governing the ATC network is a part of the preoperational experiment and these will be developed and coordinated with all agencies and organizations involved.

3.2.3 SATELLITE CONTROL CENTER

There will be at least one Satellite Control Center. It may or may not be co-located with the ATET's depending on economic tradeoffs.

The Satellite Control Center would perform the normal functions associated with the support of satellites in orbit including satellite functional commands, station keeping control, house-keeping telemetry processing and general responsibility for performance of the satellites.

3.2.4 CALIBRATION AND TRACKING STATIONS

The Calibration and Tracking Stations are at several geographical locations depending on technical and economic tradeoffs. System design would incorporate standard techniques to utilize the station tracking network for spacecraft ground communication during the launch and orbit acquisition phases.

In addition to these, it is necessary to provide within the system, calibration stations for continuous calibration and system checkout of the telecommunication link and system operation. These stations are envisioned as simply a duplication of equipment that is utilized in the mobile segment with communication links appropriately routed to the other earth segment locations.

3.3 RADIO DETERMINATION (SURVEILLANCE)

The surveillance system is designed to accommodate at least 250 aircraft simultaneously within the required area of coverage. The system should be capable of providing separation standards on the order of 30 nautical miles lateral, 2000 feet vertical and 5 minutes longitudinal. It should be an "independent surveillance" function and be able to provide some degree of flexible interrogation rate to accommodate relatively fast and slow moving mobile users. Two modes of operation are possible

as follows:

(1) For air traffic control active ranging with return links from the aircraft; all of the signal processing is performed at the Air Traffic Earth Terminal.

(2) For passive navigation the mobiles (aircraft, ships, etc.) can compute their own position location utilizing on-board clocks.

For air traffic control one signal is transmitted from the earth terminal at frequency f_1 (Figure 3.3-1) to one of the satellites on a continuous basis (for example S_1). The aircraft receives this signal at frequency f_2 and periodically returns it along with altitude and aircraft identification data to both satellites simultaneously using a single frequency, f_3. All aircraft transmissions are automatic and are timed relative to all others so that they arrive sequentially at each satellite in a time division multiple access format. The composite signal is relayed from each satellite to the earth terminal at frequencies f_4 and f_5. The Air Traffic Earth Terminal then identifies each aircraft signal and performs all computations to determine the aircraft positions.

For the passive navigation mode of operation the Air Traffic Earth Terminal emits two signals at frequencies f_1 and f_6. The signals received at each satellite are adjusted, relative to time delay, to compensate for the range differences in the links from the satellites to the earth terminal. The two signals received at the mobiles can then be utilized (with the on-board clock) to compute position on the mobile.

The surveillance signal transmitted to each mobile contains two components, the ranging waveform and a system control and surveillance data channel. Similarly, the signal returned by the mobiles contains, in addition to the repeated ranging waveform, a system control and surveillance data channel. Both digital and sine wave analog ranging waveforms are being considered for the system. An analog ranging system can provide more rapid acquisition, an important feature in a time division multiple access system. On the other hand, the digital signal, if properly designed, could provide some protection against multipath and other radio interference. Selection of a ranging waveform is somewhat dependent on whether an analog or digital voice modulation technique is used.

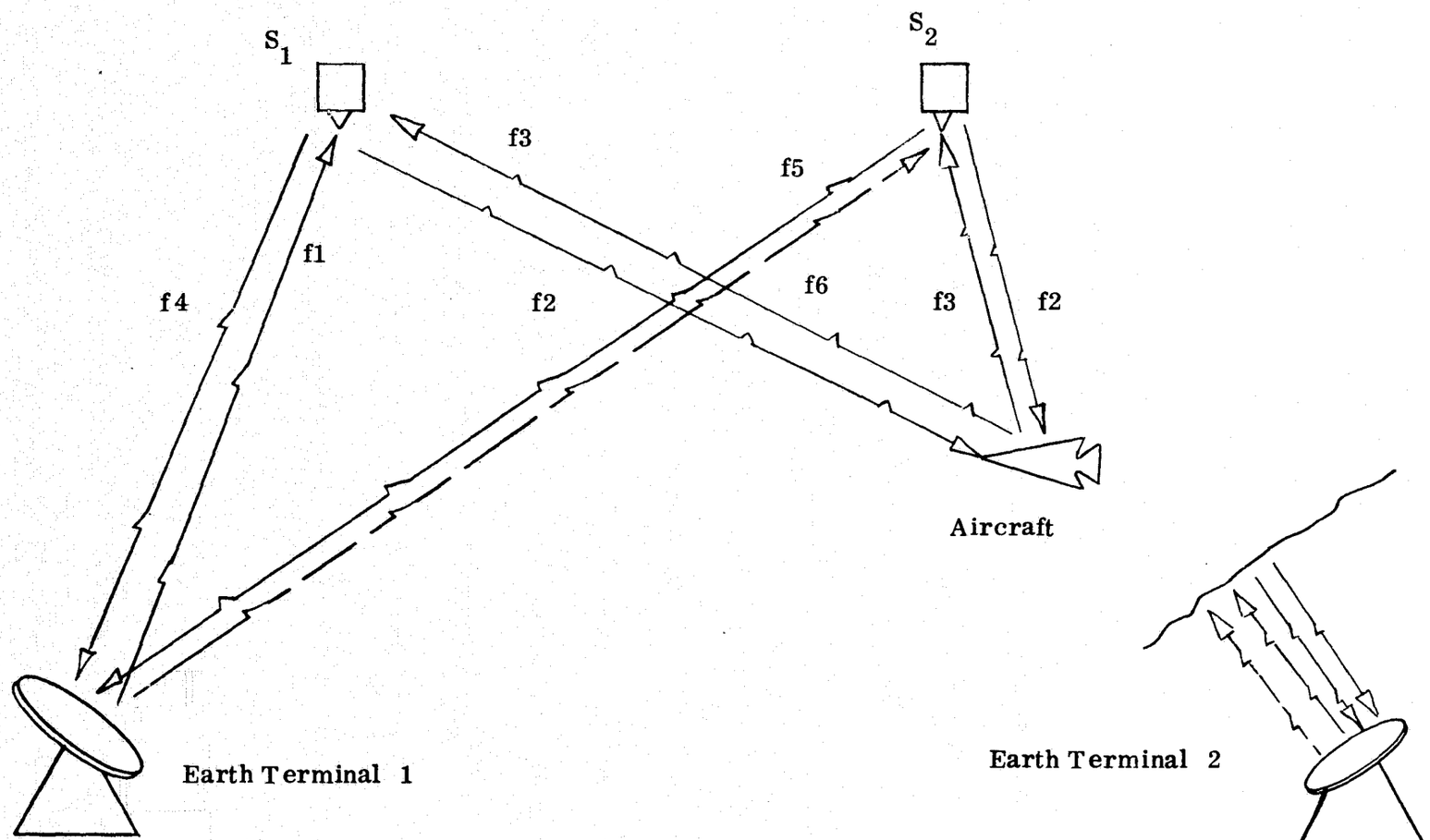


Figure 3.3-1. SYSTEM CONFIGURATION FOR SURVEILLANCE

Considerable attention must be devoted to the choice of the ranging waveform. Multipath measurements are, of course, necessary to support these studies.

3.4 DATA AND VOICE TELECOMMUNICATION

The system provides voice and data channels on each satellite. The nominal goal for word intelligibility should be 95% for at least 95% of a message (articulation index of about .6). The data channel capacity is to be 1200 bits per second with a maximum bit error rate of 10^{-5}.

Both analog and digital methods of voice processing and modulation may be considered for the voice channels. Amplitude and frequency truncation along with narrow-band FM may be considered as an analog candidate. PCM, delta modulation (and its variations) and pulse duration modulation, all coupled with DPSK, may be the digital candidates. One of the major difficulties underlying the selection is the lack of a good quantitative method of comparing the channel performance of the various techniques.

3.5 SPACE SEGMENT

The following section of this report (4.0) presents the detailed design and analysis of the presented concept. The spacecraft is a synchronous, equatorial momentum-wheel stabilized design which is to be used for air traffic control experiments in aeronautical services, thus it is a very basic satellite in that no extraneous experiments are included. As can be seen in Figure 3.5-1 the satellite consists of the main spacecraft module, (a parallelepiped), two large solar arrays, and several earth pointing antennas. The weight distribution is given in Table 3.5-1. The major subsystems which are discussed in further detail in Section 4.0 are communications, power supply, telemetry and command, thermal control, and attitude and orbit control. A brief discussion of each of these follows.

3.5.1 COMMUNICATION SUBSYSTEM

The communication subsystem receives signals at C-band, L-band, and VHF. The signals are amplified, filtered, and converted to the intermediate frequency. The signals are then directed to one of three IF amplifiers, where they are further amplifier and filtered. The output signals of the IF amplifiers are directed to the transmitter, up-converted, filtered, and amplified to the power level required for transmission, in either C-band, L-band, or VHF.

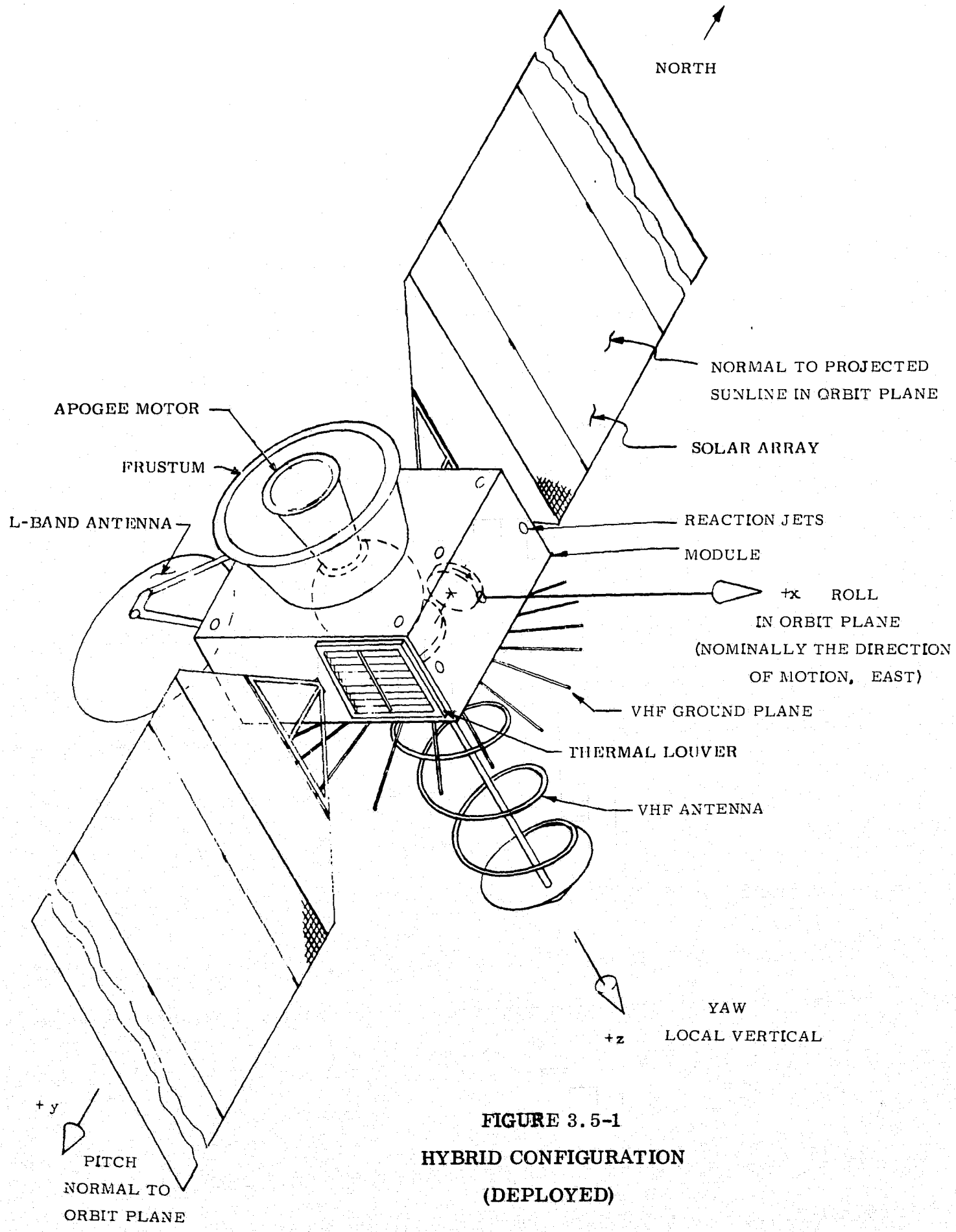


FIGURE 3.5-1

HYBRID CONFIGURATION

(DEPLOYED)

Table 3.5-1 Hybrid Spacecraft Weight Summary

Item		Weight
Power System	210.4	
TM and Command System	26.3	
Communication System	74.3	
Antenna System		
• L Band	5.0	
• VHF Band	8.0	
Stabilization and Control System	49.9	
Auxiliary Propulsion System	74.9	
Thermal Control System	15.0	
Electrical Distribution System	30.0	
Structural System	85.7	
Apogee Motor Inerts (burn-out)	46.4	
Weight Growth	61.6	
Total Payload		687.5
Apogee Motor Propellant*	614.5	
Separation Weight		1302.
Adapter (launch vehicle)	53.	
Gross Weight		1355.

*Includes 5.4 lbs. of low performance expendable inerts.

The transponder has flexibility, in that signals received in any band may be switched to any of the frequency bands for transmission.

The transponder makes efficient use of three identical IF amplifiers, in that any one of the IF amplifiers may be switched (by ground command) to any one of the received signals. Redundancy at IF is achieved economically, by means of switching.

The transponder has good capability for simultaneously handling signals on all three frequency bands. This would permit, for example, an L-band and a VHF signal to be received from the same aircraft at the same time. Analysis of propagation effects (fading, absorption) would be facilitated.

The transponder has good reliability, in that redundant up- and down-converters, IF amplifiers, local oscillators, and power amplifiers are proposed.

The communication subsystem utilizes a simple, deployable, helix antenna for the VHF band. At L-band a reflector-type antenna is used, with unequal beamwidths which provide near optimum coverage. A small electromagnetic horn provides the coverage needed for the C-band communication links to the satellite control centers. During the transfer orbit, a low-level signal, with small cross-polarized component, will be radiated from a C-band linear dipole array.

For purposes of this study the coverage areas reflected in the system guidelines have been accepted. Further studies of the operational situation may result in slightly different coverage requirements. Small changes in the reflector antenna (at L-band) and in the horn antenna (at C-band) may accommodate the new requirements.

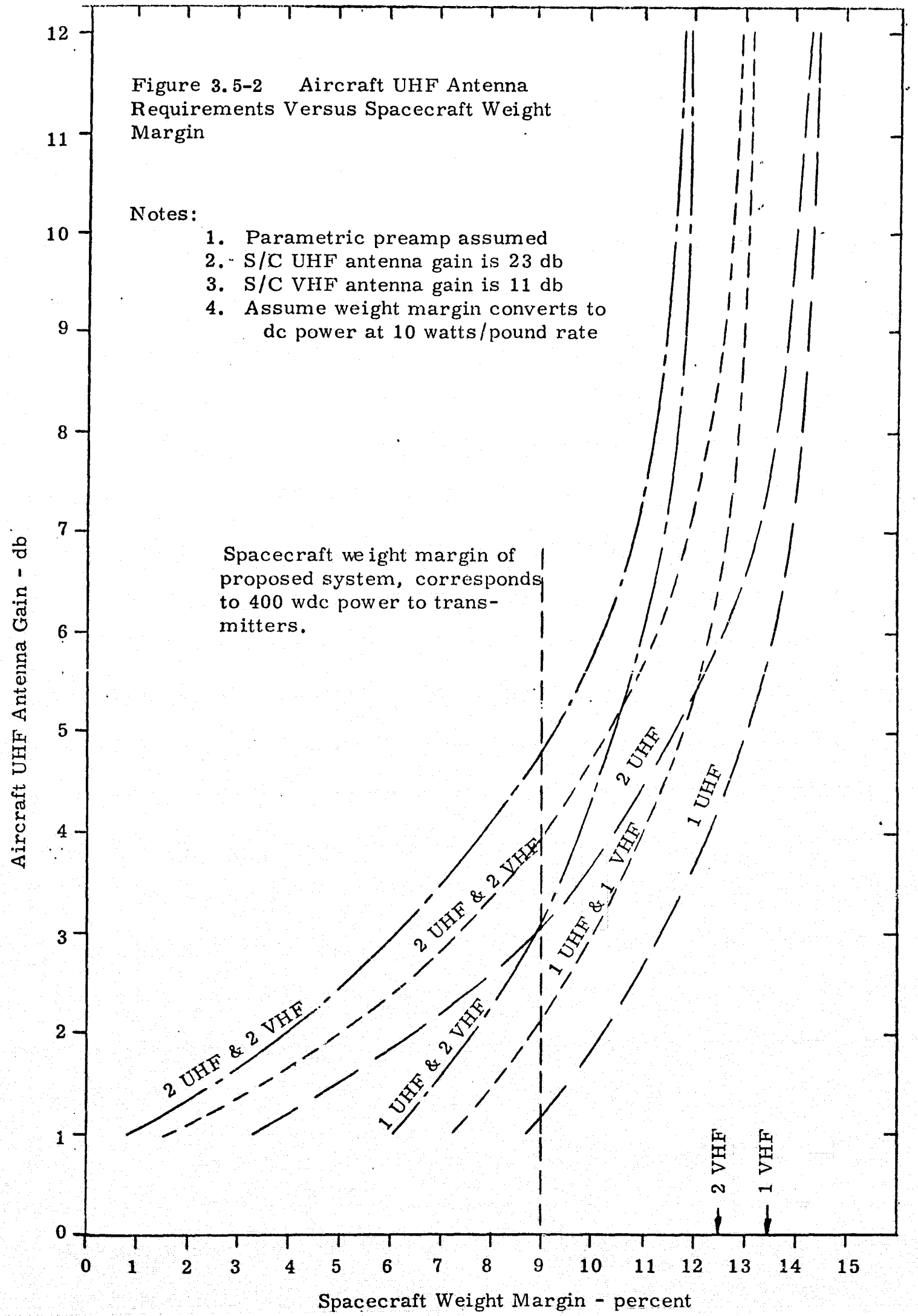
The communication subsystem avoids the need for new and unproven components and techniques. Lengthy and expensive development efforts are thus obviated. The exception may lie in the area of L-band, solid-state, power amplifiers, where values of efficiency, reliability, and cost are not as well defined as at lower frequencies.

With the present spacecraft design, the weight margin is only 9%. This margin is very sensitive to aircraft antenna gain, as can be seen in Figure 3.5-2. In the figure, 1 VHF and 1 UHF refer to a group of 1 voice, 1 digital and 1 surveillance channels transmitted at VHF or UHF, respectively; similarly, 2 VHF and 2 UHF refer to 2 voice, 2 digital and 1 surveillance channels. The spacecraft design proposed in this report provides 400 watts of dc power for the communication transponder and requires an aircraft antenna gain of 5 dB, at UHF, for full communication capability.

Figure 3.5-2 Aircraft UHF Antenna Requirements Versus Spacecraft Weight Margin

Notes:

1. Parametric preamp assumed
2. S/C UHF antenna gain is 23 db
3. S/C VHF antenna gain is 11 db
4. Assume weight margin converts to dc power at 10 watts/pound rate



At the present early stage of conceptual spacecraft design, it is desirable to have a spacecraft weight margin of 15%. To achieve this value requires an aircraft antenna gain much in excess of 12 dB. Such high gains are not practical. Consequently, the confidence level in the spacecraft design is not as high as desirable.

3.5.2 POWER SUBSYSTEM

The power system configuration chosen is capable of efficiently meeting the spacecraft load requirements and is commonly known as a Direct Energy Transfer (DET) System. It is similar to that used on the S^3 and IMP-I spacecrafts. Power is provided by the solar array during sunlight operation and by hermetically sealed nickel-cadmium storage batteries during solar eclipses. A high efficiency boost converter is provided to boost the battery voltage and to provide a regulated voltage to the loads. The battery system consists of two identical battery packages which share applied loads. This approach provides versatility for satellite thermal design, CG and inertia control, and ease of installation, as well as facilitating battery charger design. The battery system is designed for normal operation at approximately 40 percent depth-of-discharge at synchronous orbit conditions for a design lifetime of five years in orbit. Battery disconnect plugs are provided to facilitate battery control modes before launch and in-flight battery conditioners are implemented to allow reconditioning of the batteries due to possible failure modes that would impose additional cycles or deeper depth-of-discharge on the batteries. The bus tie relay allows the two solar array power buses to operate independently or in parallel for failure mode consideration. The power system estimated power loading is shown in Table 3.5-2.

Telemetry equipment performs the functions of multiplexing and formatting of housekeeping data from all spacecraft systems for transmission to the control ground station. Analysis of this data permits ground monitoring of equipment configuration and major operating parameters. The command system receives, decodes and executes ground commands which control the operating status of spacecraft equipment. T&C transmitters and receivers operate at VHF utilizing a common omnidirectional antenna; they are independent of the communications repeater. Equipment redundancy is utilized to achieve high reliability in both functions.

Table 3.5-2

Power System Night/Day/Transfer Orbit

Average Power Loads

System	Average Night Loads (watts)	Average Day Loads (watts)	Average Transfer Orbit Loads (watts)
T & C	18	18	18
Att. Cont.	42	42	30
Comm.	45	400	2
Power	25	45	10
Totals	130	505	60

3.5.4 THERMAL CONTROL SUBSYSTEM

Temperature control for the Hybrid is achieved by employing a system of louvers, heat pipes, super insulation, and thermal control coatings. The louvers are mounted to honeycomb panels located on the north and south sides of the spacecraft. By virtue of the square cross-section chosen for the equipment module, the north-south faces present large flat surfaces onwhich solar impingement is minimized. The bulk of the electronic components are mounted directly to the interior surface of the honeycomb. Heat pipes are embedded in the panel and distribute the heat load over the entire face from which it is radiated directly to space.

With the exception of the louvered and passive areas on the north-south faces, the entire equipment module is covered with super-insulation. The insulation reduces the dependence on thermal coatings to a minimum and insures that the heat

of the critical components will be directed through the louvers which provide a variable thermal resistance which is a function of temperature.

The equipment module is divided into two temperature control compartments or regions. The first, hereafter referred to as Region I, contains six square feet of thermal louvered area located on the north and south facing sides. The batteries and housekeeping equipment items are housed in this compartment. Thermal control is provided to maintain the temperature of the component mounting base plate between 0°C and 10°C for all orbit conditions.

Region II houses the communication equipment. Temperature control is achieved by means of thermal coatings applied to the north and south facing sides. It is estimated that a temperature range between 10°C to 40°C may be maintained on the equipment mounting baseplate surface.

By thermally isolating the temperature sensitive components from those which are not critical with respect to temperature, it is possible to meet all thermal requirements. Further, in the case of the batteries, a relatively low temperature prolongs life. (The ability to accept a charge is diminished but the gain in life is more important.) It is for this reason that the temperature range of Region I is shifted downward and is narrow compared to Region II.

3.5.5 ATTITUDE AND ORBIT CONTROL SUBSYSTEM

The following provides a brief summary description of the attitude and orbit control approaches which have been tentatively selected for the Hybrid. It will be injected by an Advanced Delta launch vehicle into a 28.5 degree inclined transfer orbit to synchronous orbit attitude. Passive spin stabilization will be utilized for attitude control of the spin-stable satellite following separation from the spinning third stage of the Delta, during coasting in the transfer orbit and injection at apogee into a synchronous-equatorial-circular (SEC) orbit using a separate solid rocket motor, and possibly during initial correction of this orbit to remove in-plane injection errors.

Catalytic hydrazine thrusters aligned with the spin axis will be used for spin axis precession and for translation orbit control as indicated in Figure 3.5-2. Telemetered sun sensor/POLANG data will be utilized on the ground for attitude determination as the basis for jet commands to yield the required spin axis precessions.

Following injection into SEC orbit, the spacecraft will be despun, the solar panels deployed, and the desired earth-oriented reference attitude will be acquired.

This orientation consists of the +x (roll) axis lying in the orbit plane, nominally pointed along the eastward direction of motion for a SEC orbit; the +y (pitch) axis normal to the orbit plane, nominally pointed south for a SEC orbit; and the +z (yaw) axis in the orbit plane, pointed towards the center of the earth along the local vertical. (See Figures 3.5-1 and 3.5-3.)

Acquisition of the reference orientation is accomplished by ground command of the catalytic hydrazine thrusters located on the ±x sides and the -z side of the satellite for 3-axis torqueing. Telemetered data from the solar panels, from one of two 2-axis sun sensors located on the ±x sides and from one of two 2-axis earth sensors located on the +z side are used for attitude information during the acquisition maneuvers.

These same sensors and torquers, together with a momentum wheel, are used to maintain the reference orientation to within 0.5 degree about all three axes during the planned 5-year mission. The momentum wheel is run at a high bias speed with its spin axis parallel to the spacecraft y axis so as to provide gyroscopic stability to the indicated accuracy for several days about the spacecraft x-z axes in the orbit plane. Limited up-down accelerations of the momentum wheel are effected by the on-board controller as needed for closed-loop pitch stabilization about the z axis.

Ground-originated jet commands for corrective precession of the spacecraft y axis or to cause the momentum wheel to return to its nominal bias speed should only be required every 1 - 2 days.

The solar panels are single axis driven about the y axis at the nominal orbital rate. Similarly infrequent incremental drive commands from the ground should be all that's required for the panels to track the sun to the needed accuracy of several degrees.

Final SEC orbit correction, and East-West station keeping and station relocation as required are provided by ground command of the central jets on the ±x sides of the satellite.

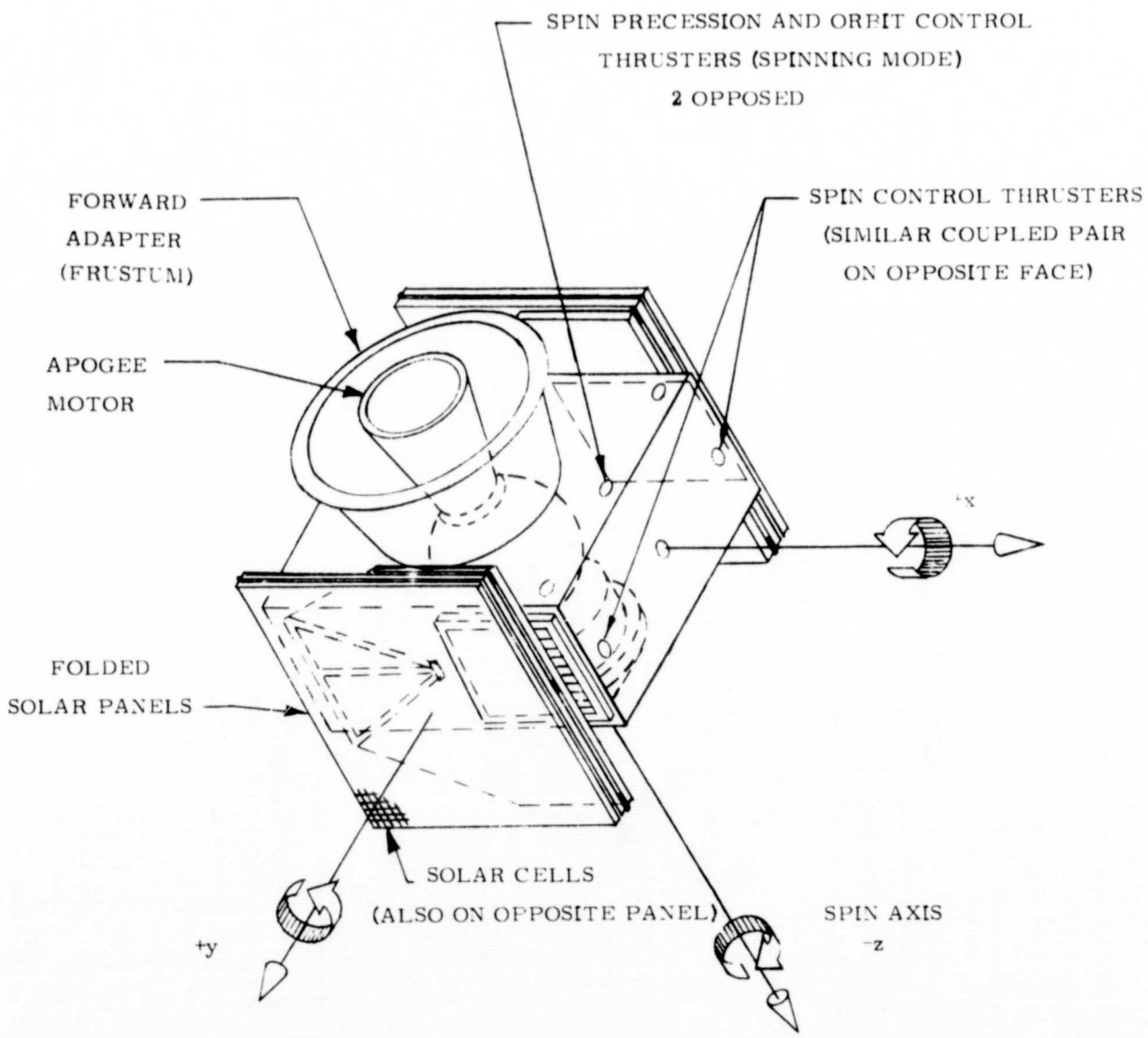


FIGURE 3.5-2

HYBRID CONFIGURATION

(STOWED)

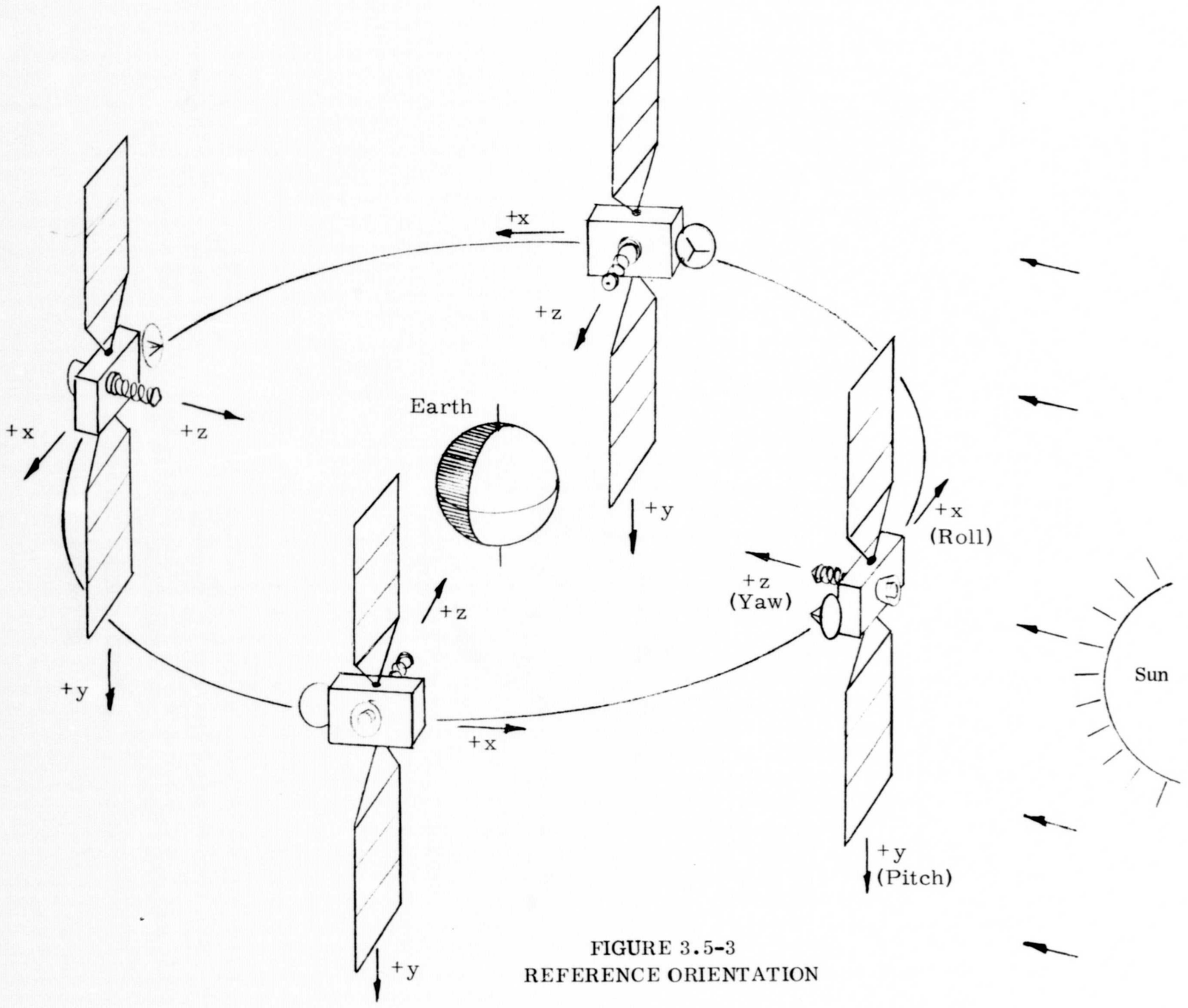


FIGURE 3.5-3
REFERENCE ORIENTATION

4.0 SPACECRAFT DESIGN

This section of the report presents in detail the back-up-data, analysis and trade-offs as well as more detailed descriptions of the satellite sub-systems which were performed during the course of the conceptual design study program. A more general description of the satellite was presented in Section 3.0.

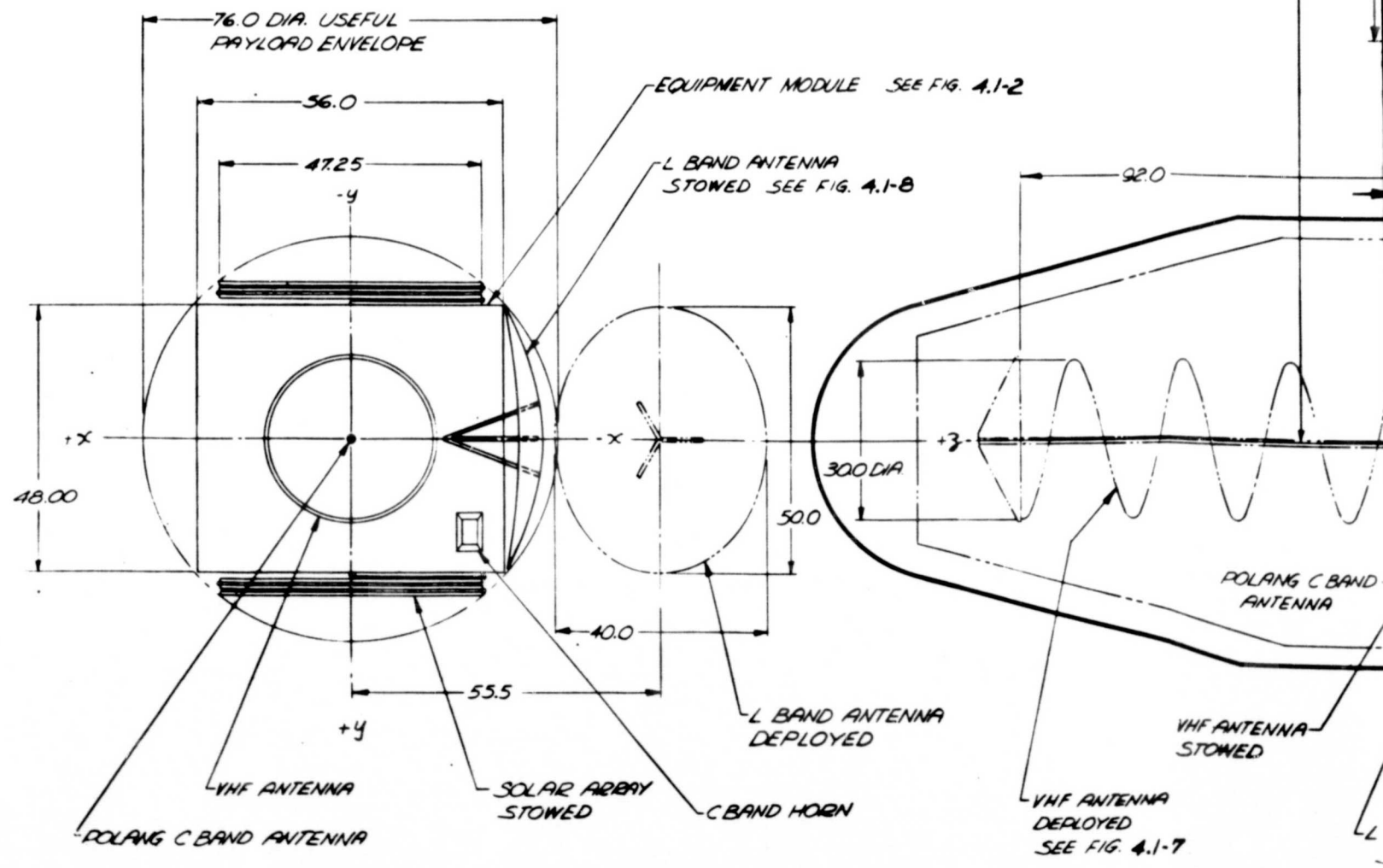
4.1 MECHANICAL DESIGN DESCRIPTION

4.1.1 INTRODUCTION

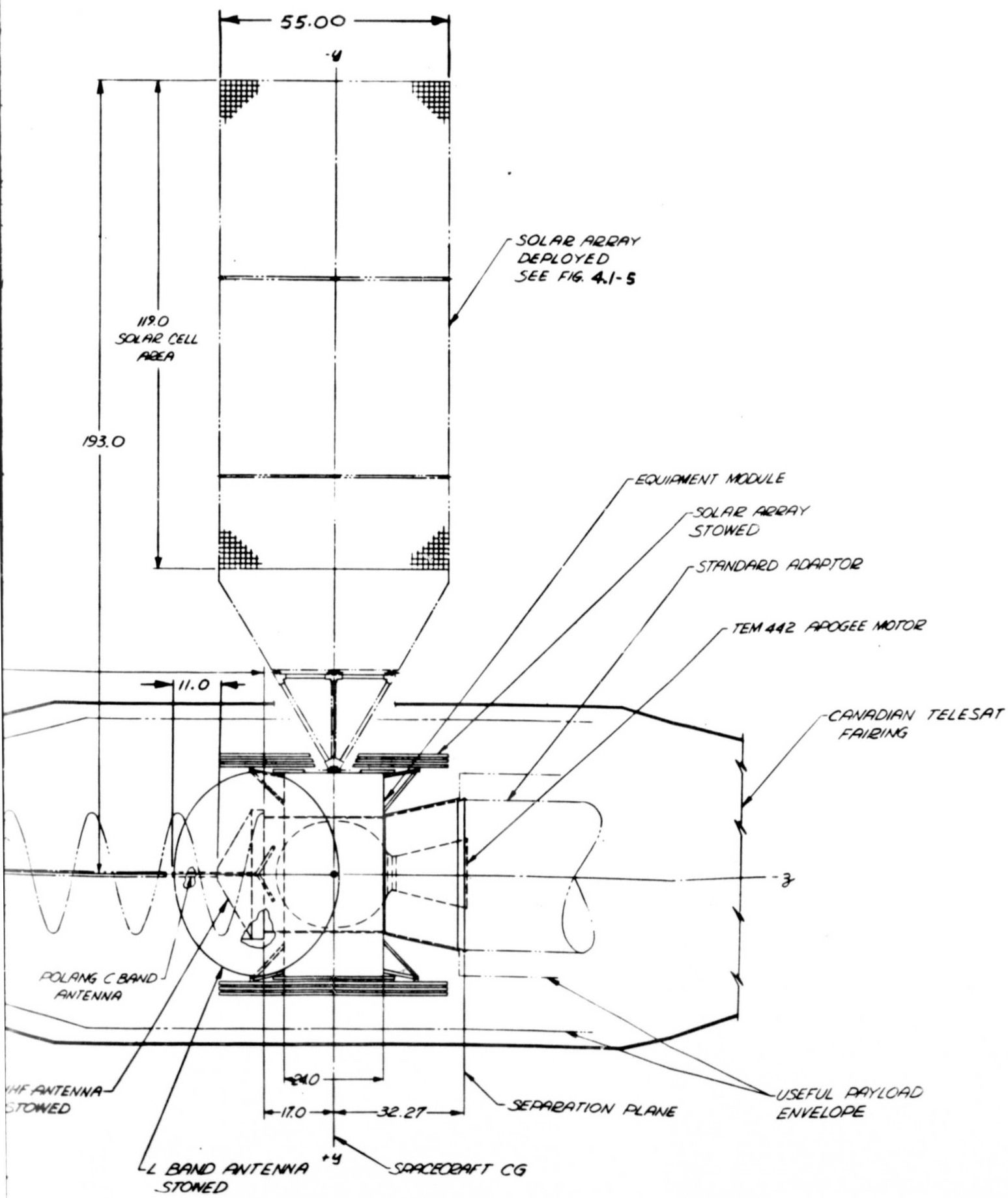
The primary satellite structure consists of a lower frustum, torque tube and module. It supports a symmetrical 900 watt solar array, a VHF Helix Antenna, a parabolic L-band antenna externally and a TEM 442 apogee motor internally. The spacecraft is supported on a standard Delta adapter and is packaged within the Canadian Telstat fairing as shown in Figure 4.1-1. The weight of the spacecraft at separation is approximately 1302 lbs. (including 60 lbs weight growth).

4.1.2 EQUIPMENT MODULE

Construction details of the equipment module are shown in Figure 4.1-2. The design is built around a 28 in. dia. central thrust cylinder which supports the apogee motor as well as the basic module structure. The thrust cylinder is fabricated of .040 inch thick aluminum alloy. It will have an internal ring for support of the apogee motor and external ribs and rings for support of the module structure. The forward end of the honeycomb frustum is attached to the aft ring of the thrust cylinder. The aft ring of the frustum is designed to mate with the adaptor section of the booster, with provisions for the attachment of a marmon clamp. The forward end of the thrust cylinder is the mounting ring for the VHF antenna package. The module, measuring 24 x 48 x 56 inches is attached to the thrust cylinder by 6 honeycomb bulkheads. Two are on the x axis and 4 parallel to the y axis. The latter contains provisions for mounting the solar array drives. The external side surfaces of the module are honeycomb panels with imbedded heat pipes spaced within them for thermal control. The four top and four bottom covers on the equipment module are honeycomb panels.



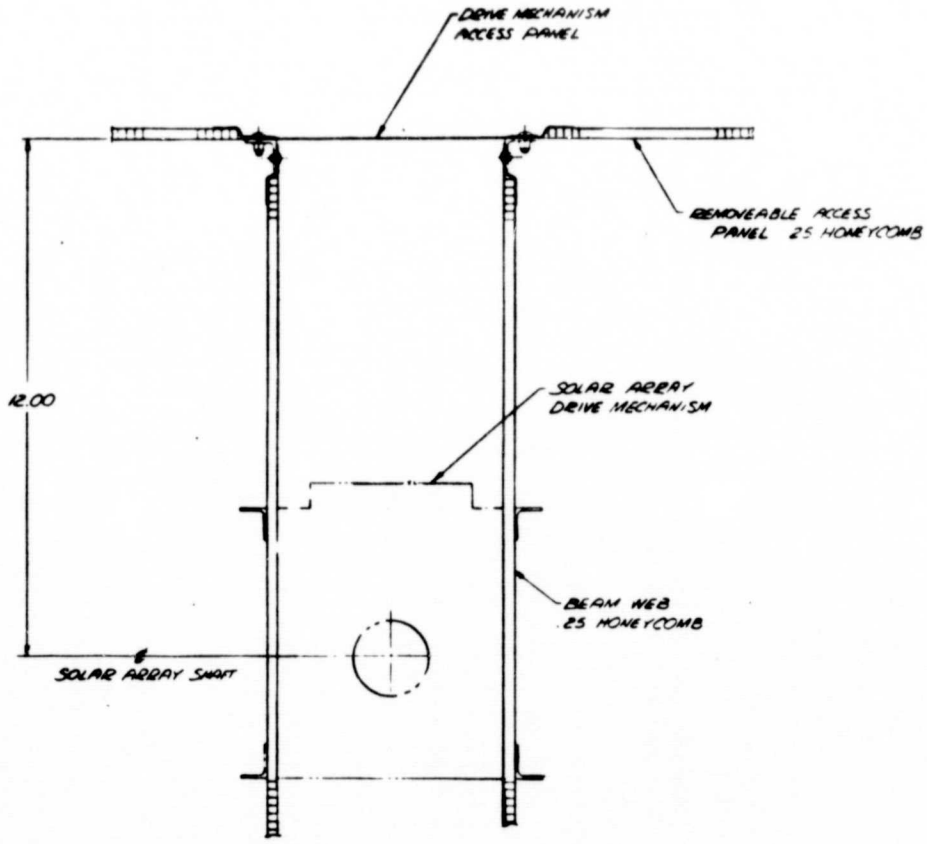
FOLDOUT FRAME

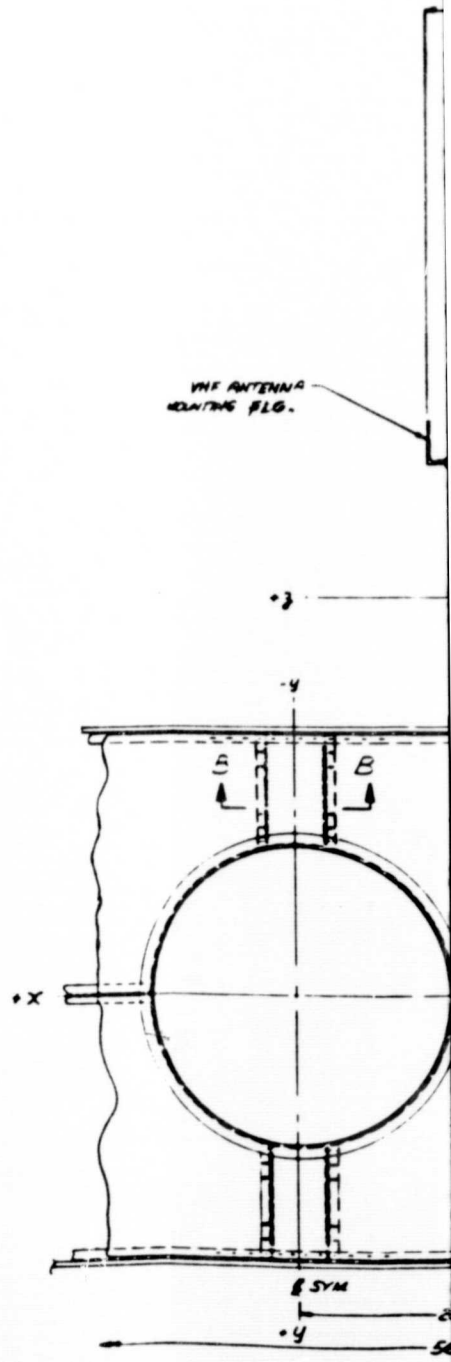


EARTH ORIENTED SPACECRAFT
ROTATING SOLAR ARRAY

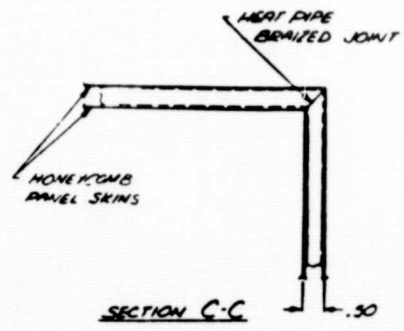
FIG. 4.1-1

FOLDOUT FRAME

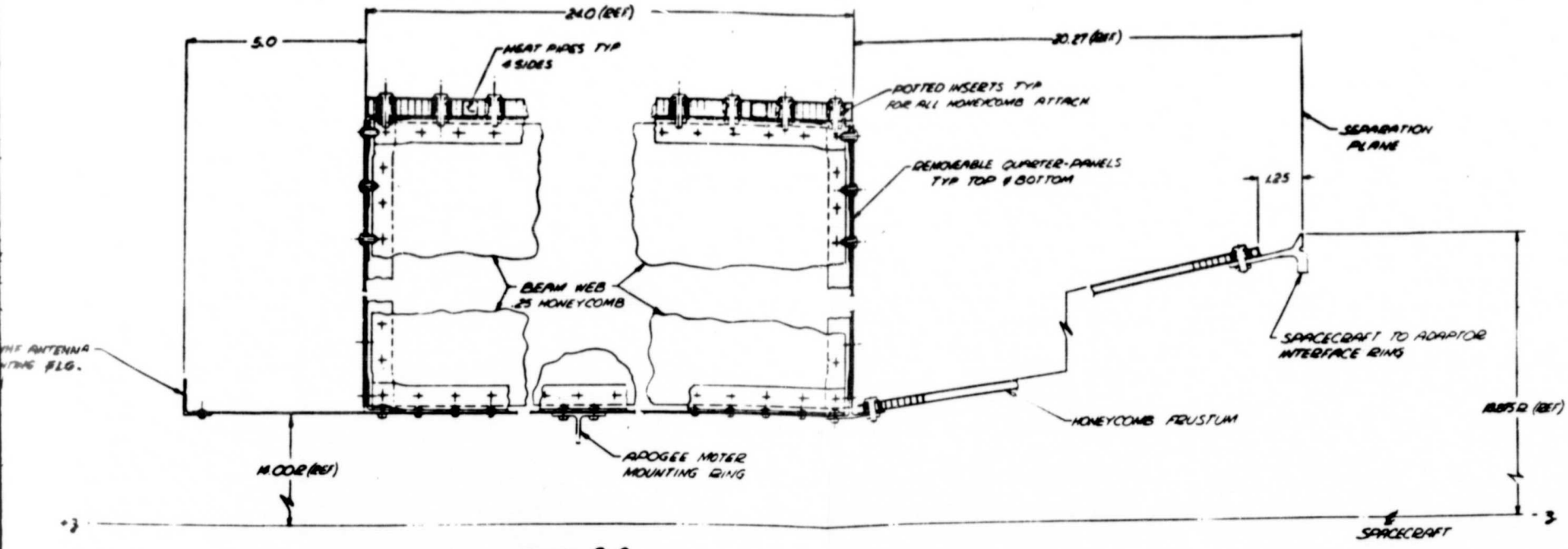




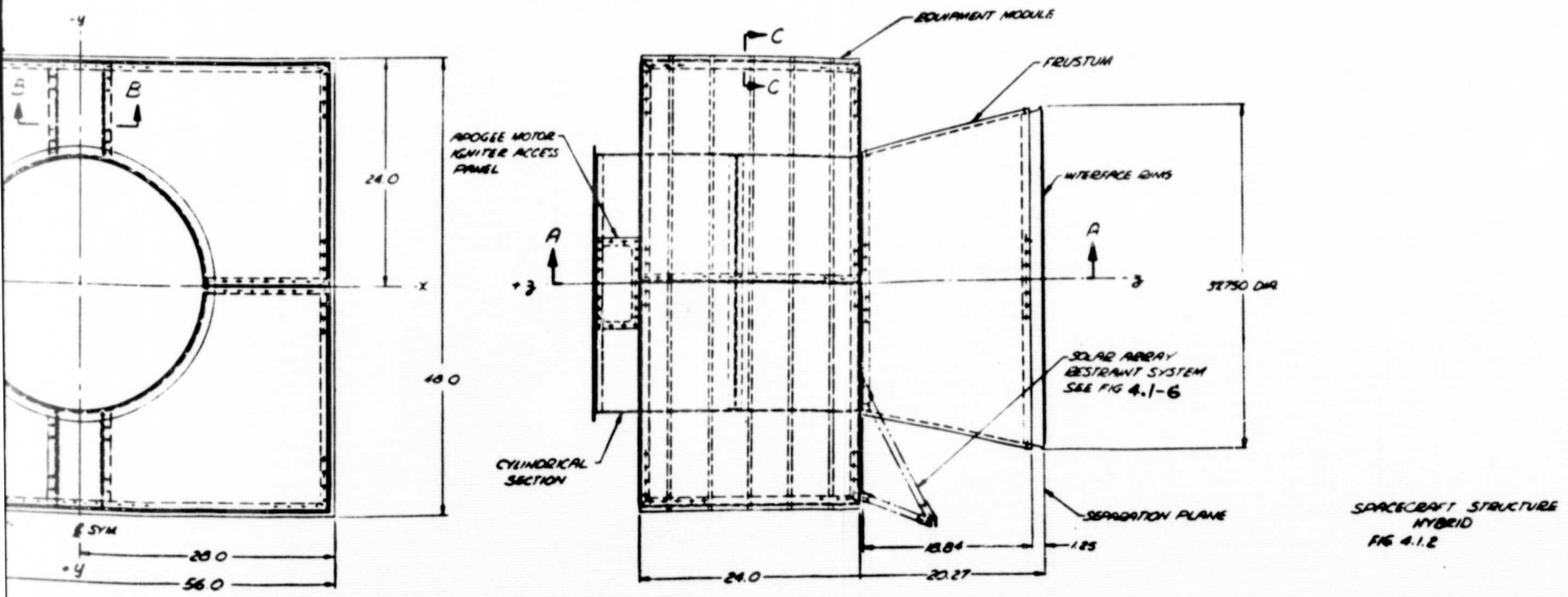
SECTION B-B



FOLDOUT FRAME



SECTION A-A



SPACECRAFT STRUCTURE HYBRID
FIG 4.1.2

FOLDOUT FRAME
1
2

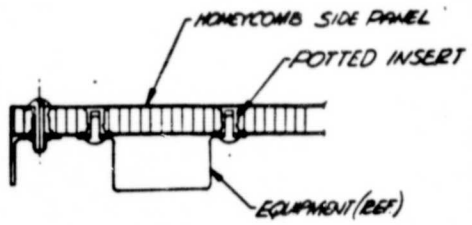
and are removeable for ease of access. The equipment installation within the module is shown in Figure 4.1-3. It is distributed to minimize the offset between the center of gravity and the center line of the spacecraft.

The thermal installation for the spacecraft is shown in Figure 4.1-4. It contains thermal blankets, louvers and heat pipes.

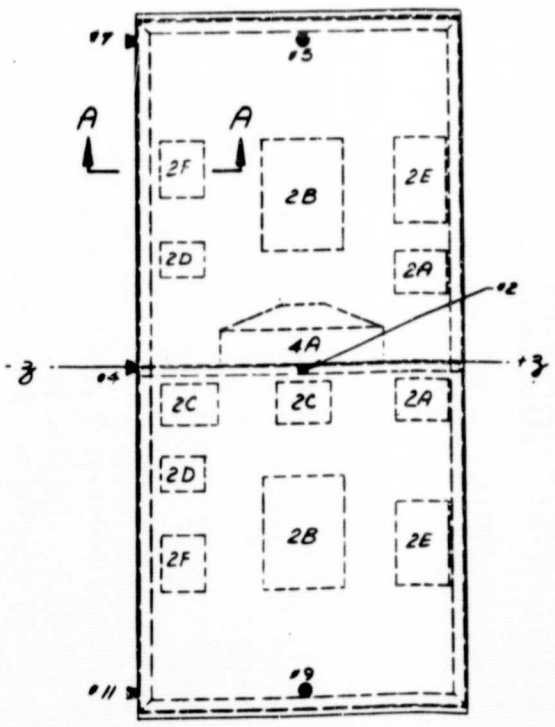
A more precise explanation of the thermal analysis leading to this design is given in Section 4.4. To briefly summarize however, the module is segregated into the thermally isolated compartments. The +x compartment containing the batteries, momentum wheel and telemetry and command equipment is actively controlled by thermal louvers while the object of the -x chamber which contains the communications equipment is to dissipate all possible excess heat using high emittance passive coatings. Equipment within the module is bolted to the side panels containing the embedded heat pipes. The heat pipes in turn efficiently transfer the heat to the control surfaces. The joint between equipment and panel is a highly conductive one using large areas and conduction filler agents. All external module surfaces except the ±y side are covered with super insulation as is the inside and outside of the thrust frustum. Insulation is also installed within the module as a compartment separator. Note the placement of the internal blanket which group the bottles and thrust cylinder in the -x space while placing the solar array drive in the +x compartment. Another significant feature of the design is the horizontal placement of the heat pipes so a more realistic "zero gravity" simulation is obtained when the spacecraft is in the launch or more importantly its test position.

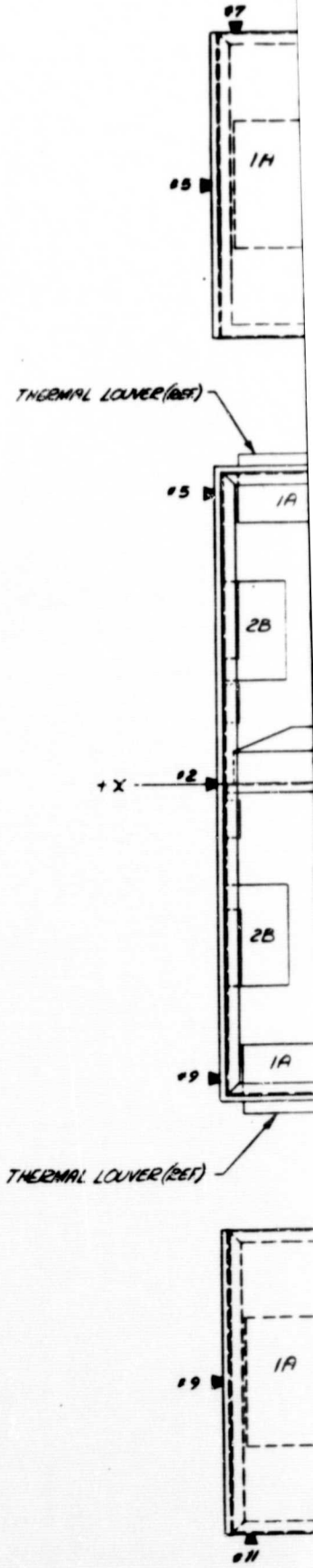
4.1.3 SOLAR ARRAY

Each panel of the solar array is assembled in four sections. Three of these sections are aluminum honeycomb sandwich while the fourth, being only a spacer, is a truss of aluminum tubing. The design is shown in Figure 4.1-5. The two outermost panels are identical. The inboard panel has essentially the same dimensions but is trapazoidal in plan form inboard of the solar cells. Each honeycomb panel is .75 inches thick and has an edge member of light aluminum channel. Solar cells are not placed on the entire panel because of shadowing considerations. An



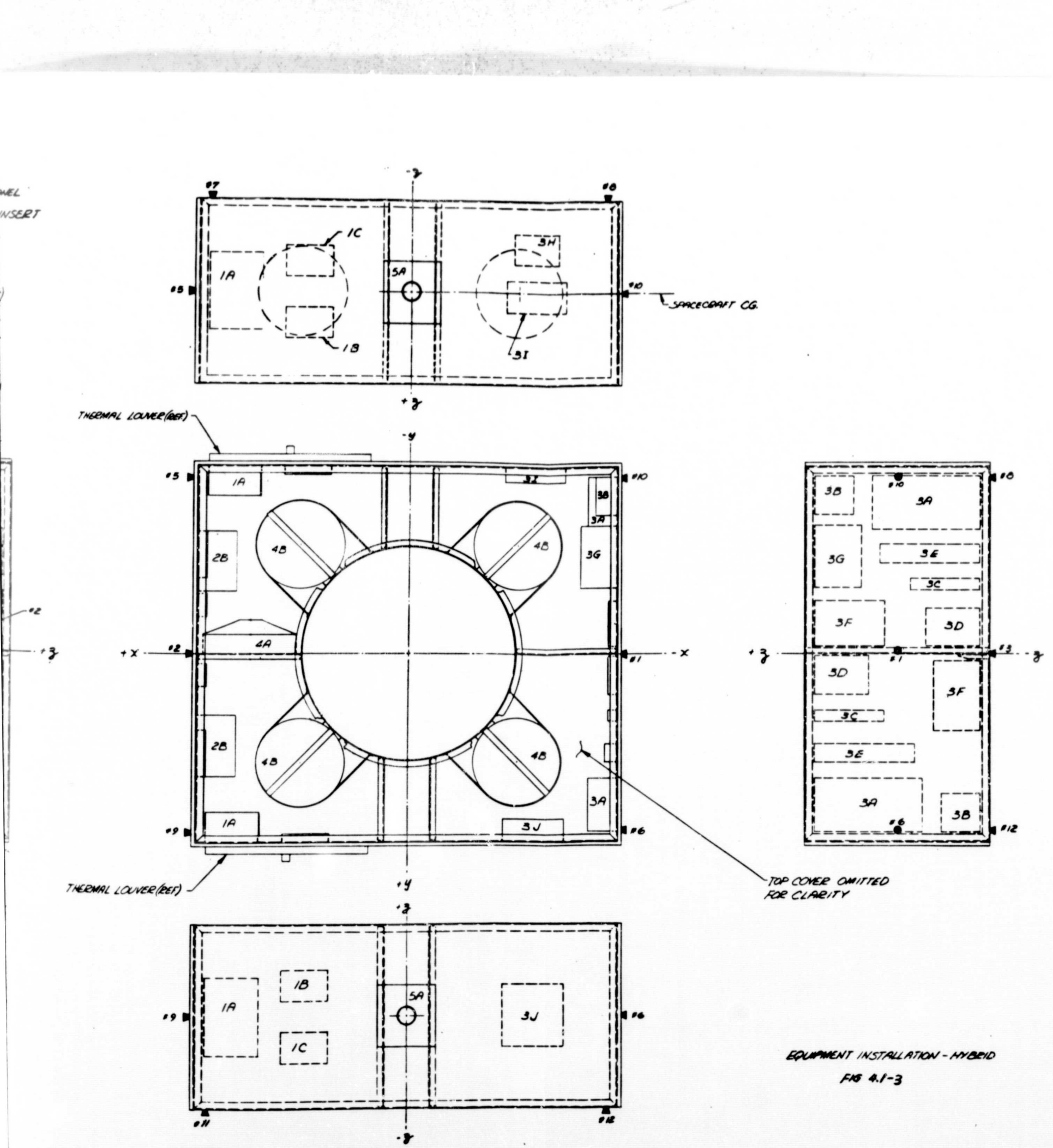
SECTION A-A





ITEM	PART	REQ
1A	BATTERY	2
1B	BATTERY CHARGER	2
1C	BATTERY DISCH. CON"	2
2A	COMMAND RECEIVER	2
2B	COMMAND DECODER	2
2C	COMMAND REGULATOR	2
2D	DIPLEXER	2
2E	TM XMITTER	2
2F	TM REG. & SIGNAL CONDITIONER	2
3A	DUAL MODE REPEATER L&C BAND	2
3B	ANTENNA ELECTRONICS	2
3C	C BAND TWTS	2
3D	C BAND TWTS POWER SUPPLY	2
3E	L BAND TWTS	2
3F	L BAND TWTS POWER SUPPLY	2
3G	NARROW L BAND MODE	1
3H	NARROW L BAND XMITTER	1
3I	VHF RECEIVER	1
3J	VHF XMITTER	1
4A	MOMENTUM WHEEL	1
4B	HYDRAZINE TANKS	4
CONTROL JETS #1 THRU #12		12
5A	SOLAR ARRAY DRIVE	2

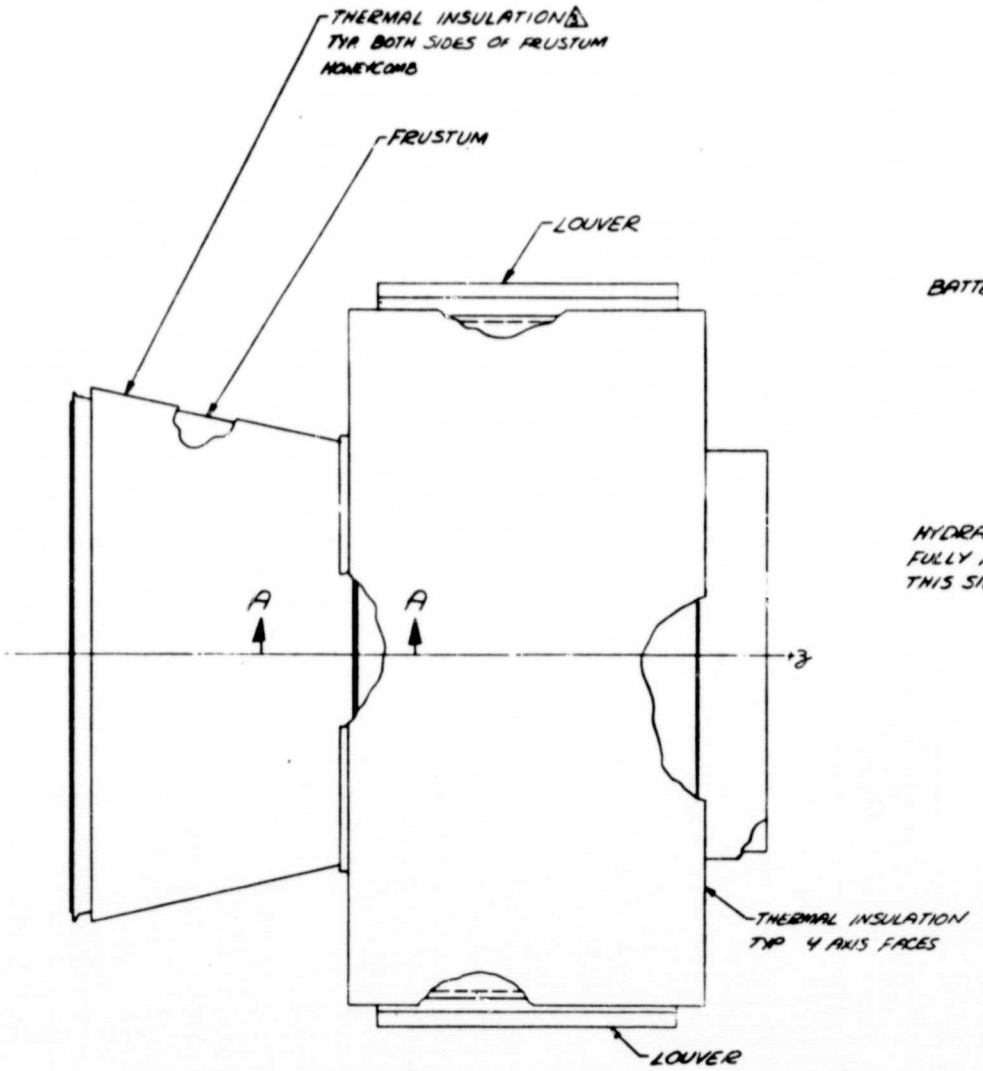
FOLDOUT FRAME
1

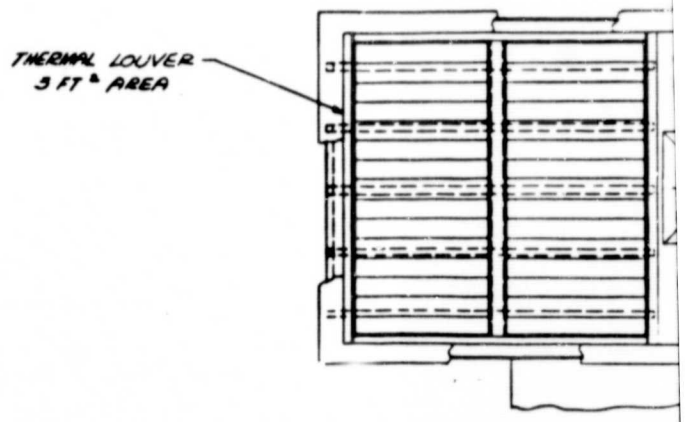


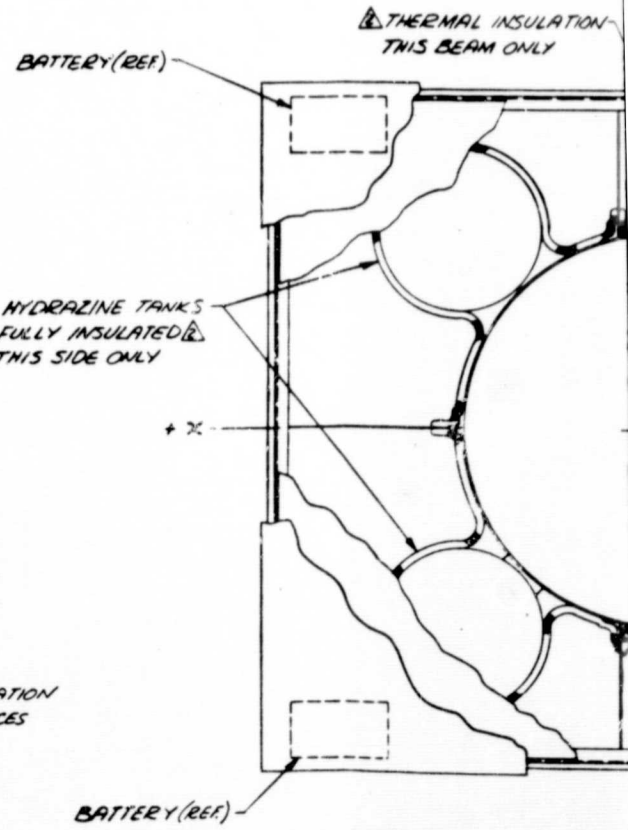
EQUIPMENT INSTALLATION - HYBRID

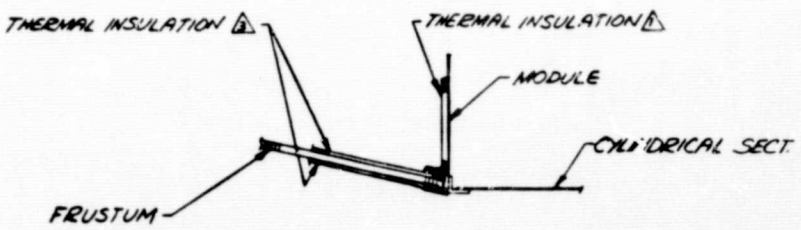
FIG 4.1-3

FOLDOUT FRAME 2

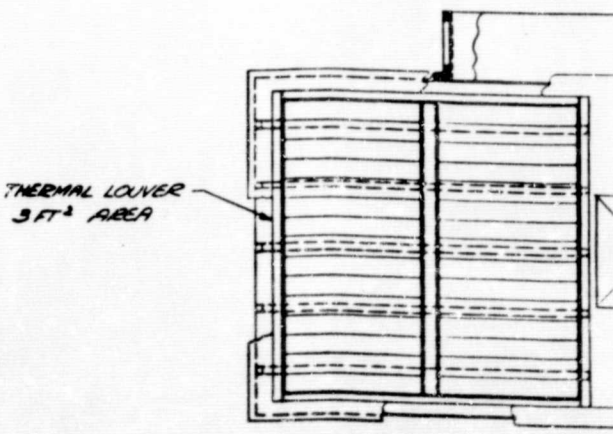






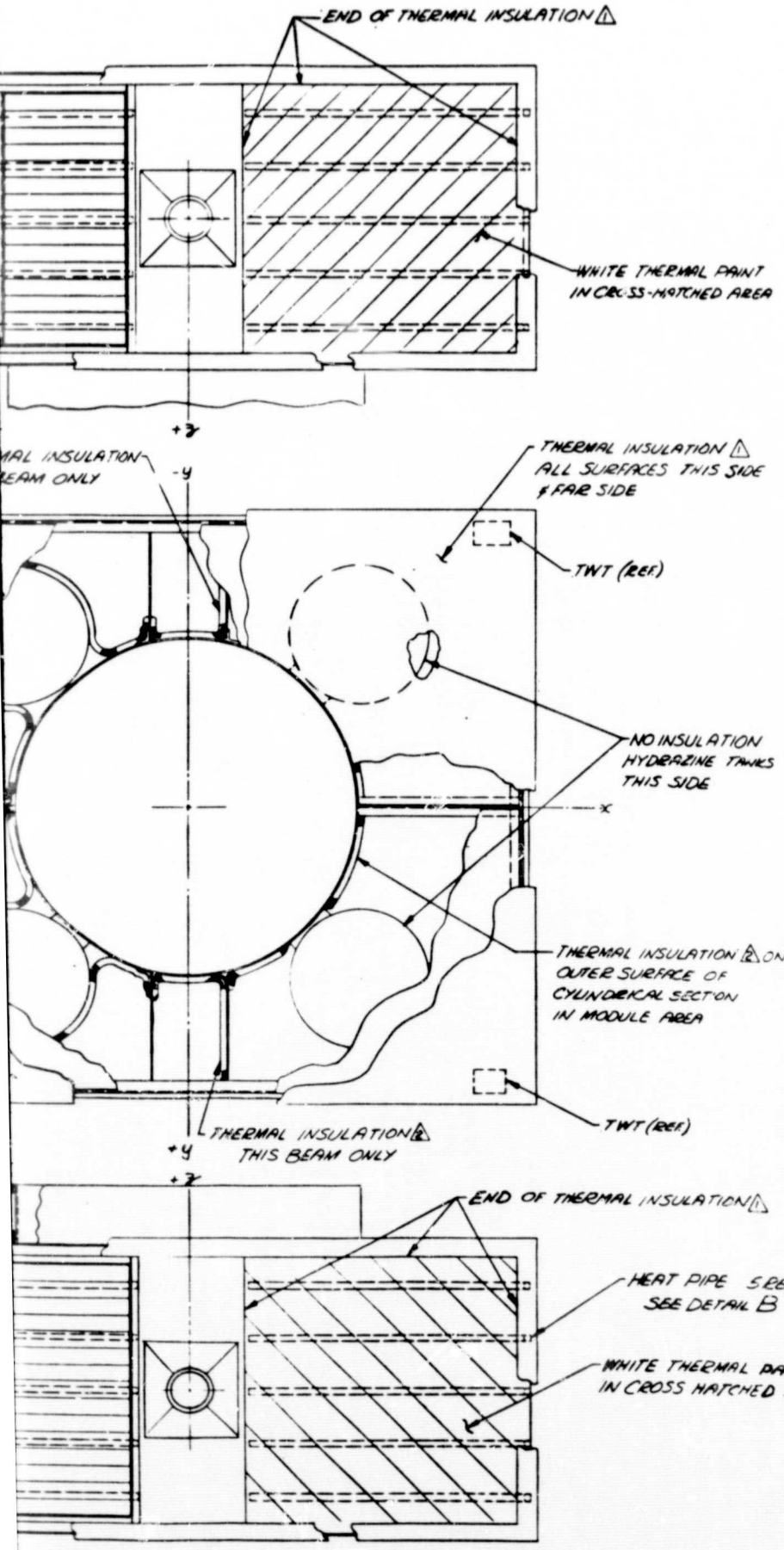


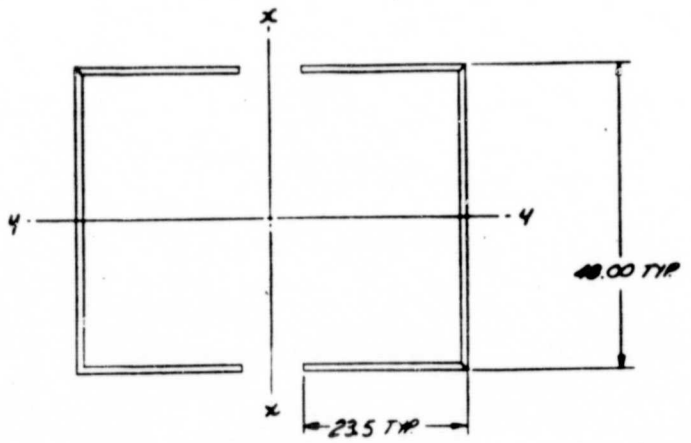
SECTION A-A



FOLDOUT FRAME

1





DETAIL B
HEAT PIPES

⚠ THERMAL BLANKET: OUTSIDE COVER 5 MIL KAPTON; 30 SHEETS .25 MIL ALUMINIZED MYLAR; INSIDE SHT 5 MIL ALUMINIZED MYLAR

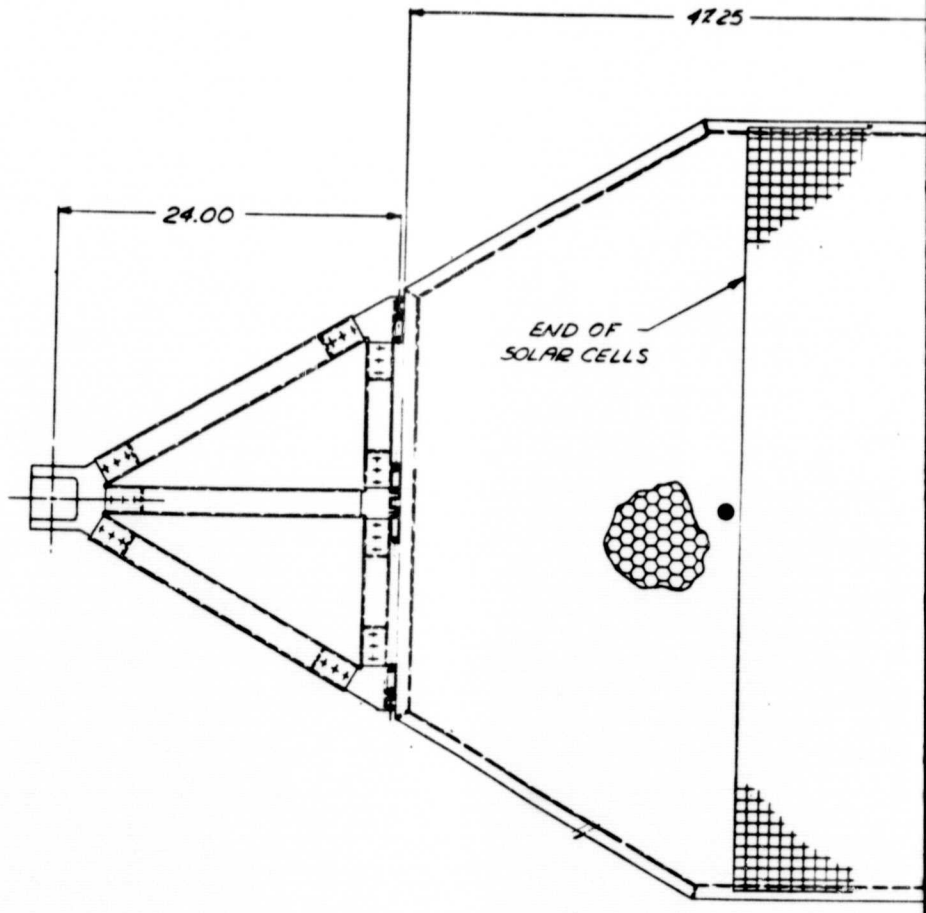
⚠ THERMAL BLANKET: 30 SHEETS .25 MIL ALUMINIZED MYLAR

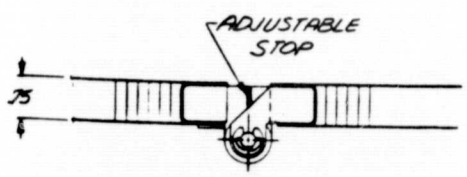
⚠ THERMAL BLANKET: OUTSIDE COVER 5 MIL KAPTON; 15 SHEETS .25 MIL ALUMINIZED MYLAR; INSIDE SHEET 5 MIL ALUMINIZED MYLAR

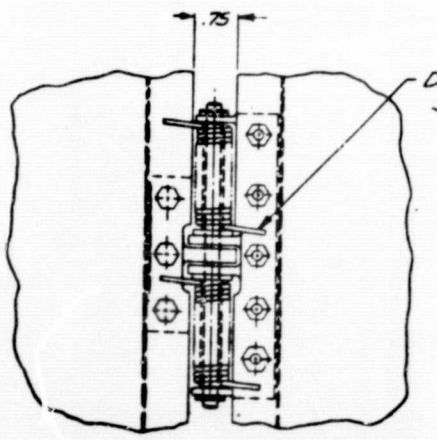
THERMAL CONTROL SYSTEM
HYBRID

FIG. 4.1-4

FOLDOUT FRAME



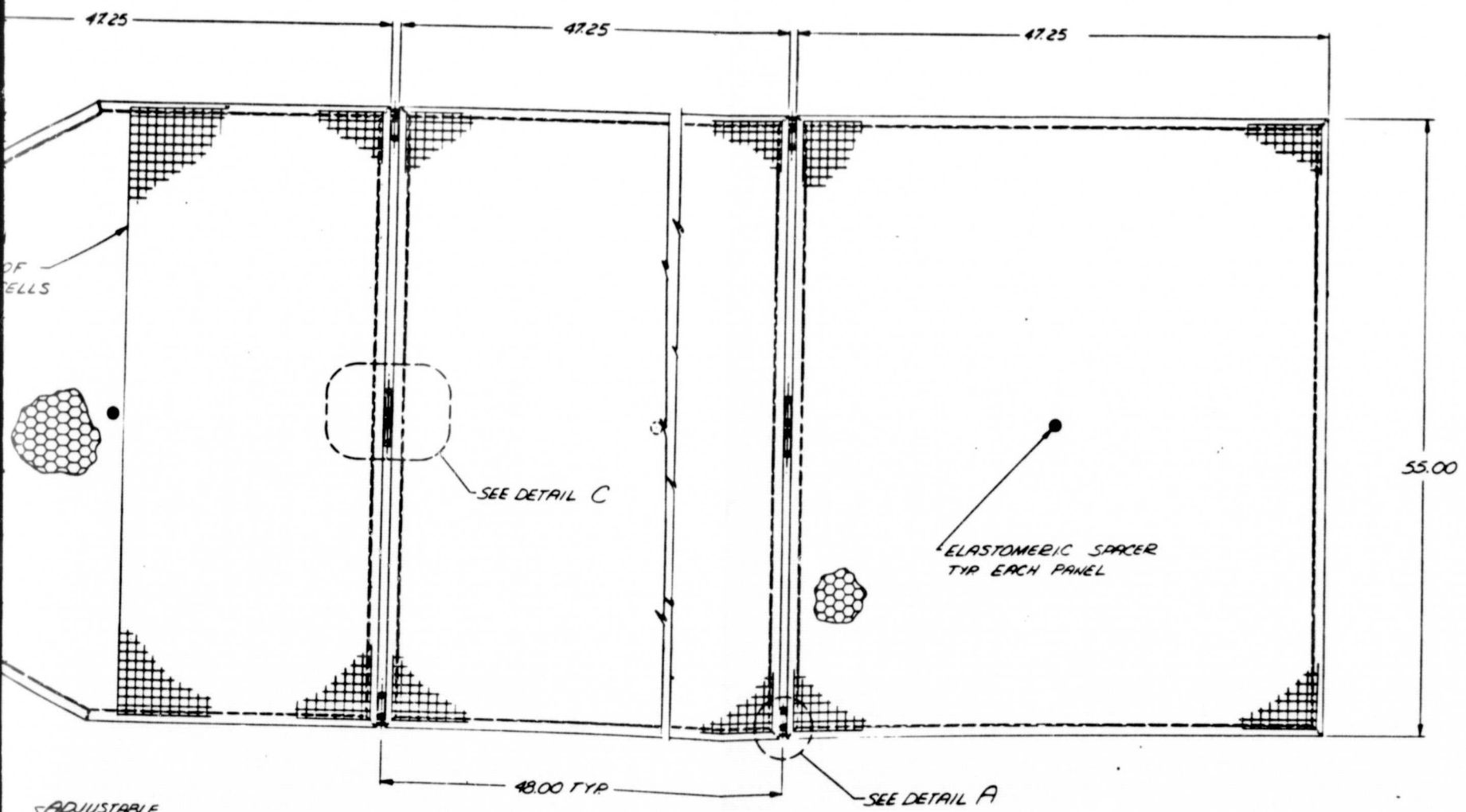


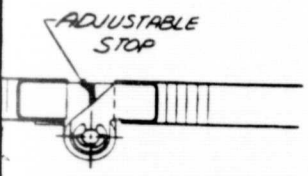


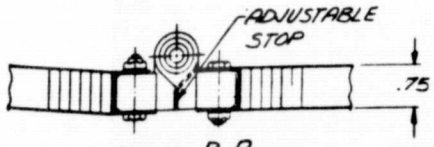
DETAIL C

FOLDOUT FRAME

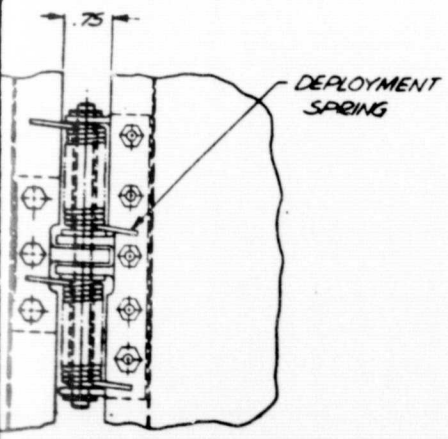
1



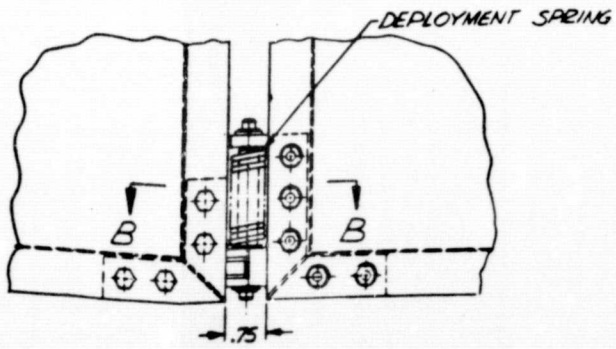




SECTION B-B



DETAIL C



DETAIL A

SOLAR ARRAY
DETAILS - HYBRID
FIG. 4.1-5

FOLDOUT FRAME

interference lock at each hinge provides rigidity for the panel when fully deployed. Outrigers from the equipment module support the stowed solar panel during launch. In the stowed configuration there are exposed solar cells on both sides of the spacecraft. A pyrotechnic release mechanism shown in Figure 4.1-6 allow the panels to deploy on command. The aft surface of the solar panels are black thermal coating selection of which is discussed in Section 4.4.

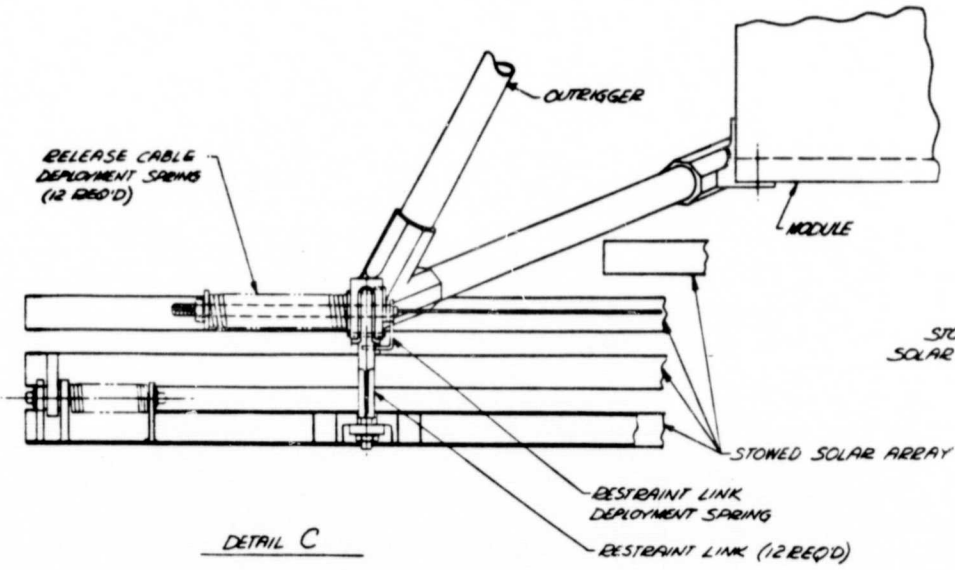
4.1.4 VHF ANTENNA

The VHF antenna shown in Figure 4.1-7 is a 92 inch long 30 inch diameter helix supported by a 0.50 inch dia. hingelock Tubular Extendible Element (TEE). The radiating element is fabricated from 0.50 inch diameter aluminum thin walled tubing. Its shape is maintained by longitudinal dacron cord or kapton strips. The end of the TEE is attached to the conical fiberglass end cap. A ground plane of rods deployed by flexures is also part of the antenna system. During launch the assembly is packaged in a 4.25 inch high 31.00 inch diameter container mounted on the forward end of the thrust cylinder even though the antenna would fit within the fairing in its deployed configuration. (In order to withstand the launch loads, its stiffness and weight would have to increase considerably. This would also be detrimental to the inertial configuration of the satellite as well as being a potential problem in the spin mode.) The cover is held down at its center by a mechanical latch incorporated into the deployment mechanism. When the unit is activated the conical end cap is released thus releasing the ground plane and deploying the antenna.

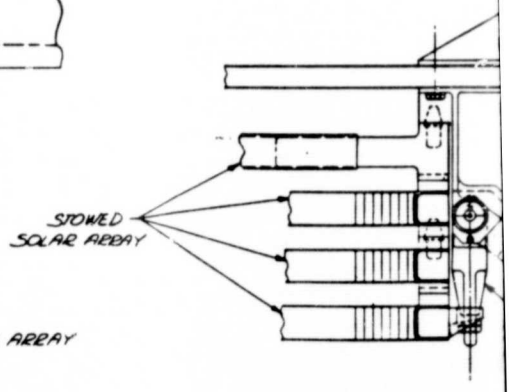
4.1.5 L-BAND ANTENNA

The L-band antenna shown in Figure 4.1-8 is a parabolic reflector having an eliptical plan view. The major axis of which is 50 inches and the minor axis 40 inches. It has an F/D of approximately 0.4. It is fabricated from an aluminum lattice type frame with an attached fine mesh screen for a reflecting surface.

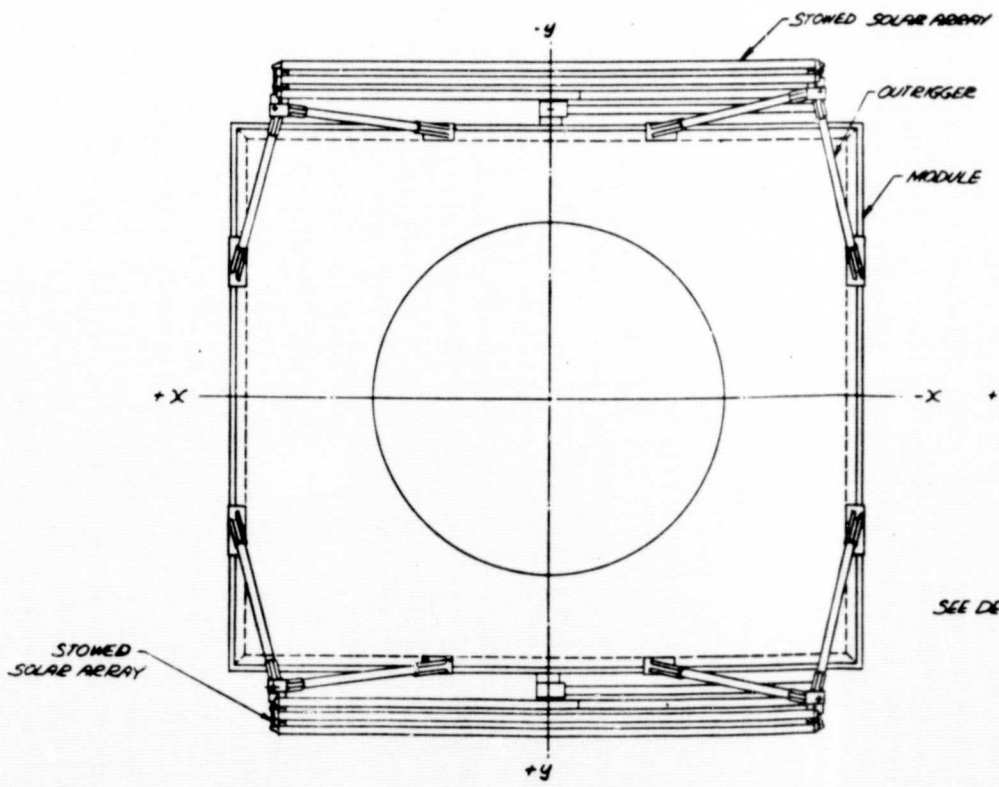
During launch the dish is stowed along the -x side of the spacecraft and is held in place by the solar panel locks as shown in Figure 4.1-8 . It is deployed



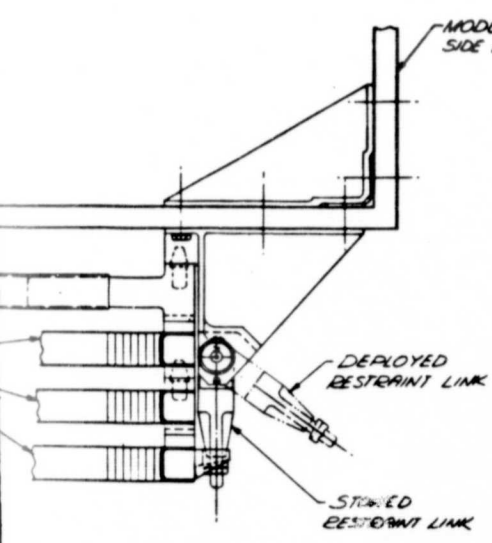
DETAIL C



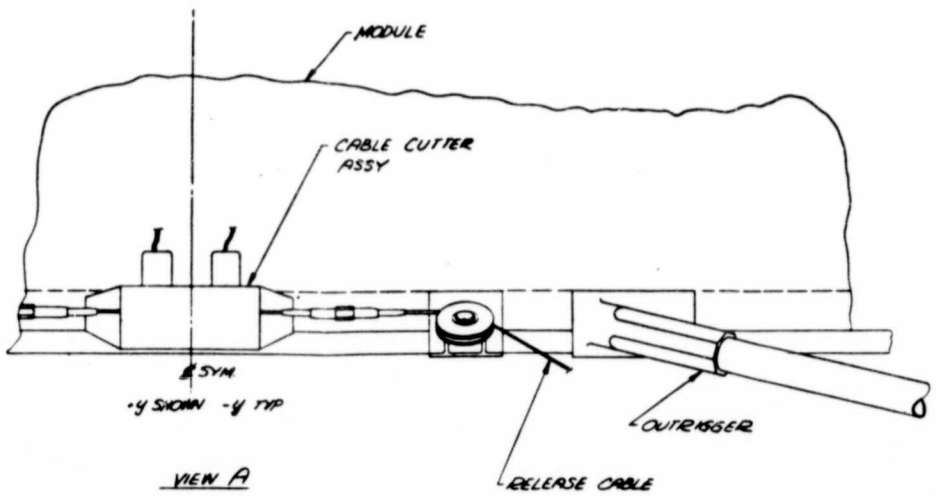
SECTION B-B



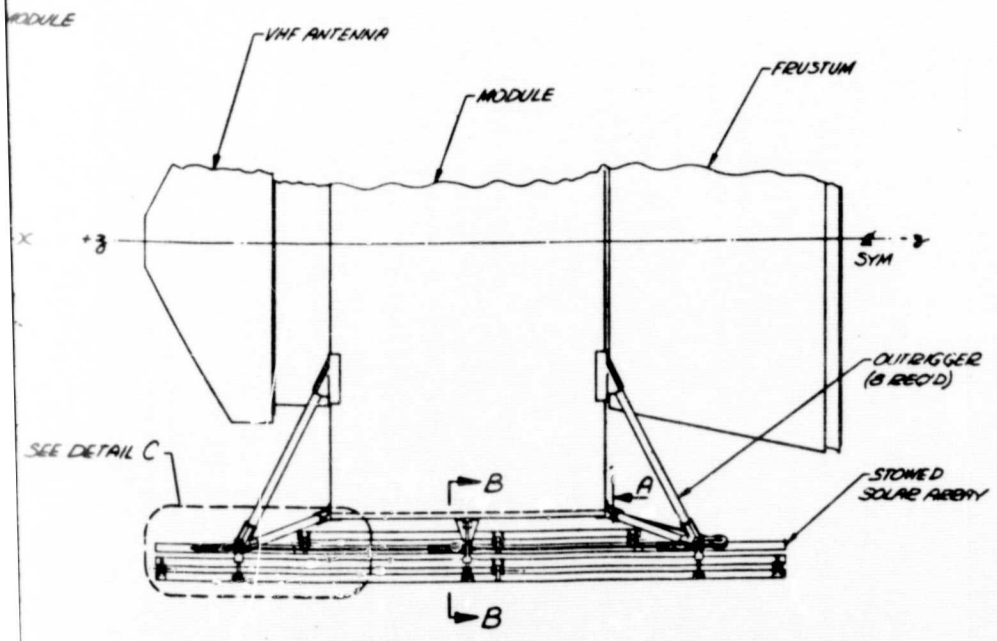
FOLDOUT FRAME
1



SECTION B-B

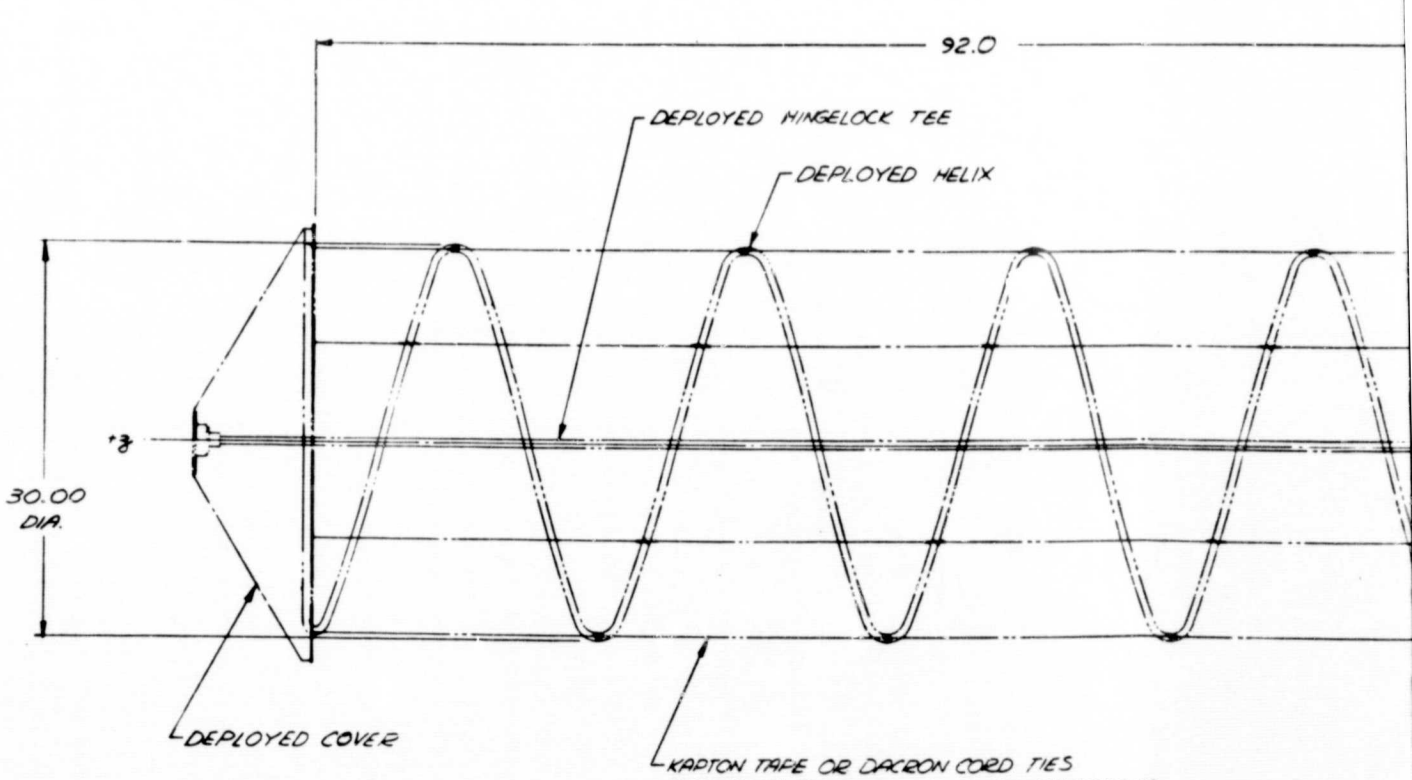


VIEW A

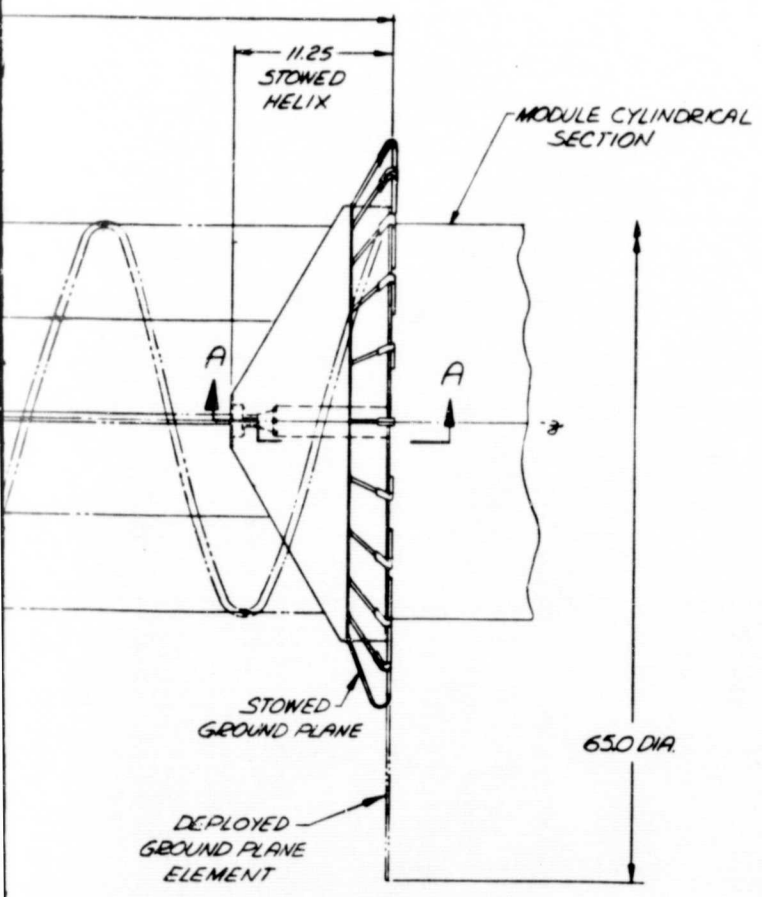


SOLAR ARRAY RESTRAINT & RELEASE SYSTEM
FIG. 4.1.6

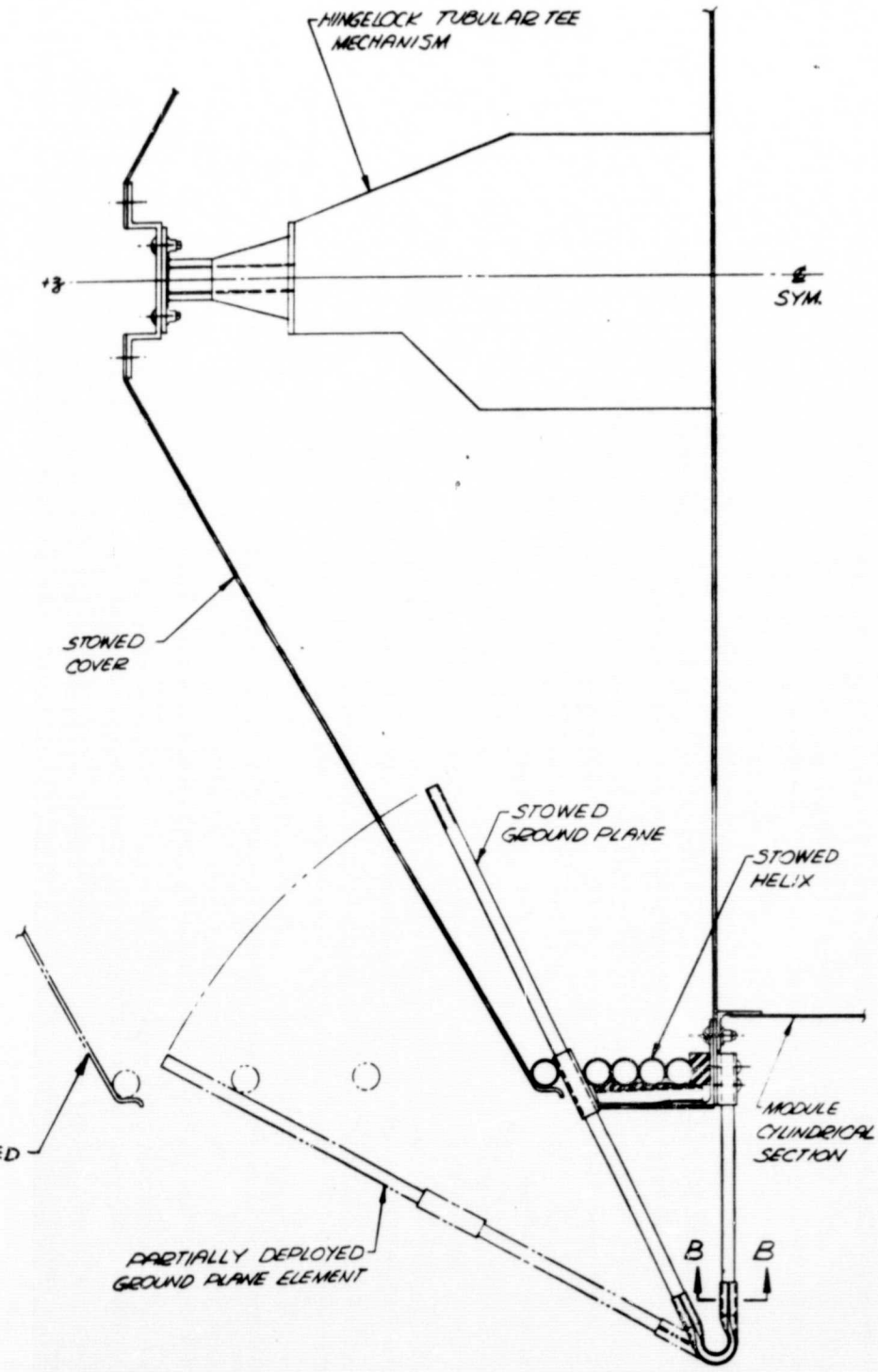
FOLDOUT FRAME



FOLDOUT FRAME
1



SECTION B-B

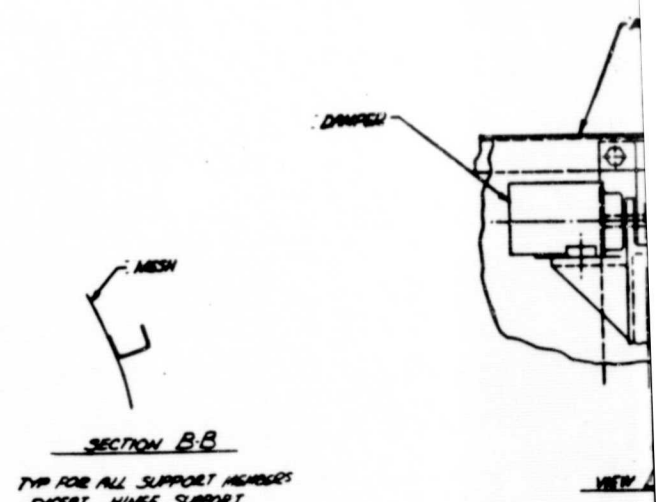


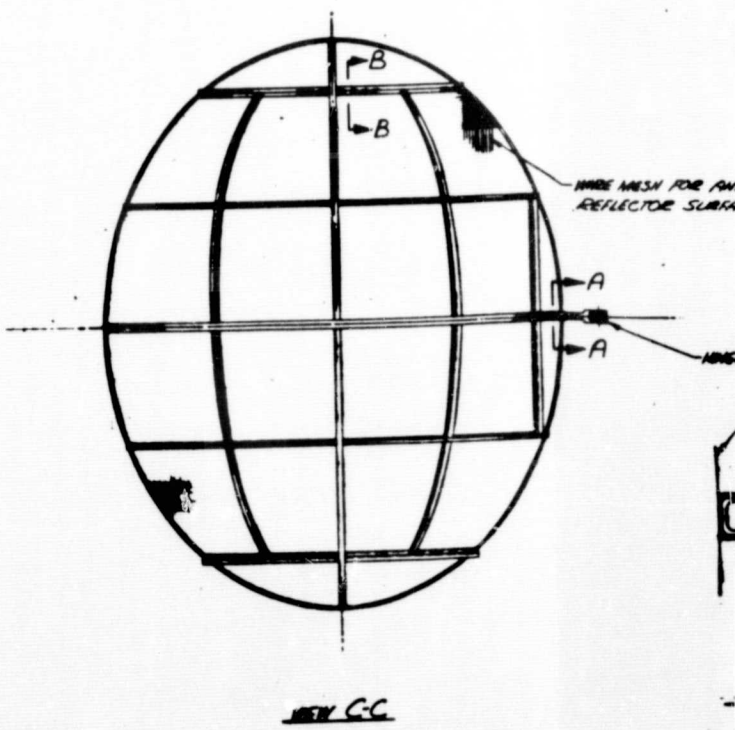
SECTION A-A

VHF ANTENNA

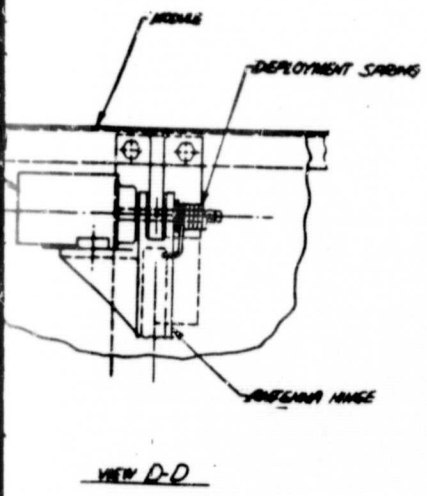
FIG. 4.1-7

FOLDOUT FRAME



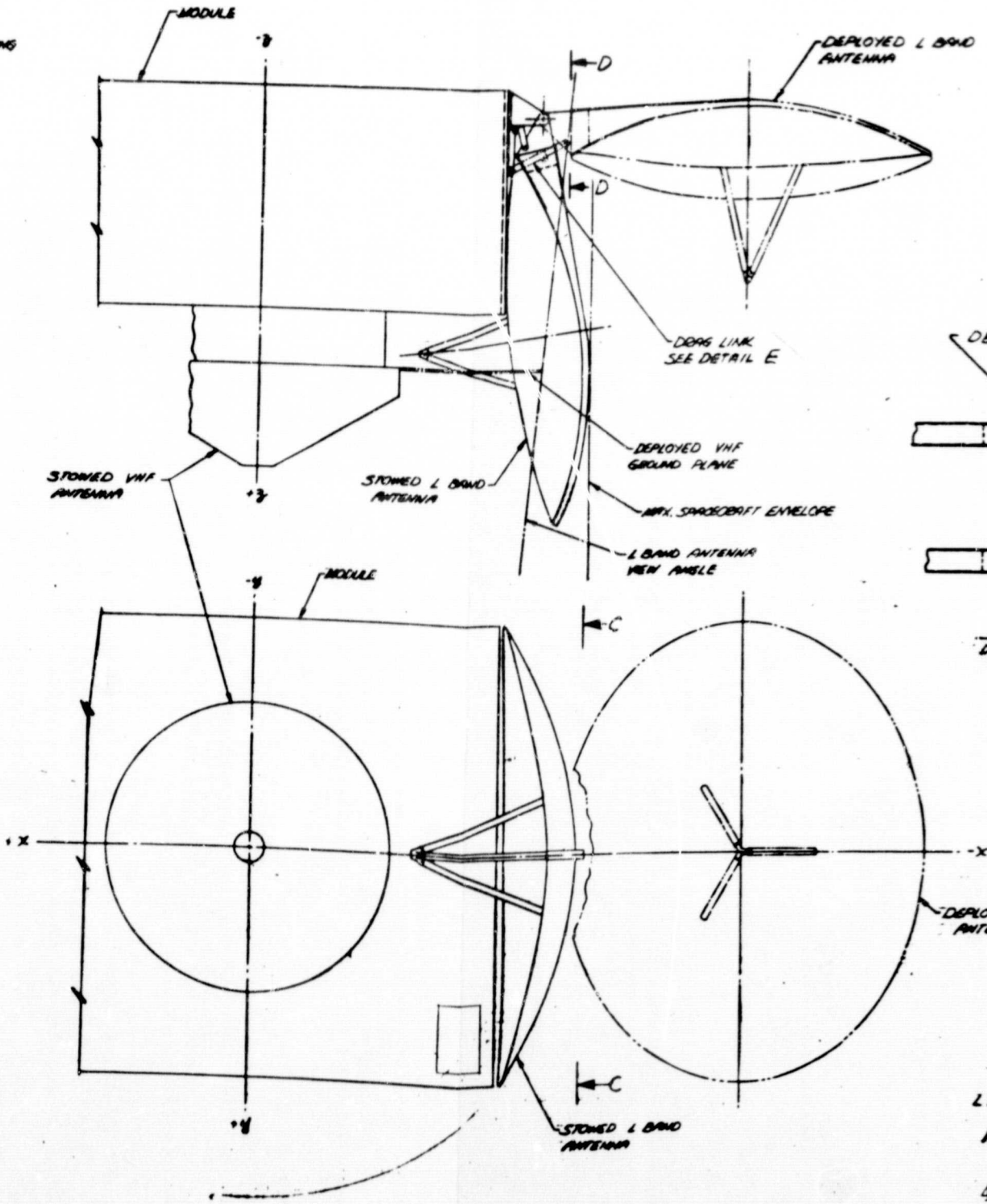


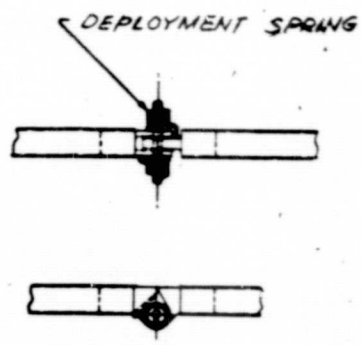
FOLDOUT FRAME



VIEW D-D

SECTION A-A





DETAIL E
DRAG LINK

L BAND ANTENNA

FIG 4.1-8

FOLDOUT FRAME

on a short link along the -x axis a distance sufficient to eliminate interference with the VHF ground plane. The assembly is spring powered. Dampers are used for limiting deployment accelerations. The shift in the spacecraft c. g. due to the antenna deployment is in the opposite direction to the c. g. shift caused by the paddle deployment. This is important to preserve the c. g. location for attitude control.

4.1.6 POLANG ANTENNA

The POLANG antenna is a one inch diameter rod, eleven inches long located on top of the VHF antenna cover. The POLANG antenna utilizes a slip joint to disconnect when the VHF antenna is deployed.

4.2 STRUCTURAL DESIGN AND ANALYSIS

4.2.1 SUMMARY

Preliminary structural analyses, Appendix A, verify the structural integrity and compliance to the structural dynamics criteria of the Hybrid design illustrated in Figure 4.1-1.

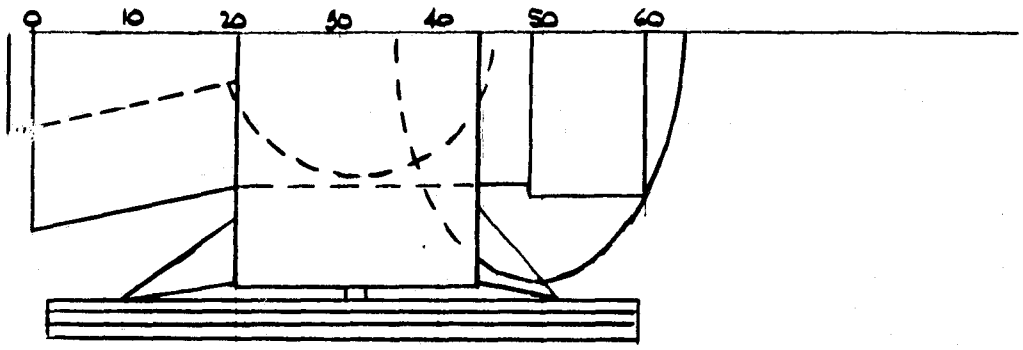
The design criteria is consistent with "Summary of Structural Design Requirements" issued March 16, 1970. The loading environments associated with first and second stage flights were utilized for preliminary analyses, and the resulting shears, bending moments, and axial loads are presented in Figure 4.2-1 . The launch vehicle interface loads are 7020 lbs-shear, 231,400 in. lbs. - bending moment, and 22800 lbs.- compressive axial load. The major structural subsystems and their preliminary design environments are presented in Table 4.2-1.

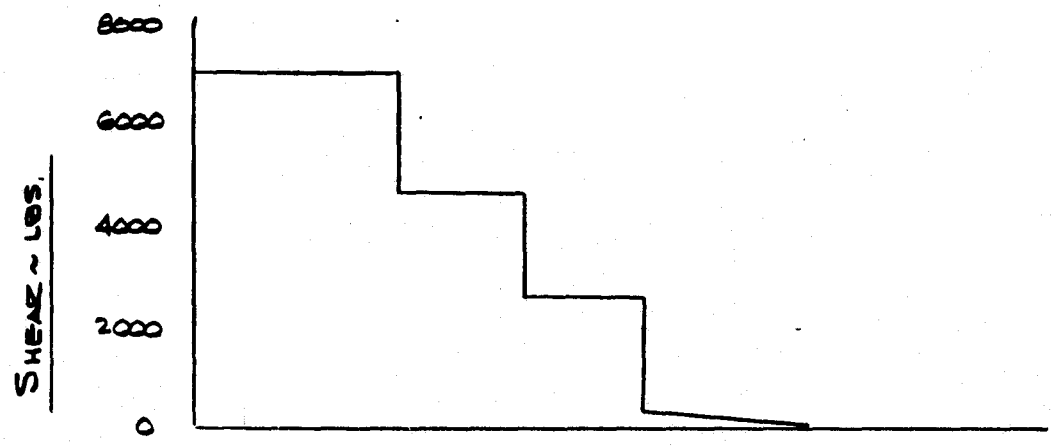
4.2.2 SOLAR ARRAYS

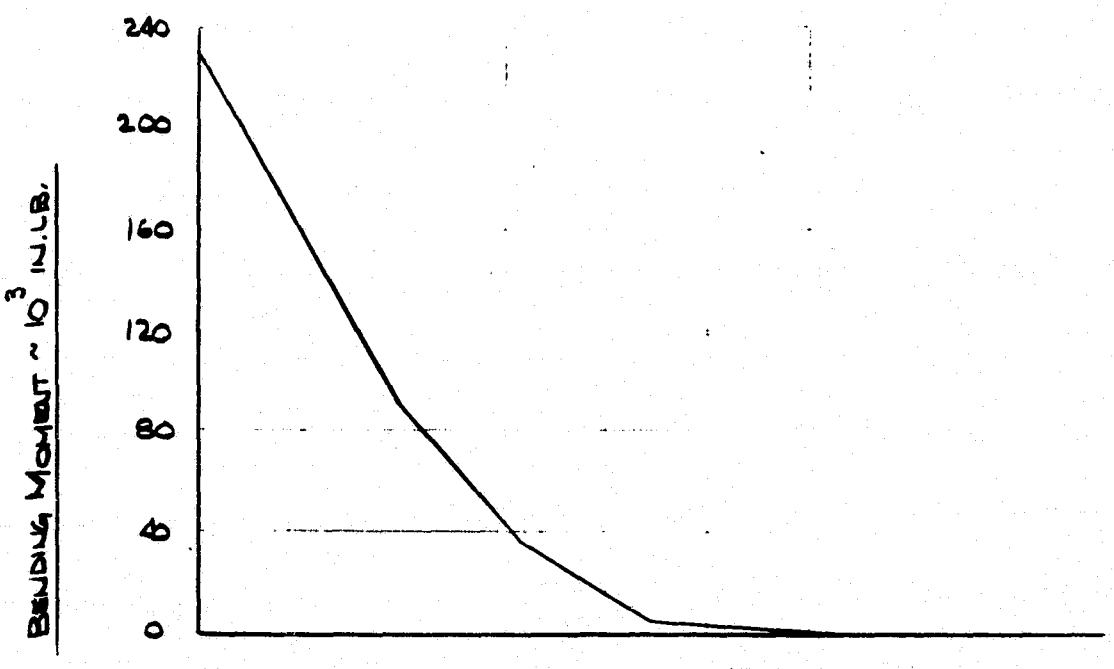
The launch configured solar arrays, as shown in Figure 4.1-5, are supported by outriggers from the top and bottom of the main module, and are also attached to the module at the mid point of the 55 inch sides of the panels. Thrust, Z axis, loads are assumed tak by the two attachments at mid span of the 55 inch side. Lateral loads, both X and Y ar sumed to be taken by the outriggers. The goal of the 6

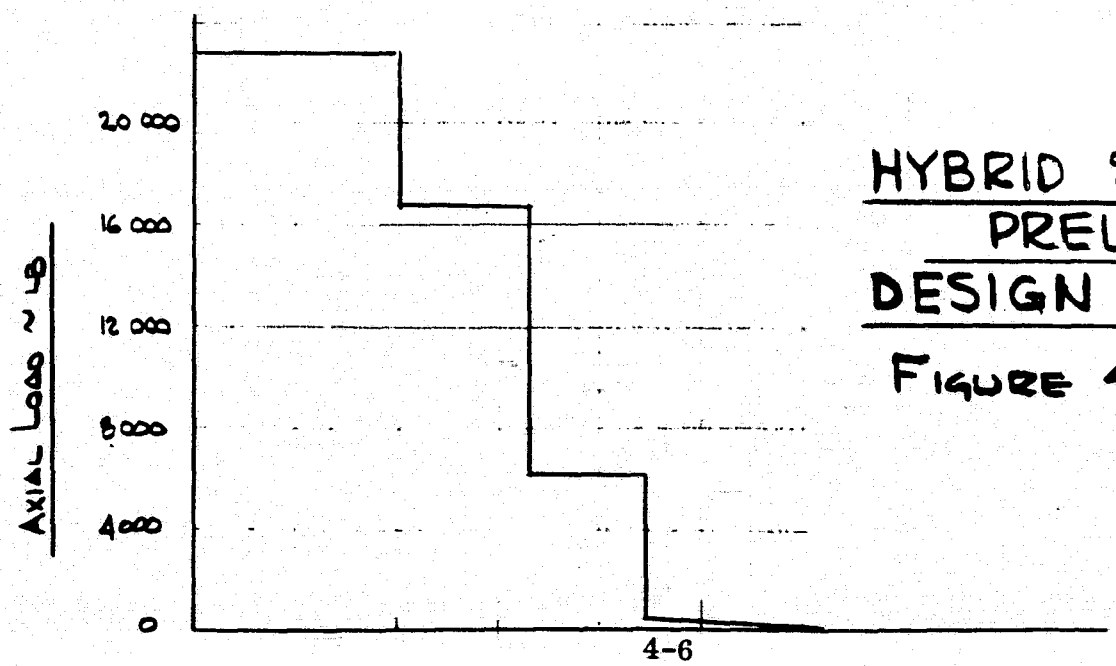
Table 4.2-1 Structural Subsystems - Design Conditions

Item	Design Environment
Solar Arrays	Orbital Dynamics
Module Structure	
Sides	Thermal Control
Tops and Bottoms	Strength
Bulkheads	Strength
Cylinder	Strength
Lower Frustum	Launch Dynamics









HYBRID SPACECRAFT
PRELIMINARY
DESIGN LOADS

FIGURE 4.2-1

attachments per array is to alleviate the loads on the solar array drive mechanism during the launch phase.

When stowed, there is approximately 0.5 inch clearance between the 0.75 inch honeycomb sandwich panels. If during lateral vibration two adjacent panels were to become "out of phase" with one another the 0.5 inch clearance is insufficient. The maximum panel deflection is 0.4 inch. To preclude slapping of adjacent panels, spacers of an elastomeric material, having a high damping capacity, are located midway along the 47 inch panel width at the top, middle, and bottom of the panel. For the normal occurrence when the 3 panels of an array are vibrating "in phase" analysis indicates the slight curvature of the panel, radius of curvature = 560 inches, causes no problem to the solar cells.

In the orbital configuration the loads are insignificant. The stiffness of the deployed array however, is very significant to the characteristics of the attitude control system. For preliminary work a design goal natural frequency of 0.5 cps was established as the minimum value which would preclude adverse coupling of the control system and flexible arrays. The stiffness of the honeycomb sandwich panel was therefore established by orbital requirements. The thickness of the panel was limited to approximately 0.75 inch by the stowed payload envelope, and the face sheets yielding the desired stiffness were calculated to be 8 mils in thickness.

4.2.3 MODULE

The module's interior and exterior primary structural panels have been conservatively designed to preclude buckling. This is considered desirable in order to obviate possible deleterious effects on the thermal paint applied to the panels. Further investigation need be made to substantiate this requirement. If buckling proves to be permissible, a conventional thin sheet metal design will be configured and a trade-off of cost and weight will be conducted for the two designs.

All panels, i.e., sides, top, bottom and interior bulkheads, are of aluminum honeycomb core sandwich configuration for minimum weight design to satisfy the buckling criteria. The side panels are 0.5 inch thick with .012 inch faces, predicated upon thermal considerations as heat pipes are submerged within the

panels. The face sheet thickness of the side panels is also required for thermal control (i. e., conduction between heat pipes). All other panels are 0. 25 inch thick with 0. 005 inch faces to satisfy the nonbuckling criteria. The resulting sandwich design shows high strength margins of safety. The analyses of the module structure are presented in Appendix A.

4. 2. 4 CYLINDER/FRUSTUM

The backbone of the structural system is the combined cylinder and frustum load path.

The structural design of the 28 inch diameter cylinder, located within the module, was based on a strength, buckling, criteria. The construction is . 040 aluminum alloy skin stiffened in the Z direction by 8 extruded angles. At the top and bottom of the cylinder are machined rings which allow the loads from the module and arrays to be introduced to the cylinder. The bottom cylinder ring also serves as an interface with the frustum. At the middle of the cylinder is a ring which serves as the attachment of the apogee motor to the spacecraft. The analyses of the combined lateral and thrust loads on the cylinder are presented in Appendix A.

The structural design of the 20 inch high frustum was dicated by launch dynamic requirements. In the launch configuration design goals of 25 cps laterally, and 40 cps longitudinally have been established as minimum values. The frustum has been designed as a 0. 25 inch thick sandwich structure to minimize weight. Face thicknesses of 0. 006 inch aluminum alloy are analytically sufficient to withstand the design loads. However, faces of 0. 014 inch are required to obtain desired spacecraft lateral natural frequency.

4. 2. 5 VHF ANTENNA

Although not considered primary structure an analysis was performed on the feasibility of stowing the VHF antenna. The helical antenna consists of a spiralled 0. 50 inch diameter 0. 020 wall aluminum tube and has a free length of 92 inch. When compressed to a packaging length of approximately 4. 5 inch, a torsional shear

stress of 13800 psi is developed. This is compared with an assumed allowable working shear stress of 20,000 psi. A force of 7.25 pounds is required to compress the antenna.

4.2.6 PRELIMINARY STRUCTURAL DYNAMICS

Based on previous Delta flight data, it is evident that if the fundamental lateral and longitudinal launch configured spacecraft frequencies exceed 25 cps and 40 cps respectively the vibratory environment to which the spacecraft is subjected will be lessened. These frequencies therefore were established as minimum design goals. Preliminary calculations indicate the lateral frequency to be 25 cps and the longitudinal to be 79 cps. The analyses are presented in Appendix A. In the orbital configuration the aforementioned 0.5 cps design goal for the solar arrays was established. A preliminary analysis of a "free-free" rigid module and flexible array is also presented in Appendix A.

4.3 MASS PROPERTIES

The three primary results of the mass properties study are as follows:

(1) the design is within the weight budget but with questionable growth margin suitable for preliminary design

(2) the proper spin-to-transverse inertia ratios for passive spin stability of the spacecraft is verified

(3) the feasibility of coincident centers of apogee engine burn, mass, and expendibles has been demonstrated.

The present payload weight is 626 lbs. within the allowable weight of 687.5 lbs. This however, represents only a 9.0 percent weight growth margin. Previous experience indicates this a high risk margin for preliminary design. (A 10% weight growth margin was stated as the systems guideline.)

The spin-to-transverse inertia ratios of the spacecraft in the stowed configuration as taken from Table 4.3-9 are, $I_{zz}/I_{xx} = 1.41$, and $I_{zz}/I_{yy} = 1.96$.

The coincidence of the three centers, apogee engine burn, mass, and expendibles is achieved by locating the propellant tanks as shown in Figure 4.1-3, and locating the module equipment, Table 4.3-8, such that its center of mass is 0.8 in. above the center of burn.

The location of module equipment also compensates for the eccentricity, off the z axis, of the L band antenna.

Table 4.3-1 presents an overall weight summary. Tables 4.3-2 through 4.3-8 present the detailed systems weight summaries. Table 4.3-9 presents the inertial and centers of mass breakdowns.

Table 4.3-1 Hybrid Spacecraft Weight Summary

Item		Weight (lbs.)
Power System	210.4	
TM and Command System	26.3	
Communication System	74.3	
Antenna System		
• L Band	5.0	
• VHF Band	8.0	
Attitude Control System	49.9	
Auxiliary Propulsion System	74.9	
Thermal Control System	15.0	
Electrical Distribution System	30.0	
Structural System	85.7	
Apogee Motor Inerts (burn-out)	46.4	
Weight Growth	61.6	
Total Payload		687.5
Apogee Motor Propellant*	614.5	
Separation Weight		1302.
Adapter (launch vehicle)	53.	
Gross Weight		1355.

*Includes 5.4 lbs. of low performance expendable inerts.

Table 4.3-2 Power System Weight Summary

Item		Weight (lbs.)
1. Battery	(2)	51.8
2. Battery Charge Regulator	(1)	3.0
3. Solar Array Paddle	(2)	103.6
4. Solar Array Orientation System	(2)	27.0
5. Battery Discharge Regulator	(2)	8.0
6. Voltage Limiter	(2)	6.0
7. Power Control Unit	(1)	11.0
Total Weight		210.4

Table 4.3-3 Telemetry and Command Weight Summary

Item	Weight (lbs.)
1. Command Receivers (2)	2.6
2. Command Decoder (2)	8.0
3. Command Regulator (2)	1.0
4. TM Multiplexer (2)	8.0
5. TM Switching Unit (1)	1.0
6. TM Transmitters (2)	0.8
7. Diplexers (2)	2.0
8. T & C Antenna Hybrid (1)	1.9
9. T & C Antenna Elements (4)	1.0
Total Weight	26.3

Table 4.3-4 Communication System Weight Summary

Item	Weight (lbs)	
1. Diplexer	1.7	
2. Pre-amplifier	0.5	
3. Down-Converter	1.8	
4. Up-Converter (5)	2.1	
5. PA Driver + Hybrid (5)	1.6	
5. Power Amplifier (5)	20.8	
		28.5
VHF		
1. Diplexer	1.5	
2. Pre-amplifier	0.5	
3. Up-Converter	0.2	
4. PA Driver + Hybrid	2.0	
5. Power Amplifier	20.8	
		25.0
C-Band		
1. Diplexer	1.0	
2. Pre-amplifier (2)	0.5	
3. Down-Converter	1.4	
4. Up-Converter (2)	1.8	
5. Power Amplifier (2)	0.5	
		5.2
IF Amplifier (3)	4.5	4.5
Synthesizer (2)	8.0	
Switches	1.5	
		9.5
IF Switching Matrix	1.6	1.6
Total		74.3

Table 4.3-5 Attitude Control System Weight Summary

Item	Weight (lbs)
1. Electronics	6.
2. Momentum Wheel	30.
3. Attitude Determination	11.
4. Passive Damper	2.9
Total	49.9

Table 4.3-6 Auxiliary Propulsion System Weight

Item	Weight (lbs)
1. Propellant Tanks (4) (11.5" dia)	9.2
2. Propellant	
Attitude Control	18.0
Orbit Control	32.6
3. Pressurant	1.0
4. Fill and Drain Valve (2)	.6
5. Pressure Transducers (2)	.6
6. Isolation Valve (4)	2.5
7. Thermocouple (2)	.1
8. Filter (2)	.8
9. Fitting and Lines	2.5
10. 0.5 #F Thruster and Valve Assembly (10)	5.5
11. 5.0 #F Thruster and Valve Assembly (2)	1.5
Total	74.9

Table 4.3-7 Structural System Weight Summary

Item	Weight (lbs)
1. Separation Ring	3.3
2. Lower Frustum	8.3
3. Module Support Ring - Lower	1.9
4. Module Support Ring - Upper	1.2
5. Apogee Motor Ring	3.7
6. Cylinder (Stiffened)	11.9
7. Module Structure (including solar array support structure)	55.4
Total	85.7

Table 4.3-8 Miscellaneous Weight Breakdowns

The following three tables are detailed breakdowns of items presented in previous tables and are not additive with the previous tables.

Item	Weight (lbs)
Module Structure Weight Summary (see Table 4.3-7)	
Sides	20.9
Top and Bottom Skins	9.8
Bulkhead Webs	3.9
Bulkhead Framing Members	2.5
Edging Members	6.3
Miscellaneous	6.0
Solar Array Retention Mech.	6.0
Total	55.4
Solar Array Weight Summary (see Table 4.3-2)	
Cell Stack	27.4
Thermal Paint	6.2
Structure	
Faces	24.5
Glueline	12.2
Core	19.9
Edging Members	6.6
Tubing, Fittings (Attachment Sect.)	5.0
Hinges	1.8
Total	103.6
Module Equipment Weight Summary (see Table 4.3-9)	
Attitude Control	49.9
Auxiliary Propulsion (less propellant and tanbs)	15.1
Power (less array & orientation mech.)	79.8
Communication	74.3
Thermal	15.0
Electrical Distribution	30.0
Telemetry and Command	26.3
Total	290.4

Table 4.3-9 Mass Properties Summary

Component		Wi (lb)	Zi (in)*	Ixxcg (slug ft^2)	Iyycg (slug ft^2)	Izzcg (slug ft^2)
1. Separation Ring		3.3	0.	.864	.864	.244
2. Lower Frustum		8.3	9.66	1.220	1.220	.483
3. Module Support Ring (Lwr)		1.9	20.27	.099	.099	.080
4. Module Support Ring (Upper)		1.2	44.27	.063	.063	.051
5. Cylinder		11.9	34.41	.381	.381	.505
6. Module Structure**		55.4	32.27	3.677	4.174	6.128
7. Module Equipment		290.4	33.07	21.068	16.352	48.886
8. Propellant and Tanks ***		---	---	---	---	---
• Post Separation		59.8	32.27	2.772	2.772	5.385
• Post Deployment		17.6	32.27	.940	.940	1.826
9. Apogee Motor Fuel****		614.5	32.27	9.569	9.569	9.720
10. Apogee Motor		46.4	27.25	2.368	2.368	.886
11. Solar Array		---	---	---	---	---
• Stowed		103.6	32.27	22.853	10.049	21.493
• Deployed***		103.6	32.27	446.256	5.702	438.696
12. Solar Array Drive		27.0	32.27	3.742	.063	3.727
13. L Band Antenna		---	---	---	---	---
• Stowed		5.0	49.27	.584	1.659	1.348
• Deployed		5.0	49.27	.292	3.559	3.540
14. VHF Band Antenna		---	---	---	---	---
• Stowed		8.0	54.77	.990	.990	.194
• Deployed		8.0	54.77	3.436	3.436	.194
15. Apogee Motor Ring		3.7	32.27	.044	.044	.089
Total	Post Separation****	1240.4	32.27	70.294	50.667	99.219
	Post Deployment	583.7	32.27	484.450	39.265	505.335

* Measured from separation plane

** Includes solar array retention mechanism

*** Cell surface normal to x axis

**** ΔW between post separation and post deployment is due to the expenditure of the 614.5 lbs of apogee motor propellant and 42.2 lbs. of hydrazine propellant for attitude and orbit control.

4.4 TEMPERATURE CONTROL SUBSYSTEM

4.4.1 SYSTEM DESCRIPTION

Temperature control for the Hybrid module is achieved by employing a system of louvers, heat pipes, super insulation, and thermal control coatings as shown in Figure 4.1-4. The louvers are mounted to honeycomb panels located on the north and south sides. By virtue of the square cross-section chosen for the equipment module, the north-south faces present large flat surfaces to which solar impingement is minimized. The bulk of the electronic components are mounted directly to the interior surface of the honeycomb. Heat pipes are embedded in the panel and they distribute the heat load over the entire face from which it is radiated directly to space.

With the exception ot the louvered and passive areas on the north-south faces, the entire equipment module is covered with super insulation. The insulation reduces the dependence on thermal coatings to a minimum and insures that the heat of the critical components will be directed through the louvers which provide a variable thermal resistance which is a function of temperature.

The equipment module is divided into two temperature control compartments or regions. The first, hereafter referred to as Region I, contains six square feet of thermal louvered area located on the north and south facing sides. The batteries and housekeeping equipment items are housed in this compartment. Thermal control is provided to maintain the temperature of the component mounting base plate between $0^{o}C$ and $10^{o}C$ for all orbit conditions.

Region II houses the communication equipment items. Temperature control is achieved by means of thermal coatings applied to the north and south facing sides. It is estimated that a temperature range between $10^{o}C$ to $40^{o}C$ may be maintained on the equipment mounting baseplate surface.

By thermally isolating the temperature sensitive components from those which are not critical with respect to temperature, it is possible to meet all thermal requirements. Further, in the case of the batteries, a relatively low temperature prolongs life. (The ability to accept a charge is diminished but the gain in life is more important.) It is for this reason that the temperature range of Region I is shifted downward and is narrow compared to Region II.

The structural mounting surface of a component shall normally be the heat dissipation surface. To minimize temperature gradients within the component, all parts which are high dissipators will be thermally coupled to this mounting surface (heat sink). The average component surface emittance shall be greater than 0.85.

The narrow temperature limits in Region I are realized by virtue of the louvers which control the radiative heat rejection resistance as a function of component temperature, and the fact that the heat losses or gains from the apogee motor and attendant structure are minimized because of the super insulation.

In general, the equipment items whose temperature is to be controlled are mounted directly to the north and south facing honeycomb panels or baseplates. This results in maximum heat rejection capability and minimizes the temperature gradient between a given electronic package and the thermally controlled surface. This is especially significant in the case of the thermal louvers which adjust their opening angle and therefore radiative heat rejection as a function of baseplate temperature and not necessarily component temperature.

The exterior (space-facing) surface of the component mounting baseplates are covered with an optical solar reflector (vapor deposited silver on fused silica) coating and sized to handle the upper limit of component dissipation at the maximum allowable operating temperature. For instance, louvers of six square feet active area will reject 140 watts at 50^{o}F (10^{o}C) when the spacecraft is orientated such that the solar direction is 30^{o} with respect to one of the louvered panels. This orientation only occurs during the solstice orbits but represents a maximum heating condition and dictates the hot case environment. In like manner, the cold case environment is predicated on an equinox orbit when no solar input occurs on the radiating surfaces.

The same considerations exist for the passive radiating surfaces assigned to Region II. For the tentative design value of 300 watts, 9.5 square feet of radiating surface is required during the worst case equinox orbit. In region II, thermal compensation is not aided by louvers and the decrease with temperature is relatively steep with decreasing power. When the minimum power level is fixed (perhaps from failure mode analyses), it may be desirable to incorporate some louvered area to assure a lower bound minimum temperature at reduced power dissipation levels.

By virtue of the temperature control louvers and thermal isolation from the apogee motor and housing, temperature control within Region I is relatively tight. Of course, the predictable range is a strong function of component heat dissipation variation and the heat leaks or gains to the region. The accuracy with which a detailed thermal model can be used to predict these heat leaks is a function of the complexity of the geometry. In the case of the apogee nozzle which is sunlit at a variable angle during approximately 12 hours out of each 24, the heating effect due to solar input is difficult to calculate with a high degree of accuracy. In addition, the average orbit solar input will be a function of the time of year; the difference between equinox and solstice orbits will be considerable. It is for this reason that the apogee motor and related support structure is thermally decoupled from Region I which contains the temperature sensitive equipment items.

Super insulation blankets are used to thermally isolate the equipment modules from space and to insure that component heat dissipation is directed to the north and south radiating panels. This is especially important in the case of Region I, which contains the louvers; the capability of the louvers to maintain narrow temperature limits depends on their capability to impose and vary heat rejection resistance over a large range and this can only be achieved if the heat transfer is such that the louvers cannot be bypassed. The thermal super insulation blankets consist of 30 sheets of 1/4 mil aluminized mylar. When the blanket is mounted to an exterior surface, an outer face sheet of 20 mil kapton is used. The kapton protects the blanket from the space environment, but more important, provides the optical values (absorptivity and emissitivity) which will maintain a surface temperature to help minimize net heat losses and gains through the blankets.

As shown in Figure 4.1-4, "C" shaped heat pipes are incorporated in the equipment mounting surfaces (honeycomb baseplates) of each region. The pipes are spaced approximately 4 inches apart in parallel planes. When used in this fashion the heat pipes serve to distribute component heat over the entire surface of the radiating panel and virtually eliminate temperature gradients so that the entire surface may be utilized for component mounting. The pipes minimize thermal problems associated with mounting high dissipators with small volume directly to the radiating plates.

4.4.1.1 Thermal Louvers

At a given point in its mission profile the various spacecraft components will be subjected to different degrees of heating caused by solar thermal radiation and internal power dissipation. The parameters which in most cases control the spacecraft heat rates are the solar absorptance factor (α) and the emittance factor (ϵ). The solar absorptance determines how much solar thermal radiation the spacecraft will absorb and the emittance regulates the amount of thermal energy radiated to space. The ratio α/ϵ controls the spacecraft's equilibrium temperature.

If the changes in internal power dissipation or external heat fluxes are severe, it is not possible to maintain the internal component temperatures within the allowable design temperature limits unless the α/ϵ ratio can be varied. A very popular and reliable method which effectively gives a variable α/ϵ ratio is through the use of thermal louvers. When the louver blades are open, the effective α/ϵ ratio is low (low α, high ϵ) and when the blades are closed, the effective α/ϵ ratio is high (low α, low ϵ). In effect, the louvers act as a "thermal valve" to regulate the flow of heat out of the spacecraft. This property, when properly utilized, provides an additional thermal design tool in that louvers reduce the dependence of the spacecraft on the value of optical coatings which have a tendency to degrade from their nominal values during a long-term mission.

Thermal louvers consist of a rigid, light weight polished aluminum frame which contains low-friction pivots for the louver blades. The blades are thin, highly polished, specular finish aluminum and are actuated by bimetallic sensors which are located in a housing thermally insulated from outside influences. The bimetallic sensors expand and cause the louver blades to open, thus allowing more heat to be radiated to space. The opening and closing temperatures of the blades are regulated by adjusting the bimetallic sensors. It should be noted that the louver blades are independently actuated (one bimetallic sensor per pair of louver blades) providing a redundant system. The typical louver has 10 or more pairs of blades so that in case of failure of one actuator, the overall system degradation is small. These louvers have been employed on many spacecraft and have proven to be a reliable temperature control system.

Thermal louvers recommended for Region I of the spacecraft are shown on Drawing 4.1-4. They are mounted directly to the north and south facing honeycomb panels.

4.4.1.2 Thermal Coatings

Solar reflector coatings ($\alpha/\epsilon \ll 1$) must be employed when the amount of solar energy input to the spacecraft surface must be minimized while as much thermal energy as possible is concurrently emitted. Thermal analyses of the Hybrid spacecraft have shown the desirability of covering the external surfaces of the north and south panels behind the louvers with such a coating.

The low α is desirable to minimize solar input when the sun strikes the north-south faces obliquely. A high ϵ is required to maximize heat rejection to space, thereby minimizing the louver area.

In selecting a solar reflector coating, both initial values of α and ϵ and any changes in these values during a mission lifetime are important. Most solar reflectors are subject to optical and/or physical degradation in the space environment, while others may be difficult to handle, apply, or maintain in the ground environment.

For long life missions in the range of 2 to 5 years, degradation of α can be large for all white paints. For this reason, the use of a second surface mirror coating system is recommended. Such a coating is vapor deposited silver on 8 mil thick fused silica called an Optical Solar Reflector (OSR). This coating exhibits little or no degradation in the space environment. It has been flown on Lunar Orbiter and OSO spacecrafts and has been extensively tested in the laboratory. The present design is predicated upon the use of OSR.

A secondary choice is the less costly series emittance coating system of silver-teflon. The series emittance thermal control coating consists of a transparent (to the solar spectrum) dielectric film over a highly reflecting metallic substrate. The reflectance of the metal primarily controls the solar absorptance; the thickness of the transparent film governs the emittance. This coating system has certain advantages over the OSR; however, it is still in the development stages.

4.4.1.3 Multilayer Insulation

The critical components in the Hybrid are to be thermally controlled through the use of louvers. In order to make full use of the temperature control derived by the use of radiating windows and thermal louvers, all heat rejected should pass through these areas. In practical applications this requirement can only be approached through the use of insulation systems.

The most efficient and reliable thermal insulation concept yet found for spacecraft applications is the multilayer system. This insulation represents at least an order of magnitude reduction in thermal conductivity over all other insulating systems, and is the most efficient insulation on a weight to thermal resistance basis. These multilayer insulations are composed of a large number of very thin layers of material having a high infrared reflectance separated by either continuous or discontinuous layers of a very low conductance material, or by physically deforming the reflective layers so as to provide effective separation of adjacent layers with a minimum of contact conductance. The reflective layers are usually a very thin (1/4 mil) film of plastic such as Mylar or Kapton supporting a vacuum-deposited layer of aluminum, silver or gold. A variety of spacer materials such as silk or nylon netting foam and organic or glass fibers have been used for both aerospace and commercial application. Integral spacers have been developed by such methods as crinkling or dimpling the metalized films, or by bonding small areas of fibers to one surface of the reflective sheet.

The advantages of using this multilayer insulation on the equipment module are summarized in the following list:

1. Minimizes uncontrolled heat rejection.
2. Reduces the solar flux input.
3. Reduces the antenna and solar array reflected solar flux input.
4. Provides large thermal time constant during occult.
5. Most efficient insulation on a weight to thermal resistance basis.

4.4.1.4 Heat Pipes

A heat pipe is a device which exhibits very high effective thermal conductance per unit weight. The device consists of a container tube, a wicking structure in contact with the inside diameter of the tube and a working fluid. In operation, heat is supplied at one end of the pipe, causing evaporation of the working fluid. This vapor then flows to the other end of the pipe where heat is removed, causing the vapor to condense. The condensate is returned to the heat source region by the capillary action of the wicking structure, thus provising closed cycle performance.

Heat pipes may be classified as to their purpose or end use in the thermal control system. If high heat transport is required, then the heat pipe design is optimized to provide high conductance at a low weight. In some instances, however, it may be desirable to design some of the heat pipes such that they exhibit nearly isothermal performance over a wide power range. Such performance characteristics may be required in order to prevent distortion of critical structural elements of the spacecraft due to thermal expansion. Isothermal heat pipes are designed by providing reseservoirs of noncondensible gases suitably connected to the condenser sections of the pipes. As the input power to the evaporator is varied, the amount of gas in the condenser changes, varying the effective condenser area and thereby providing nearly uniform temperature operation.

Annular wicks composed of wire screen or porous or sintered metal have been used. Longitudinal grooves cut in the I. D. of the container tube can also serve to provide the necessary capillary pumping pressure. However, doubt exists concerning the applicability of 1-g testing of this type of heat pipe. The most efficient state-of-the-art design is currently the artery type wick. This design consists of a thin wire screen annulus to which is connected a small diameter artery near the center of the heat pipe. Since the annulus is thin, the thermal resistances encountered in transferring heat into and out of the pipe are minimized. The bulk of the condensate return is via the artery. Owing to the larger flow area the frictional drag is reduced. This, in turn, allows the heat pipe to operate at higher power levels without encountering burnout or nucleate boiling.

4.4.2 ANALYSIS

4.4.2.1 Thermal Control of Module Equipment

The initial thermal design of the Hybrid satellite module indicates that it is feasible to control the temperature of all components within acceptable limits. The two basic temperature criteria which dictate the design are that the batteries must be maintained at $41^{o}F \pm 9^{o}F$ ($5^{o}C \pm 5^{o}C$) and that the hydrazine subsystem temperature must not go below $41^{o}F$ ($5^{o}C$). These conditions are met by placing the batteries with other housekeeping components in the louvered compartments and by assuring a good thermal path between the passively controlled equipment such as the TWT's and the hydrazine bottles.

The thermal analysis consisted of evaluating the average temperatures of the louvered compartment (Region I) and the passively controlled compartment (Region II). The utilization of the heat pipes on the module skin on which the components are mounted insures uniform distribution of the heat generated internal to the module as well as the impinging solar energy. Hence, an average temperature is determined rather than temperature maps. As the program progresses and finalized design information becomes available, more definite conclusions will be obtained for the thermal gradients in the system.

The assumptions made in the analysis refer mainly to the performance of the louvers, heat pipes, passive coatings and super insulation. The effective emittance of the louvers was taken to vary with blade angle as shown in Figure 4.4-1. The curves shown are based on the total area of the louvers which include the frame as well as the actuator housing. The negative values of F_{ϵ} for the sunside at 10^{o} or smaller opening blade angle indicate that heat is flowing into the system. The curves were generated based on employing an optical solar reflector (OSR) with $\alpha/\epsilon = 0.2/0.85$ behind the louvers on the surfaces where the components are mounted. The passive area which controls the temperature of Region II is also assumed to have $\alpha/\epsilon = 0.2/0.85$.

The leakage through the super insulation as a function of the average internal temperature is shown in Figure 4.4-2. Since it is expected that the temperatures

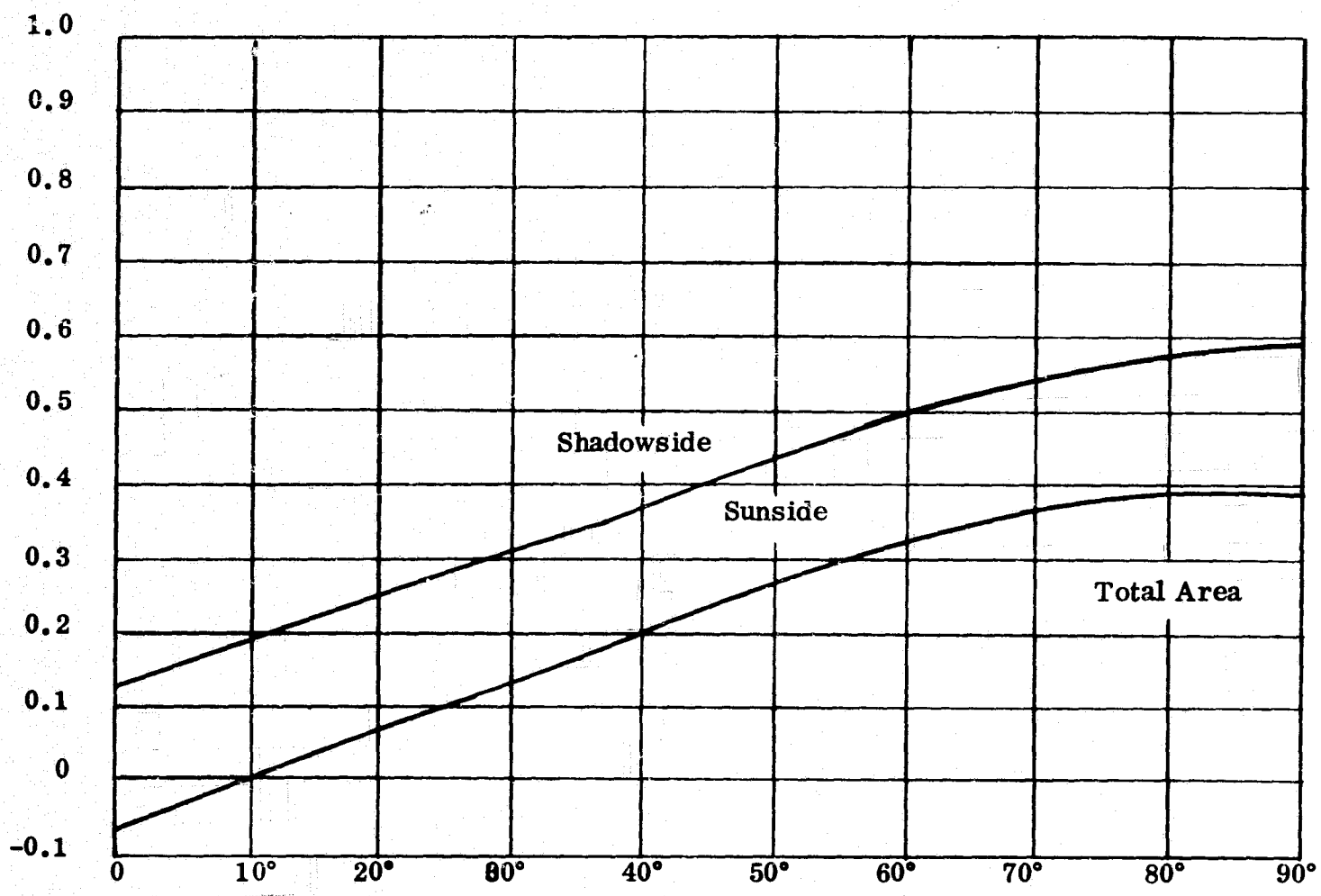


Figure 4.4-1 . Louver Effective Emissivity vs. Blade Opening Angle

of the two regions will not be radically different, Figure 4.4-2 was utilized in the analysis by taking the leakage to correspond to the arithmetic average of the temperatures of the regions. The effective emittance between the components and the inner surface of the super insulation was taken as 0.02 and the effective emittance of the blankets was assumed to be 0.01. The external temperature of the Kapton cover (α/ϵ = 0.4/0.8) was based on orbital flux averages. The high resistance and time constant of super insulation blankets allow for such simplifications.

The analysis did not include the thermal effects of the mounting structure, the VHF housing, ground plane and antenna. All these items will be thermally controlled by passive means so that their temperature will be of the same order as that inside the module in order to reduce the energy interchange with the module. The influence of the solar panels was included in terms of a wattage input to the thermal control surfaces. A conservative value of 140°F (60°C) was considered for the temperature of the panel, and the module was assumed at 50°F (10°C). It was estimated that a conservative but realistic IR input would be 40 watts to the louvered compartment when the louvers are open and some 50 watts to the passively controlled compartment. These values were incorporated in the analysis for "hot case" evaluation. The input was not considered during "cold case" operation.

Figure 4.4-3 gives the average temperature of the louvered compartment as a function of internal dissipation. Figure 4.4-4 shows the temperature of the passively controlled region. The upper lines in these figures correspond to a "hot case" evaluation when the spacecraft is orbiting during winter or summer solstice with a worst case 6.5° off-north tilt due to orbit inclination and attitude control errors. (See Figure 4.4-5) These curves also reflect the IR input from the solar panels.

4.4.2.2 Solar Panels

The most effective thermal design for the solar panels would be one that incorporates a coating of high emittance on the back surface in order to minimize the temperature at which the solar cell operates. Since the orbit considered is synchronous and albedo effects are negligible, the coating chosen was 3M black with an emissivity higher than 0.85. The panel honeycomb thickness was dictated by structural

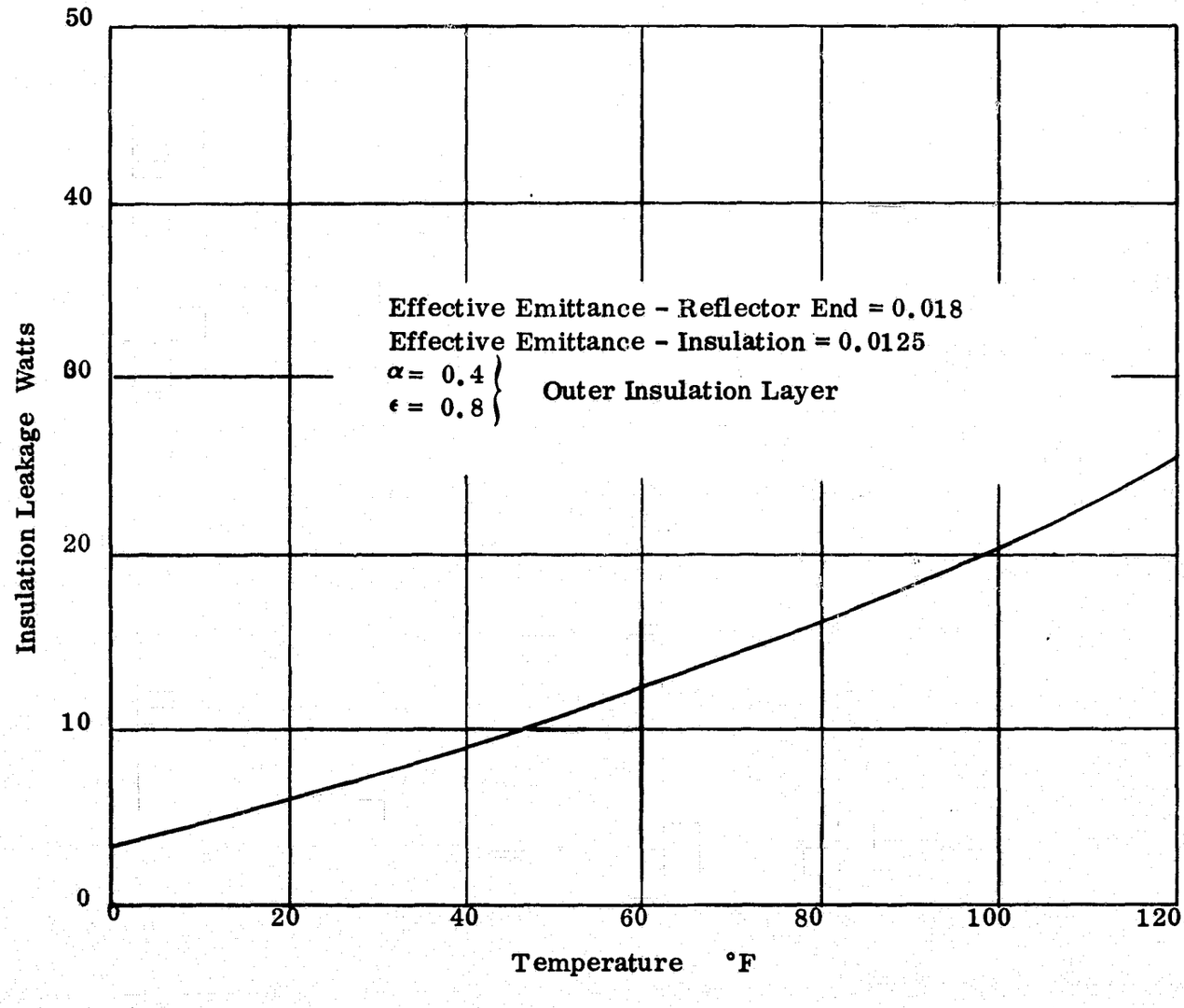


Figure 4.4-2 Orbital Insulation Heat Leakage vs. Average Regions Temperature

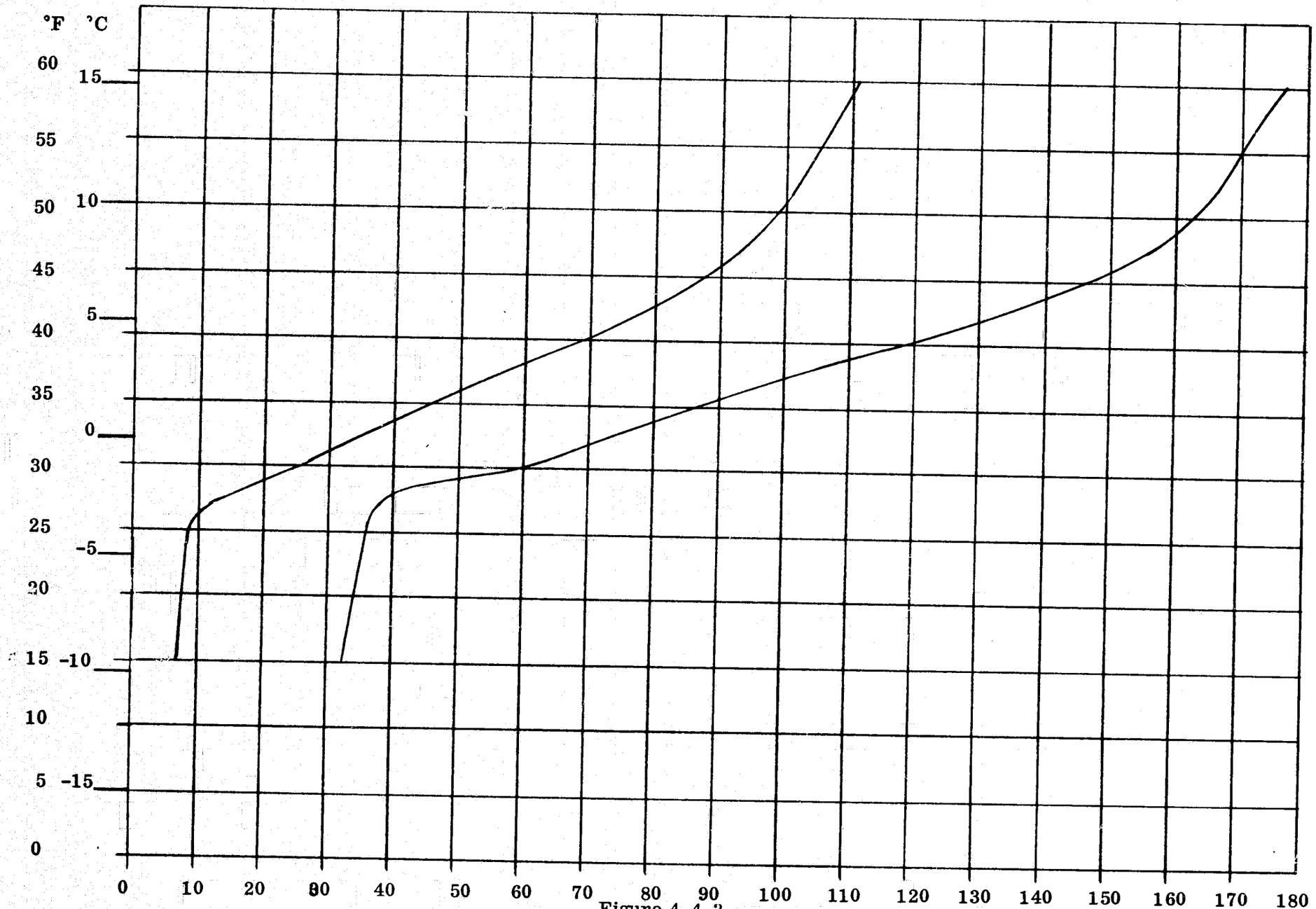


Figure 4.4-3

Active Module Temperature

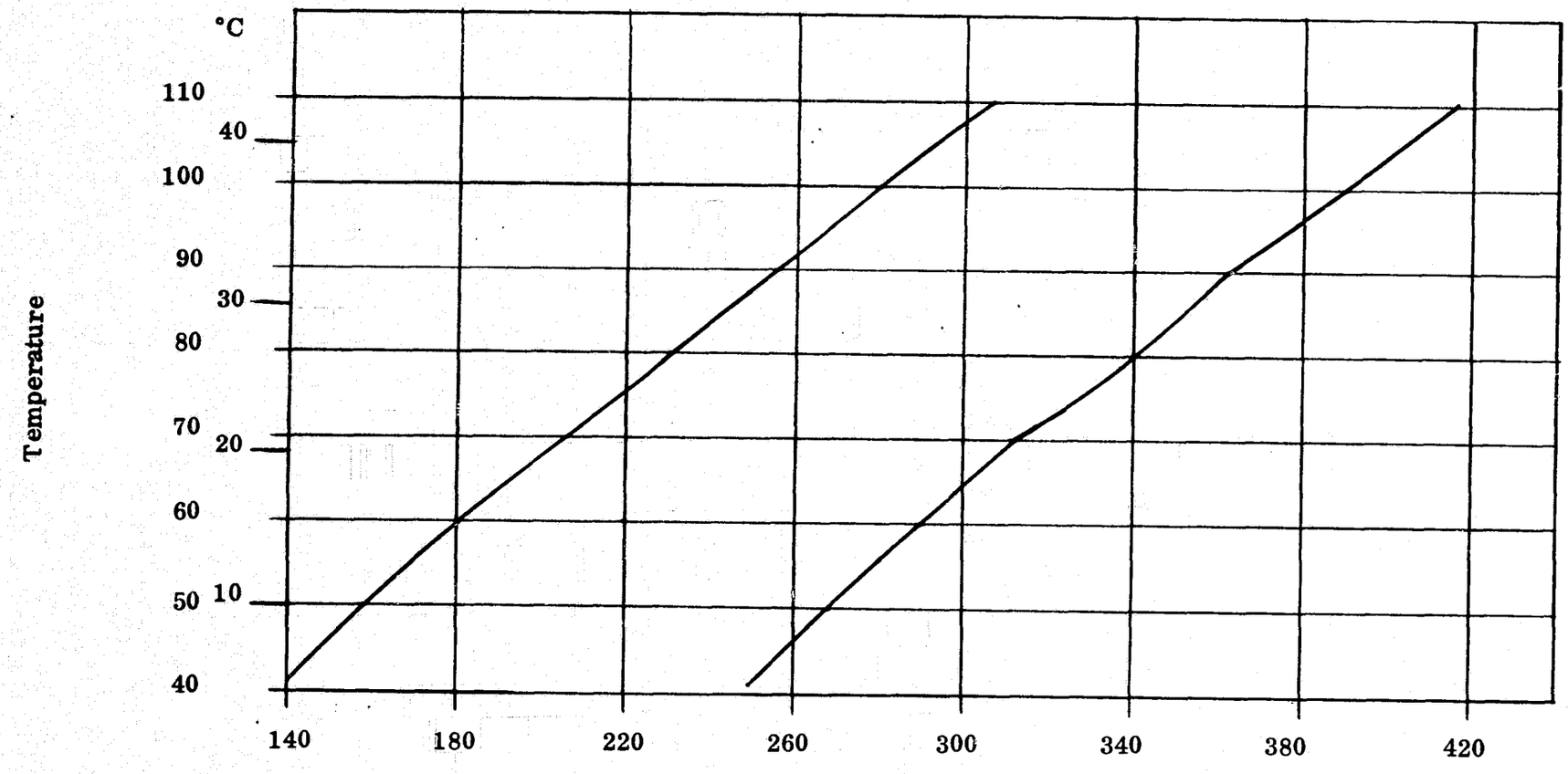


Figure 4.4-4

Passive Module Temperature

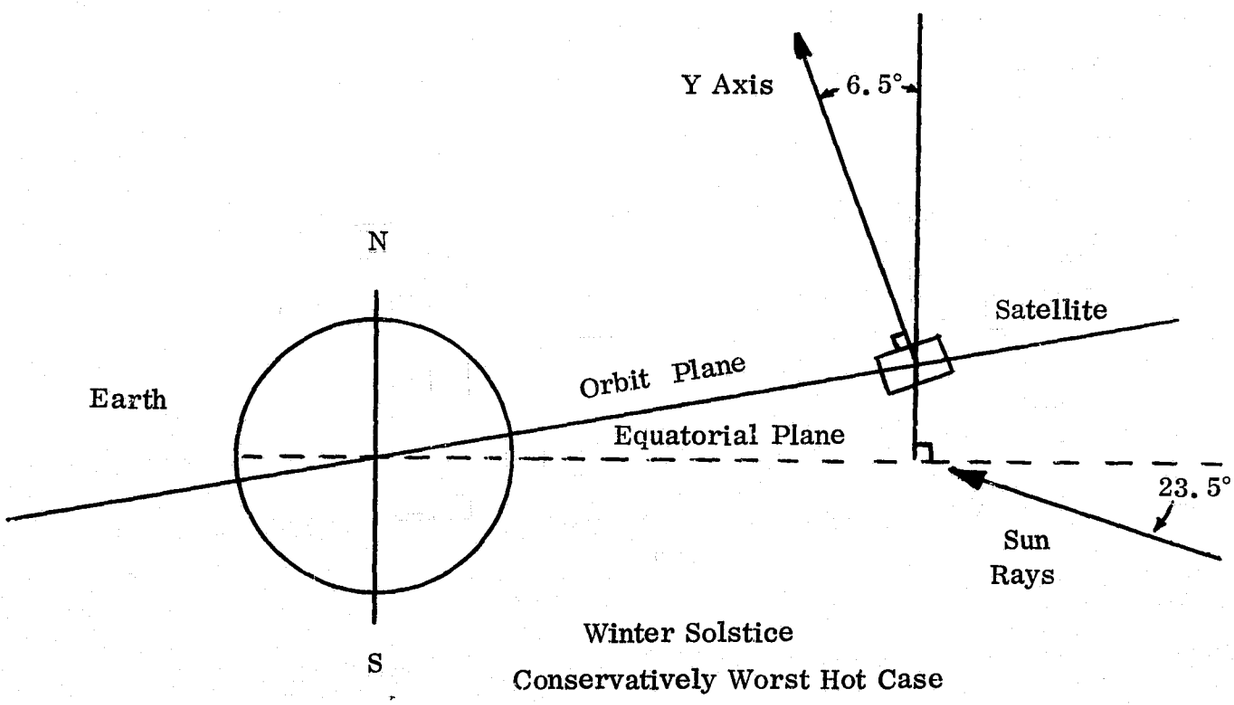


Figure 4.4-5 INCIDENT SOLAR ANGLE AT SOLSTICE

considerations to be 0.75 inch. Although a reduced thickness would be essential to low thermal gradients across the panel, the gradients realized in the present panel design are about $4^{o}F$ and are tolerable.

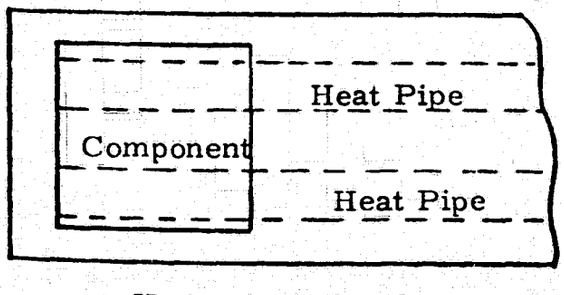
The results of the analysis of the panels are presented in Figure 4.4-6 which shows the solar cell temperature (based on $\alpha/\epsilon = 0.68/0.85$) and the gradient across the panel as a function of emittance of the back surface. The solar flux was conservatively assumed to be 468 Btu/hr ft^2.

4.4.2.3 Heat Pipe Spacing

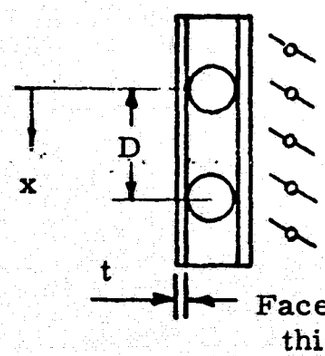
A major goal in the thermal design will be to evenly distribute the power dissipation throughout the system in order to minimize the temperature gradients. The tolerances will dictate the number of heat pipes to be used and the lay-out configuration.

Important areas of investigation are heat pipes spacing and the transfer of heat from a dissipating component across the interface which connects to a heat pipe. Experience on the ATS program has shown that the bulk of the gradient occurs across such interfaces. In pursuing an optimum design, the heat pipes will be located with respect to the components in such a way as to balance the power output as well as insure heat sharing between surfaces exposed to environmental fluxes and purely radiating surfaces. The complete analysis will be based on a multi-node mathematical model which will include the radiative resistance of the louvers as a function of heat sink temperature and incident solar angle.

The approach to be used in evaluating the incorporation of heat pipes in the system may be illustrated by the following analysis which pertains to the temperature distribution between two constant temperature heat pipes imbedded in a honeycomb panel to which a louver assembly is attached. The configuration is shown below.



Honeycomb Panel



Thermal Louver Blades

Face sheet thickness

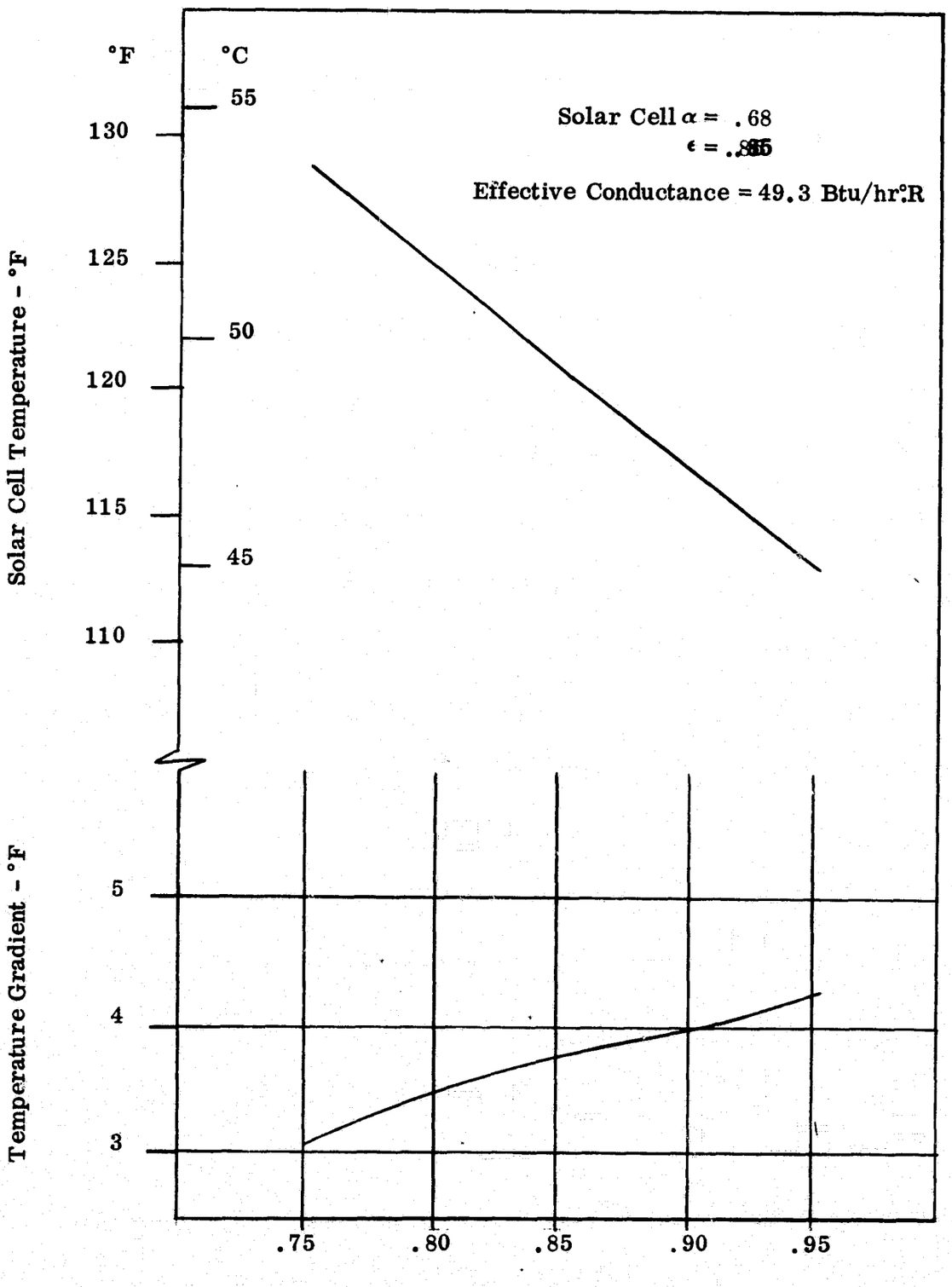


Figure 4.4-6

Solar Cell Temperature and Gradient Across Panel
versus
Emissivity of Back Facesheet

Due to the symmetry, it is necessary to consider only the values of x between 0 and D/2. An energy balance on an element Δx wide located at a distance x from the heat pipe is shown in Figure (B).

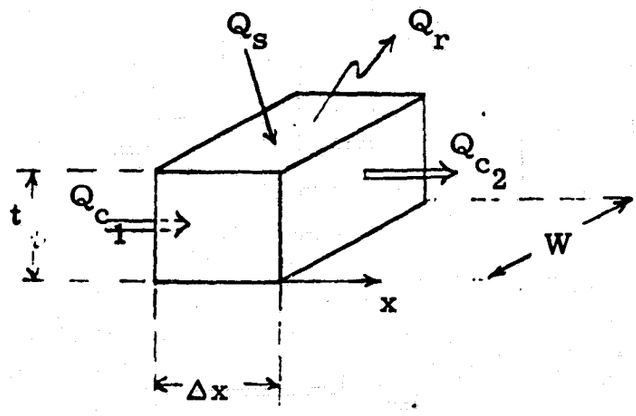


Figure (B) Energy Balance

The corresponding steady-state heat balance equation is:

$$Q_s - Q_r + Q_{c1} - Q_{c2} = 0 \qquad (1)$$

or

$$Q_s w\Delta x - \epsilon_c \; w\Delta x \; \sigma T^4 + ktw \left.\frac{dT}{dx}\right|_{x} - ktw \left.\frac{dT}{dx}\right|_{x+\Delta x} = 0 \qquad (2)$$

where:

Q_s = solar input per unit area to louver assembly when louver skin is inclined to sun

w = width of the panel to which louver is attached

Q_r = heat radiated from the louvered skin = $w\Delta x \; \epsilon_c \; \sigma T^4$

ϵ_c = effective emissivity of the louver array

σ = Stephan - Boltzmann constant

T = Temperature at location x

Q_{c1} = heat transfer by conduction into the element at x

$$ktw \left.\frac{dT}{dx}\right|_{x}$$

k = thermal conductivity of louvered skin

t = skin thickness

Q_{c2} = heat transfer by conduction out of the element at at $x + \Delta x$

$$ktw \left.\frac{dT}{dx}\right|_{x + \Delta x}$$

In the limit as Δx approaches zero, equation (2) may be written

$$Q_s = \epsilon_c \sigma T^4 + kt \frac{d^2 T}{dx^2} = 0 \qquad (3)$$

Equation (3) is a nonlinear second-order differential equation. The following linearization is introduced:

Let $$T = T_m (1 + \eta), \quad \eta << 1 . \qquad (4)$$

where

T_m is the mean temperature of the heat pipe.

Then $$T^4 = T_m^4 (1 + 4\eta + 6\eta^2 + 4\eta^3 + \eta^4) \approx T_m^4 (1 + 4\eta) \qquad (5)$$

To further simplify the form of the equation, let

$$\eta = \tau - 1/4$$

Then equation (4) becomes:

$$T = T_m (\tau + 3/4),$$
$$T^4 \approx 4T^4_m \tau \qquad (6)$$

and $$\frac{d^2 T}{dx^2} = T_m \frac{d^2 \tau}{dx^2}$$

The linearization form of equation (3) is

$$ktT_m \frac{d^2 \tau}{dx^2} - 4\epsilon_c \sigma T_m^4 \tau = -Q_s$$

$$\frac{d^2 \tau}{dx^2} - b\tau = -a \qquad (7)$$

Where $$a = \frac{Q_s}{ktT_m} \qquad b = \frac{4 \sigma \epsilon_c T_m^3}{kt}$$

Equation (7) is a linear second order differential equation. Boundary conditions in terms of temperature are derived from the fact that there is no conductive heat exchange at the mid-point between the two pipes and that the temperature at the heat pipe location (x = 0) is equal to T_m. In terms of τ, the boundary conditions are:

$$\left.\frac{d\tau}{dx}\right|_{x=\frac{D}{2}} = 0 \qquad (8)$$

$$\tau \Big|_{x=0} = 1/4 \qquad (9)$$

The solution of equation (7) is

$$\tau = \frac{a}{b} + C_1 e^{x\sqrt{b}} + C_2 e^{-x\sqrt{b}} \qquad (10)$$

Using equations (8) and (9), the constant of integration can be obatined and equation (10) becomes:

$$\tau = \frac{a}{b} + (1/4 - a/b)\left(\cosh x\sqrt{b} - \tanh \frac{D\sqrt{b}}{2} \sinh x\sqrt{b}\right) \qquad (11)$$

Equation (6) is used to relate τ to T and (11) may be written:

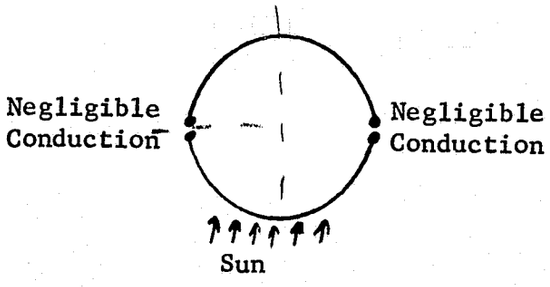
$$T = T_m \left[3/4 + a/b + \left(\cosh\sqrt{b}\, x - \tanh \frac{D\sqrt{b}}{2} \sinh x\sqrt{b}\right)\right] \qquad (12)$$

The above equation was solved using the Com-Share computer. The fin thickness t was taken as 0.030 inches corresponding to two 0.015 inch thick honeycomb face sheets. The louvers emittance was taken as 0.9. An effective emittance of 0.9 corresponds to a maximum gradient case and may be theoretically approached for open louvers in the absence of solar input. Results based on a mean heat pipe temperature of 104°F (40°C) show that a mid-point temperature decrease of 6°F will not be exceeded.

4.4.2.4 Temperature and Distortions of Tubular VHF Antenna

The thermal control of the tubular extendible VHF antenna consists of maintaining the temperature within reasonable values so that the structural integrity

of the element is not impaired during long-time mission, and confining the temperature gradients to as low a value as possible in order to eliminate the associated thermal deflections. Since the element is of the HINGELOCK type, perforation is necessary to reduce the severe gradients that could develop under the condition of the solar rays being normal to the line joining the points where interlocking tabs are employed as shown in the sketch. The gradients are theoretically eliminated when the percentage of the element surface which is perforated, x, obeys the condition $x = \frac{\alpha_o}{\alpha_i}$



Worst Case Gradients

where α_o and α_i are the external and internal solar absorptance, respectively. In order to maintain the perforated area a minimal, $_o$ must be as low as possible, whereas α_i must be high. These conditions are achieved by silverplating the external surface and coating the inner surface with black paint. Thus $\alpha_o = 0.10$ and $\alpha_i = 0.9$ leading to a required 11% surface perforation. The average temperature of the element will be 235°F (113°C).

Perforation of the helix tubular element may also be necessary. The percentage of perforation will be less than 11% since the helix element is seamless. This small amount of perforation will not be detrimental to the antenna characteristics.

4.5 ATTITUDE AND ORBIT CONTROL

4.5.1 MISSION SEQUENCE, OPERATION AND REQUIREMENTS SUMMARY FOR CONTROL

The launch vehicle is assumed to be the DSV-3L/ID(N_2O_4)/TE 364-4 Delta with 9 strap-on Castor solids and the large 84-inch diameter fairing. A candidate ascent trajectory consists of a near East launch from ETR, into essentially a 100 n. mi. parking orbit, and injection at the first equatorial crossing into a 28.5-degree inclined transfer orbit to synchronous altitude. Injection into the desired synchronous, near equatorial, circular orbit occurs at second apogee at about 53° West longitude some 16.9 hours after lift off. Alternatively, injection into the transfer orbit can be effected at the second equatorial crossing in the parking orbit. Injection at first apogee of the transfer orbit some 6.4 hours after lift off also yields a favorable longitude injection station of about 90° West. This ascent trajectory provides less time in the transfer orbit for ground determination of the proper attitude and timing for the apogee injection maneuver, however.

The subject launch vehicle can inject a total payload of 1355 pounds into the indicated transfer orbit when the large fairing is used. A spacecraft aft adaptor which remains with the launch vehicle represents 53 pounds of this weight.

The spacecraft will be separated from the spinning (70-90 rpm) third stage of the Delta while in the attitude required for the transfer orbit injection maneuver. A partial spin down from 90 rpm to about 45 rpm about the z axis will then be effected (to reduce subsequent precession control propellant requirements), using an outward-firing jet couple located at the corners on the $\pm$ x sides of the spacecraft near the plane of the spacecraft CG (Figure 4.5-1). Thereafter, passive spin stabilization will be used for attitude control during the transfer orbit and during the synchronous orbit injection and initial correction maneuvers.

An approximate 127-degree yaw precession (for first or second apogee injection) of the separated, spinning spacecraft about an axis parallel to the line of apsides of the transfer orbit is next accomplished by ground command to orient it as required for the apogee injection maneuver. Asymmetric pulsing of one thruster from

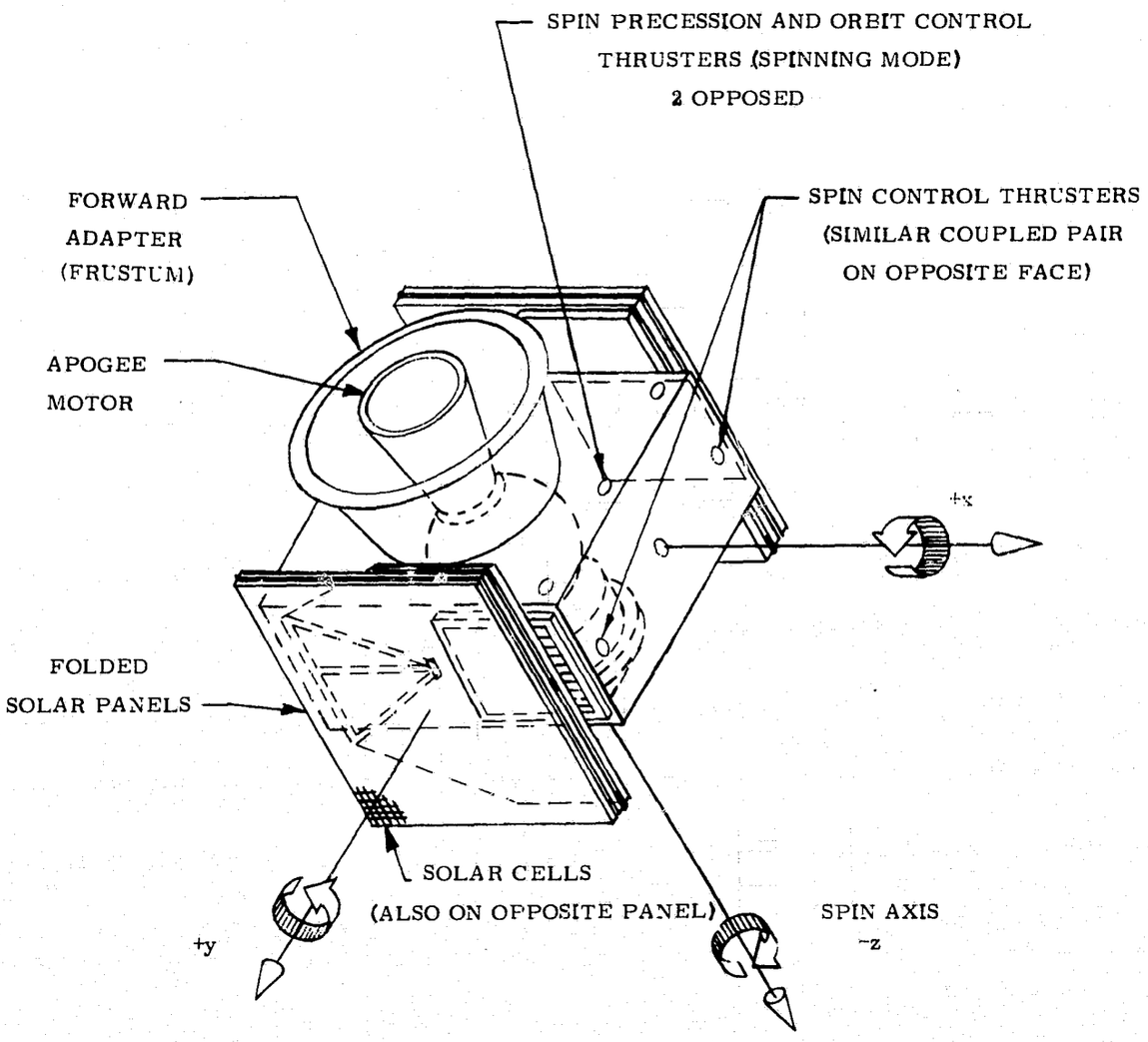


FIGURE 4.5-1 HYBRID CONFIGURATION (STOWED)

the central pair of the diametrically opposed, spin precession thrusters with thrust axes parallel to the spin axis will be used for this purpose (Figure 4.5-1).

The apogee injection stage must provide a velocity impulse of about 6030 ft/sec to accomplish the indicated apogee maneuver. Following injection into the synchronous near-equatorial orbit and identification of any existing period/eccentricity injection errors, initial orbit correction maneuvers can be accomplished. By thus making the indicated initial period and eccentricity correction maneuvers (coordinated so as to reduce the required velocity impulse) as soon as possible while still spinning, unwanted satellite eastward/westward drifts relative to the earth can be minimized.

Because of the associated large velocity impulse requirement, provision has not been made for orbit control propellant to provide North-South station-keeping against inclination perturbations for the planned 3-5 year mission. However, a demonstration of this capability for a limited period of time can be effected. Correction of the expected small initial inclination errors is thus not warranted (a relatively large velocity impulse would also be required). An initial inclination bias of several degrees can probably be used to center the inclination "drift" changes about a near zero value.

The indicated "spin axis" precession control thrusters can be employed for the ground based orbit correction maneuvers, using asymmetric thrusting of one thruster to precess the spinning spacecraft to the proper orientation and symmetric thrusting of the pair of diametrically opposed thrusters to provide the required corrective velocity impulse. Propellant requirements have been sized to cover a full 360-degree precession maneuver and a corrective velocity impulse of 300 ft/sec. This impulse is a very conservative value compared to the expected in-plane injection errors.

Orbit corrections could also be provided during the spinning mode by appropriately pulsing the central radial-firing thruster mounted on the +x side of the spacecraft (Figure 4.5-1). Associated disturbance torques would be acceptably small since the thrust vector of this jet can be closely aligned with the spacecraft CG for both the stowed and deployed configurations.

Orbit corrections can be made following deployment and acquisition of the earth-referenced attitude using these same jets. These thrusters are also used for East-West stationkeeping and station relocation maneuvers as later discussed.

Following initial synchronous orbit correction maneuvers, the spacecraft will be despun using the previously indicated jet couple located near the corners of the $\pm x$ sides. The solar panels will next be unfolded. Three-axis jet torqueing will then be provided by means of the thrusters aligned with the original spin (z) axis and the jets on the corners of the $\pm x$ sides (for torqueing about this z axis) as shown in Figure 4.5-2. These thrusters are used for ground command acquisition of the reference earth-oriented attitude which is shown in Figure 4.5-3. This reference orientation consists of the +y (pitch) axis of the satellite normal to the orbit plane, nominally parallel to the earth's south pole for an equatorial orbit; the +x (roll) axis in the orbit plane and perpendicular to the y axis, nominally pointed East along the direction of motion for a circular orbit; and the +z (yaw) initial spin axis directed towards the center of the earth along the local vertical. The solar panels are driven about the y axis so as to be normal to the projected sunline in the orbit plane.

Further clarification of the relationship of the satellite body axis frame (x y z) and the earth-oriented, orbital reference frame (X_E, Y_E, Z_E) to which it is desired to align the body axes is given by Figure 4.5-4. Roll, pitch and yaw angle errors are depicted therein, representing Euler angle deviations of the body frame from the reference frame.

It was noted that the spacecraft layout will be planned so that the plane of the jets mounted on the $\pm x$ sides will closely coincide with the CG of the stowed, fully-loaded and of the deployed, apogee-motor-expended spacecraft. Further, the drive axis for the solar panels will be located very close to the deployed spacecraft CG. This will minimize the solar pressure disturbance torques acting on the spacecraft. Periodically varying torques about the y axis will be produced by the varying solar aspect of the earth-tracking satellite body. An essentially inertially-fixed bias torque will be caused by a CP-CG deviation along the y axis. This torque can be increased (or decreased) at solstice conditions due to a bias torque introduced by the sun illuminated top or bottom of the spacecraft.

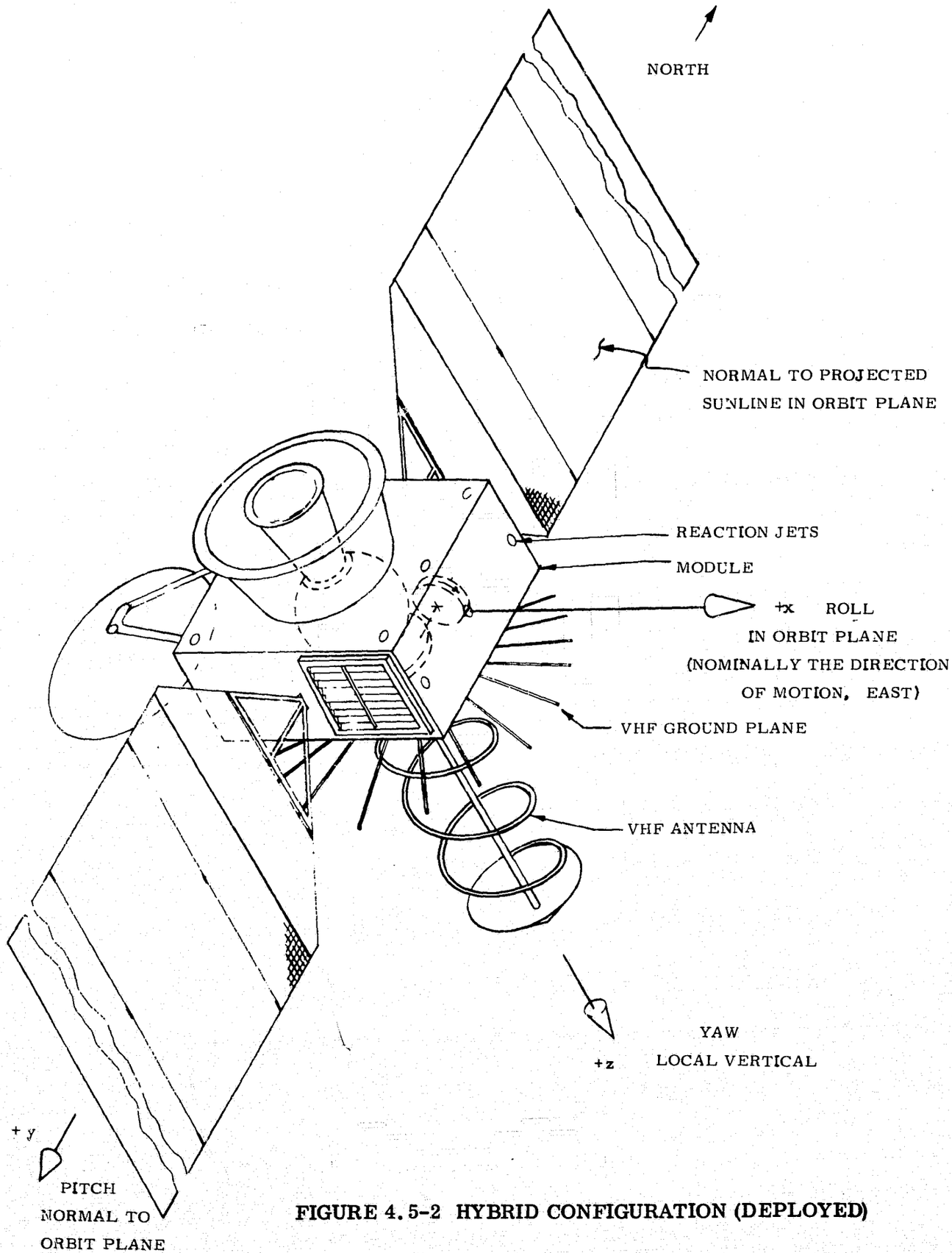


FIGURE 4.5-2 HYBRID CONFIGURATION (DEPLOYED)

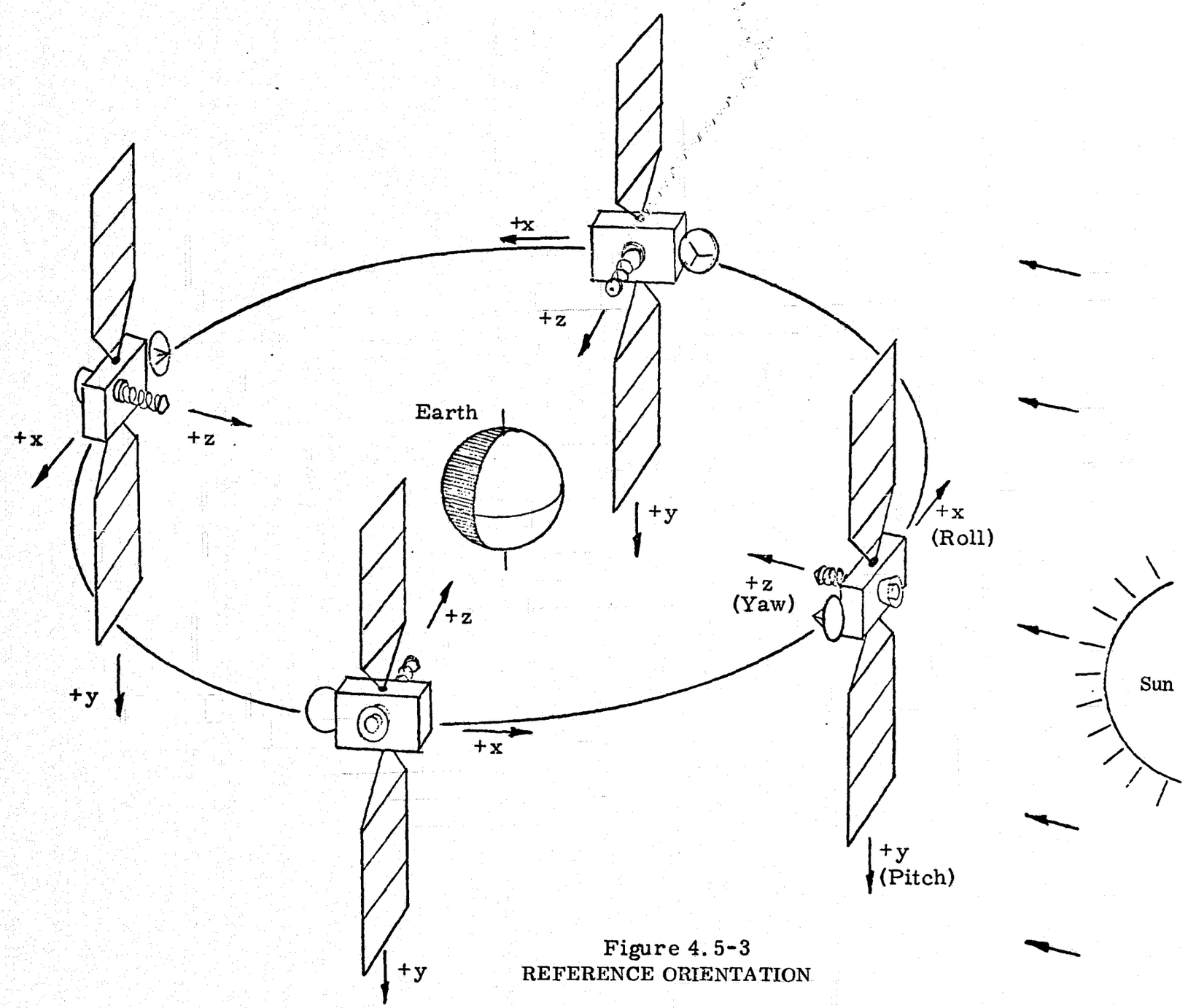


Figure 4.5-3
REFERENCE ORIENTATION

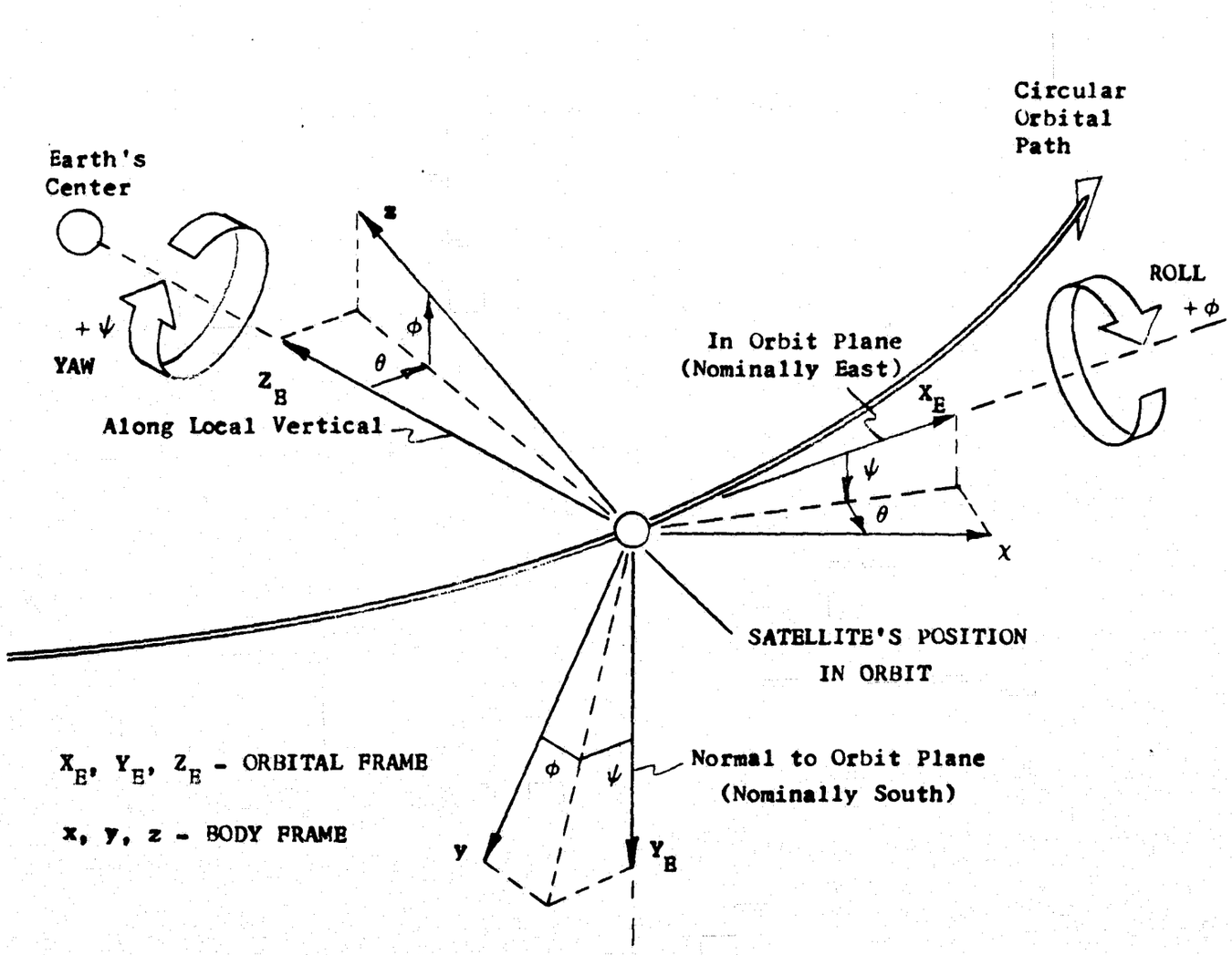


FIGURE 4.5-4 VEHICLE CENTERED ORBITAL AND BODY REFERENCE FRAMES

Following acquisition of the earth-referenced orientation, the momentum wheel aligned with the y axis will be accelerated to its bias speed. The jet thrusters will be used to counter the associated reaction torque on the spacecraft. The normal operational control mode designed to maintain the reference orientation can then be initiated.

An attitude and orbit control approach for the operational control mode has been tentatively selected based on the objectives of meeting performance requirements with the highest reliability and within acceptable ground command/control requirements for an operational satellite system. This philosophy has led to the design approach that the attitude and orbit control jets are only to be fired by ground command, for any control mode. Further, many of the attitude control and all of the orbit control functions have been assigned to the ground command/control station, thereby minimizing the complexity of the on-board controller.

With the conceptual control approach under consideration, it should not be necessary for the ground station to initiate jet commands for attitude corrective maneuvers any more often than every 1-2 days, and far less often for orbit corrective maneuvers. Hence, the associated command/control functions (including communications and ground computation) represent reasonable requirements for an ultimate operational spacecraft system.

Figures 4.5-2, 4.5-3, 4.5-4 and 4.5-5 provide an indication as to the attitude control approach envisioned for the normal operational mode. As previously stated, it is desired to have the z (yaw) axis of the satellite track the local vertical and the y (pitch) axis remain normal to the orbit plane. The solar panels are to be driven around the y axis so as to be normal to the projected sun line in the orbit plane. It is noted that the expected orbit inclination variations of the spacecraft (up to ± 2 degrees over its 5-year mission) will introduce a figure "8" pattern into its z-axis ground aim point, with latitude excursion equal to the inclination angle.

A near-constant-speed pitch momentum wheel (spin vector along the +y axis) will be used to provide a natural gyroscopic stability of the satellite about its x/z (roll/yaw) axes in the orbit plane. The major requirement for this gyro stiffness is that it must stabilize against the dominant solar pressure disturbance torques to a

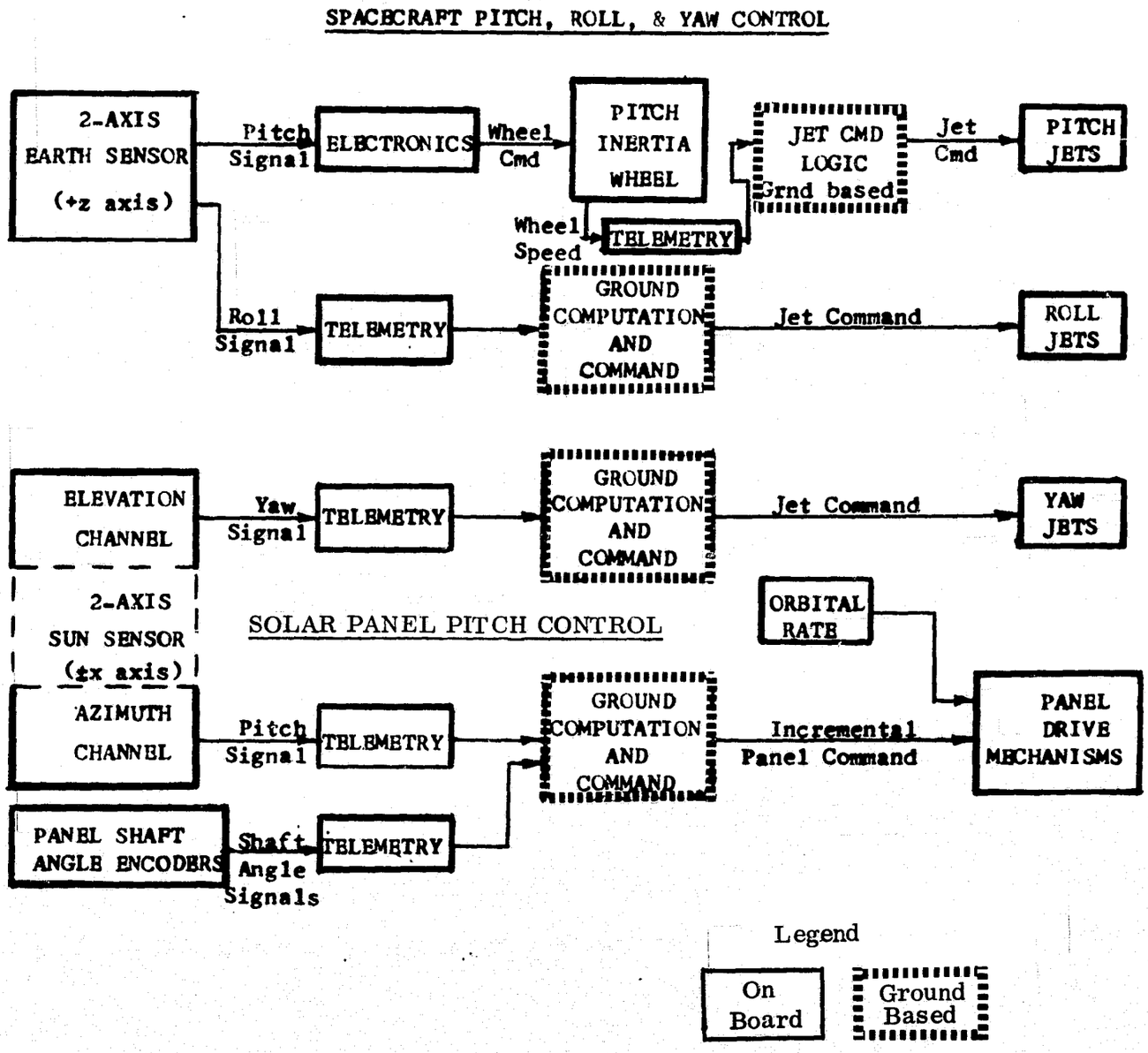


FIGURE 4.5-5 ATTITUDE CONTROL SYSTEM BLOCK DIAGRAM (OPERATIONAL MODE)

roll/yaw angle accuracy of about 0.5 degree between ground-originated, precession correction (jet) commands every 1 or 2 days. Thus, no on-board closed-loop control of roll or yaw is planned in the operational mode.

Roll angle data for the ground-based roll control loop are available at any time for telemetering to the ground. A 2-axis roll/pitch earth sensor is used for this purpose, looking along the +z axis of the spacecraft. Yaw angle data are provided near an orbit sunrise/sunset condition by sun elevation angle data from one of the two 2-axis sun sensors looking parallel to the $\pm$x axes of the satellite. These solar elevation angle data must be provided over a range of $\pm$26 degrees to accommodate summer/winter solstice conditions and expected orbit inclinations.

The sun azimuth angle data from these sun sensors, together with relative panel/satellite angle data, are used near the terminator plane to maintain acceptable sun-pointing accuracy for the two independent solar panel drive loops. These signals can be processed via the ground station as shown in Figure 4.5-5 to yield infrequent incremental corrective drive commands for the array drive mechanisms which are open-loop controlled to the nominal orbital rate. A sun alignment accuracy of several degrees is all that is required.

A pointing accuracy in pitch (East-West) to the local vertical of $\pm$0.5 degree is desired as well as in roll (North-South). Since no gyroscopic stability is provided in pitch (around the y axis), it is planned that on-board, closed-loop nulling of pitch error signals from the 2-axis earth sensor will be provided. Limited up-down accelerations of the inertia wheel (still preserving a minimum bias speed by infrequent, ground commanded jet firings as necessary) can be used for this purpose to minimize limit cycle motions and propellant expenditures.

Propellant is provided for an East-West stationkeeping velocity impulse of 35 ft/sec (7 ft/sec per year for 5 years) and a station relocation impulse of 25 ft/sec. The central, radial-firing thrusters aimed through the CG and parallel to the x axis (velocity vector) are used for this purpose based on ground-originated firing commands.

In sizing the propellant tanks, a 50 percent contingency was added to the calculated attitude control propellant requirements for spin and for earth-referenced control. The latter includes stabilization against the dominant solar pressure disturbance torque for 5 years.

In order to improve mission reliability, standby/functional redundancy has been provided for the attitude control sensors and torquers and for the orbit control thrusters for both the spin control and earth-oriented operational control modes. In addition, backup, degraded-performance operational control modes have been considered to cover a possible failure of the momentum wheel. In one mode the panels would be driven at 16 rpm to provide an equivalent gyroscopic stabilizing effect.

Pitch angle control around the y axis is a potential problem in this mode. The pitch error signal for this closed-loop control would be provided by one of the earth sensors as is the case for the normal operational control. However, corrective torqueing actions must be generated by on-board up/down acceleration commands to the panel drive loops, instead of to the momentum wheel as in the normal mode.

The stability effects of using the panels as a gyro "rotor" when they are not rotationally symmetric about the y drive axis and can dissipate significant energies via internal damping are also matters of concern.

4.5.2 APOGEE MOTOR

The apogee motor must provide a velocity impulse of about 6030 ft/sec in order to inject the spinning spacecraft into a synchronous, equatorial orbit. This maneuver is accomplished at apogee of the 28.5-degree inclined transfer orbit with a perigee altitude of 100 n.mi. and an apogee altitude of 19,323 n.mi. Actually, the velocity impulse can be reduced if an initial inclination bias of 2 degrees is employed in order to bias the inclination drift due to orbital perturbations about a near zero value. However, the full velocity impulse has been conservatively assumed for this study.

The apogee motor considered for this application is a modified Thiokol TE-M-442 motor with a 1.85-inch belly band. This motor is predicted to have an expended case weight of 46.4 pounds and to provide a propellant specific impulse of 295.4 sec., together with low performance expendables weighing 5.35 pounds with a specific impulse of 80 sec.

The start-burn weight for the apogee maneuver is taken to be 1355 pounds (the assumed payload capability of the improved Delta launch vehicle into the indicated transfer orbit)minus 53 pounds (the aft spacecraft adapter which remains with the launch vehicle). Accordingly, the weight of the high performance propellant required for the apogee maneuver is 609.1 pounds. The total propellant weight, including low performance expendables, is thus 614.5 pounds.

4.5.3 ATTITUDE CONTROL SYSTEM (ACS)

4.5.3.1 ACS Control Modes

General

There are four different attitude control modes which must be considered:

- o Spin control, employed during the transfer orbit, the apogee injection maneuver and the initial synchronous orbit correction maneuvers.
- o Acquisition, employed during acquisition of the reference earth-oriented attitude.
- o Operational, employed throughout the assumed 5-year mission in synchronous orbit to preserve the reference earth-oriented attitude.
- o Backup Operational, employed as a degraded performance control mode in synchronous orbit in the event of a failure of the momentum wheel used for 2-axis gyroscopic stabilization in the operational mode.

Most of the attitude control system (ACS) analysis to date has dealt with the operational mode as being the most critical. However, conceptual approaches have been defined for the other control modes which will also be briefly described in the following material.

Spin Control Mode

A basic constraint placed upon the spacecraft design is that its spin moment of inertia while stowed (solar panels folded) be greater than its transverse

moments of inertia by at least 20 percent. Hence, the spacecraft represents a stable spinning body while in the stowed condition. Passive spin stabilization of the satellite is accordingly fully effective. Its planned use permits long-term control in this mode (from several days up to a month or more).

Adequate electrical power for all spacecraft housekeeping functions can be generated by the solar cells on the outward-facing, stowed solar panels as long as the spin axis is maintained reasonably orthogonal to the sunline. The batteries can also meet this power requirement for a fairly extended period of time in the absence of solar power.

When the satellite is separated from the Delta third stage, it will be spinning at rates up to 70-90 rpm about its z axis. The despin thrusters (couple) shown in Figure 4.5-1 will be ground commanded to reduce the spin rate to about 45 rpm. This spin rate will still provide adequate spin stabilization against all disturbance torques, whether caused by natural sources or spin-thrust axis misalignments during the apogee maneuver. By thus lowering the spin rate, propellant requirements for the various spin precession maneuvers are reduced, as are spin acceleration loadings on the spacecraft during the apogee maneuver.

Use of the conventional sun sensor - Polang approach is planned for spin axis attitude determination on the ground. This method was employed for the early ATS vehicles and other satellites. Telemetered data from either of two wide angle ($\pm$ 30 degrees), 2-axis sun sensors looking along the $\pm$x axes of the spacecraft (transverse to the spin axis) are used in this mode, together with a polarized antenna signal. These are the same sun sensors that are used for 2-axis solar aspect data during the subsequent acquisition and operational control modes.

Spin axis precession control as needed (e.g., to reorient the apogee motor thrust axis to the attitude required for the apogee maneuver) is accomplished by ground originated commands to one of the two (redundant) spin precession control thrusters shown in Figure 4.5-1. Use of a 0.5 pound$_F$ catalyzed hydrazine thruster for this purpose yields a fully adequate 0.1 deg/sec. precession rate and permits a flight proven thruster design to be chosen, as discussed in Section 4.5.4.

Initial synchronous orbit correction maneuvers, for quick elimination of period errors causing unwanted satellite longitude drifts, can be effected by ground command firing of both of these diametrically opposed thrusters. Spin precession commands would first be sent from the ground so as to orient their thrust axes in the required inertial direction for the corrective maneuver.

It is noted that orbit correction maneuvers can also be made in the spinning mode by ground command firing (at the appropriate spacecraft attitude and orbit position) of the central thruster that is mounted on the +x side (Figure 4.5-1). The thrust vector of this jet is closely aligned with the spacecraft CG for both the stowed and deployed conditions.

A passive damper is employed to damp coning motions during the spin control mode. Active control damping is not required since the satellite is designed to be passively spin stable.

Acquisition Control Mode

Following injection into synchronous orbit and completion of any desired initial orbit correction maneuvers, the satellite will be despun using the indicated spin control thrusters. The solar panels will then be deployed.

Three-axis jet torqueing can then be provided by means of 0.5-pound$_F$ hydrazine thrusters located on the -z side and near the corners of the $\pm$x sides of the spacecraft. (Section 4.5.4 describes the appropriate use of these thrusters for attitude control in some detail.)

The first step in acquisition of the reference, earth-oriented attitude is to direct the solar panels towards the sun. Solar power can then be utilized and the batteries conserved. The panels will be initially locked with the cell-mounted side facing along the +x or -x axis of the spacecraft, depending on whether the subsequent earth acquisition maneuver is to be performed near the orbit sunrise or sunset condition as next discussed (See Figure 4.5-3).

General orientation of the +x or -x side of the spacecraft towards the sun as desired can be effected by ground command of the appropriate pitch/yaw jets

based on telemetered data on the output power level of the solar panels. Alternatively, coarse sun sensors located around the sides of the satellite can be used for this purpose.

Once the sun is brought within the field-of-view of one of the two wide angle, 2-axis sun sensors looking along the +x or -x axes of the spacecraft, final alignment of this axis to the sunline can be effected. This is done by ground commanding the pitch/yaw jets so as to null the telemetered sun azimuth (pitch) and elevation (yaw) angle signals from this sensor.

As the satellite moving in orbit approaches the sunrise (sunset) condition near the terminator plane, a slow earth search rate will be initiated about the sun-stabilized +x (-x) axis. As the +z axis of the satellite is thus caused to rotate about the sun line, the earth will ultimately come within the field-of-view of the earth sensor. Stabilization of the +z axis to the local vertical can then be accomplished. This is done by commanding the roll/pitch jets so as to null the roll and pitch angle error signals from the earth sensor. The solar panels will then be unlocked and driven at the preset nominal orbital rate so as to track the sun.

The y axis at this point will be normal to the ecliptic plane. A yaw maneuver can then be performed if necessary (i.e., for other than an equinox condition) to make it normal to the orbit plane. This is accomplished by commanding the yaw jets so as to produce the proper sun elevation angle signal from the 2-axis sun sensor. The reference orientation will then essentially have been established for the satellite.

The momentum wheel will next be brought up to its bias, gyroscopic-stabilization speed of 1400 rpm. The hydrazine thrusters providing a torque couple about the y axis are used to stabilize the spacecraft during wheel spinup. On-board, closed-loop nulling of the pitch error signal from the 2-axis earth sensor is employed to provide this stabilization. This completes the acquisition sequence.

Operational Control Mode

The primary attitude control requirements to be met during the operational control mode include the following:

- To maintain the reference earth-oriented attitude (+z axis along the local vertical and +y axis normal to the orbit plane) with an accuracy of $\pm$ 0.5 degree about all three body axes. (A North-South or East-West, roll or pitch angle error of 0.5 degree corresponds to a latitude or longitude deviation of the z-axis ground aim point of 2.8 degrees.)
- To drive the solar panels around the y axis so as to align them to the projected sunline in the orbit plane to within several degrees.
- To maximize the ACS reliability for the projected 5-year mission lifetime by the use of flight proven components wherever possible and by standby or functional redundancy for critical elements subject to realistic weight and/or power constraints.

With regard to the third requirement, a particular point of emphasis in the evolution of a tentative ACS design concept was to minimize the on-board controller functions (e.g., control of the attitude control jets) where possible. At the same time, reasonable operational command/control requirements on the ground control station have been maintained. Thus, it was desired that systemmatic ground command control functions, such as jet commands to correct attitude errors, should be required no oftener than every 1-2 days, less often if possible.

In order to meet the overall control accuracy requirements, the earth and sun sensor accuracy specifications were taken to be 0.1 degree desired, 0.25 degree maximum. It has been previously noted that sustained North-South station keeping is not planned for the subject pre-operational hybrid design because of the large velocity impulses associated therewith. (Short period demonstration of such a capability is possible.) The orbit inclination can probably be initially biased so as to balance the inclination "drift" due to orbital perturbations about a near zero value. This should keep the satellite subpoint latitude excursions within $\pm 2-3$ degrees in the 24-hour figure "8" pattern about the central equatorial longitude station. It should be possible to keep longitude excursions much smaller, within $\pm$0.1 to 0.2 degree.

The basic concept for the subject ACS operational control mode was described in Section 4.5.1, with a functional block diagram given in Figure 4.5-5. The key features are that the satellite is earth-oriented (local vertical/orbital plane) with the exception of the solar panels which are driven about the spacecraft y axis so as to track the sun. A large momentum wheel is employed with spin axis parallel to the satellite y axis. The natural gyroscopic stability provided by this wheel can counter the effects of all disturbance torques and maintain the y axis normal to the orbit plane as desired for periods of 1-2 days (without the need for corrective control action). See Section 4.5.3.2.

On-board closed-loop nulling of pitch angle errors about the y axis (+z axis off the local vertical in an East-West direction as detected by a 2-axis earth sensor) is provided, with torqueing accomplished by small variations in the high (1400 rpm) bias speed of the momentum wheel.

Firing of the hydrazine reaction jets for attitude error corrective torqueing about any of the three body axis can only be accomplished by ground command, and is only necessary on an infrequent basis (every 1-2 days). For this purpose, roll/pitch angle data from either of two (redundant) 2-axis earth sensors boresighted along the +z axis and yaw angle data (sun elevation angle data near the terminator plane) from two 2-axis sun sensors aligned along the $\pm$x axes are telemetered to the ground. Sun azimuth data from the sun sensors (near the terminator plane), together with relative panel/satellite angle data, are used to generate incremental corrective drive commands as required for the panels to track the sun.

It is noted as discussed in Section 4.5.3.4 that other locations and configurations were considered for the sun sensor. The indicated approach should provide adequate angle data for stabilization of the satellite in yaw and solar panels in pitch, but further studies are needed in this area.

Backup Operational Control Mode

Standby redundant sensors and reaction thrusters (for 3-axis torqueing) have been provided for the operational mode in order to enhance mission reliability.

However, weight limitations essentially preclude the inclusion of a redundant unit for the heavy (30-pound)momentum wheel and drive electronics .

Preliminary control analyses have shown that it is not sensible to use jet-only control in the event of a failure of momentum wheel. These studies revealed that the propellant consumption rate would be excessive even if thrusters much smaller than the planned 0.5 $pound_F$ jets were employed. Also, ground command control of the jets, used for reliability reasons during the operational mode, would not be practical because of the short period between jet limit cycle firings (10 to 40 seconds). Hence, the on-board controller would have to be made more complex than desired.

One alternative approach would be to use two small momentum wheels instead of one large one. Should either of the small wheels fail in orbit, the remaining wheel would still provide half the gyroscopic stabilization capability. A reasonably effective mission could thereby still be maintained. More frequent ground-originated jet commands for corrective precession torqueing would be required in this case, or larger angle excursions of the y axis from its desired orientation normal to the orbit plane would have to be tolerated. Further studies are required of the performance, reliability, weight and power of this approach compared to the tentatively selected one of a single large momentum wheel, but it is expected to be somewhat heavier.

Still another alternative backup operational control mode has been considered for use should the momentum wheel fail. This backup mode involves speeding up the drive rates for the solar panels about the y axis. A drive rate of 16 rpm for each of the two solar panels would yield a gyroscopic stability equivalent to that provided by the momentum wheel.

Using this backup operational control mode, the ground command/ control method would be essentially the same as that described for the operational control mode. However, on-board closed-loop nulling of pitch angle errors about the y axis would now have to be effected by up-down acceleration commands to the panel drive loops, a much more questionable operation compared to using the momentum wheel. Occasional ground command firing of the pitch jets so as to maintain a nominal 16 rpm drive rate for the panels would still be employed.

The solar power available from the "spinning" solar panels would be reduced by a factor of approximately $1/\pi$ compared to the normal mode of operation. Additional areas of concern are the dynamic stability effects of using the solar panels as a gyro rotor since they are not rotationally symmetric about their driven axis and can internally dissipate significant amounts of energy.

4.5.3.2 Solar Pressure Disturbance Torque Analyses

The gravity gradient and magnetic disturbance torques for the earth-oriented hybrid in a synchronous orbit are negligible compared to the solar pressure disturbance torques. These dominant solar pressure torques acting on the spacecraft have been considered from three basic aspects for the operational control mode:

- The impact they have on sizing the momentum wheel so that it can provide inherent gyroscopic stabilization about the x-z axes to an accuracy of 0.5 degree for 1-2 days.
- The secular momentum buildup they may impart to the spacecraft about any axis which must be countered by the expenditure of reaction jet propellant, based on ground commands to the thrusters.
- The time varying momentum they may impart about the y axis which is to be countered by variations in the momentum wheel bias speed, accomplished by on-board closed-loop nulling of pitch error signals from the 2-axis earth sensor.

Two types of solar pressure torque analyses have been conducted. The so-called nominal analysis used a best estimate modeling of spacecraft component areas and reflectivities with no tolerance effects included. The tolerance torque analysis considered the effects of various mechanical/reflectivity tolerances on key spacecraft components. These nominal and tolerance torques were then combined to determine the total disturbance effects of interest. These included the expected precession of the gyroscopically-stabilized, spacecraft y axis during an orbit and the attitude control propellant required to remove accumulated solar pressure momentum.

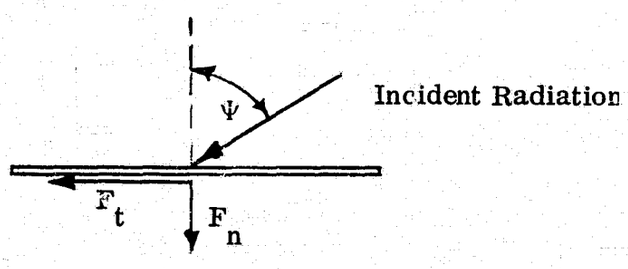
In order to most directly examine these effects, the solar torques are calculated in a pseudo inertial, satellite-projected sunline reference frame (X, Y, Z). This consists of the +X axis lying in the orbit plane pointed towards the sun projected therein, the +Y axis normal to the orbit plane pointed South for an equatorial orbit (nominally parallel to the spacecraft +y axis), and the +Z axis in the orbit plane normal to the projected sunline.

Solar Pressure Torques - Nominal

A simplified model of the hybrid configuration illustrated in Figure 4.5-2 was developed for use in assessing the level of cyclic and bias solar torques and resulting y axis precession angles during earth orbit for equinox and solstice sun locations. The model, consisting of flat and cylindrical surfaces equivalent in area to those of the proposed configuration, is detailed in Appendix B where surface properties and sample calculations are also described.

The equations used have been derived in the literature based on the usual photon momentum transfer theory and the appropriate geometric treatment of surfaces exposed to solar flux. Normal (F_n) and tangential (F_t) components of force are defined for flat and cylindrical surfaces as follows:

Flat Plate



where;

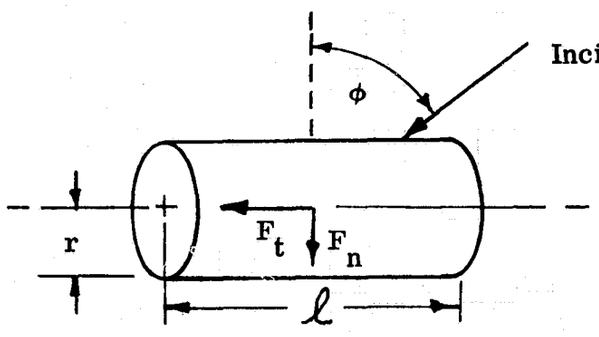
$$F_n = \left[(1 + s\rho)\cos^2\psi + \frac{2}{3}\rho(1-s)\cos\psi\right] P_f A_p \quad (1)$$

$$F_t = \left[(1-s\rho)\cos\psi\sin\psi\right] P_f A_p \quad (2)$$

P_f = Solar pressure, 1×10^{-7} lbF/ft^2

A_p = Plate surface area, ft^2

Cylinder



where $F_n = \left[(1+s\rho/3)\cos^2\varphi + \rho(1-s)(\pi/6)\cos\varphi\right] P_f A_c$ (3)

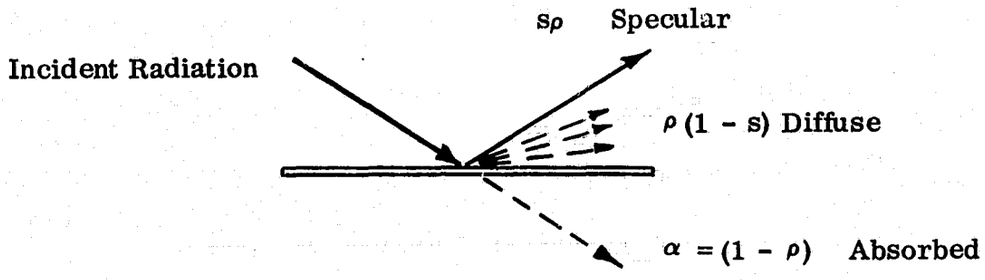
$F_t = \left[(1-s\rho)\cos\varphi\sin\varphi\right] P_f A_c$ (4)

A_c = Projected cylinder area, $2r\ell$, ft^2

and where

ρ = fraction of incident radiation reflected

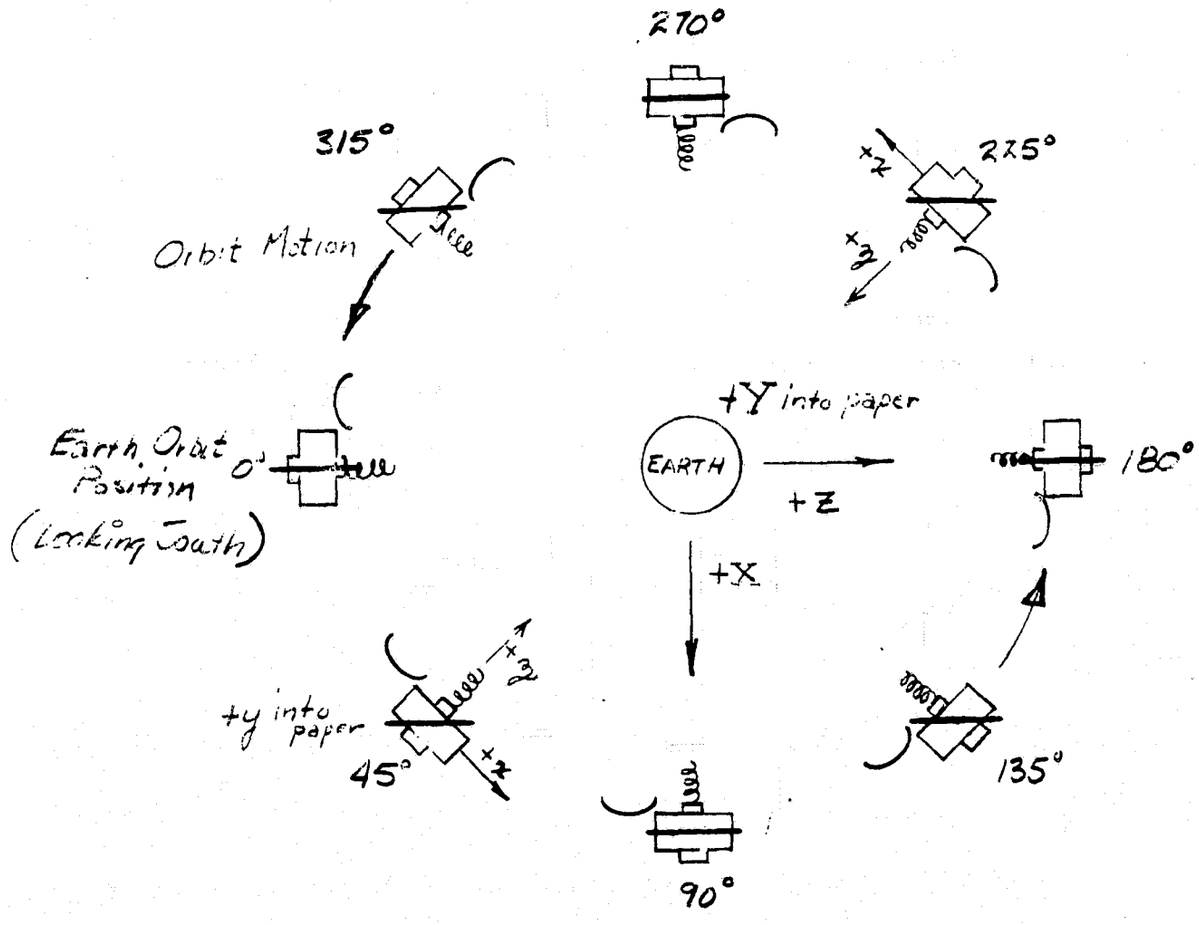
s = fraction of reflect radiation which is specular



Values of ρ, s, areas and the force equation coefficients are listed in Appendix B for the fourteen surfaces which make up the model.

Forces on the various surfaces were calculated and moments summed at eight orbital locations as shown in Figure 4.5-6, where the pseudo inertial (satellite-projected sunline) and body axis frames are also indicated. The net torque for each location determined at equinox and solstice sun positions is plotted in Figure 4.5-7 from values tabulated in Table 4.5-1. Shadowing effects are included therein.

The spacecraft is symmetrical about the x and z axes when viewed from any direction in the xz plane (see Figure 4.5-2). Thus there are no net torques about the x and z axes in equinox orbit. The spacecraft is unsymmetrical about the y axis and Figure 4.5-7 illustrates the associated variation in solar torque for varying solar aspects. The accumulated positive angular momentum during the first half



DEFINITION OF AXES:

1) Satellite - Projected Sun - Origin; CG of Spacecraft

$\bar{X}$ = Unit vector in orbit plane a long projection of sun line from SC CG; positive toward Sun CG

$\bar{Y}$ = Unit vector, normal to orbit plane, positive in direction opposite to orbit rate direction

$\bar{Z}$ = Unit vector, such that $\bar{Z} = \bar{X} \times \bar{Y}$

2) Spacecraft Body Axes - Origin; CG of spacecraft

x = Along spacecraft velocity vector, positive indirection of flight

y = Through solar panel axis, positive toward south

z = Positive toward center of earth

Note: All axes coincident at 0°, the point of initial acquisition.

Figure 4. 5-6 Orbital Geometry for Solar Torque Calculations

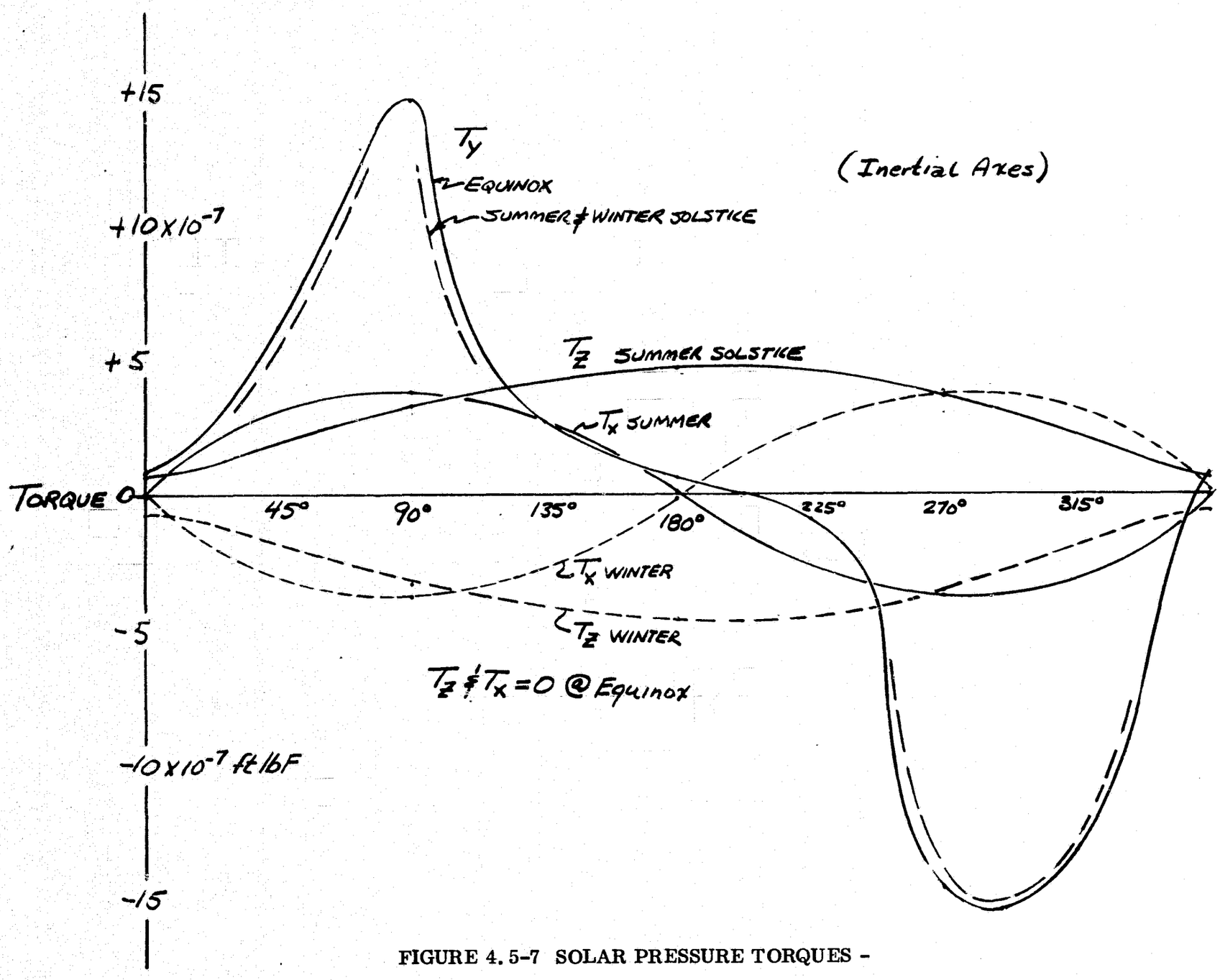


FIGURE 4.5-7 SOLAR PRESSURE TORQUES - NOMINAL CASE

Table 4.5-1

Solar Pressure Torque Summary - Nominal Case

Torque (Pseudo Inertial)	Orbit Position								
(10^{-7} ft-lb F)	Sunrise 0^o	45^o	Noon 90^o	135^o	Sunset 180^o	225^o	Midnight 270^o	315^o	Net Accumulation of Angular Momentum, ft-lb F-sec. (Per Orbit)
Torque around Y axis, T_y									
Equinox Orbit	+.850	+6.22	+14.59	+2.70	+.625	-.900	-14.59	-13.20	-5.22×10^{-3}
Summer & Winter Solstice Orbits	+.500	(+5.66)	+14.22	(+2.33)	+.550	(-1.00)	-14.22	(-12.32)	-6.08×10^{-3}
Y axis precession torques (Summer Solstice Orbit; Winter Opposite Sign)									
Torques about Z axis, T_z	+.725	---	+3.35	---	+4.66	---	+3.67	---	$+27.35 \times 10^{-3}$
Torques about X axis, T_x	-.0408	---	+3.78	---	+.242	---	-3.78	---	≈ 0 ($\pm 10.75 \times 10^{-3}$ per half orbit)

equinox orbit is less than the negative momentum accumulated during the second half, leaving a net negative accumulation as listed in Table 4.5-1. Solstice orbits slightly reduce the y axis torques, with both winter and summer orbits having the same sign. The net momentum accumulation, however, increases by 20%.

As the orbit goes from equinox to solstice, increasing solar torques are introduced about the X and Z axes which result in precession of the spacecraft y axis (parallel to the spin axis of the stabilizing momentum wheel). Both the summer and winter orbit induced torques are mirror images of each other as seen in Figure 4.5-7. However, the Z torques are all positive in the summer and all negative in the winter with net momentum being accumulated during any three months. The plus and minus X torques cancel each other over an orbit.

Solar Torques Due to CG - CP Deviations

Calculated center-of-gravity/center-of-pressure (CG/CP) location deviations along the spacecraft x, y, and z axes are given in Table 4.5-2 for the following maximum tolerance conditions:

Item	Description
1	Tolerance on capability of locating the spacecraft CG.
2	Size tolerance of solar panels. This affects both CG and CP variations along all 3 axes to different degrees.
3	Effect of manufacturing variations on relative reflectivity of solar panel arrays. This differential reflectivity for the solar panels affects the CP along the spacecraft y axis only, producing a constant bias torque about the pueudo inertial Z axis. This corresponds to sinusoidally varying torques about the spacecraft x and z axes, displaced in phase by 90 degrees.
4	Bearing and hinge-pin clearances in the solar array supports, affecting both the CG and CP along the spacecraft x and z axes as the spacecraft rotates in orbit. This yields effectively a fixed bias torque about the y axis.

Table 4.5-2

CG-CP Deviation Summary

(Maximum Tolerances)

	ITEM	S/C CG Deviation, ft. β_x	β_y	β_z	S/C CP Deviation, ft. γ_x	γ_y	γ_z
1.	Satellite CG Tolerance	.0083	.0083	.0083	NA	NA	NA
2.	Solar Panel Size Tolerance	.00016	.0006	.00016	.0025	.0083	.0025
3.	Reflectivity Differences, Solar Panels	NA	NA	NA	NA	.00066	NA
4.	Solar Panel Bearing & Hinge Tilts	.00045	NA	.00045	.00622	NA	.00622

Table 4.5-3 shows the resulting incremental solar torques due to the above, about the pseudo inertial (satellite-projected sunline) Y and Z axes. Items 1, 2, and 4 are most significant, whereas item 3 is inconsequential.

Detailed calculations for the values given in Tables 4.5-2 and 4.5-3 are presented in Appendix C.

Attitude Disturbance Effects of Solar Pressure Torques

The nominal and tolerance solar pressure torques that were calculated in the preceding sections were combined to determine how they might perturb the desired spacecraft orientation. (Associated attitude control impulse requirements are covered in Section 4.5.4.3.) Of particular concern was the possible precession of the spacecraft y axis about the pseudo inertial X/Z axes. It is desired to keep such angle excursions within ± 0.5 degree for 1-2 days. This will obviate the need for any more frequent ground-originated jet commands for precession correction and result in acceptable ground command/control operational procedures.

Figure 4.5-8 presents a plot of the precession angles for the spacecraft y axis about the X and Z pseudo inertial axes for a worst case solstice condition. It can be seen that the precession about the Z axis reaches a maximum of only 0.1 degree and essentially reduces to zero after one full orbit. The secular buildup in total precession angle about the X axis during one orbit is only about 0.3 degree. Hence, by appropriate biasing of the initial y axis orientation about the X axis, precession correction commands from the ground would not be required for three full orbits while still keeping the X axis angle error within 0 ± 0.5 degree.

A change of only 4.6 rpm in the momentum wheel bias speed of 1400 rpm is all that is required to counter the accumulated momentum under one-half cycle of the T_Y curve shown in Figure 4.5-7. This is accomplished by on-board closed-loop nulling of pitch angle error signals.

As a concluding comment upon these solar torque analyses, it is noted that a careful effort was made to obtain a realistic estimate of the nominal and tolerance disturbance torques. Additional tolerance analyses were performed as described in Appendix B to evaluate the effects of variations in the assumed values for ρ and s

Table 4.5-3
Solar Torques Due to Tolerance Effects

Torques about Z-axis (Psuedo Inertial)					Angular Momentum Per Orbit ft - lb F - sec
	Item	Force, lb.	Moment arm, ft.	Solar Torque ft - lb	
1.	S/C CG Tolerance	186.5×10^{-7} (satellite, total)	$\beta_y = .0083$	1.55×10^{-7} (BIAS)	
2.	Solar panel size tol.	117.8×10^{-7} (Panels)	$\gamma_y - \beta_y = .0077$	$.907 \times 10^{-7}$ (BIAS)	
3.	Differential reflectivity	$.0097 \times 10^{-7}$ (ΔF panels)	11.1	$.108 \times 10^{-7}$ (BIAS)	
$\Sigma T_z = 2.56 \times 10^{-7}$ (BIAS)					22.0×10^{-3}

Torques about Y-axis (Pseudo Inertial)					
	Item	Force, lb.	Moment arm, ft.	Solar Torque ft - lb	
1.	S/C CG Tolerance	186.5×10^{-7} (satellite total)	$\beta_z = .0083$	1.55×10^{-7} (OSCILL)	0
2.	Solar panel size tol.	139.4×10^{-7} (panels + bases)	$\gamma_z - \beta_z = .00234$	$.326 \times 10^{-7}$ (BIAS)	
4.	Bearing & Hinge tol.	139.4×10^{-7} (panels + bases)	$\gamma_z - \beta_z = .00577$	$.804 \times 10^{-7}$ BIAS)	
$\Sigma T_y = 1.55 \times 10^{-7}$ (OSCILLATING) + 1.13×10^{-7} (BIAS)					9.76×10^{-3}

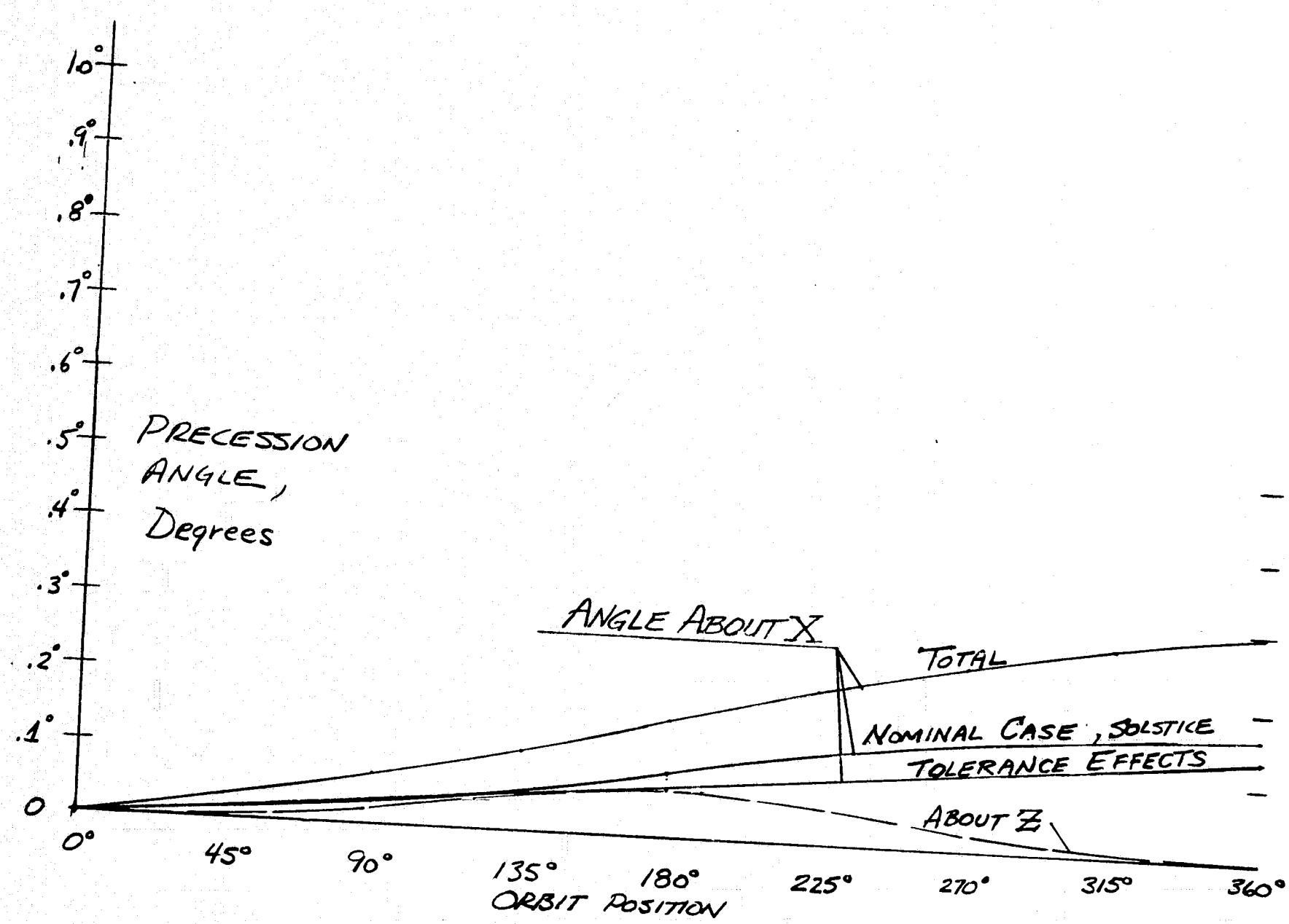


FIGURE 4.5-8 SPACECRAFT Y-AXIS PRECESSION

for the various elements making up the spacecraft structure. These led to even lower values for the solar torques.

The calculated solar torque values were surprisingly low. However, even if they should prove to be bigger by a factor of 2, 3 or even 6 than these values, the attitude control concept described herein should still be effective. Precession corrective torqueing commands would be required every 2 or 1 or 0.5 days instead of every 3 days as the analyses indicated. The additional attitude control propellant required would be quite small. Further solar torque analyses are needed to further substantiate these studies.

4.5.3.3 Pitch Axis Control Analysis

The preceding section dealt with the quality of gyroscopic stabilization provided by the momentum wheel about the roll/yaw (x/z) axes in the presence of the dominant solar pressure disturbance torques. That section also showed that only relatively small excursions in the bias speed of the momentum wheel are required to compensate for the cyclically varying solar pressure torque about the y axis. Also, infrequent ground commanded firing of the pitch jets will be all that is needed to counter any secular build-up of momentum about the y axis. The momentum wheel can thus be kept rotating near its desired nominal bias speed of 1400 rpm.

An additional pitch axis control analysis has been performed to examine the general problem of the precision or resolution of wheel speed control required to ensure accurate pitch angle limit cycle control for realizable disturbance torque levels. The torque levels considered ranged from a low value of 0.33×10^{-6} ft-lb, through an intermediate value of 0.92×10^{-6} ft-lb, and up to a near maximum value of 1.84×10^{-6} ft-lb.

The simplified equations of motion employed for this analysis were the following:

$$\Delta H = I_w \Delta \omega$$

$$\Delta H = Tt$$

$$T = I_{s/c} \alpha$$

$$\theta = (1/2) \alpha t^2$$

where,

ΔH = change in momentum, ft-lb-sec

I = y axis inertia (w-wheel, s/c-spacecraft), slug-ft^2

t = time, sec

$\Delta\omega$ = initial change in momentum wheel speed, rad/sec

T = torque, ft-lb

α = angular acceleration, rad/sec^2

θ = angular excursion about spacecraft y axis, rad

A scallop limit cycle operation (control action at only one deadband boundary) was assumed for this analysis as depicted in Figure 4.5-9. Using the given equations, the angular excursion (θ) about the spacecraft y axis which would accumulate during the time required for various torque levels to null the initial spacecraft rate caused by an initial impulsive change in wheel speed ($\Delta\omega$) were calculated. These angle data are presented in Figures 4.5-10, together with a cross plot of the time required for the given torque levels to null the initial spacecraft rate caused by any given $\Delta\omega$ value. Separate plots of these time-to-null values versus $\Delta\omega$ for various torque levels are also given in Figure 4.5-11.

It is noted that in a scallop limit cycle mode, as shown in Figure 4.5-9, the subject time-to-null would represent half the limit cycle period and the $\Delta\omega$ value would represent half the wheel speed change required at the crossing of the angle control boundary to reverse the limit cycle trajectory. Again, this control impulse is provided at only one side of the angle control boundary for a scallop (soft) limit cycle, namely the side towards which the existing disturbance torque causes the spacecraft to drift.

Soft, scallop limit cycle control would result in lower wheel drive power requirements compared to hard, two-boundary limit cycle control. However, the data shown in Figure 4.5-10 indicate that in order to be able to realize soft limit cycle control with acceptably small angle excursions, unrealistically fine speed control

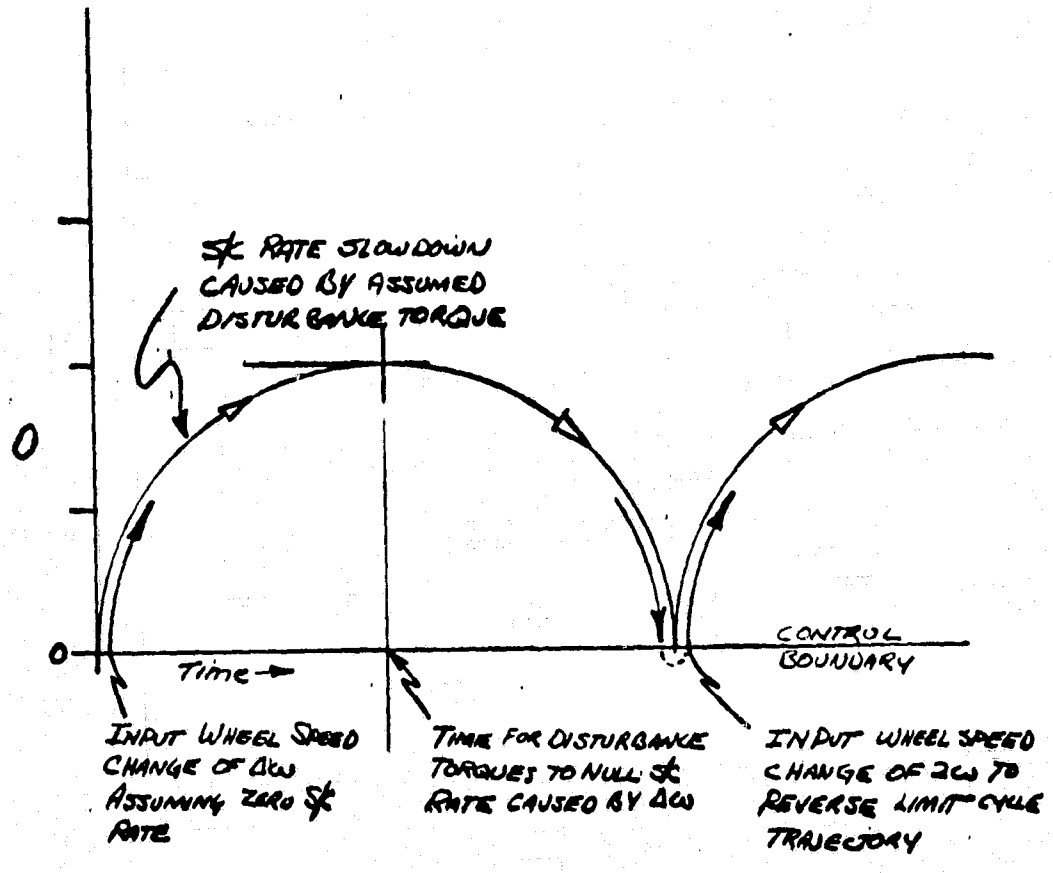


FIGURE 4.5-9 LIMIT CYCLE MODEL

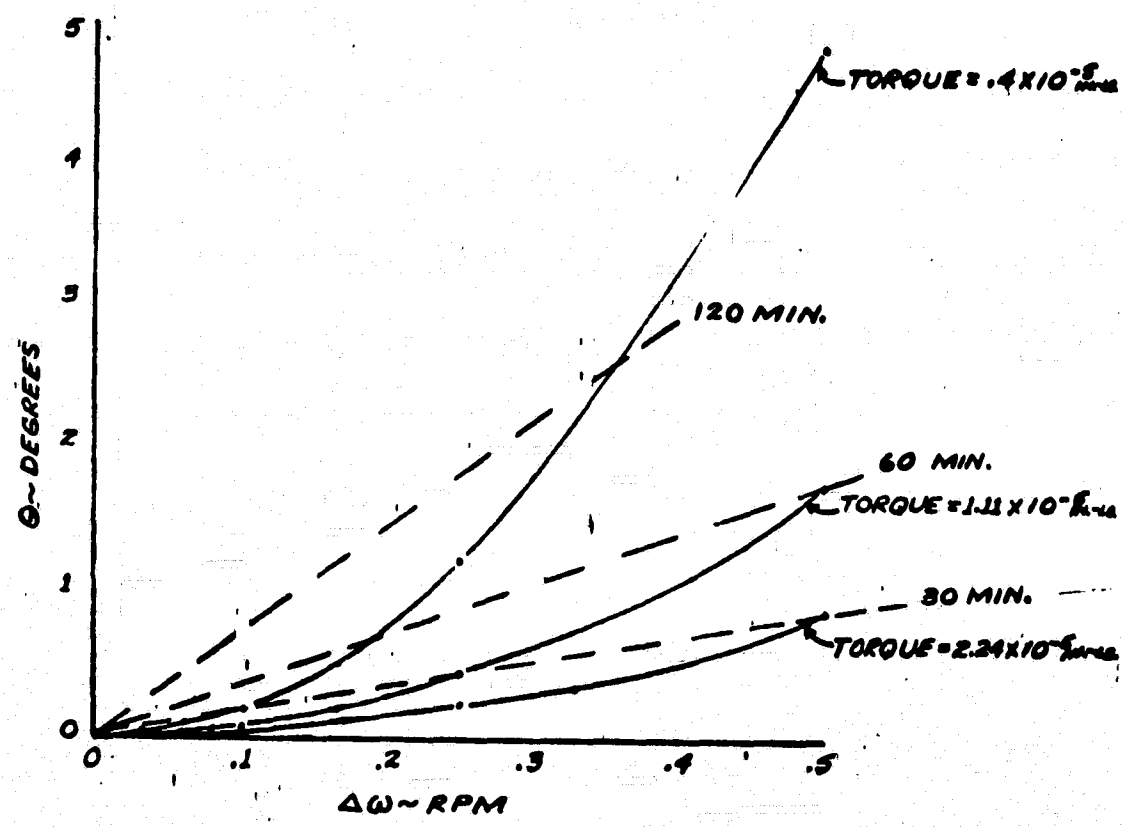


FIGURE 4.5-10 ANGULAR EXCURSION (θ)
vs.
WHEEL SPEED CHANGE (Δω)
(Zero S/C Rate Before Δω)

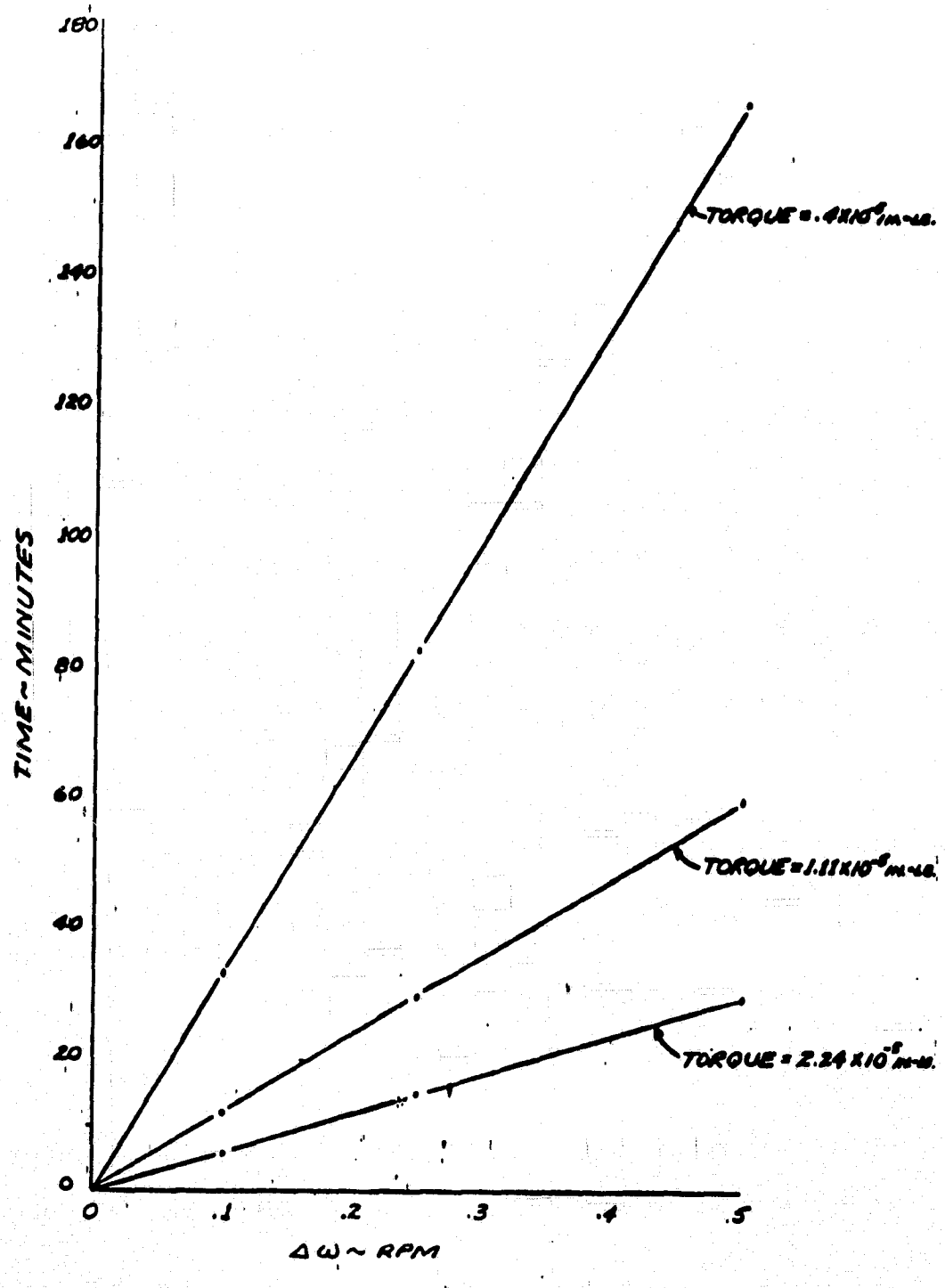


FIGURE 4.5-11 TIME TO NULL S/C RATE vs. WHEEL SPEED CHANGE (Zero S/C Rate Before Δω)

of the large momentum wheel would be required. This result is based upon assumed low natural disturbance torques of the order of 10^{-6} ft-lb.

However, the on-board momentum wheel drive control loop could be operated in a simple pulsed mode, based on maintaining the pitch angle error within a preset deadband. The disturbance torque associated with momentum wheel slow-down between successive power pulses to the wheel would then far overshadow the expected solar pressure torque. An acceptable scallop limit cycle mode could thus be established with a duty cycle of about 20 to 25 percent and with a period of about 5 seconds for an angle excursion of about $\pm$ 0.25 degree.

These and other wheel drive approaches require further study.

4.5.3.4 Sensors

As indicated previously, the sensors required for the various ACS control modes and for incremental solar panel pointing corrections in pitch are:

- Two, 2-axis earth sensors (standby redundant) looking parallel to the +z axis of the spacecraft.
- Two, 2-axis wide angle sun sensors (essentially redundant) looking parallel to the $\pm$ x axes of the spacecraft.

A resolution/accuracy capability of 0.1 to 0.25 degree is required for each of these sensors. Summary data are next provided regarding candidate earth sensors and sun sensors.

Earth Sensor

Several existing earth sensors appear to be applicable for pitch and roll attitude determination for the Hybrid. Their characteristics are summarized in Table 4.5-4. These are of two general types: scanning and static radiometric. The static sensors (Quantic and Barnes) have no moving parts, but have conical fields of view. The scanners can be single-axis (TRW Vela) or two-axis (LMSC) configurations, and have fan-shaped planar fields of view.

Table 4.5-4
EARTH SENSOR CANDIDATES

	HONEYWELL	TRW	QUANTIC		LMSC	BARNES
DESIGNATION	DYG774A1	VELA/Visor	Static (no mirror)	IV A	NOHS Dual Scan (Null Op H.S.)	HAHS Earth-Lunar Modified (No Gimbals) (Hi Alt. H.S.)
TYPE	Radiation Balance	Scan Thru	Rad. Bal.	Rad. Bal. Edge Trkr.	Scan Thru 45^{o} Off Along Lats.	Rad. Bal. Edge Trkr.
MOVING PARTS	NO	YES 5 Hz	NO	YES Thermo-Static, Non Periodic	YES 4 Hz	NO
ACCURACY $\pm 3\sigma$	0.1^{o}	$<0.1^{o}$	0.1^{o}	0.03^{o}	0.017^{o} - 0.068^{o}	0.1^{o}
OUTPUT D - Digital A - Analog	A	A	A, 1v/deg or .5v/deg	A or D Ser/Par	D, $.01^{o}$/Digit A, 1v/deg	A, 1v/deg
LINEAR RANGE	$\pm 70^{o}$	$\pm 2.3^{o}$ min $\pm 19.3^{o}$ max	$\pm$ 5 deg	$\pm$ 10 deg	$\pm 10.24^{o}$ pitch $\pm 2.56^{o}$ roll	$\pm 0.5^{o}$ brk @ 1^{o} $\pm$10 deg Satura.
SPECTRUM MICRONS	11-20	14-17	22-40	14-16	14.1-15.8	13.7-16.3
AXES	2	1	2	2	2	2
WEIGHT, HD WEIGHT, ELEC. TOTAL WT.	6.5 — 6.5	~3.0 ~5.0 8.0	7.0 — 7.0	4(7)=28.0 10.0 38.0	4.0 — 4.0	2.0 — 2.0
VOL. HD. VOL. ELEC. TOTAL VOL (cu. in)	30 95 125	~175 ~200 ~375	(8diax7) 350 — 350	4(116)=464 464+	(4.25x4.5x7.00) 134 — 134	(3diax7) 50 — 50
ALT. NM	100-60,000	Synch.	Synch.	80-25,000	Synch.	Synch.
POWER, watts	6.0	~7.0	2.2@ 22-31 vdc	22-34	5.0@28vdc	1.5@ 22-29.5vdc
SUN REJECTION	Acc: $\sim 0.25^{o}$	Avoid	Avoid by Switching	Avoid by Switching	Pitch-Switches Roll-uses Std. Chord	Avoid by Switching, Not inhibited
DETECTOR	Thermistor Bolometer (7)	Thermistor Bolometer (1)	Thermocouples (24)	(48)	Thermistor Bolometer (2)	Thermo-piles (16)
REMARKS	Needs more development	In-Orbit 1967 Visor qual.	Qual. for AF, ATS	Qual. 30g sine, Life '66	Qual. design proof, life test compl.	Thermopiles qual. 35g -195+100C

Figure 4.5-12 shows how the single scanning mirror of a typical sensor scans the earth in a North-South direction. The Lockheed sensor, for instance, derives pitch and roll angle information as shown in this figure. Pitch attitude (in this orientation of the sensor) is determined by computation of the sensed difference between two earth chord lengths which are separated by 12 degrees. Roll attitude is derived by timing the horizon-to-center crossing in each direction along one chord.

Sun avoidance capability in one form or another is provided for all the sensors considered. In the pitch axis, the Lockheed sensor substitutes a "standard" chord electrically for that chord in the scan plane intercepting the sun. Roll information is then derived by timing horizon crossings in the other scan plane, out of the sun's view.

It should be noted that use of the LMSC earth sensor here for illustrative purposes does not signify final selection of that sensor at this time, but the derivation of two-axis information from a single scanning mirror makes this concept attractive from a weight and power point of view. The attitude control system weight budget reflects the assumed use of 2 redundant LMSC earth sensors, at 4 pounds each.

Two-Axis Sun Sensors

A wide-field, two-axis solar aspect sensor with a resolution/accuracy of 0.1 to 0.25 degree is required for the Hybrid. It is planned to use two such sensors, essentially redundant, aligned parallel to the $\pm$ x axes of the spacecraft, for all of the basic control modes (spin, acquisition, operational and backup operational). A wide elevation field-of-view (FOV) in the plane normal to the orbit plane for the operational mode is necessary to account for the sun's annual excursion in declination, amounting to $\pm$ 23.5 degrees, and for several degrees of orbital inclination. The total FOV requirement is thus about $\pm$ 26 degrees minimum, but a safer margin is provided by a FOV of $\pm$ 30 degrees.

The azimuth FOV requirement in the orbit plane is essentially the same in order to provide a wide sun acquisition cone. In addition, a wide FOV in the azimuth channel permits sun pointing corrective commands for the solar panels to be calculated in the operational mode for large portions of the orbit path near the

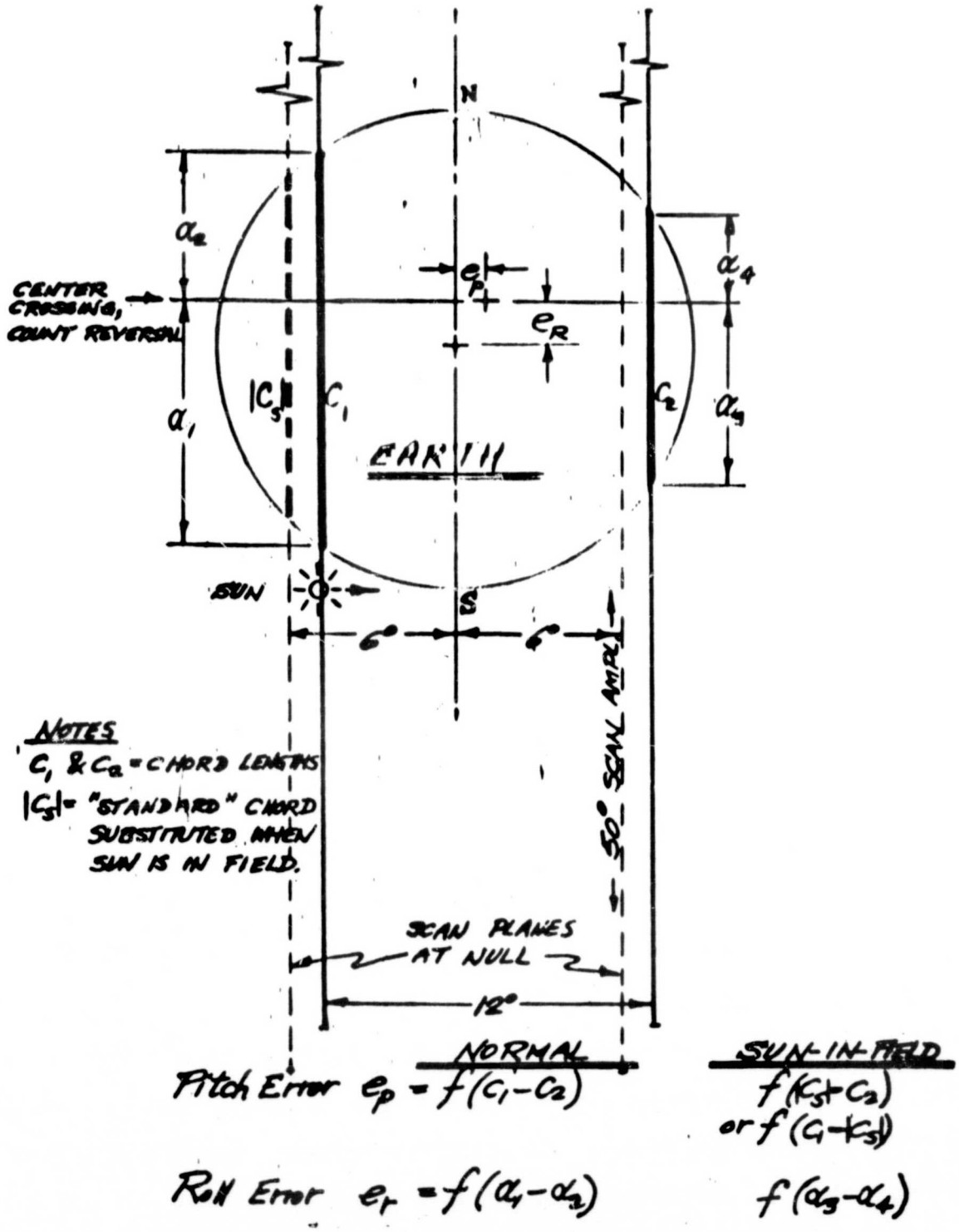


FIGURE 4.6-12 LMSC "NOHS" SCAN GEOMETRY

terminator plane. Nearly one-third of the orbit can be so covered with an azimuth FOV of $\pm$ 30 degrees.

Consideration was given to placing the 2-axis sun sensors on the solar panels rather than on the $\pm$ x sides of the satellite. The panel location for the sensors would have the advantage of providing solar aspect data (with derivable panel/satellite roll, pitch and yaw information) continuously over the full orbit as the panels track the sun. However, significant disadvantages are that low level signal leads would have to be brought across the rotating panel joints, and care would have to be taken in folding the solar panels so as not to damage the sun sensors. Two-axis sun aspect data for the indicated portions of the orbit path near the terminator plane are fully adequate for purposes of satellite yaw control and panel pitch control. Hence, it was tentatively decided to locate the sun sensors on the $\pm$ x sides of the satellite. Further studies are needed in this area.

Table 4.5-5 lists several types of wide-field sun sensors (both analog and digital) with appropriate associated performance and physical characteristics. All of these sensors are passive, strapped-down devices with no moving parts. All use silicon photovoltaic cells which peak near 0.8 micron wavelength, just outside the visible range. Response time is of the order of 5 to 10 microseconds.

Budgeted weight for the optics, detector, and associated electronics 2 (redundant) 2-axis sensors is 3 pounds maximum. The favored EOS and BBRC candidate sensors appear capable of meeting this weight limit, including their processing electronics.

The Electro Optical Systems Inc. Radiation Tracking Transducers (RTT) are designed for mechanical attachment to any "standard" lens such as the wide-field PAXAR identified in the table. However, the narrower the field (e.g., 60^{o} instead of 180^{o}) the better the resolution capability of the system.

TRW Systems Inc. also builds sun sensors for many aerospace programs. However, their analog sensors used the EOS RTT which is described herein.

Table 4.5-5
Sun Sensor Candidates

Supplier	Bendix		Ball Bros.	E.O.S.		Adcole	
Type	Wide Field Sun Seeker	Binary Output Sun Sensor	Fine Sun Sensor Assembly	RTT (Detectors)		Solar Aspect Sensors/ Electronics	
Model No.	1771858	1771982	SS 100	XY20B	XY20E	10941/ 235	11974/ 11962
Characteristic	*	*					
Analog/Digital	An.	Dig.	An.	An.	An.	Dig.	Dig.
Sensitive Axes	2	2	2	2	2	1	2
Total Wt., lb.	.19		~.68	~.5**	~.5**	2.26	2.8
Size	1.9"dia. x 20"	~1.5"dia. x 6"	2.8" x 1.7x 1.8	2.62" dia. max. x ~2.7" lg.		see below, detector and electronics	
Power, watts	.005		~1.0	no electr.		.27	---
Linearity over	5%	NA	~1%	2%	8% @.025"	---	---
Angular Range	±10°	NA	±5	8% @ .100"		---	---
Resolution, Noise	inf.	NA	inf.	~inf. .003°	~inf. .003°	0.5°	0.5°
Optics	Glass Cover	Mask Only	Glass Cover	No Optics Supplied		Internal	
Field of View	180°	(to order)	30°	±.225" ±.100"	± .225" max ± .025" useful	±32° x 2°	±64° x ± 64°
Size: dia x lg.	1 7/8" x2"	NA	NA	Above are detector dimensions: F.O.V. depends on lens		NA	NA
Detector	Quad. 2/axis	---	Quad. 2/axis	1 →		#10941	#11974
Type	Silicon		Silicon	Silicon →		Silicon	
Signal gradient	1.8 max / deg.	---	35 μa/min 5 " "	.25 mv/ mw/.001 in. →		NA	NA
Size	Included in integrated package			1.2" dia x .9" lg		2@ 1.2" x 1.7" x .9"	3.2" x 3.2" x .8"
Weight	(.19 lb)		(0.38 lb)	.06 lb →		2@ .13 lb	.5 lb
Electronics	Not Supplied		2 diff amp. + 4 amp + pwr. sup.	Not Supplied		#235 2 req.	#11962
Size			3" x 3" x 2"			2 req. 4.6" x 2.0" x 3.3"	6.5" x 4.5" x 2.3"
Weight			(~0.3 lb)			2@ 1.0	2.3 lb

* Detector only

** With 180° PAC "Paxar Periphoto" f/6.3, 2.62 dia x 1.75 lg lens, .35 lb plus housing

4.5.3.5 Torquers

The torquers employed for attitude control of the Hybrid include reaction jets which are used for torqueing about all axes during the spin, acquisition, operational and backup operational control modes and a large momentum wheel which is used for gyroscopic stability about two axis and limited torqueing about the third axis during the operational mode. The configuration and operation of the jets are described in detail in Sections 4.5.1 and 4.5.4. The intended use of the momentum wheel is discussed in Sections 4.5.1 and 4.5.3.2. The characteristics of the proven momentum wheel design being considered for this application are summarized in Table 4.5-6.

4.5.3.6 Estimated ACS Weight/Power

Based upon the tentative selection of components indicated in the foregoing sections, the estimated weight and power requirements for the ACS are summarized in Table 4.5-7. As noted, the control electronics listed in this table include those needed for the Auxiliary Propulsion System (APS). The rest of the hardware and propellant weights for the APS are separately covered in Section 4.5.4, however.

4.5.4 AUXILIARY PROPULSION SYSTEM (APS)

The auxiliary propulsion system (APS) must provide the thrusters and total impulse needed for attitude control in the spin, acquisition, operational and backup operational control modes. In addition, it must fulfill the requirements for synchronous orbit correction maneuvers (300 ft/sec) in the spinning, operational and backup operational modes and for subsequent East-West station keeping and station relocation maneuvers (60 ft/sec) in the operational and backup operational modes. Thrust levels in the 0.5 to 1 pound range for spin precession control and in the 1-5 pound range for orbit control are needed.

The APS is to meet the indicated propulsion requirements for a mission duration time of up to 5 years. A major consideration in the definition of a preferred APS is the use of flight proven hardware wherever possible, and the use of redundancy for all critical elements to further enhance mission reliability.

Candidate Momentum Wheel Characteristics

(Bendix Type 1880026)

Item	Value
Spin Inertia (slug - ft^2)	0.0647
Nominal Momentum -1400 rpm (ft-lbs-sec)	9.5
Stall Torque (oz-in)	20
Stall Power (watts, both phases)	53
Overall dimensions (inches) - outer diameter	12.125
- height	4.75
Weight (lbs, not including external electronics)	19.5
Synchronous speed (rpm)	1430

TABLE 4.5-6

Estimated ACS Weight and Power

Item		Weight (lb) Ea.	Weight (lb) Total	Power (watts) Ea.	Power (watts) Total	
Attitude Determination						
Earth Sensor (including electronics) (2)		4	8	5	10	
Sun Sensors and electronics (2)		1.5	3	1	2	
Subtotal			11		12	
Momentum Wheel						
Wheel	(1)	19.5	19.5	--	--	
Wheel Electronics	(1)	10.5	10.5	53	53	max.
				20	20	avg.
Subtotal			30		53	max.
					20	avg.
Control Electronics (ACS/APS)	(1)	6	6	20	20	max.
				10	10	avg.
Subtotal			6		20	max.
					10	avg.
Passive Damper	(1)	2.9	2.9			
Total			49.9		85	max.
					42	avg.

TABLE 4.5-7

4.5.4.1 Selection of a Preferred APS

Several propellants were considered for the reaction jets with particular attention given to ammonia and hydrazine. The required, relatively high thrust levels and large impulse values, together with the advanced state of thruster and feed system development and considerable amount of flight experience, made hydrazine the preferred choice.

A number of companies, including Hamilton Standard Division of United Aircraft, TRW/Systems, Rocket Research Corporation and Marquardt, have for some time been developing, testing and refining hydrazine feed system components and thrusters covering a wide thrust range. A variety of systems have been qualified, placed in production, and are in operational use on ATS, Intelsat and Air Force satellites.

Recent development has concentrated on the 0.1-lb. thrust level and on systems delivering millipound thrust levels. Catalytic thrusters at 0.5-lbF and above can be tailored for steady state or pulsed operation and are available in production models that have been qualified and flight proven. Table 4.5-8 provides summary data for some of these candidate hydrazine thrusters.

The spacecraft is spin-stabilized during its coast period in the transfer orbit and during its synchronous orbit injection and initial correction maneuvers. Following this, the vehicle is despun, its solar panels are deployed, and it is stabilized using a momentum wheel and jet torquers (3-axis). Attitude control thrusters at the 0.5-lb thrust level are needed to provide an adequate precession rate capability while spinning. Higher thrust levels are not needed because the satellite has been designed with a maximum moment of inertia about its stowed spin axis, thus making it inherently spin stable. This same thrust level can be used during the deployed operational mode because of the gyroscopic stability provided by the momentum wheel running at a high bias speed.

Redundancy trade-off studies are discussed in the following section as regards a preferred configuration of the 0.5-lbF thrusters to meet all attitude control requirements. Also, as will be further discussed therein, orbit control requirements

Catalytic Hydrazine Thrusters

Thrust lb F	Hamilton Standard	Rocket Research	TRW
5	ATS-III Flight Tested Intelsat IV Similar to III Development problems with hard seat torque motor valves.	MR 50A Lockheed P-95 Satellite; 4 thrusters per module. All mode operation - Blowdown pressurization. Second order of 120 units, 4 units to AVCO proposed for Mars Lander (Viking 1973)	Intelsat III system: Blowdown 3.5→1.2 lb F 90% steady state, 10% pulse (.080 on/.520 off) 2 redundant systems (2 tanks, 2 thrusters each)
1	Development Thrusters	MR 50A and MR 6A operated in the 1 lb-F range	Development thruster used for effect of environments on catalysts. (1967 Monopropellant Symposium)
0.5	Development Thruster	MR 6A thruster (classified HPM) 6 thruster, steady state operation, repressurization blowdown mode; supplying fourth system. Proposed for GE ERTS	Suggested for FHC ATS F&G; All mode operation with plenum or NH_3 for low thrust. (Proposed all ammonia system determined to be optimum)
.0.1	Proposed for GE ATS F&G Extensive valve-thruster test. Pulse mode (.075 and .100 sec) and life testing	MR74 All mode development thruster. Proposed to GE for ATS F&G. Units to be delivered to JPL.	Development Thrusters
Notes	Extensive analytical effort at UA Research Labs on catalytic bed processes. Data on Mid Range Thrusters, 5, 25, 15, 150, 200 lb-F	.05 lb-F Early development Proposed for Grand Tour mission Integrated plenum system delivered to GSFC	Plenum systems being flown on AF satellites

TABLE 4.5-8

while spinning can be fully satisfied by symmetric firing of a central pair of the 0.5-lbF thrusters aligned with the spin axis. Alternatively, appropriate pulsing of the outward firing jet on the + x side (near the plane of the spacecraft CG) can be used for orbit control in this mode. Orbit control following deployment will be effected by use of the latter jets, activated by ground command at the appropriate position in orbit.

For those jet configurations where a central jet(s) aimed through the CG parallel to the x axis (velocity vector) is considered for deployed orbit control, the 5.0-lbF thrust level is favored for fast, efficient orbit correction maneuvers, while still permitting flight proven thrusters to be chosen.

4.5.4.2 Thruster Configurations

Various configurations of jets (location and number) were studied in arriving at a preferred configuration that would meet all thruster requirements with full backup redundancy for any failed thrusters. The proposed 12-jet layout seen in Figures 4.5-2 and 4.5-13 was arrived at through the logic next discussed.

The four-thruster diagram (Figure 4.5-13) represents a minimal, non-redundant configuration. There is no redundancy in translational thrust along the spin axis while spinning. in spin/despin (with unbalanced forces) around the spin axis, nor in in-orbit translational thrust. Translational maneuvers can only be performed in one direction in orbit. Since there is no torque around the x axis, precession of the momentum wheel spin axis (y) in any inertial direction is accomplished by combining z axis maneuvers with y axis torqueing. Such maneuvers would mean moving the +z axis off the local vertical, possibly causing the antenna to lose the earth. Alternatively, by waiting until 6 hours later in orbit, torqueing about the z body axis could yield the same precession direction in inertial space.

It is seen that the 4, 8 and 12a jet configurations do not have a thruster dedicated solely to in-orbit translational maneuvers. These are accomplished by firing an appropriate pair of parallel spin/despin jets, with a pulsed attitude control duty cycle in case of a thrust imbalance.. With four jets there is no backup. With eight or twelve jets (as in 8 and 12a) failure of one spin jet would mean that orbital corrections could only be made in one direction in orbit.

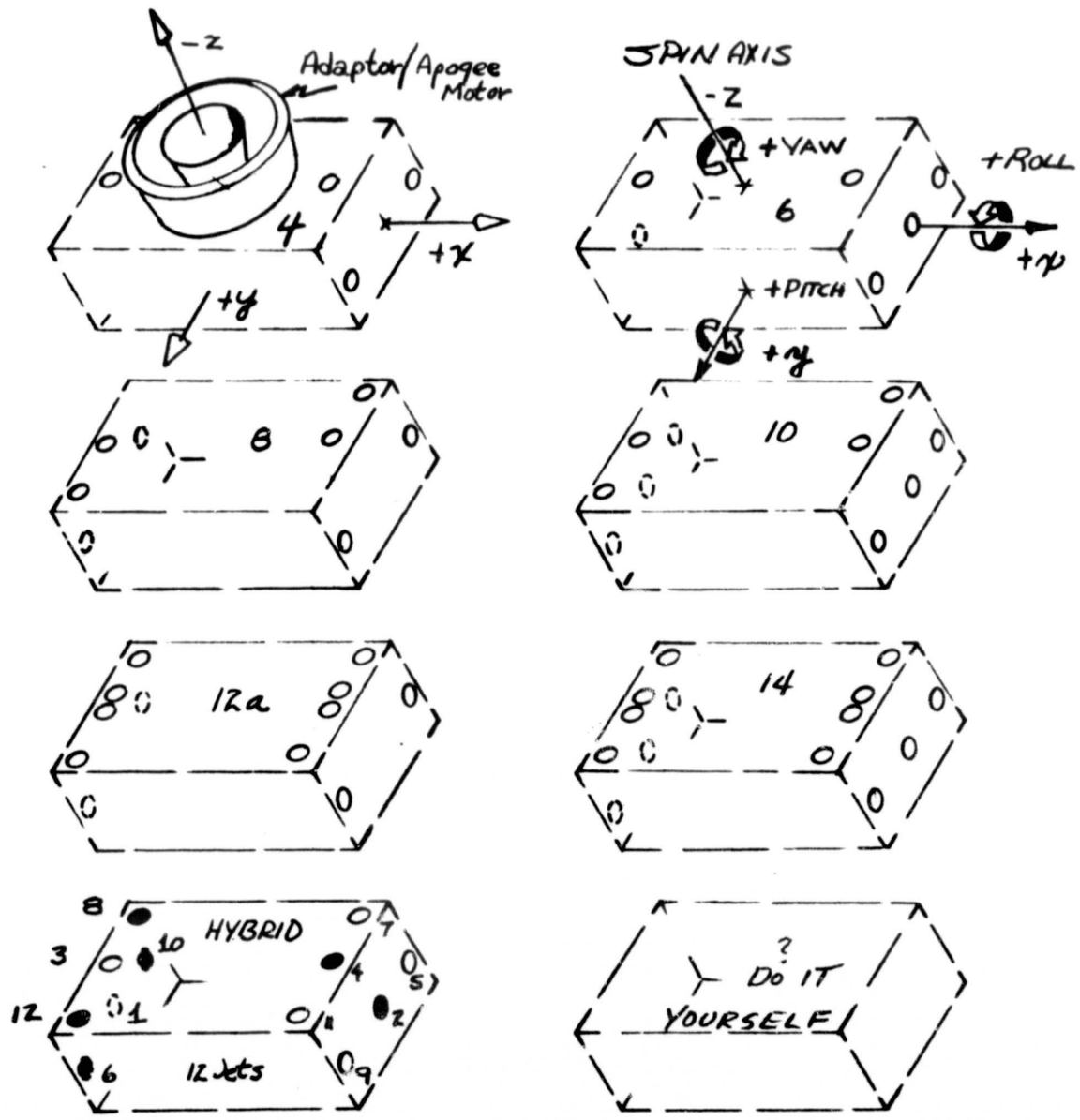


FIGURE 4.5-13 ALTERNATE JET CONFIGURATIONS

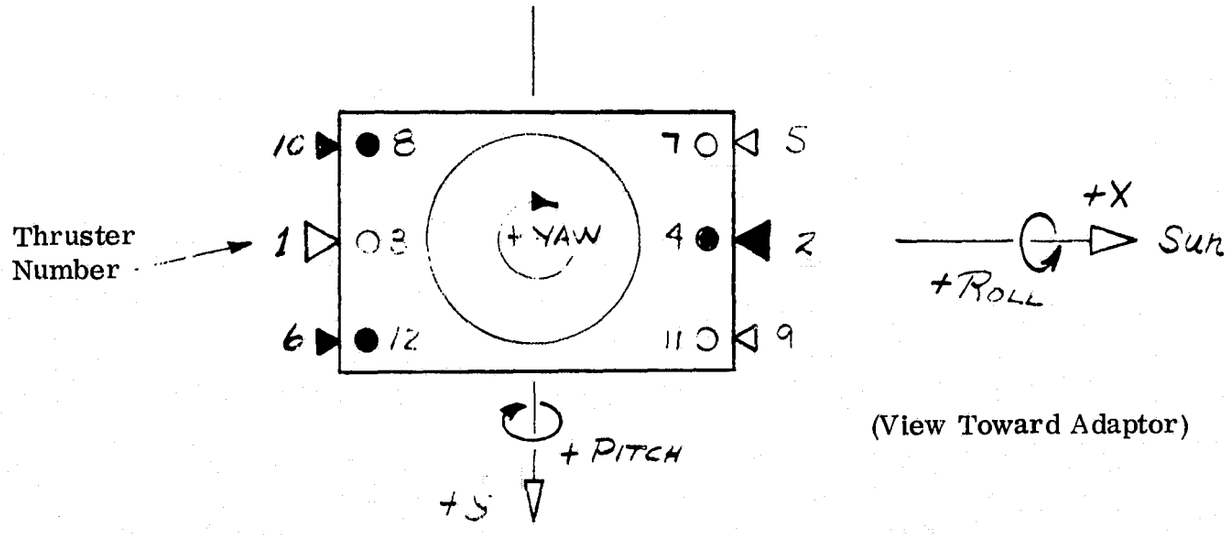
The eight-thruster configuration provides spin/despin couples around the spin axis with redundant single-thruster operation, an inefficient non-redundant torque around the x axis, and a redundant and coupled torque around the y axis. Failure of the x axis torquer would require going back to y axis maneuvers as a back-up to provide momentum wheel spin axis precession in any direction.

The 12a thruster configuration provides full redundancy for the jets on the adaptor side of the module. Instead of placing the four additional jets side by side with those on the eight jet diagram, they are, as shown, placed opposite. This has the advantage of providing not only redundancy, but an efficient torque around x. The backup mode for x axis torque is then the same as the normal mode for eight jets, meaning that there is no need for y axis maneuvers which move the +z axis off the local vertical and thus distrub the earth-pointing antennas. Another advantage of this configuration over the previous one is that redundant jets are provided for translational thrust along the spin axis while in the stowed mode. These jets are located midway between the stowed panels, thereby avoiding any contamination danger to the panels.

The right column of configurations shows what results when two opposing translational jets are added. If one of the two fails, its function can be taken over by the spin jets. In this case, the translation jets could be chosen with a greater thrust, i.e., 5 lbs, with all other jets at .5 lbs each.

Another option would be to add only one translational thruster and utilize symmetric thrusting of the spin control jets for backup translational maneuvers.

The twelve jet configuration, shown lower left, was tentatively selected as a suitable compromise between simplicity and redundancy. The thrusters are grouped on two isolatable manifolds (odd numbers/open symbols/System A and even numbers/black symbols/System B) to compensate for valve open or catalyst bed failures. Prime and backup jet utilization for this configuration is summarized in Figure 4.5-14 for the Hybrid orbital configuration. During the transfer orbit when the stowed satellite is spinning, the two central +z firing jets are used for precession and orbit control.



- Orbital Configuration -

	Roll		Pitch		Yaw		Translation
	+	-	+	-	+	-	
Primary (All Jets)	11 & 12	7 & 8	8 & 12	7 & 11	9 & 10 (Coupled Torques)	5 & 6	1 or 2
Backup (Sys. A fail)	12 & 4	8 & 4	8 & 12	4	10	6	6 & 10 or 2
Backup (Sys. B fail)	11 & 3	7 & 3	3	7 & 11	9	5	1 or 5 & 9

NOTES:

- Odd # Thrusters = Sys A; Even # = Sys B
- Thrusters # 1 & 2 = 5 lbF, # 3, 4, 5, 6, 7, 8, 9, 10, 11 & 12 = 0.5 lbF
- Thrusters torquing uncoupled except for primary yaw
- The Y axis (yaw) is the transfer orbit spin axis.
- Thrusters 3 & 4 used for spin precession and orbit control while spinning.

Figure 4.5-14 Hybrid Configuration, 12 Jet Utilization

Further jet configuration studies are needed to explore possible elimination or relocation of some of the thrusters. This could permit better use of the flexibility in inertial precession of the spacecraft y axis (normal to the orbit plane) that is made possible by body-mounted thrusters on the earth-oriented Hybrid.

4.5.4.3 Impulse Requirements and Propellant Load

The APS design to provide three axis attitude control and orbit control for the Hybrid has been sized to fulfill the following specific requirements:

- Partial despin from maximum initial 90 rpm of Delta third stage to 45 rpm.
- Approximate 127-degree yaw precession to apogee injection orientation.
- Initial synchronous orbit correction, consisting of a 360-degree spin axis precession and a velocity impulse (ΔV) of 300 ft/sec to correct in-plane errors only.
- Despin from 45 rpm to 0 rpm and acquisition of earth-referenced orientation.
- East-West station keeping and station repositioning, consisting of a ΔV of 35 ft/sec (7 ft/sec/yr x 5 yr) for station keeping and a ΔV of 25 ft/sec for repositioning.
- Stabilization for 5 years against the dominant solar pressure torque.
- Spin up of solar panels to 16 rpm for wheel failure backup mode.
- 50 percent attitude control contingency.

Propellant calculations were made using current values for spacecraft inertias and mass and thruster moment arms, and specific impulses of 200 seconds and 230 seconds for pulsed and sustained thruster operations, respectively. These calculations indicated a total propellant load of 50.6 pounds, with 18 pounds for

attitude control and 32.6 pounds for orbit control. As noted, a 50 percent contingency was included for attitude control. No such reserve was added for orbit control because of the very conservative velocity impulse value used (300 ft/sec) for synchronous orbit correction maneuvers.

4.5.4.4 APS Configuration/Layout

Figure 4.5-15 illustrates the location of the jets and propellant tanks in relation to the apogee motor within the equipment module. Redundancy considerations and the design goal of maximizing the spin axis moment of inertia dictated a multitank arrangement close to the center of gravity.

The four hydrazine tanks, equally spaced around the apogee motor, are connected in opposite pairs to two thruster manifolds (systems A and B) while crossover lines equalize ullage pressures for tank pairs. Latching isolation valves and an interconnect line are configured to allow either or both tank sets to feed either or both thruster manifolds. This allows freedom in isolating thruster and thruster valve open failures as well as preventing total propellant loss. Latching isolation valves allow periodic use of particular thrusters in either System A or B where other partially failed or degraded components exist, as well as use of residual propellant in isolated tanks. Systems A and B each provide a 3-axis torqueing capability and a translation or orbit control capability.

Tank volumes were determined using propellant density at 70^{o}F. A 33% ullage volume was added to allow blow down operation of the feed system. Detailed studies of thruster operation and performance at final tank pressure will be necessary to determine the optimum ullage volume and initial pressurization level. It may be desirable to include a small high pressure nitrogen bottle to repressurize the system to its initial level after partial propellant usage or as backup pressurization.

While solenoid valves remain a potential problem, concerted efforts in recent years by hydrazine system suppliers, in the areas of contamination control, materials selection, and mechanical design have resulted in a number of proven dependable designs. Further, the APS system has been designed with considerable flexibility and redundancy, both in propellant feed and in jet utilization, so as to ameliorate the effects of any valve failures. The estimated weight for the APS is itemized in Table 4.5-9. It totals 74.9 pounds.

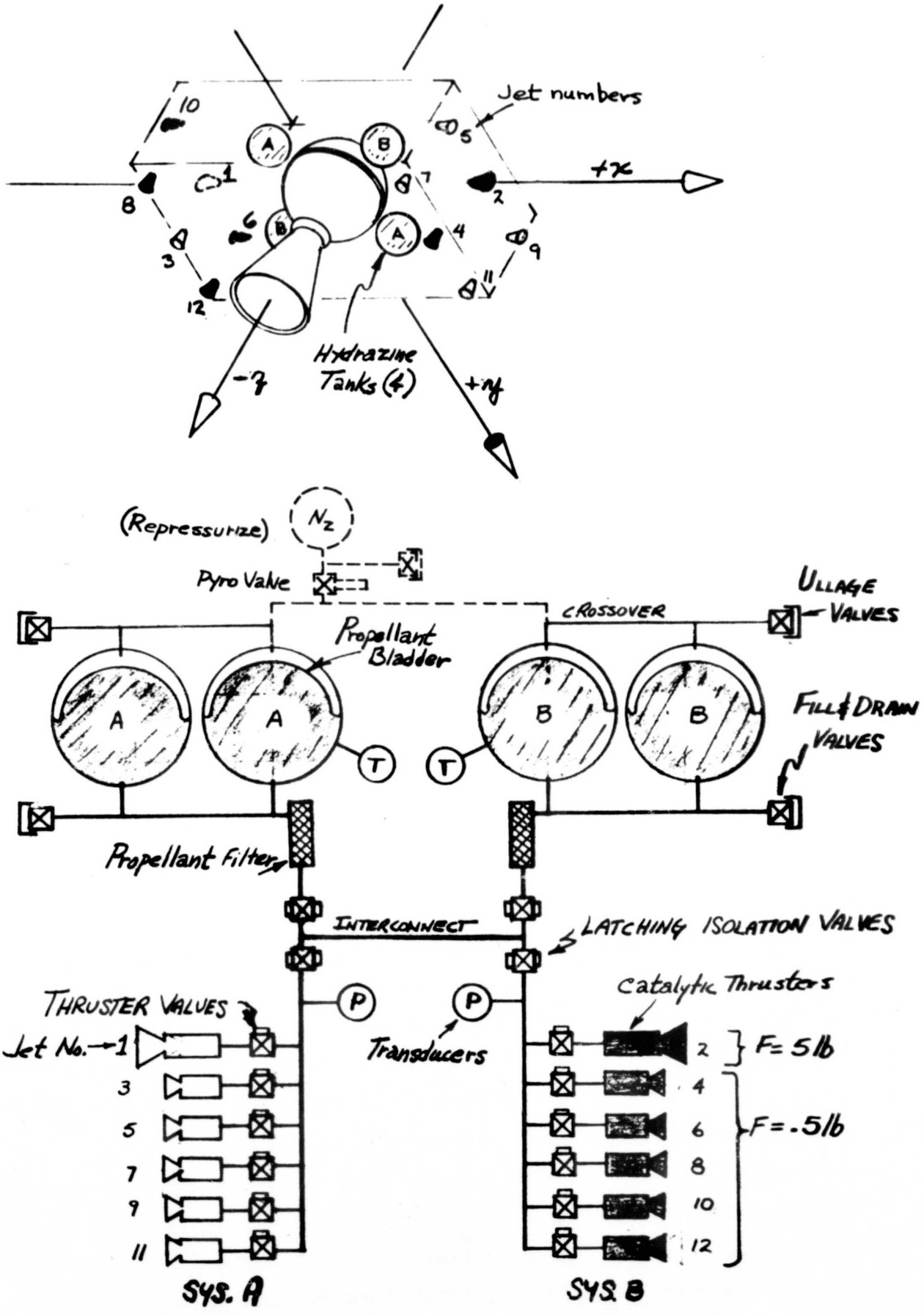


FIGURE 4.5-15 HYBRID CONFIGURATION

12 Jet, 4 Tank Schematic Layout

Table 4.5-9

Auxiliary Propulsion System Weight

Item	Quantity	Weight (each) (lbs)	Weight (total) (lbs)
Propellant Tanks	4 (11.5" dia)	2.3	9.2
Propellant			
Attitude Control			18.0
Orbit Control			32.6
Pressurant			1.0
Fill and Drain Valve	2	.28	.6
Pressure Transducers	2	.32	.6
Isolation Valve	4	.63	2.5
Thermocouple	2	.06	.1
Filter	2	.40	.8
Fitting and Lines		2.51	2.5
0.5 #F Thruster and Valve Assembly	10	.55	5.5
5.0 #F Thruster and Valve Assembly	2	.75	1.5
			74.9

4.6 COMMUNICATION SUBSYSTEM

4.6.1 INTRODUCTION

The communications subsystem possesses the necessary capabilities to perform aeronautical experiments in both the VHF and the UHF (L-band) frequency bands. These experiments consist of voice, digital data and surveillance signal relaying through the communications subsystem transponder from ground stations to aircraft on a two-way basis. Two equatorial synchronous satellites will be used to provide the required communications and surveillance functions. Dual satellite range surveillance is used and communications will be shared between the satellites. The assumptions used in this report are summarized in Table 4.6-1.

From Table 4.6-1 it is noted that a tradeoff must be made in order to establish definitive requirements for the communications subsystem. In particular, UHF and VHF RF link power budgets must be established for the spacecraft/aircraft transmission links to determine the number of voice and digital data channels which the satellite can support. These link power budgets are given in Table 4.6-2 for the UHF and VHF links. In the UHF case, the resultant carrier-to-noise density ratio (C/N_o) is given as a function of the spacecraft transmitter power, receiver or aircraft antenna gain, fading and receive system noise temperature.

The UHF C/N_o is given in Table 4.6-3 for four antenna gain values and for two receiver types; receivers with parametric and transistorized preamplifiers are considered. Different levels of signal fading and antenna temperatures are given for the different aircraft antenna gains. This is because low gain antennas are more susceptible to signals (multipath) and noise emanating from the earth.

The required DC power for links using the four specified aircraft antenna gains and the two receiver types are given in Table 4.6-4. The required RF power is that value necessary to meet the C/N_o values of Table 4.6-1 and the required DC power is three times the RF power. It is seen that the voice links require much more power than do the other links and have the greatest impact on the combination of channels that the spacecraft can support. The support limitation must be based upon the amount of regulated DC power available from the power subsystem. In section 4.9

Table 4.6-1

Assumptions

I Two ground stations - one station on each side of the Atlantic Ocean

II Transmission frequencies

a) Between satellite and aircraft:

VHF, 118 to 136 MHz

UHF, 1540 to 1655 MHz

b) Between Satellite and ground:

C-band

III Signal Channels

a) Voice:

- Maximum consistant with available power and assumed coverage.
- Carrier-to-noise Density Ratios of at least 49 dB-Hz per channel

b) Digital:

- Maximum consistant with available power and assumed coverage
- Carrier-to-Noise Density Ratios of at least 42.1 dB-Hz per channel

c) Surveillance:

- One channel at each frequency band per satellite having at least 43 dB-Hz C/N_o

IV Spacecraft UHF antenna gain of 23 dB. (for assumed coverage)

V Spacecraft VHF antenna gain of 11 dB.

VI UHF aircraft antenna gains of 2, 4, 7 and 12 dB to be considered.

VII VHF aircraft antenna gain of 0 dB.

Table 4.6-2 UHF & VHF Link Power Budgets

Parameter	Value UHF	VHF
Frequency, MHz	1600	118-136
Trans. Power, dB	P_T	P_T
Trans. Ant. Gain, dB	+ 23.0	11.0
Trans. to Antenna Loss, dB	- 1.0	- 1.0
Pattern Loss, dB **	- 3.0	- 1.0
Space Loss, dB	- 187.6	-166.6
Fading, dB	- FAD	- 6.0
Rcvr. Ant. Gain, dB	+ G_R	0
Rcvd. Signal Power, dBw	$P_T + G_R$ - FAD - 168.6	P_T - 163.6
Receiver Noise:		
Ant. Temp. ^oK (Sky + Sidelobes)	T_A	1,000*
Noise Figure, dB	F	3.0
Losses (L), dB	1.5	1.6
System Temp. (T_S), ^oK (L&F as Ratios)	T_A + 290 (LF-1)	2,550
Power Dens. (KT_S), dBw/Hz	-228.6 + 10Log T_S	-196.8
Carrier-to-Noise	$P_T + G_R$ - FAD - 10 Log T_S + 60	P_T + 33.2

* Nominal worst case. The normal operating antenna temperature is expected to be somewhat lower.

** At edge of coverage region.

Table 4.6-3 UHF Link Power Budget For Four Aircraft Antenna Gains

Mobile Antenna Gain, dB	2	4	7	12
FAD, dB	3	2.5	2	1.5
T_A, ^oK	330	200	150	150
System Temperature, ^oK				
2.3 dB Parametric Amp	730	600	550	550
4.9 dB Transistor Amp	1300	1170	1120	1120
Carrier-to-Noise Power Density Ratio Per Channel, db-Hz				
Parametric Amp	$P_T + 30.4$	$P_T + 33.7$	$P_T + 37.6$	$P_T + 43.1$
Transistor Amp	$P_T + 27.9$	$P_T + 30.8$	$P_T + 34.5$	$P_T + 40.0$

Table 4.6-4 UHF Transmitter Power/Aircraft Antenna Gain Tradeoff for Down Link

Signal Channel	Transmitter DC Power, Watts* Aircraft Antenna Gain, dB			
	2	4	7	12
1 - Voice				
Parametric	216	102	42	12
Transistor	387	198	84	24
1 - Digital				
Parametric	44	20	8	3
Transistor	78	40	17	5
1 - Surveillance				
Parametric	55	26	11	3
Transistor	98	52	21	6

* Assumed 33% transmitter efficiency

Note:

Method of multiplexing multiple channels has not been chosen. Therefore, straight power addition may be assumed when considering multiple simultaneous channels.

it is stated that the power subsystem can provide 550 watts of regulated DC power. Of this amount, only about 400 watts can be made available to the communications subsystem.

The DC power required to support the VHF links is tabulated in Table 4.6-5. These values were obtained by equating the VHF C/N_o of Table 4.6-2 to the required C/N_o of Table 4.6-1. These calculations assumed aircraft VHF antenna gains of 0 dB.

Tables 4.6-4 and 5 provide a measure of the required transmitter DC power for each type of signal channel; the resultant power requirement for multiple simultaneous channels may then be approximated by straight addition of the per channel requirements. This approximation was used to plot the curves in Figure 4.6-1. In the figure, 1 VHF and 1 UHF refer to a group of 1 voice, 1 digital and 1 surveillance channels transmitted at VHF or UHF, respectively; similarly, 2 VHF and 2 UHF refer to 2 voice, 2 digital, and 1 surveillance channels. The figure shows three groups of curves plotted as a function of aircraft antenna gain: 1) 1 and 2 UHF with no VHF, 2) 1 and 2 UHF with 1 VHF and, 3) 1 and 2 UHF with 2 VHF. The figure also shows the points corresponding to 1 and 2 VHF channel groups.

The spacecraft system proposed in this report provides 400 watts of DC power to the transmitters and corresponds to a spacecraft weight margin of nine percent as shown in Figure 4.6-1. The point where this line intersects any of the curves indicates the required aircraft UHF antenna gain to operate with the proposed spacecraft when the indicated simultaneous channel combinations are set up; these points are tabulated in Table 4.6-5A. The maximum channel capability is taken as 2 UHF and 2 VHF as shown in the transponder block diagram in Figure 4.6-2. Figure 4.6-1 shows a 5 dB aircraft UHF antenna is required to operate with 2 UHF and 2 VHF channels simultaneously. While gains as high as 5 dB can be obtained with the simpler antennas such as slot-dipole and cavity backed spirals, the gain over most of the antenna field of view would be more like 4 dB.

The main feature of the curves in Figure 4.6-1 is the way the aircraft antenna gain must increase in order to increase the spacecraft weight margin.

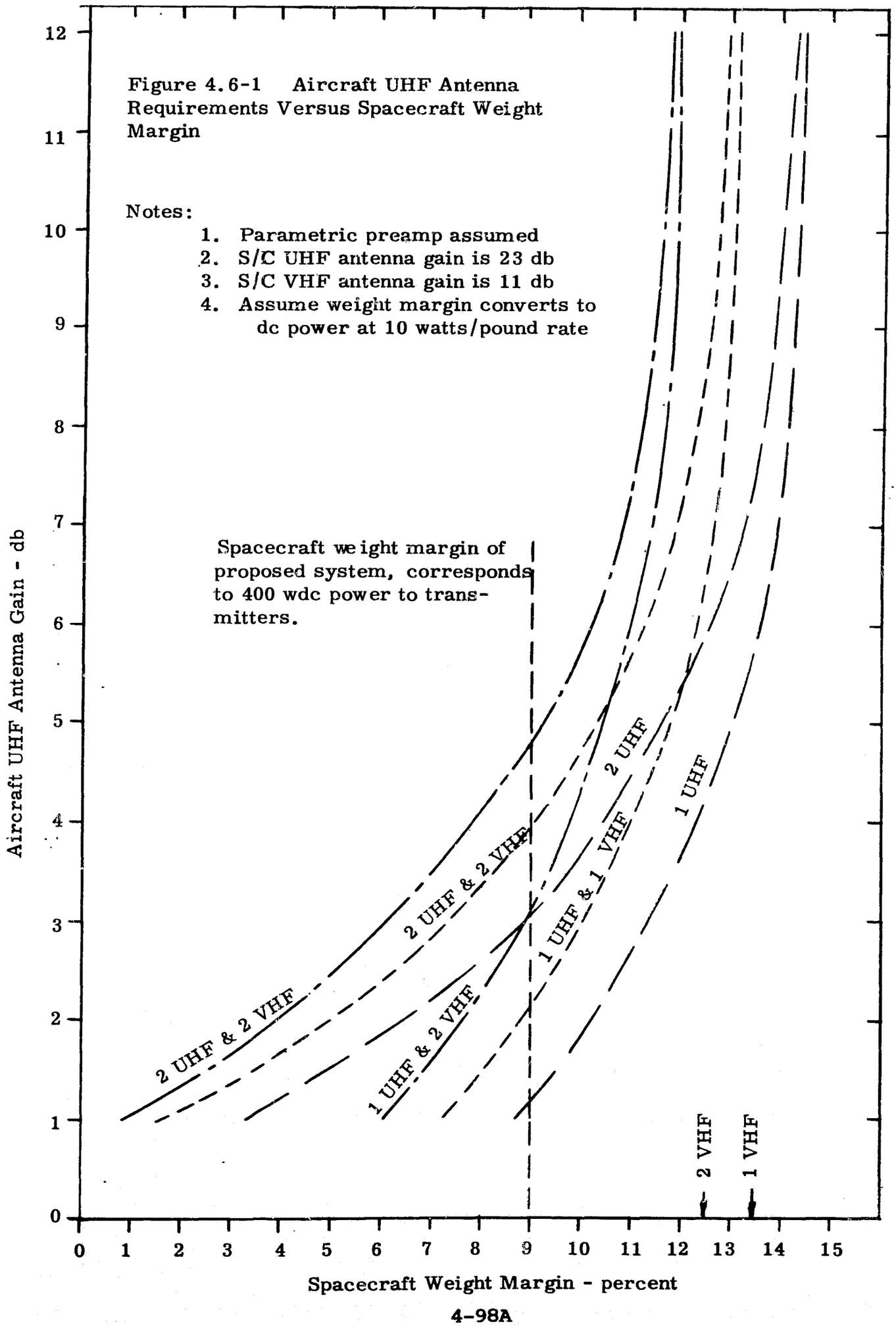

Figure 4.6-1 Aircraft UHF Antenna Requirements Versus Spacecraft Weight Margin
Notes:
1. Parametric preamp assumed
2. S/C UHF antenna gain is 23 db
3. S/C VHF antenna gain is 11 db
4. Assume weight margin converts to dc power at 10 watts/pound rate
Spacecraft weight margin of proposed system, corresponds to 400 wdc power to transmitters.
2 UHF & 2 VHF
2 UHF & 2 VHF
1 UHF & 2 VHF
2 UHF
1 UHF & 1 VHF
1 UHF
2 VHF
1 VHF
Aircraft UHF Antenna Gain - db
Spacecraft Weight Margin - percent
0 1 2 3 4 5 6 7 8 9 10 11 12 13 14 15
0 1 2 3 4 5 6 7 8 9 10 11 12

Table 4.6-5 VHF Transmitter DC Power Requirements

Signal Channel	Power* (watts)
1 - Voice	63
1 - Digital	13
1 - Surveillance	16

* Assumes transmitter efficiency of 60%. Laboratory VHF power amplifiers have been operated with efficiences up to 80%. Therefore, it is reasonable to expect that 60% efficiency could be achieved in a practical spacecraft transmitter design.

Note:

Method of multiplexing multiple channels has not been chosen. Therefore, straight power addition may be assumed for a first order analysis. However, present frequency assignments in the VHF band may severely restrict the freedom to choose a multiplexing method. The assumption of straight power addition is therefore optimistic.

Table 4.5-5A Required Aircraft UHF Antenna Gain for Indicated Operating Mode

Operating Mode	Minimum Gain (dB)
1 UHF	1
2 UHF	3
1 UHF and 1 VHF	2
1 UHF and 1 VHF	4
1 UHF and 2 VHF	3
2 UHF and 2 VHF	5

If the weight margins were to be increased from 9 to 11 percent by reducing DC power, the aircraft antenna gain would need to be increased on the order of 2 dB. The trend of the curves indicates that even a 12 dB aircraft antenna would not be adequate if the weight margin were increased to 15 percent - a margin which is very desirable at this early point in time. The data in Figure 6.4-1 is accurate only in the vicinity of the 9 percent margin line; for margins greater than about 11 percent and less than about 7 percent, the intent of the curves is only to show the trend.

The UHF and VHF links in the reverse direction (aircraft-to-satellite) will perform at about the same level as the satellite-to-aircraft links. The aircrafts would be capable of supporting power amplifiers somewhat more powerful than those used in the satellite; and low noise preamplifiers can be used in the satellite. Earth based interfering signals may be the major problem area.

The transmission frequency for the links between the satellite and ground stations could be VHF, UHF or C-Band. Since the larger ground stations now in existence are equipped for C-Band operation, it is assumed that the Hybrid system will also use C-Band. The Hybrid system could then operate with the 40-foot antenna located at Mojave, California, the 85-foot antenna at Rosman, North Carolina and the NASA 40-foot transportable stations. The RF links would operate at frequenciew in C-band.

The RF power budget for the C-band links are given in Table 4.6-6 for an assumed 40-foot ground antenna. The satellite antenna gain at 4000 MHz is chosen to be 12.6 dB minimum and will result in about 1 dB of pointing loss at the extreme limits of coverage. The resulting C/N_o at the ground terminal is then 74.1 dB above the transmitter power. Now, if all five of the channels (2 voice, 2 digital and 1 surveillance) are amplified in one power amplifier, the required RF power is as shown in Table 4.6-7. When the C-band link is given a 10 dB margin over the VHF or UHF links, and an allowance of 3 dB is assumed for linearization, the required total RF power is 156 milliwatts. This level of RF power can be obtained with solid state devices at 4000 MHz and would require less than about 2 watts of DC power. In the case of the C-band up-link, more RF power is required but kilowatts of power are available at the ground stations at 6000 MHz.

In summary of the above discussions and link performance tradeoffs, a table of nominal RF amplifier power levels has been developed and is given in Table 4.6-8.

Table 4.6-6

C-Band Link Power Budget

Parameter	Up-Link	Down-Link
Frequency, MHz *	6,000	4,000
Transmitter Power, dBW	P_T	P_T
Trans. Antenna Gain, dB	+ 54.5	+ 12.6
Space Loss, dB	-200.0	-196.4
Antenna Pointing Loss, dB	-1.0	-1.0
Atmospheric loss, dB	-0.4	-0.7
Rcvr. Ant. Gain (40 ft), dB	+ 12.6	+ 51.0
Rcvd. Signal Power, dBW	P_T - 134.3	P_T -134.5
Receiver Noise:		
Antenna Temp. (T_A), °K	290	40°
Receiver Temp (T_R), °K	1160	60°
Noise Density (KTs), dBW/Hz	-197.0	-208.6
Carrier-to-Noise Power Density Ratio, dB-Hz	P_T + 62.7	P_T + 74.1

* Nearly identical results will be obtained if the 5000-5250 MHz aeronautical band is used since constant area and constant gain antennas are assumed at opposite ends of the link.

Table 4.6-7 C-Band Transmitter Power Requirements

Signal Group (All On One Carrier)	Required Transmitter Power	
2 - Voice Channels (C/N_0 = 59 dB-Hz/CH)*	17.9 dBm	62 milliwatts
2 - Digital Channels (C/N_0 = 52.1 dB-Hz/CH)*	11.0	12
1 - Surveillance (C/N_0 = 50.0 dB-Hz/CH)*	6.0	4
Total Signal Power	18.9	78
Intermodulation Loss, (3 dB)	3.0 dB	78
Total Power Required	21.9	156

* The C-Band C/N_0 requirements are taken to be 10 dB greater than the VHF and UHF values so that noise contributions from the satellite-ground links are negligible.

Table 4.6-8 Power Amplifier Requirement Summary

Signal	RF Power, Watts		
	UHF	VHF	C-Band
1 - Voice	70[1] 40[2]	50	-
2 - Voice	70[3]	100	-
2 - Digital	50[4] 30[5]	20	-
1 - Surveillance	15	10	-
2V, 2D & 1S	-	-	0.2

Notes:

(1) To operate with G_A = 2 dB and parametric amplifier or G_A > 4 dB and transistor preamp.

(2) All cases except as noted in Note 1.

(3) To operate with G_A = 4 dB and parametric preamp.

(4) To operate with G_A = 2 dB and transistor preamp.

(5) All cases except as noted in Note 4.

4.6.2 COMMUNICATIONS TRANSPONDER DESCRIPTION

The proposed communications subsystem uses an integrated transponder as shown in Figure 4.6-1A. Signals received at VHF, UHF, or C-Band are down converted to a common IF of 136 MHz. A switching matrix is then used to select one of three IF amplifiers. The signal is down-converted again to a frequency of 40 MHz, level adjusted, filtered, and then routed to the proper up-converter and power amplifier through a second switching matrix. By integrating the transponder as shown, a much more flexible and adaptable system is obtained. A received signal can be routed through any of the three IF amplifiers, of which only two are required at one time. Thus full IF redundancy is obtained with only one additional amplifier.

A TDA preamplifier is proposed for the C-Band link while a transistorized preamplifier is proposed for the VHF link and a parametric amplifier is proposed for the UHF link receiver. A parametric amplifier is proposed at UHF since the associated noise figure is about 2.5 dB better than for a transistor amplifier Additionally, a parametric amplifier is assumed at some of the aircraft terminals on the UHF down-link, and hence may be available for satellite use.

The two down-converter mixers for the UHF and C-Band receivers are commercially available. Mixers with doubly-balanced Schottky diodes will be used at both UHF and C-Band. The first IF is selected to be at 136 MHz and thus VHF requires no mixer.

The IF distribution switching matricies are implemented by the use of single-pole double-throw relays. These relays are connected to achieve the multipole, multithrow functions required by the system. The relays proposed are miniature (Teledyne 420 series) and are mounted in a TO-5 can. The small size of the relay minimizes stray capacitance and makes it suitable for use at frequencies well above 136 MHz.

The RF power amplification configuration is shown to the right of the transponder block diagram. At both VHF and UHF it is proposed to turn on (by ground command) individual low power transmitters as needed. Output of the transmitters will be added by switching in appropriate RF combining circuits. The

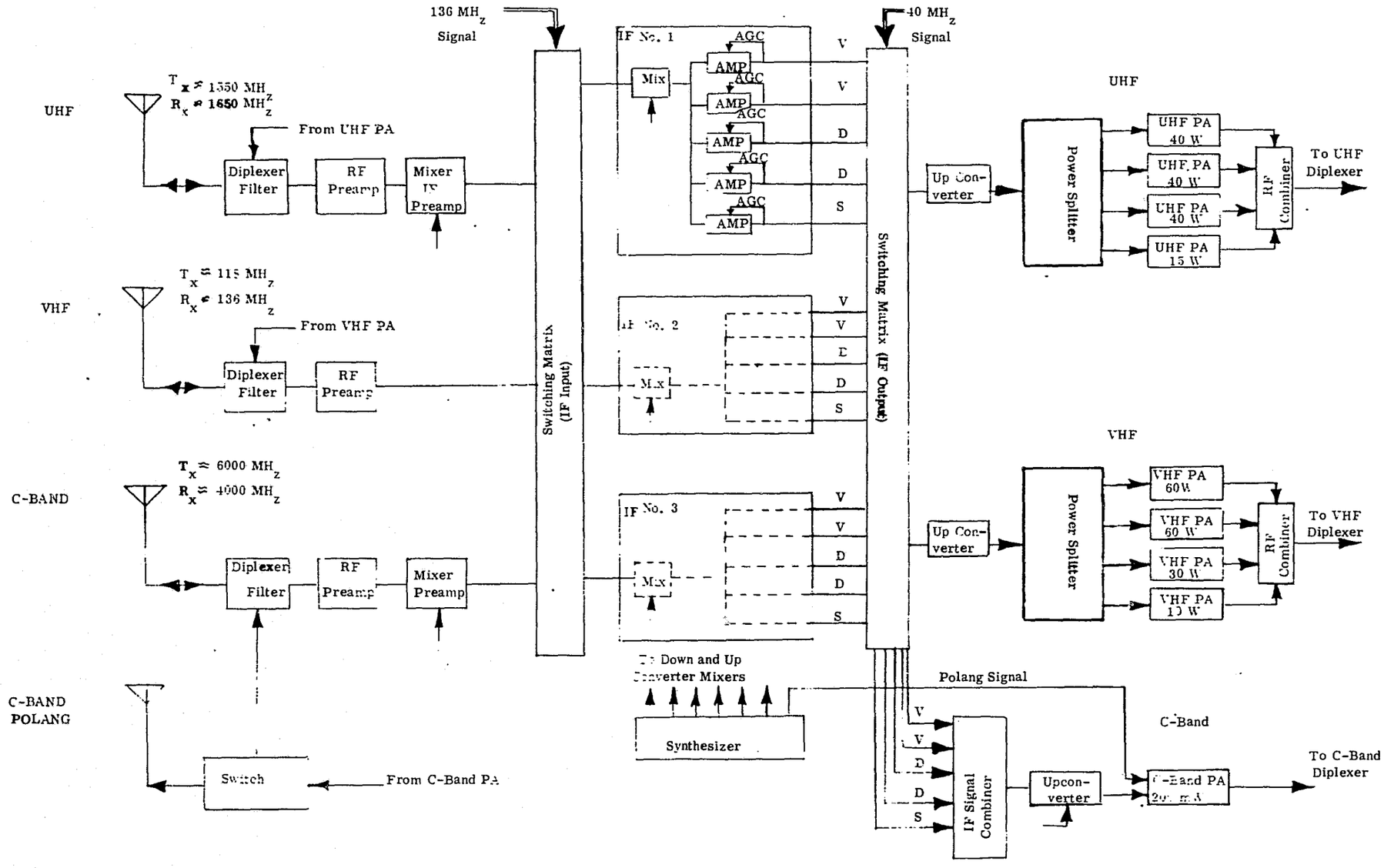


FIGURE 4.6-1A. INTEGRATED COMMUNICATIONS TRANSPONDER

significance of this approach is that three identical 40 watt amplifiers can be used at the 1550 MHz UHF-(L-Band) frequencies. At the 40-watt level solidstate amplifiers can be used instead of traveling wave tubes.

The use of 40 watt amplifiers at UHF instead of 65 watts (2 dB less power) means that the aircraft antenna gain must be at least 4 dB to meet the assumed 49 dB-Hz C/N_o voice channel requirement. Actually, a 2 dB antenna gain would provide a reduced quality but useable link. Also, voice modem designs are continuously being improved and projections indicate that the required C/N_o may be reduced from 49 dB-Hz to about 46 dB-Hz in the near future.

At VHF, separate 60 watt amplifiers are used for the two voice channels. Again, the advantage of 60 watts at VHF is that solidstate amplifiers become practical. Also, amplification of the voice signals in separate amplifiers eliminate the problem of intermodulation in the amplifier. Adequate frequency separation is required to permit low-loss RF power combining.

During the ATS F&G study, numerous trade-offs were conducted by Fairchild Hiller and Philco-Ford comparing a TWTA vs solid-state amplifiers for L-Band power amplifiers. The reduced cost and weight associated with the solid-state amplifiers led to the use of transistor amplifiers (one at 1800 MHz, and one at 1550 MHz) rather than a single dual mode TWTA.

A block diagram of the proposed configuration for each of the amplifiers is shown in Figure 4.6-2. The 1800 MHz amplifier uses four RCA TA7205 transistors in parallel to produce 20-W output power. The output stage is preceded by five single transistor stages which provide more than 30 dB gain and raise the up-converter output level to that required to drive the output stage. The 1550 MHz amplifier uses eight parallel-combined RCA TA7205 stages to produce 40-W output power. The output stage is driven by two similar stages in parallel, preceded by four single transistor drive stages.

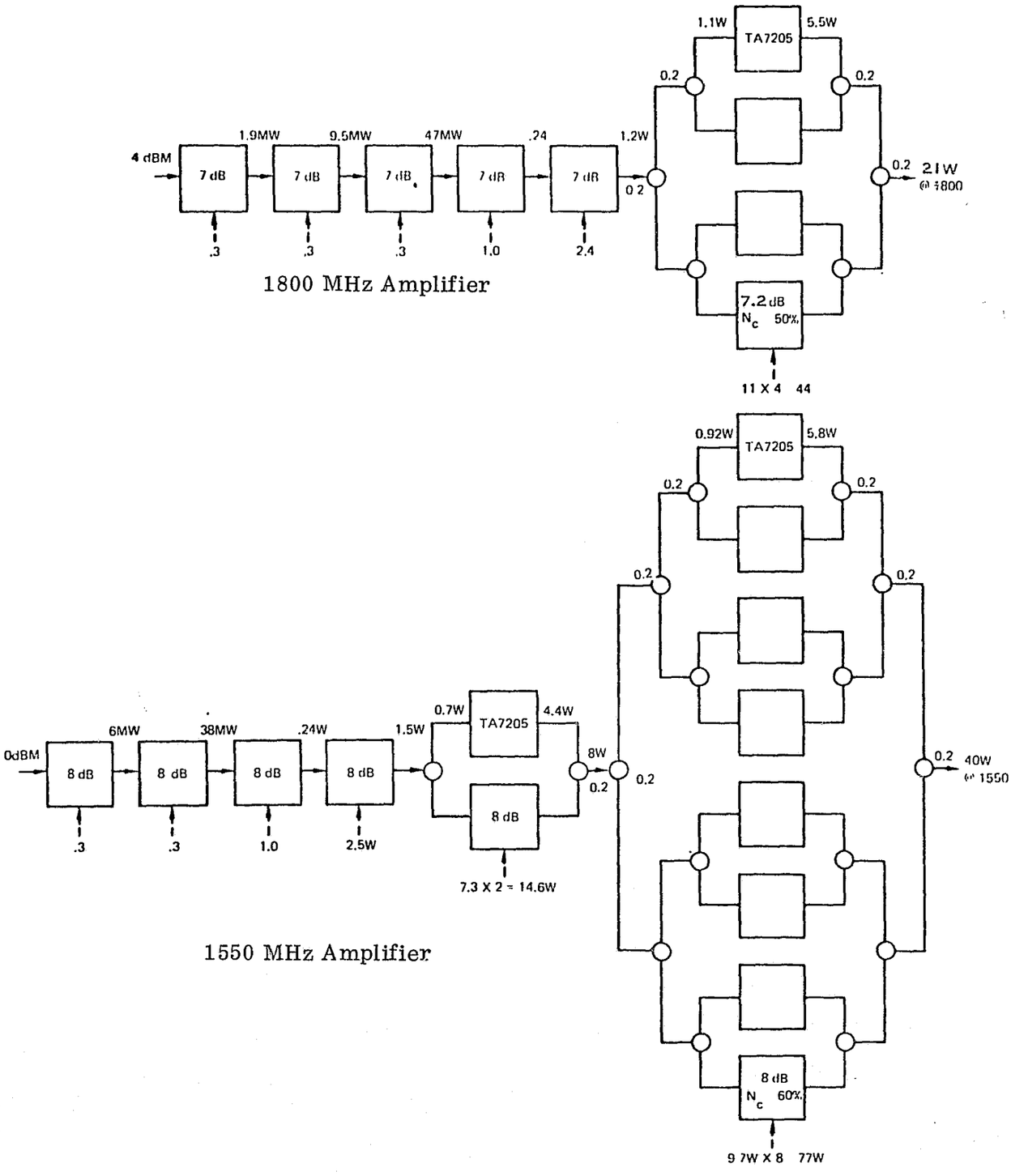


Figure 4. 6-2 Solid State L-Band Power Amplifier Configurations

Comparison of TWTA and Solid State Approaches

A comparison of the relative advantages of TWTA and solid state amplifiers for the L-band power amplifier is given in Table 4.6-9. As may be seen from the table, the solid state approach results in higher dc-to-RF efficiency, lower weight, and considerably lower cost.

The TWTA efficiency averages 26%. The efficiency of the transistor amplifier is conservatively rated 33%, with experimental data to date in vicinity of 40%. The more pessimistic efficiency numbers have been used, because of the possibility that the transistor operating voltage may have to be reduced, to lower the stress levels. In addition, lower power levels may be necessary, in order to reduce the junction temperatures. Further improvements in the amplifier efficiency as part of the flight model development cycle would probably result in an efficiency between 35 and 40% including temperature margins and yield margins for such factors as transistor matching and batch variations.

The total weights of the two approaches differ significantly, with two TWTA's 10 lb. vs. two transistor amplifiers at 4 lb. The weight of the transistor configuration could be reduced from that shown by careful design and more sophisticated packaging if desirable.

Reliability estimates based on parts counts and previous flight history show the transistor amplifiers to be superior.

Table 4.6-9

Comparison of TWTA and Solid State
L-Band Power Amplifiers

	TWTA	Solid State
Efficiency	26%	32%
Weight	10 lbs	4 lbs
Reliability	0.991	0.9998
Relative Cost	1.0	0.3

ATS Breadboard Results

Breadboard design and test of several L-band power amplifiers was carried on in order to assess the feasibility of the solid-state amplifier approach and to provide better definition of various performance parameters such as gain, efficiency, bandwidth, and stability. Tests were made on both single stage and multiple stage amplifiers. The results of this breadboard work is described below.

Single Transistor Amplifier Design and Construction

The breadboard amplifiers used the RCA TA7205 transistor. This transistor is rated to deliver 6 watts RF at L-band with a gain of 7 dB and collector efficiency of 50%. The coaxial package of this transistor results in very low emitter and collector lead inductances which eases matching to input and output 50-ohm lines and allows good heat conduction from the collector stud. The TRW 2N5483 was also evaluated, but performance was found to be less satisfactory with this device. Both stability and bandwidth were poorer due to higher lead inductances.

The TA7205 transistor in a coaxial cavity design may be operated with good gain at frequencies up to 2300 MHz. However, a strictly coaxial layout poses problems in regard to electrical tunability and heat conduction from the collector. Therefore, a "hybrid" approach was chosen in the design of the Philco-Ford amplifier which places the transistor in a coaxial mount but uses microstrip circuits for input and output matching.

The electrical equivalent circuit of the amplifier is shown in Figure 4.6-3. . The low impedances of emitter and collector are matched to the 50 ohm input and output lines by stripline sections of 8 and 7 ohms characteristic impedance. The dc blocking capacitors are placed in the input and output lines. Chokes and bypass capacitors are arranged in the usual way to provide collector dc supply voltage and to self bias the emitter in the event of large overdrive or instability during RF tuning. The shunt capacitor in the output is used for tuning of the output match.

Details of the mechanical design are illustrated in Figure 4.6-4. The transistor is mounted coaxially into a hole in a block of aluminum of which the upper and lower surface is used as ground plane for the input and output striplines. The 7- to 10-watts of dissipated dc power in the collector must be conducted from the collector stud to the block. A beryllium oxide ring in the collector mount serves this purpose. No detectable thermal slump of the output power after switching on the amplifier has been observed, which demonstrates that the heat sinking provisions are satisfactory.

Single Transistor Amplifier Performance

The measured performance of the 1800 MHz amplifier module is shown in Figures 4.6-5 & 6 . This initial data was taken with a voltage of 28 V. More recent tests conducted at 25 V indicates very similar results.

Figure 4.6-5 shows output power and collector efficiency for 1-W input power and a collector voltage of 28 V in the frequency band from 1760 to 1860 MHz. At each test point, the output shunt capacitor was retuned for maximum power output. Power output is essentially constant at 5-1/2 W and efficiency increases with frequency from 50 to 55%.

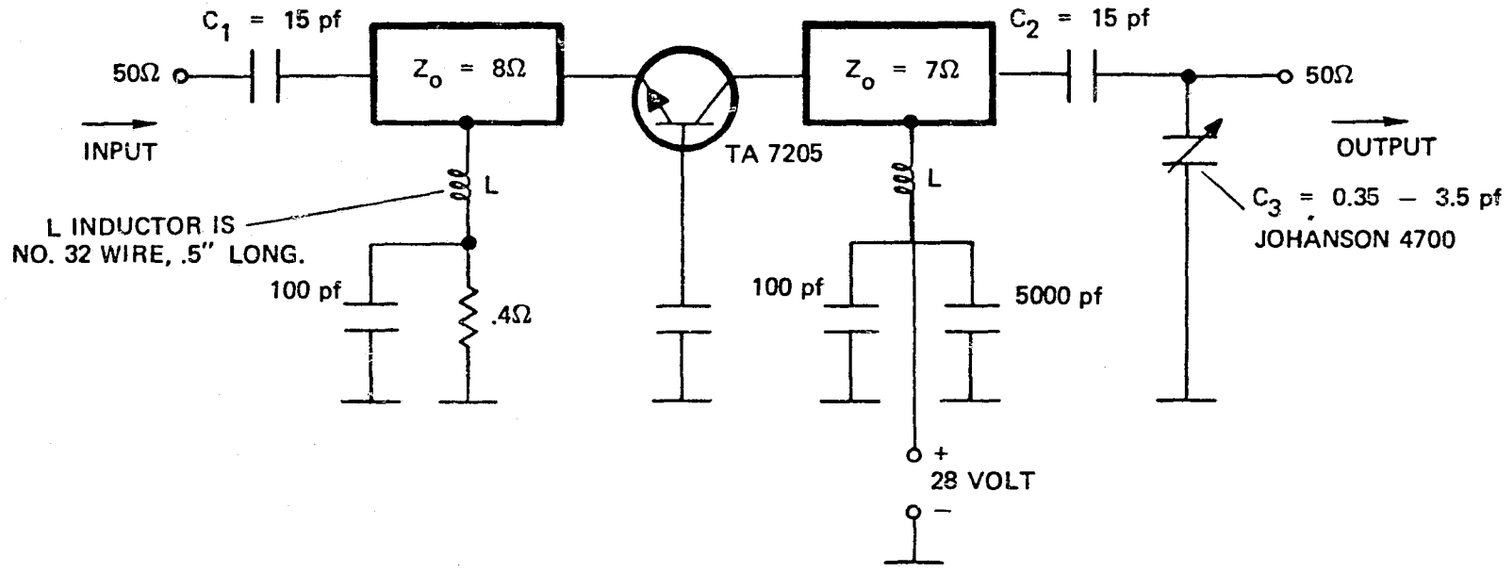


Figure 4.6-3 1800 MHz Amplifier - Equivalent Circuit Diagram

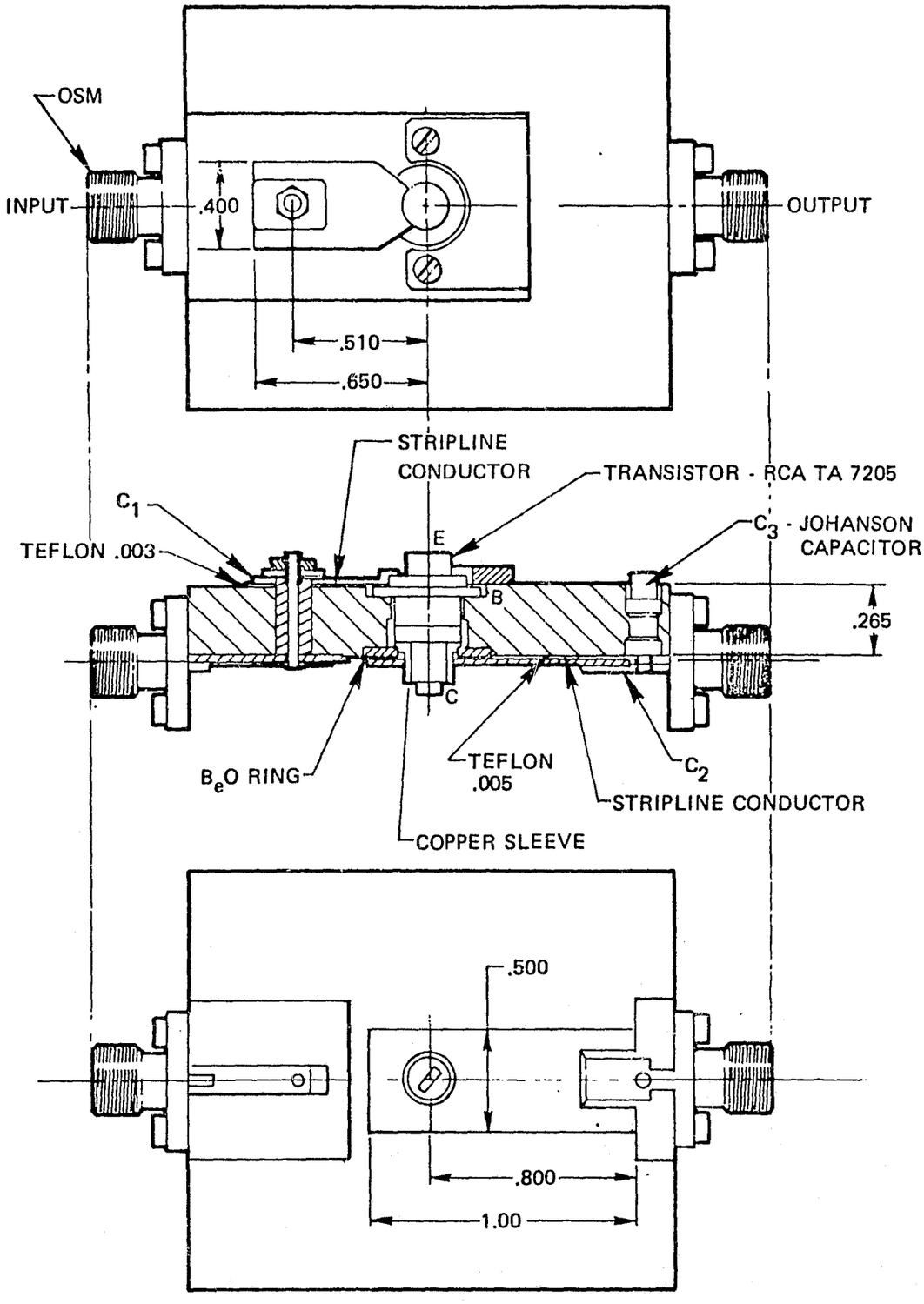


Figure 4.6-4 Power Amplifier Mechanical Design

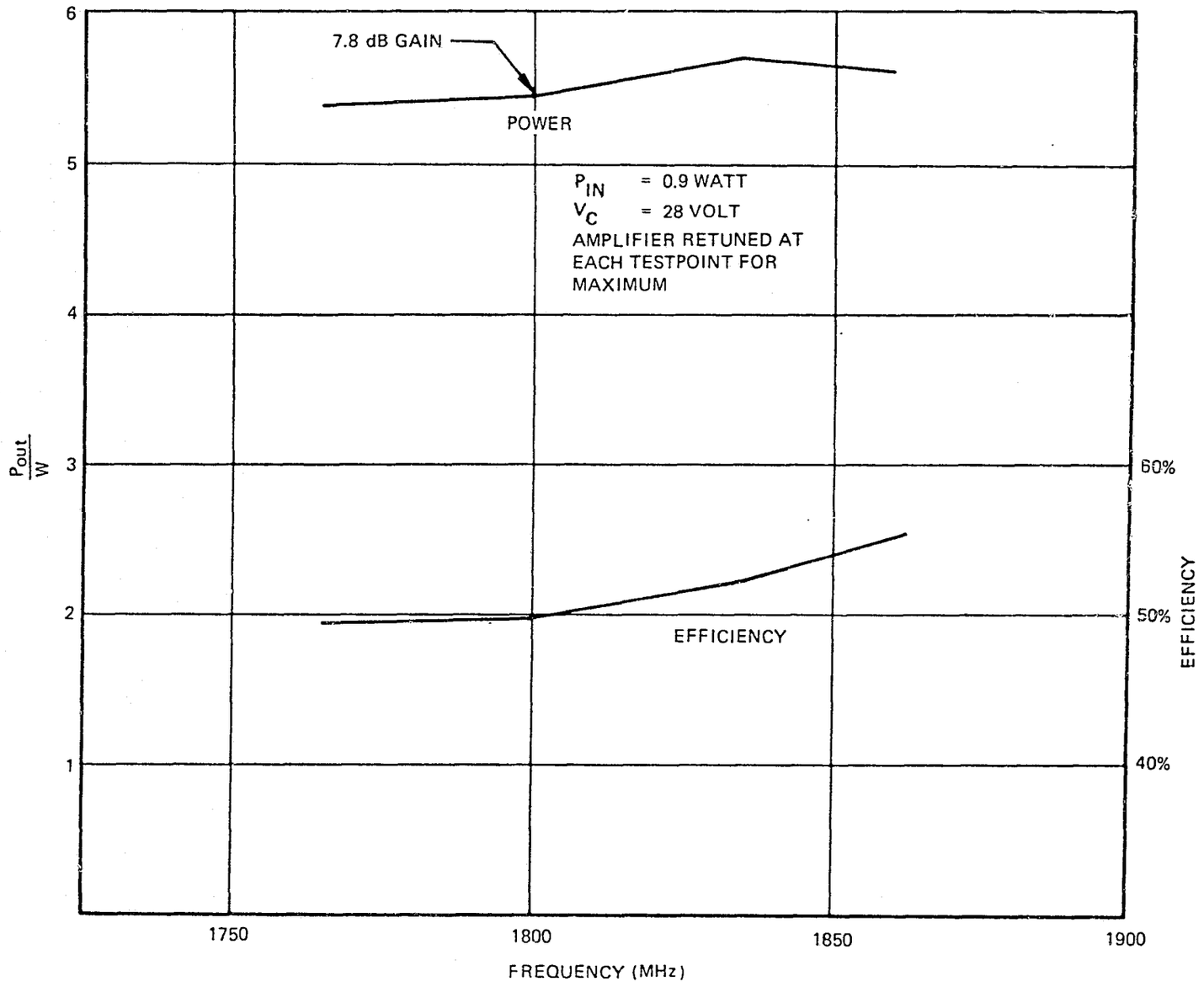


Figure 4.6-5 L-Band Power Amplifier Performance (with Collector Retuning)

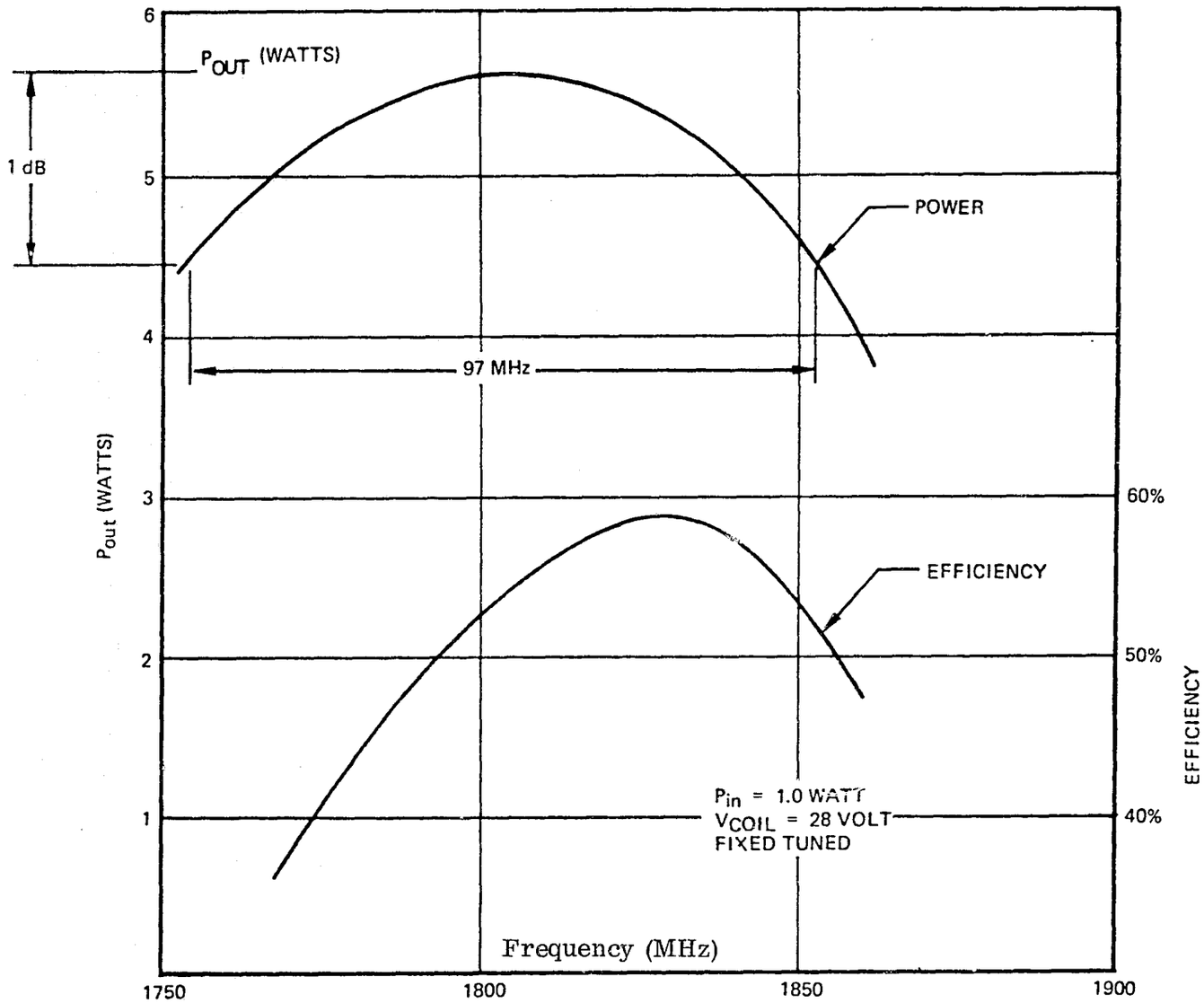


Figure 4.6-6 L -Band Amplifier Performance (Fixed Tuned)

Figure 4.6-6 shows output power and collector efficiency of the same amplifier fixed tuned for optimum performance at 1800 MHz. The 1-dB bandwidth is about 97 MHz. Notice that the efficiency peak at 1860 MHz is not coincidental with the maximum power.

At VHF frequencies (118 MHz), power transistors are available which can produce more than 30 watts output per stage. Paralleling of two such stages to produce the required 60 watts output will be much less difficult than at UHF. DC-to-RF efficiencies of 60% can be achieved in the VHF band. The 10 watt and 30 watt amplifiers will utilize the same driver stage as used with the 60 watt amplifiers.

The C-Band power amplifier requirement is for nominally 200 m W and will be obtained easily with solid state devices. Just recently Microwave Semiconductor Corporation introduced the MSC 3005 power transistor. The MSC 3005 has produced 5 watts at 3 GHz with a gain of 5 dB and 30 percent efficiency. This device should be capable of producing 0.2 watts at 3.7 to 4.2 GHz without much difficulty.

The IF amplifiers use double conversion in order to obtain a frequency where the closely spaced narrow band signals can be properly filtered and level controlled. Crystal filters are commercially available with center frequencies up to about 60 MHz and bandwidths from 0.01 percent to 3 percent of the center frequency. The proposed signal bandwidth is about 100 kHz. This bandwidth will insure that all signals are adequately filtered so that negligible RF power will go into noise. It is also wide enough to accommodate the signals with instabilities on the order of 1 PPM and doppler shifts that could be experiences with high speed aircraft.

The transponder uses a frequency synthesizer to develop the local oscillator signals (approximately 15 required). This approach minimizes the number of oscillators required and simplifies the design requirements to stabilize the oscillators.

4.6.3 COMMUNICATION ANTENNAS

4.6.3.1 C-Band Earth-Viewing Horn Antenna

The C-band earth-viewing horn antenna must provide an antenna pattern which covers the ground stations, as viewed from synchronous orbit. The angular separation of the ground stations (with one located on the U. S. East Coast and the other on the European West Coast) will not exceed 13^{o} or so. The width of the beam in the North-South direction is not critical. A minimum coverage of 9^{o} is sufficient. The requirements on the antenna may be summarized as follows:

Frequency - Transmission over the frequency range of 3700 to 4200 MHz and reception over the frequency range of 5900-6400 MHz.

Gain - Gain of 11.6 dB minimum in the direction of the ground stations, at the transmitting frequencies. Gain on reception may be as low as 0 dB.

Polarization- Polarization to be linear.

To fulfill these requirements, a simple electromagnetic horn, rectangular in shape, is proposed. The aperture dimensions of the horn are 4.75 inch (H-plane) and 7.35 inch (E-plane). The length of the horn is 12 inches; this length permits a total flare angle of 40^{o}. The gain in the direction of the ground stations (assumed to be 6.5^{o} off-axis, or less) is 14.1 dB at the low end of the transmit band (see Table 4.6-10). The margin on the critical down-link is thus 2.5 dB; as a consequence, the C-Band transmitter may be reduced from a power level of 200 mw to just over 100 mw. Alternatively, the size of the C-band horn could be reduced.

The gain of the horn on receive is 18.4 dB (6400 MHz) -- a value much in excess of what is needed. In view of the fact that the size of the horn is dictated by transmit requirements, the large receive gain is achieved at no penalty to the spacecraft.

Table 4.6.10

Performance of C-Band Earth-Viewing Horn Antenna

	Frequency	
Half-Power Beamwidths	6400 MHz	3700 MHz
H-plane	26°	45°
E-plane (1)	14.	24
Gain		
Peak	19.2 dB	14.4 dB
±6.5° (H-plane)	18.4	14.1

(1) Polarization is such that electric vector is parallel to the North-South axis of earth.

An alternative arrangement to the use of a single C-band horn is the use of two separate horns. One would cover the transmit band and a separate horn would cover the receive band. This arrangement would ease the C-band diplexing problem slightly. If orthogonal linear polarizations were utilized for receive and transmit, an additional 20 dB of isolation could be achieved. Separate horns would then be preferred, since the receive horn would be quite small (aperture size less than four square inches).

4.6.3.2 POLANG Antenna Considerations

The functional requirements of the POLANG antenna are:

- Purity of linear polarization, aligned along spin axis.
- Omni-directional pattern response, about spin axis.
- Medium gain, about 6 dB or so.

The transmission of a pure linearly polarized signal is an ideal case which cannot be obtained in practice. The proximity of the spacecraft, with its complex surface, imposes boundary conditions that introduce irregularities in the pattern and introduce higher magnitude of cross-polarization than would be obtained if the antenna were in freee space or mounted on an ideal infinite ground plane. The mechanical constraints in the spacecraft dictate the use of small lightweight antenna elements. Any protrusion of the antenna must not exceed the payload envelope, otherwise complex deployable devices will be required.

It is recommended that the POLANG antenna be attached to the cover which holds the VHF helix in its undeployed conditions. This location provides a symmetric environment for the antenna and should permit good omnidirectional patterns, in a plane perpendicular to the axis of the spacecraft. If necessary, the antenna can be extended axially a small distance.

Design of the POLANG antenna will be similar to the one used on ATS-C. The antenna will consist of a three-element, full-wave dipole array, fed by a coaxial line. Gain will be about 7 dB. Length and diameter are estimated to be 11 inches and 1 inch, respectively.

The POLANG antenna will become inoperative upon deployment of the VHF antenna. A location of the POLANG antenna on or near the apogee motor was looked at. This location was discarded because of the desire to have POLANG information after firing of the apogee motor. If was feared that the antenna would suffer injury (or perhaps have to be ejected) upon the firing of the apogee motor.

Upon deployment of the helix antenna, the coaxial cable feeding the POLANG antenna must separate. Two methods of effecting cable separation may be used. The simplest scheme is to employ an explosive cutter, which severs the cable completely. If further reliability studies show this method not desirable, a coaxial sliding connector may be employed. A commercial connector, modified to reduce the separation force, will be used.

4.6.3.3 VHF Antenna Considerations

At VHF frequencies, the size of the antenna usually dictates the design, with gain and coverage becoming secondary considerations. For example, a 30-foot dish has a half-power beamwidth of 16^{o} (earth coverage) at 136 MHz. The largest reflector that can be accommodated by the Hybrid is much less than 30 feet in diameter and consequently, other antenna types, with broad beams, have to be considered.

An end-fire parasitic array (Yagi array), consisting of a driven element, single reflector element, and three directors, has been considered. Its gain is about 10 dB, its half-power beamwidth is 60^{o}, and its length is about 10 feet. There must be a second array, crossed with respect to the first one, to produce the required circular polarization. The stowage and deployment mechanism would be expected to be heavy and bulky. For this reason, the Yagi-array is not the recommended configuration.

A second end-fire antenna (and the recommended approach) is a helical beam antenna. For the helix to radiate axially, its circumference must be equal to about one wavelength. For operation in the 118-136 MHz band (wavelength in the neighborhood of 8 feet), the diameter of the helix antenna must be about 30 inches.

The maximum length of the helix antenna is limited by the following:

- size and weight of deployment mechanism
- considerations of shadowing of solar array.

For the present spacecraft concept, the limiting consideration on the length of the helix antenna is the shadowing of the solar array. As the helix length increases, the solar arrays must be moved farther away, with attendant increase in weight. A reasonable maximum is in the vicinity of 100 inch. A helix length much in excess of this value would result in prohibitive weight and size of the total spacecraft.

The requirements on the VHF antenna may be summarized as follows:

Gain -	Maximum, consistent with constraint on length.
Frequency -	118 - 136 MHz (transmission and reception).
Polarization -	circular.
Length -	Not to exceed 100 inches.

The physical characteristics of the recommended helix antenna are summarized below:

length = 92 inch

diameter = 30

no. of turns = 4-1/2

The electrical characteristics of the helix, at the two extremes of the frequency band, are as follows:[1]

118 MHz		136 MHz
0.94	circumference/wavelength	1.09
.92	length/wavelength	1.06
57^{o}	HPBW	46^{o}
11 dB	gain	13 dB
1 dB	axial ratio	1 dB

[1] Kraus, J. D., Antennas, McGraw-Hill, New York (1950) Chap. 7.

The minimum gain over the frequency band is 11 dB; the consequences of this limit are shown in the link analyses (Section 4. 6. 1).

The feed line for the helix is a coaxial cable. The helix operates against a ground plane, which is composed of 24 radial aluminum rods, 1/4-inch in diameter. The ground plane diameter is 65 inches (0. 65 wavelength at 118 MHz). The diameter of the ground plane is well in excess of a halfwavelength, which is the minimum value for a reflector.

A tubular extendible element deploys the helix to its final position. The element, which is coaxial with the helix, will have no significant effect on the radiation properties of the helix, since the longitudinal field at the axis of the helix is small.

4. 6. 3. 4 L-Band Antenna Considerations

The requirements on the L-band antenna may be summarized as follows:

Frequency - Transmission over a 20 MHz band centered on 1550 MHz and reception over a 20 MHz band centered on 1650 MHz.

Beamwidth - A halfpower beamwidth of 9. 5° in the north-south direction and 12. 2° in the east-west direction.

Gain - minimum value of 22. 0 dB

Polarization- circular

The recommended antenna for meeting these requirements is a simple cut paraboloid. The aperture of the antenna will be elliptically-shaped, with the dimensions of the aperture adjusted to give the desired beamwidths.

The calculation of reflector size proceeds from aperture distributions described by Hansen.[1] The particular distribution used is the $(1 - e^2)$ on a pedestal distribution, which seems to satisfy most needs and covers most reflectors in

[1] Hansen, R. C. Microwave Scanning Antennas, Vol. I, Academic Press, New York (1964), pp. 64-67.

actual practice. Hansen's results apply rigorously to circular apertures; extrapolation to elliptical apertures will introduce no serious errors, in view of the small amount of asymmetry present.

With the edge taper being 10 dB ($b = 1/2$, $n = 1$), the reflector dimensions are found to be 50 inches in the north-south direction and 40 inches in the east-west direction. The gain is estimated from the equation.

$$G = \eta 4\pi \ A/\lambda^2.$$

Here A is the aperture area λ is the wavelength, and η is the efficiency. The gain is estimated to be 23.4 dB (with an efficiency of 60%). Feed dissipation losses are not included in this number. With an F/D of 0.38, the angle subtended by the reflector at the focal point is 133°. A helical antenna, fed by a coaxial cable against a small ground plane, will serve as the prime focus feed for the reflector. The length of the helix, and hence its beamwidth, will be adjusted to give the proper primary illumination function.

An alternate arrangement to the conventional prime focus feed reflector described above is the paraboloid with offset feed. The feed and support trusses would not be in the radiating aperture and minimum blockage would result. However, the offset paraboloidal reflector suffers from lack of complete symmetry and, as a consequence, the cross-polarized lobes may be stronger than they would be for a symmetric situation. For the present application sidelobe levels are not of particular importance, so this defect is not a severe one.

Conflicting requirements on the reflector shape exist. A large F/D ratio yields smaller cross-polarized components, has better off-axis scanning properties, and is more tolerant of feed horn axial displacements. All of these properties are desirable. On the other hand, large F/D-ratios require larger feed horns, which are located farther away from the reflector. Both of these factors cause an increase in the weight and volume. In addition, the larger feeds associated with high F/D may introduce some feed blockage, or require more reflector offset to prevent feed blockage. The choice of F/D = 0.38 appears to be a reasonable compromise.

4.7 POWER SYSTEM DESIGN CONSIDERATIONS

4.7.1 SYSTEM CONFIGURATION

For the Hybrid power system design, certain environmental and performance parameter assumptions were made prior to the initiation of the design effort. These assumptions are listed below:

• Orbit	Synchronous, near equatorial
• Daytime regulated load	505 watts
• Night time regulated load	130 watts
• Load bus voltage	28 vdc
• Weight	Minimum, compatible with system reliability
• Power source	Nonflexible solar cell array
• Energy source	Nickel-cadmium batteries
• Worst case sun-paddle normal angle	26^{o}

Figure 4.7-1 shows one power system configuration capable of efficiently meeting the spacecraft load requirements. Such a configuration, commonly known as a Direct Energy Transfer (DET) System, is similar to that used on the S^3 and IMP-I spacecrafts. Power is provided by the solar array during sunlight operation and by hermetically sealed nickel-cadmium storage batteries during solar eclipses. A high efficiency boost converter is provided to boost the battery voltage and to provide a regulated voltage to the loads. The battery system consists of two identical battery packages which share applied loads. This approach provides versatility for satellite thermal design, center of gravity, inertia, and ease of installation, as well as facilitating battery charger design. The battery system will be designed for normal operation at approximately 40 percent depth-of-discharge at synchronous orbit conditions for a design lifetime of five years in orbit. Battery disconnect plugs are provided to facilitate battery control modes before launch and in-flight battery conditioners are implemented to allow reconditioning of the batteries due to possible failure modes that would impose additional cycles or deeper depth of discharges on the batteries. The bus tie relay allows the two solar

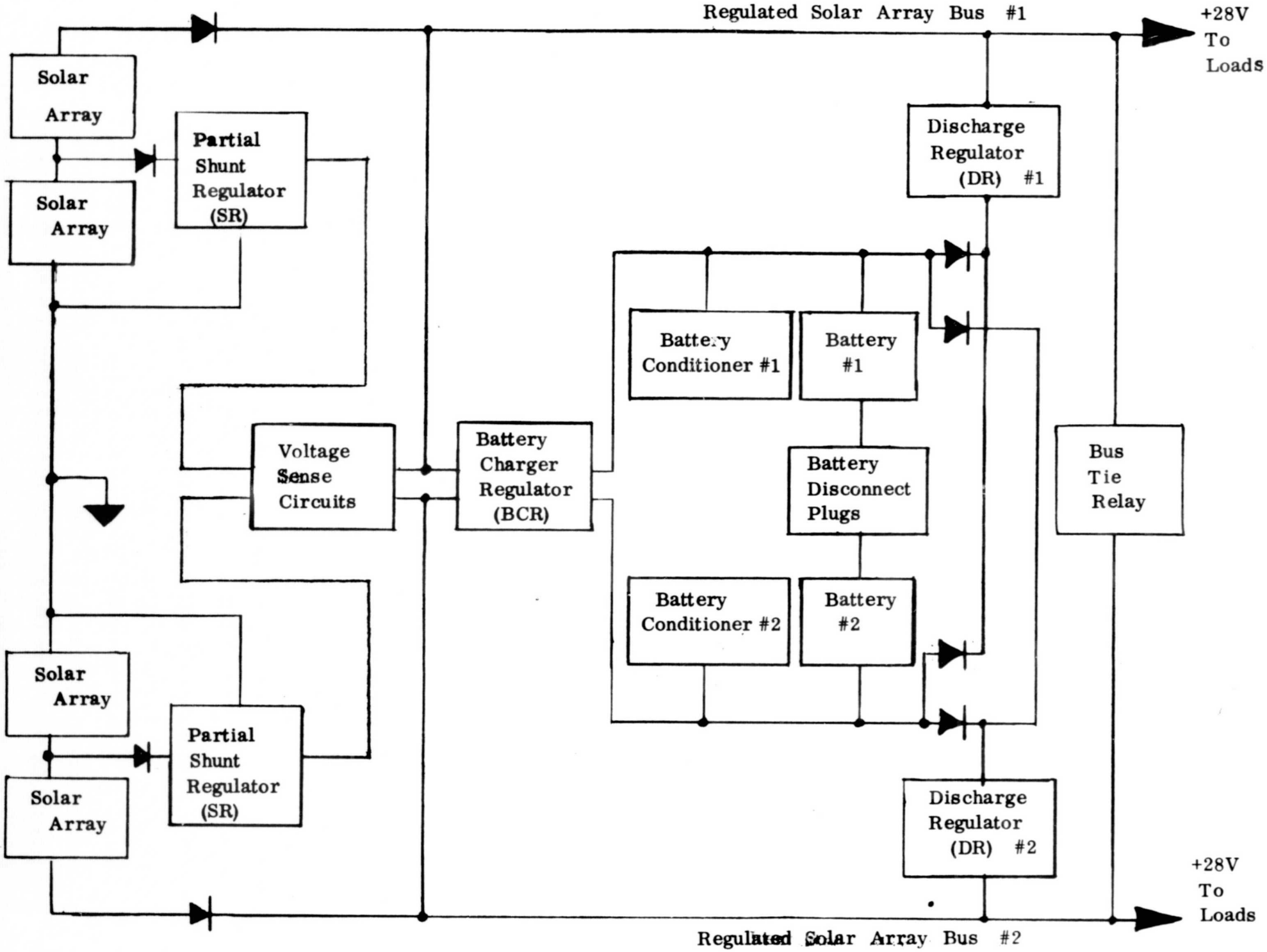


FIGURE 4.7 -1 DIRECT ENERGY TRANSFER SYSTEM

array power busses to operate independently or in parallel for failure mode consideration. The power system estimated power loading is shown in Table 4.7-1.

The lack of any series element between the solar array and the regulated load bus allows the system to supply the daytime load demands at almost 100% efficiency. A possible drawback is the discharge regulator efficiency -- typically 85% -- when the batteries must be discharged to supply spacecraft loads. As the maximum eclipse time is fixed at approximately 70 minutes in a synchronous orbit, only a significant number of daytime peak load demands, in excess of the solar array capability, would cause this configuration to lose much of its initial attractiveness. It should be noted that the initial design does not include provisions for peak load power demands.

Due to the extended mission lifetime requirement, the power system configuration of Figure 4.7-1 contains redundancy for the battery charge regulator (BCR), battery, and discharge regulator (DR) subsystems operating independently. Sufficient redundancy will be incorporated into the final design to insure power system operation in the event of a power system component failure.

4.7.2 BATTERY

Since the occult load and the solar array regulated output voltage have been defined, the battery can now be designed. The storage cell selected for this mission is a conventional hermetically sealed, sintered plate, nickel-cadmium (Ni-Cd) cell. Although both silver-cadmium and silver-zinc storage cells exhibit higher energy densities (watt-hours per pound), no data is available which indicated that these cell types can operate successfully for the mission duration. In addition, unlike the other cell types, a Ni-Cd cell can tolerate a small amount of continuous overcharge, thereby greatly reducing the complexity of the battery charge regulator.

The three factors that contribute significantly to battery performance are temperature, depth of discharge (DOD), and charge/overcharge controls. Ideally, a cell would like to see a low temperature (0° C to 20° C), low DOD, and minimum overcharge. Battery tests are presently underway at the Naval Ammunition Depot, Crane, Indiana, to determine the effect of DOD and operating temperature on

Table 4.7.-1

Power System Night/Day/Transfer Orbit

Average Power Loads

System	Average Night Loads (watts)	Average Day Loads (watts)	Average Transfer Orbit Loads (watts)
T & C	18	18	18
Att. Cont.	42	42	30
Comm.	45	400	2
Power	25	45	10
Totals	130	505	60

storage cells under synchronous orbit conditions. These tests are controlled by the Electrochemical Power Sources Section at GSFC. Real time results after five eclipse periods (equal to approximately 2.5 years in space) reveal that cells with a 40% DOD, at both 0^{o}C and 25^{o}C, and 0^{o}C cells at 60% DOD can still deliver the required ampere-hour capacity during the maximum eclipse periods with some capacity to spare. Cells at 0^{o}C and a 80% DOD are just barely able to meet the capacity requirements and could not be expected to deliver sufficient energy at the end of three years.

A reasonable extrapolation of the present data yields three possible combinations of temperature and DOD for a three-year mission: 25^{o}C and 40% DOD, 0^{o}C and 40% DOD; and 0^{o}C and 60% DOD. With a five-year lifetime imposed upon the power system, further extrapolation of the available data indicates that a battery at 40% DOD, operated at either 0^{o}C or 25^{o}C, would perform satisfactorily for five years, with the 0^{o}C battery temperature offering the higher degree of confidence. Therefore, to allow a single battery to be limited to a reasonable DOD (80%) in the event of failure, it is necessary to maintain a 40% DOD with a 0^{o}C to 25^{o}C temperature range when both batteries are in operation.

The time spent in the earth shadow by the satellite in a synchronous equatorial orbit is a varying function with the time of year as shown in Figures 4.7-2 and 4.7-3. The satellite is in the shadow for a total of 84 hours annually consisting of the penumbra and umbra times during the two equinoxes. As the satellite approaches the equinox, the time in shadow which occurs once per day, increases gradually for approximately 22 days to a maximum of 1.16 hours (70 minutes). The shadow time then cycles back to zero shadow time in another 22 days. The batteries, therefore, would be required to perform through approximately 88 charge/discharge cycles per year for a total of 440 cycles over a five-year period.

Proper power system operation requires a maximum battery terminal voltage of 26.0 volts (thereby allowing at least a two-volt drop across the battery charge regulator and two volts of boost for the discharge regulator), the number of series cells is easily calculated to be 16 cells for an even number

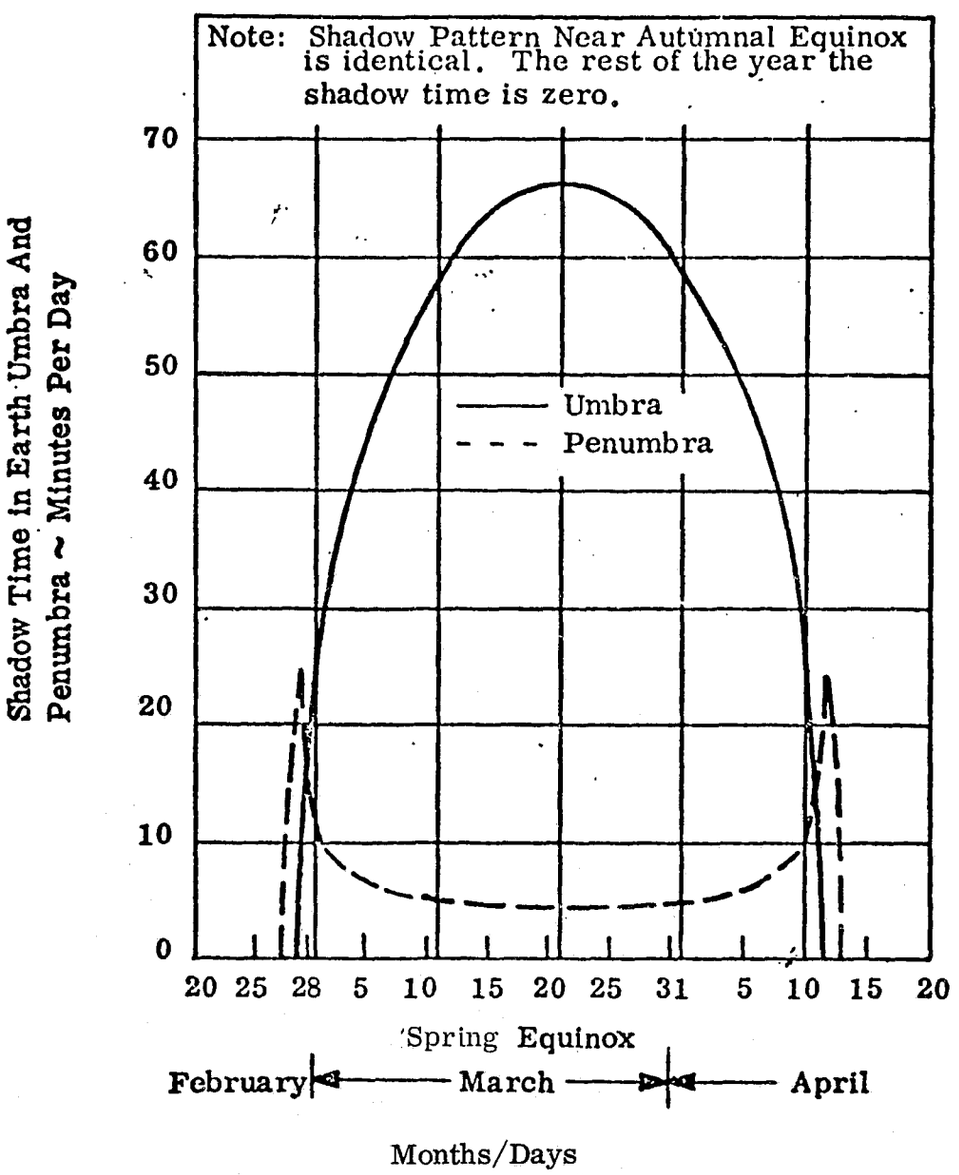


Figure 4.7-2 Umbra and Penumbra Patterns for a Synchronous Equatorial Orbit

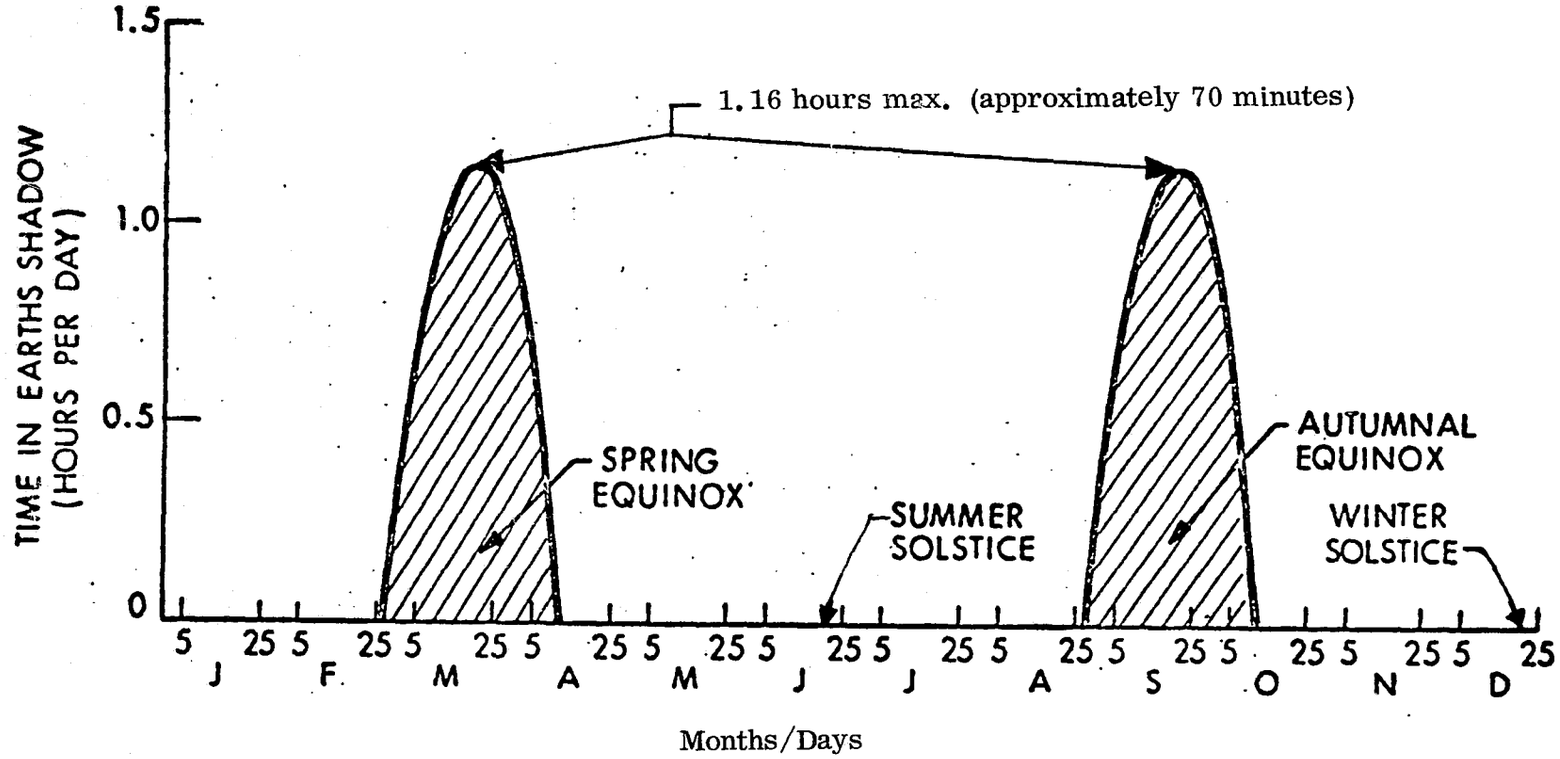


Figure 4.7-3 SHADOW TIME (COMPOSITE OF UMBRA AND PENUMBRA TIMES) FOR A SYNCHRONOUS EQUATORIAL ORBIT

of cells in the battery package. The minimum end-of-discharge voltage is chosen to be 1.1 volts per cell, while the maximum allowable charge voltage is chosen to be 1.50 volts per cell. The 1.50 volts per cell represents the maximum allowable charge voltage at $0^{\circ}C$.

The batteries must operate while being subjected to various environmental extremes and the battery must be designed with a minimum of weight and proper thermal parameters, yet be structurally secure to withstand the rigors of launch. The battery assembly must be designed so that a constant pressure is applied to the cells by the end plates when the package is assembled, thereby pre-stressing the external structure to a point considerably above the load imposed by normal internal pressures of the cells. Pre-stressing accomplishes four major functions in the battery structure.

- The cells are restrained by the frictional forces developed between cells, making the battery behave more as a solid than as a collection of individual parts.
- The cells are kept under pressure, enhancing the electrical characteristics.
- The cells are restrained from moving relative to each other and transmitting loads from the intercell connections to the terminals and the ceramic-to-metal seals.
- The cells are retained in intimate contact with heat sinks through which heat may be rejected from the battery; this is a very important function of the preloading of the cells by the pre-stressed structure.

A typical wiring diagram for the battery is shown in Figure 4.7-4. Connector J1 is the power connector, J2 provides the interface with the charger and the telemetry interface, and J3 provides the access for ground testing each individual cell of the 16-cell battery. Figure 4.7-5 shows the typical wiring for the battery return disconnect function with the two disconnect plugs. The battery returns are controlled

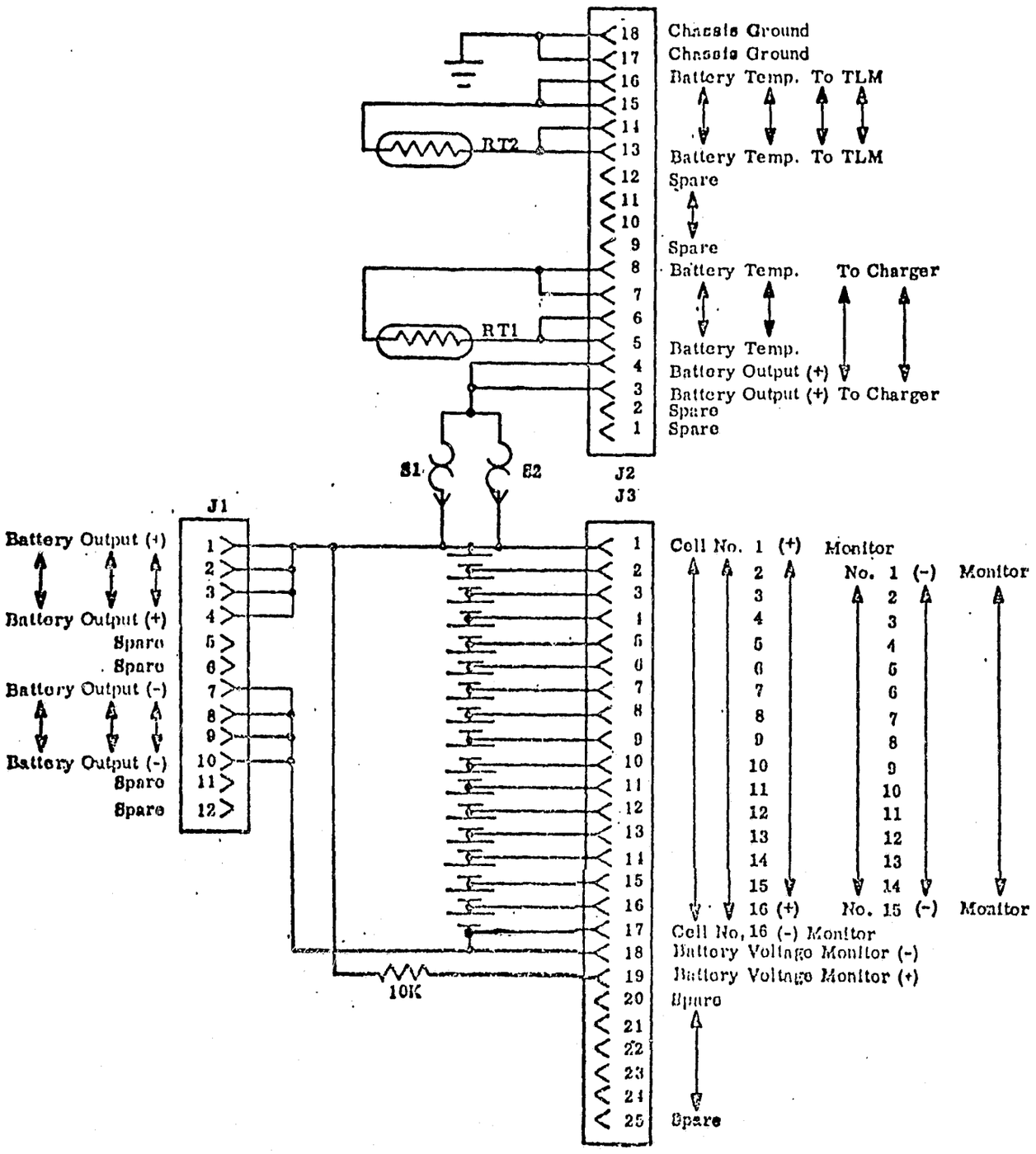


Figure 4.7-4 BATTERY WIRING DIAGRAM

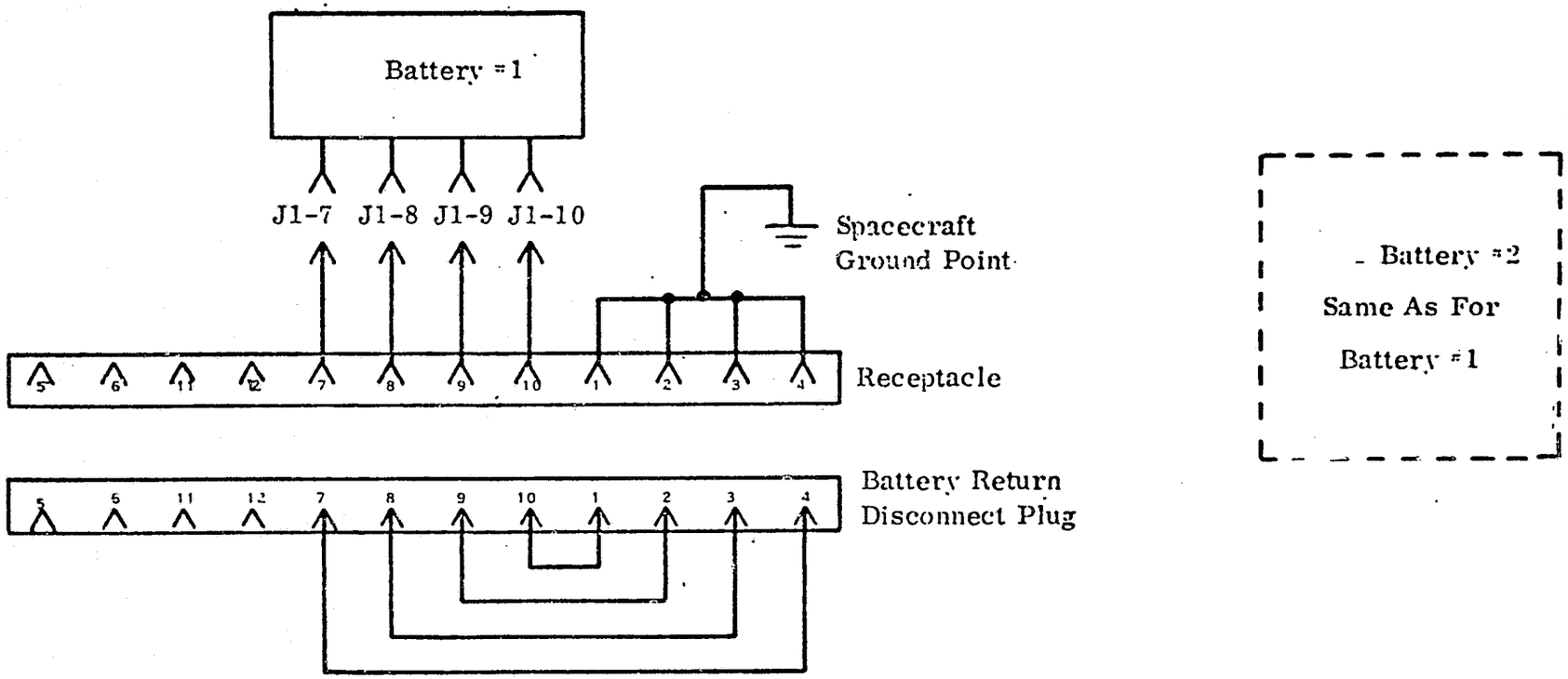


Figure 4.7-5 Battery Return Disconnect Wiring Diagram

for power removal or system shut-down during periods of non-operation or off-line battery charging. The receptacle must be located for accessibility during prelaunch checkout of the spacecraft.

4.7.2.1 Battery Sizing

For calculating the battery capacity, the following parameters are considered:

- Occult load -- 130 watts
- Discharge regulator efficiency -- 85%
- Occult period -- 1.16 hours
- Battery cell voltage -- 1.1 volts per cell
- Number of battery cells -- 16

$$\text{Amp-hours} = \frac{\text{watt-hours}}{\text{volts}}$$

$$\text{Amp-hours} = \frac{\left(\frac{130\ \text{w}}{0.85}\right)(1.16\ \text{hours})}{(1.1\ \text{v/cell})(16\ \text{cells})}$$

$$\text{Amp-hours} \cong 10$$

Using a 40% DOD for the two-battery system, the necessary capacity is:

$$\frac{10\ \text{amp-hours}}{0.40} = 25\ \text{Amp-hours}$$

To derive the 25 amp-hours with two batteries, the 12 amp-hours battery cell would not be a suitable selection due to the variation of cell capacity with temperatures as shown in Figure 4.7-6 for a 12 amp-hour cell. Therefore, the 15 amp-hour cell would be a more suitable selection at this time.

With two 15 amp-hour batteries, the power system can support a higher occult load with the same 40% DOD. The higher occult load capability is

$$\text{Load capability} = 30\ \text{amp-hours} \times 0.40$$

$$\text{Load capability} = 12\ \text{amp-hours}$$

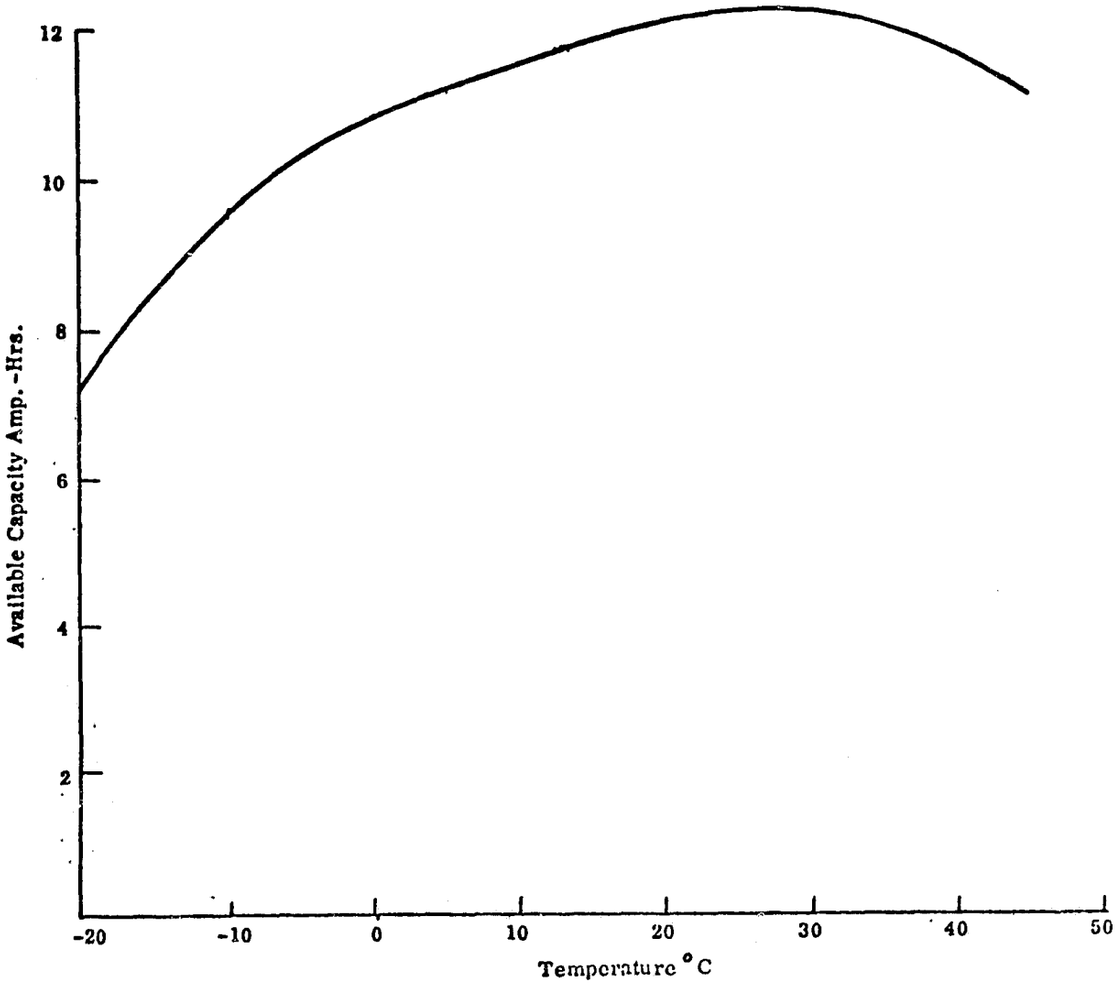


Figure 4.7-6 12 A-H Battery Capacity as a Function of Temperature

or in watts is:

$$\text{Load capability} = \frac{12 \text{ amp-hours } (1.1 \text{ v/cell}) (16 \text{ cells}) (0.85)}{1.16 \text{ hours}}$$

$$\text{Load capability} \cong 154 \text{ watts}$$

The total weight of the two batteries including case, potting, wiring, etc., is assumed to be two times 115% of the total cell weight for each battery. The 115% factor was generated from Nimbus and RAE flight battery module weights. The 16 cells for 15 amp-hour cells, weigh 22.5 pounds (1.41 lbs/cell) and each battery system will weigh 25.9 pounds or 51.8 pounds for the two-battery system.

4.7.2.2 Battery Conditioner

After long periods of use, a nickel-cadmium battery often loses some of its capacity. This phenomenon is not completely understood; however, it is known that temperatures above 25° C greatly accelerate the effect. Therefore, the batteries should be operated in a temperature environment between 0°C and 25°C. In order to have the capacility to extend the life of the battery, provision is made to discharge each battery slowly through a resistor to an average voltage of one volt per cell and then to recharge. This action should regain some of the lost capacity using a reconditioning discharge time of approximately three days. Each battery could be conditioned while the satellite is in full sunlight just prior to the beginning of the eclipse period. To discharge a 15 amp-hour cell over a three-day period, the discharge rate is:

$$\text{Discharge rate} = \frac{15 \text{ amp-hours}}{72 \text{ hours}} = .208 \text{ amp average discharge current}$$

and the resistance required per cell is:

$$\text{R/cell} = \frac{\text{Average voltage}}{\text{Average current}} = \frac{1.2 \text{ volts/cell}}{.208 \text{ amp}} = 5.8 \text{ ohms/cell}$$

The 5.8 ohms per cell multiplied by 16 cells yields a letdown resistance of 93 ohms. Since 91 ohms is a standard size, this value would be used. The average power dissipation for the resistor is:

$$\frac{(1.2 \times 16 \text{ volts})^2}{91 \text{ ohms}} \cong 4 \text{ watts}$$

4.7.3 BATTERY CHARGE REGULATOR (BCR)

The battery charge regulator consists of one trickle charger and one main charger for each battery. The basic charge regulator system block diagram is shown in Figure 4.7-7. Each main charger operates on a 50 precent duty cycle, but they do not operate simultaneously except by ground command control with the other main charger. This sequence technique permits a current of C/10 (1.5 amperes) to be delivered to each battery without loading the array with a C/5 (3.0 amperes) load normally encountered when simultaneously charging two batteries (the 1.5 ampere current level is delivered first to one battery then to the other). In this manner the battery sees a higher, more efficient, charge rate while the solar array sees the lower average current rate. The C/10 rate is selected to insure that full battery capacity is obtained during recharge as shown by the curve in Figure 4.7-8.

The charge current and voltage into the battery must be controlled so as not to damage the battery with high end-of-charge voltages or overcharge rates. For the Hybrid spacecraft, a pulse-width-modulated battery charge regulator was selected for the main battery charger circuit. The regulators must be designed to function as nondissipative, tapered current, temperature compensated, bucking chargers. The main charger initial constant current portion of the charge is accomplished at a C/10 (1.5 amperes) rate at 50% duty cycle. The charge rate is then modified (tapered) as an inverse function of battery terminal voltage and battery temperatures to approximately C/25 (0.6 ampere) rate at the 50% duty cycle rate.

The trickle chargers will provide a C/100 charge rate throughout the sunlit portion of the orbit. Following peak loading discharge or occult discharges of the batteries, the main chargers initially provide the C/10 charge rate at the 50% duty cycle unless disabled by ground command. Under the initial charging condition, the batteries are receiving the C/10 charge rate at 50% duty cycle plus the C/100 charge rate, or essentially a charge current level equal to C/9.1 (1.65 amperes). The main charger tapers its current contribution at a predetermined voltage depending upon battery temperature, thus the charging reverts back to only the constant trickle charger at C/100 plus a C/25 rate at a 50% duty cycle.

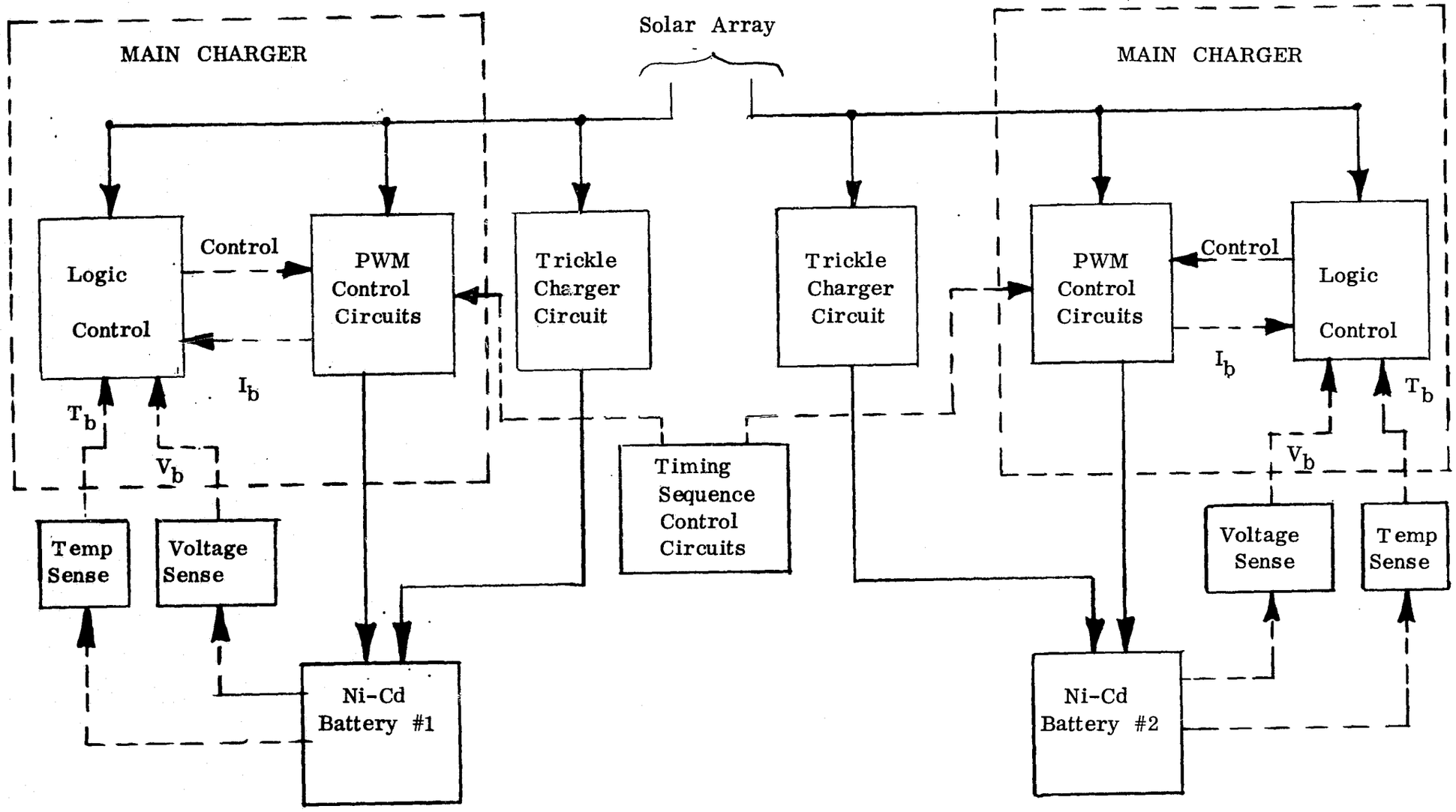


FIGURE 4.7-7 BATTERY CHARGE REGULATOR BLOCK DIAGRAM

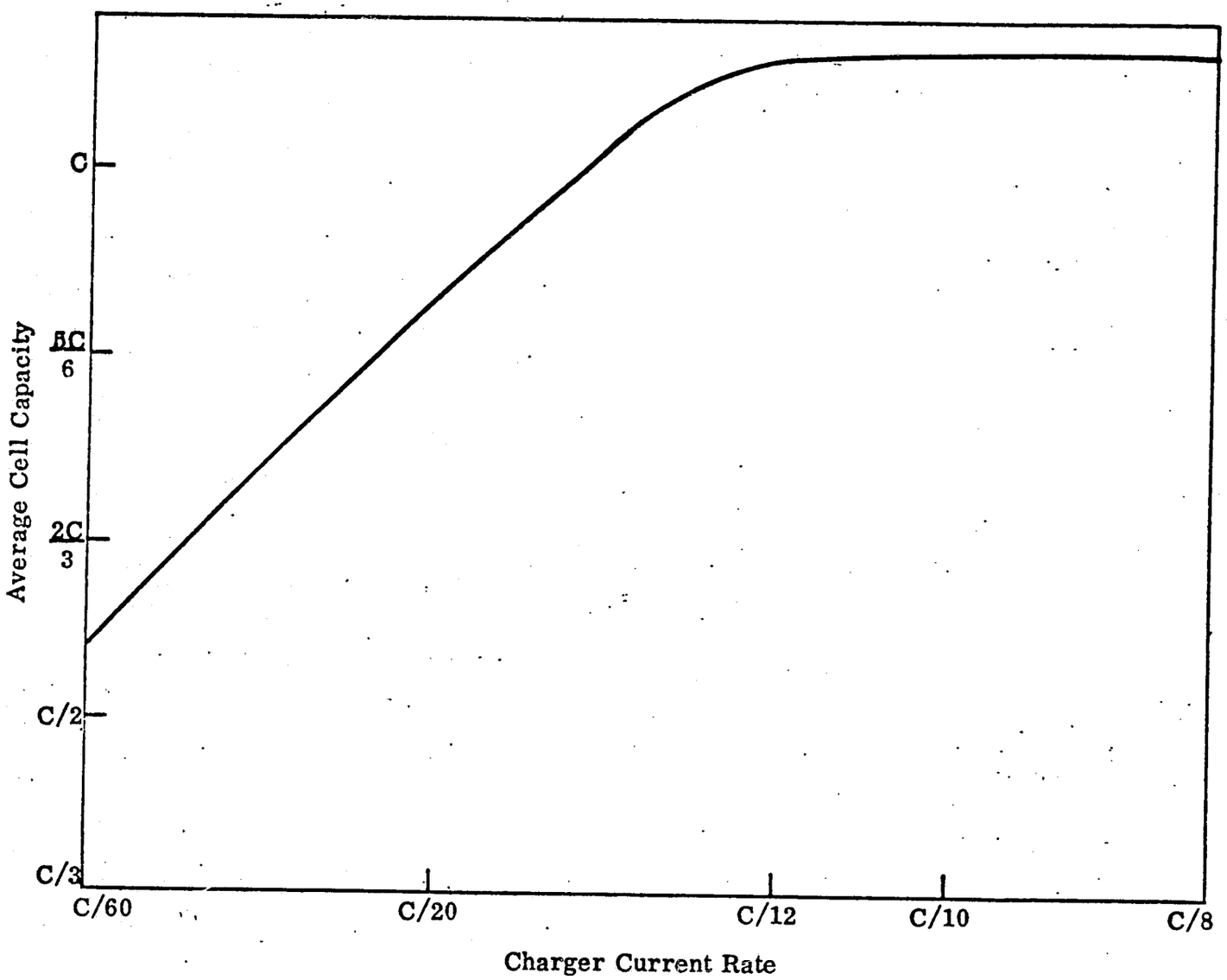


Figure 4.7-8 Recharge Capacity As A Function of Charge Current

Several other charging methods and charge controls techniques were considered prior to selecting the current-limited, temperature-compensated, charger. Due to the amount of R and D work being done on the third and fourth electrode nickel cadmium cells, it is worthwhile to explain briefly why these other charge control techniques were not selected. Even with the large amount of work expended upon third and fourth electrode systems, they have not yet been utilized as a prime battery control system on a satellite. In fact, the third electrode control only recently has been flown as an experiment in the OAO program. Since the program requires a high degree of confidence in the design-to-hardware conversion, it is inadvisable to consider using even an advanced developmental control system.

4.7.4 DISCHARGE REGULATOR (DR)

The discharge regulator will be a boost converter with a regulated 28 vdc output. Because of the high power handling requirement (at least 200 watts), the discharge regulator has been assigned a power transfer efficiency of 85%. While the assumed transfer efficiency may appear slightly conservative, the effect on the required solar array output is minimal.

A simplified diagram for one type of a boost converter is shown in Figure 4.7-9. The converter provides power in series with the battery to the loads and only the difference voltage between the battery and the required output is supplied by this circuitry. Therefore, the converter does not have to supply the total power output but only a percentage of the power. The converter operates on a pulse-width-modulation basis such that with Q1 initially turned-on, a voltage is induced in the opposite winding of T1 to supply an output voltage pulse thru CR2 to the output low pass filter network containing L1 and C1. When the output voltage is at the proper turn-off level, Q1 switches off and the energy stored in L1 is supplied to the load. When the output voltage drops to the turn-on level, Q2 turns on and provides an output pulse to the low pass filter network thru CR1. This completes one cycle for the boost converter. The pulse width of the voltage at the input to the low pass filter will vary with the battery terminal voltage and also with the load on the converter output.

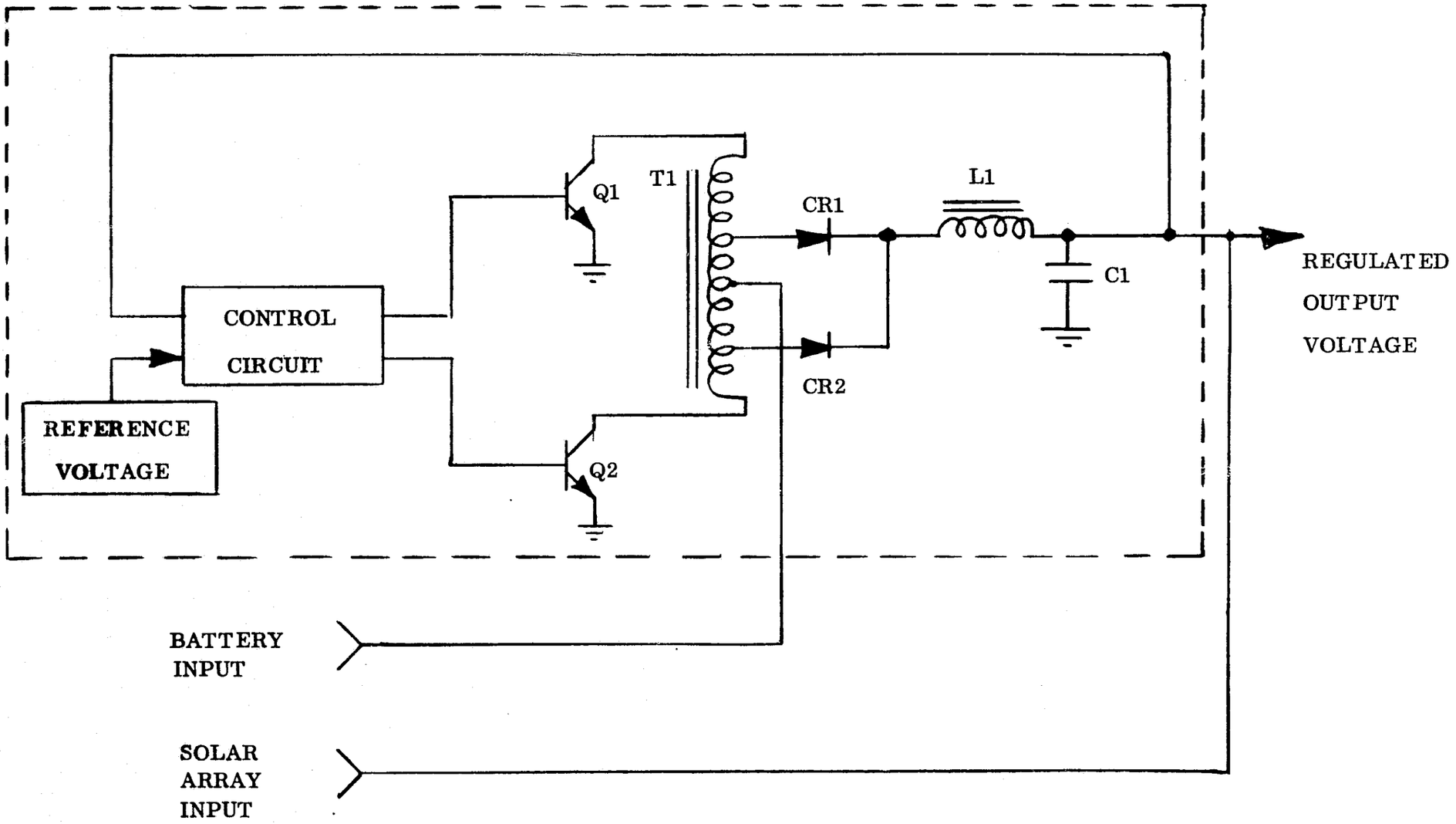


FIGURE 4.7-9 BOOST CONVERTER SIMPLIFIED DIAGRAM

4.7.5 SHUNT REGULATOR

The shunt regulator as shown in Figure 4.7-1 is a partial shunt regulator. This approach will allow most of the unneeded power to remain in the array, thereby greatly reducing the power dissipating requirement for the regulator shunt paths. This technique has previously been employed on several spacecrafts.

The Direct Energy Transfer System utilizes the partial shunt regulator in order to eliminate the need for series-type power conditioners between the solar array power source and the spacecraft loads. The shunt regulator also maintains the solar array voltage at the 28 vdc level for the spacecraft loads as shown in Figure 4.7-10. With this partial shunt configuration, the shunt power dissipation is:

$$\text{Shunt power dissipation} = (I_{SH})\ (V_R)$$

or also equals

$$\text{Shunt power dissipation} = (I_R - I_L)\ (V_{BUS} - V_U)$$

To preclude an over design for the solar array, the shunt power dissipation should approach zero watts at the end of life for the spacecraft design. Typical operating points at the beginning and end of life for the partial shunt regulated solar array are shown in Figures 4.7-11 through 4.7-14.

The tap point for the partial shunt regulator is determined by:

$$\text{Tap Point (TP)} = 100 \left[1 - \frac{V_{BUS} - V_{R\ (full\ on)}}{V_{OC\ (cold\ new\ array)}} \right]$$

where:

V_{BUS} = 28 vdc

$V_{R\ (full\ on)} \cong$ 5 vdc for a saturated transistor plus emitter resistor voltage drops.

$V_{OC(cold\ new\ array)} \cong$ 66 vdc for the total open circuit voltage for a new array when leaving the occult phase (cold new array) as shown in Figure 4.7-15.

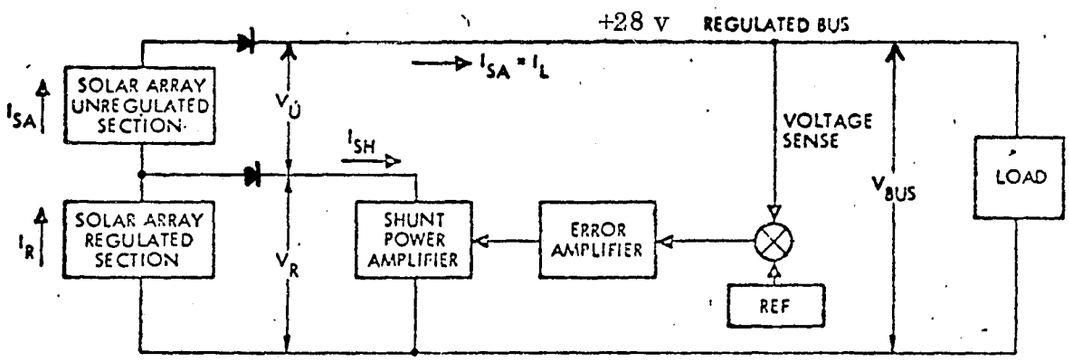


Figure 4.7-10 SOLAR ARRAY PARTIAL SHUNT REGULATOR BLOCK DIAGRAM

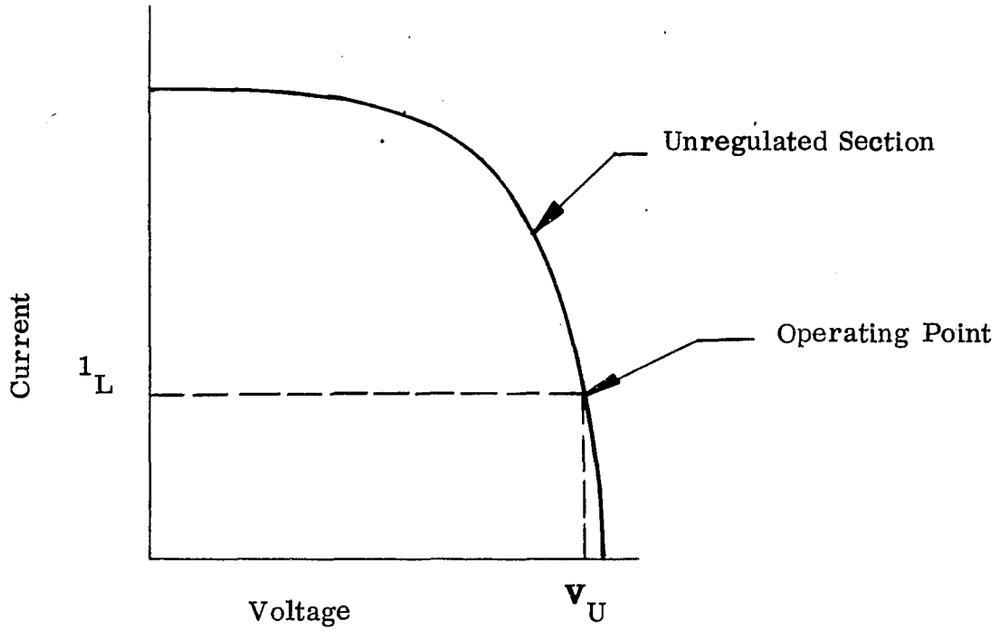


Figure 4. 5-11 SOLAR ARRAY UNREGULATED SECTION OPERATING POINT PRIOR TO END OF LIFE

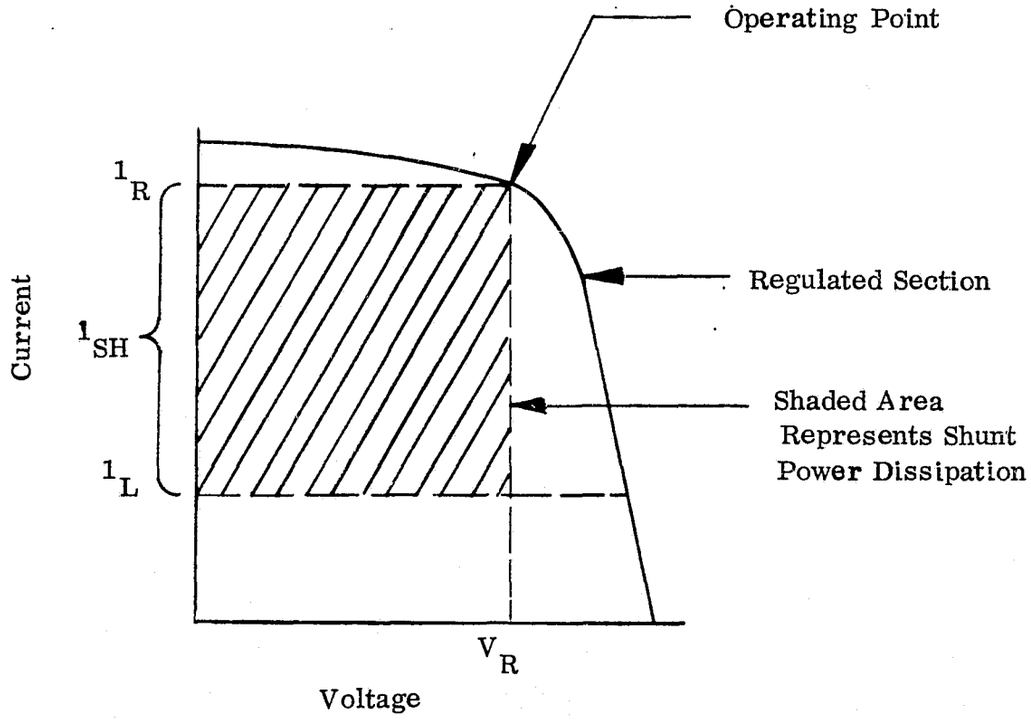


Figure 4. 7-12 SOLAR ARRAY REGULATED SECTION OPERATING POINT PRIOR TO END OF LIFE

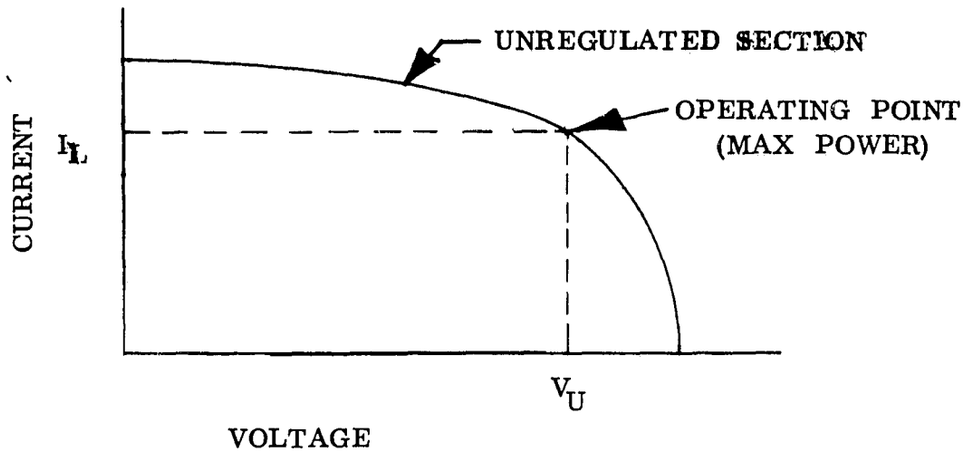


FIGURE 4.7-13 SOLAR ARRAY UNREGULATED SECTION
OPERATING POINT AT END OF LIFE

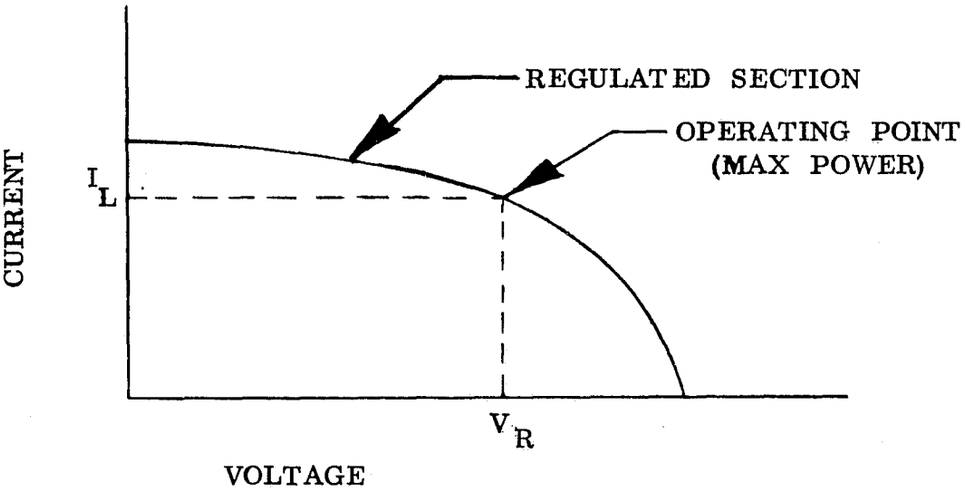


FIGURE 4.7-14 SOLAR ARRAY REGULATED SECTION
OPERATING POINT AT END OF LIFE

Then:

$$T.P. = 100 \left[1 - \frac{28 \text{ vdc} - 5 \text{ vdc}}{66 \text{ vdc}}\right]$$

$$T.P. \cong 65\%$$

The maximum power dissipation for the partial shunt regulator at zero load on the solar array bus is calculated by:

$$P_{max.\ dissip.} \cong I_{sc\ (hot\ new\ array)} \left[V_{BUS} - (1.0 - T.P.)\, V_{OC\ (hot\ new\ array)}\right]$$

For the solar array characteristics shown in Figure 4.7-15 and 4.7-16 the maximum power dissipation for the partial shunt regulator at zero load on the solar array bus would be

$$P_{max.\ dissip.} = 30.5A \left[28 \text{ vdc} - (1.0 - 0.65)\ 44 \text{ vdc}\right]$$

$$P_{max.\ dissip.} = (30.5A)\ (12.6 \text{ vdc})$$

$$P_{max.\ dissip.} \cong 385 \text{ w (worst case)}$$

The dissdipation is high due to the wide temperature range (-100°C to +60°C) for these typical solar array characteristics and the no-load condition.

4.7.6 SOLAR ARRAY

Now that the other power system components have been defined, and the day and night load profiles specified, the required solar array power output is easily obtained. Referring again to Figure 4.7-1, a power system energy balance equation is written which allows the required watt-hours of solar array energy to be calculated for any time in the mission.

The general equation for energy balance is:

$$P_A\, t_D = P_{LD}\, t_D + \left(\frac{P_{LN}}{\eta_{DR}}\right)\left(\frac{1}{\eta_B}\right) t_N$$

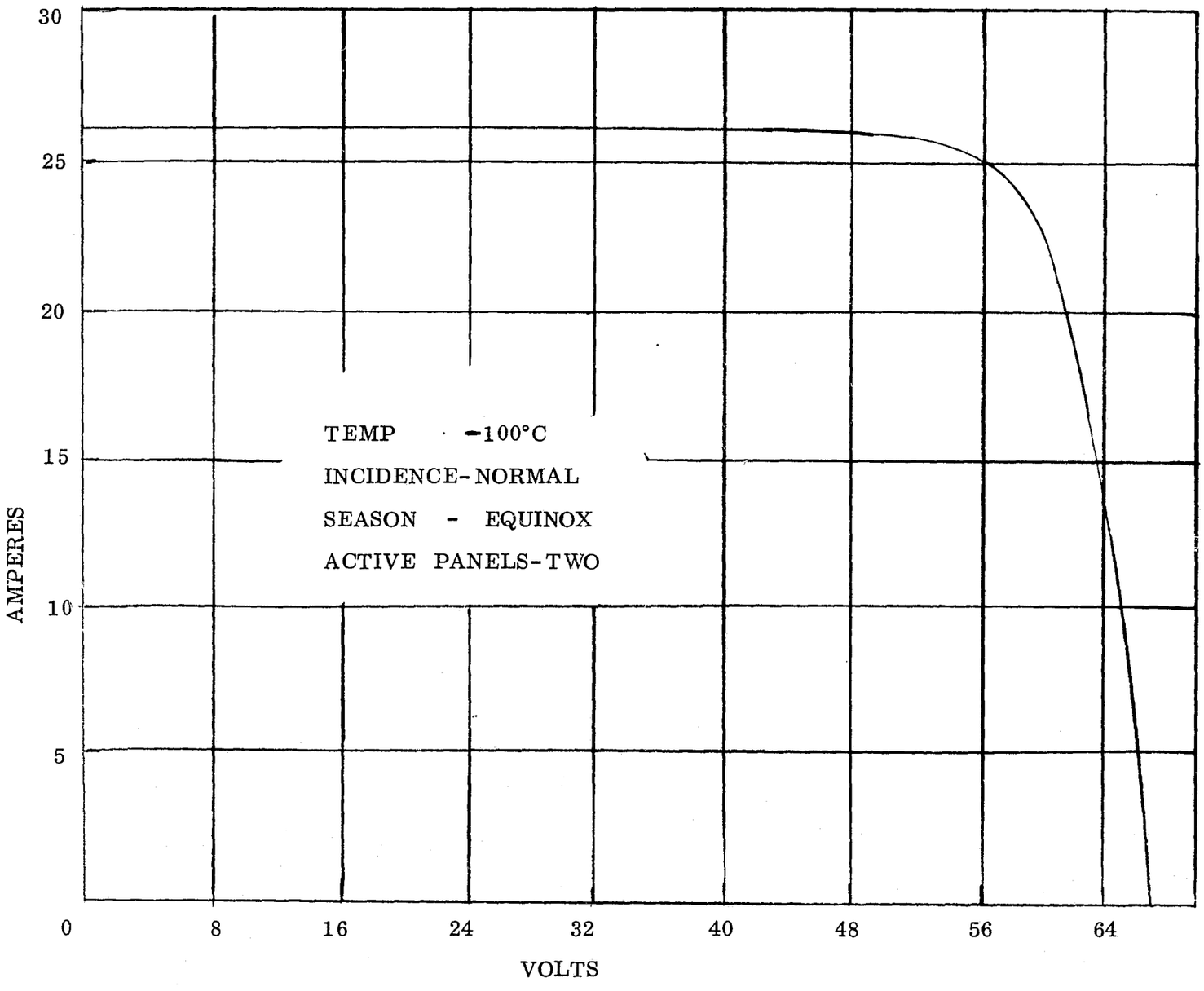


FIG. 4.7 -15 TYPICAL I-V CHARACTERISTIC OF SOLAR ARRAY UPON EXIT FROM OCCULT (BOL)

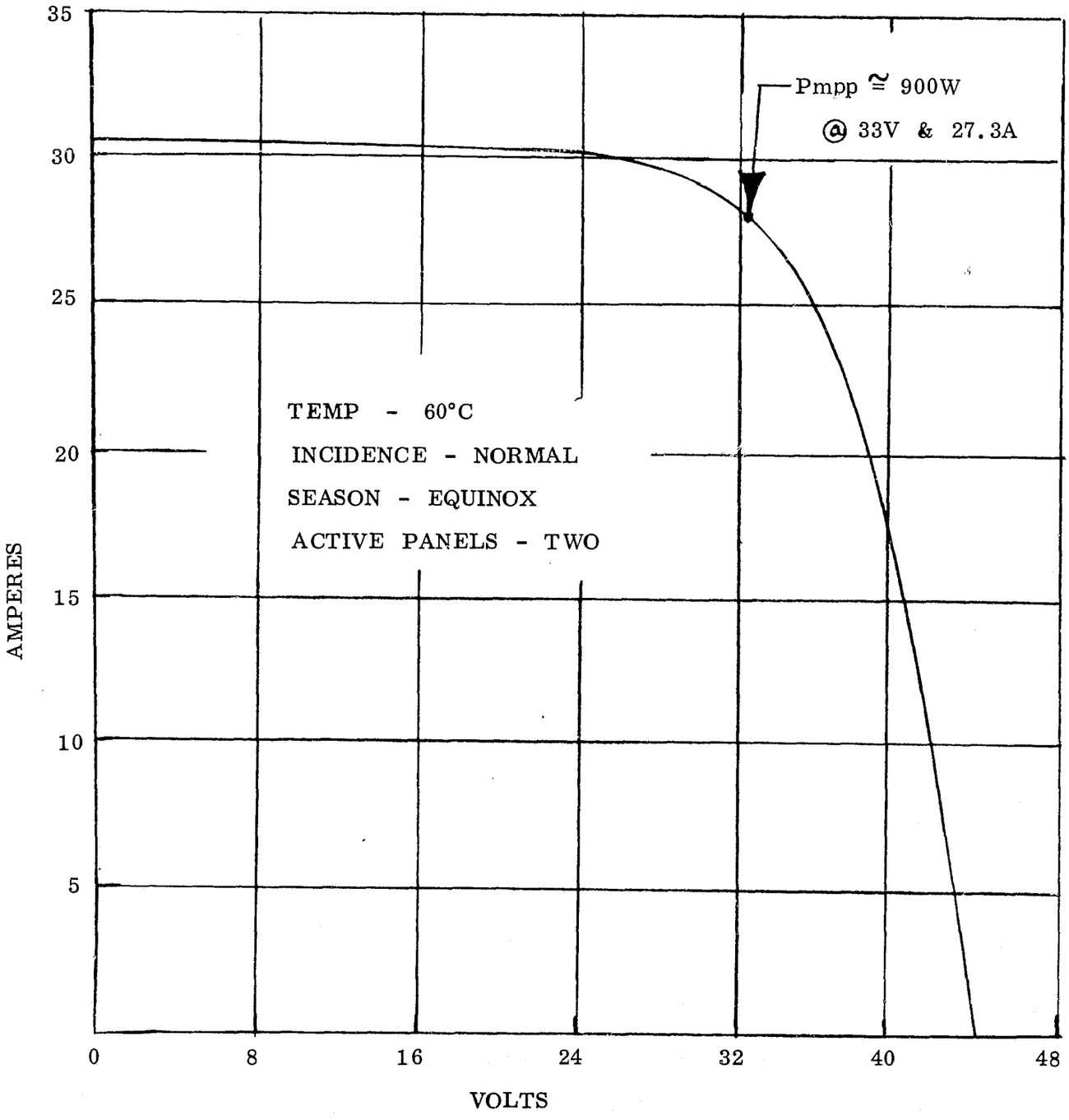


FIGURE 4.7-16 TYPICAL I-V CHARACTERISTIC OF SOLAR ARRAY (BOL)

where:

P_A = Average array power (watts),

P_{LD} = Average regulated day load power (watts),

P_{LN} = Average regulated nightime load power (watts),

t_D = Satellite day = 22.83 hours,

t_N = Satellite night = 1.16 hours

η_B = Battery discharge to charge efficiency, and

η_{DR} = Battery discharge regulator efficiency.

A worst-case battery discharge-to-charge efficiency is derived by assuming a warm environment, 35°C. At this temperature, and including trickle charge, a charge-to-discharge current ratio (C/D) could be conservatively specified to be 1.35/1. This is somewhat conservative, but of little impact, as will be seen later. An end-of-charge to end-of-discharge voltage ratio can be assumed to be 1.46/1.1. The battery watt-hour charge efficiency is given by:

$$\eta_B = \frac{(1.0 \times 1.1)}{(1.35 \times 1.46)} = 56\%$$

A more typical value is 65 percent; however, 56 percent is used for the design margin values, since it does not seriously affect the array size for this mission. Also for simplicity, the shunt regulator losses have been included with the day and night load requirements.

Substituting the design numbers into the energy balance equation and solving for the solar array power yields:

$$P_A = 505\ w + \left(\frac{130\ w}{0.85}\right)\left(\frac{1}{0.56}\right)\left(\frac{1.16\ hours}{22.83\ hours}\right)$$

$$P_A = 505\ w + 13.9\ w$$

$$P_A \cong 519 \text{ watts at end of life}$$

To insure sufficient array power at the end of life (EOL), all factors which cause a decrease in power must be taken into account in the determination of the beginning of life (BOL) power requirement. The general energy balance equation is therefore modified as follows to calculate the BOL array

$$P_{A\,(BOL)} = \left(\frac{1}{K_1} \times \frac{1}{M} \times \frac{1}{\cos \alpha} \right) P_{A\,(EOL)}$$

where:

K_1 = percentage power remaining after charged particle irridiation damage (assume 75% for five years)

M = design margin; this includes the power loss associated with ultra-violet light damage, array blocking diode voltage and line drop, changes in solar intensity, etc. (assume 90%)

α = angle between spacecraft orbit plane and incident solar radiation (assume solstice sun angle of 23.5° worst case plus 2.5° attitude inclination angle).

Therefore, the solar array power required at beginning of life is:

$$P_{A\,(BOL)} = \left(\frac{1}{0.75} \times \frac{1}{0.90} \times \frac{1}{0.899} \right) \quad 519 \text{ w}$$

$$P_{A\,(BOL)} \cong 856 \text{ watts}$$

With the two-paddle, oriented solar array, the 856 watts can be obtained with approximately 45 square feet (assume 10 W/ft^2) of solar array (450 watts) per paddle with a 44 watt margin for design contigencies. The weight estimate for one paddle is 51.8 pounds (does not include orientation system weight).

The solar cells selected for the solar array have the following characteristics:

- N-on-P silicon
- 2 x 4 cm
- Nominal 10 ohm-cm

- 10.5 percent minimum average efficiency
- 12 mils thick
- Sintered silver titanium contacts

and the selected cover glass will have the following characteristics:

- 6 mils thick
- Fused silica
- 0.400 μ cut-off filter
- Anti-reflective coating

4.7.6.1 Solar Panel Drive

There are two nominal rotation rate requirements for the solar array drives: orbital rate for the normal operational mode and a possible "spin" rate of 16 rpm for the backup operational mode. Thus the dynamic range of rotation rates for the array drives could be approximately 2300 to 1 (16 rpm for the possible backup "spin" rate to 6.95×10^{-4} rpm for the orbital rate). In addition, the drive must be capable of accepting incremental drive commands at infrequent intervals from the ground in order to correct any accumulated sun pointing errors for the array.

Table 4.7-2 presents a summary of the characteristics of typical candidate drive systems, both geared and direct driven, including an indication of the prior applications or flight status.

The Ball Brothers antenna control drive has limited angular freedom in both axes. The Sylvania and Philco-Ford drives run synchronously at 50 to 150 rpm -- too fast for use in the Hybrid without further reduction gearing. Further speed reduction to 1 revolution per day means that several additional gear passes aggregating 144,000 to 1 would be required. The Hughes proposed system is servo driven by sun orientation error signals, and is not designed for continuous rotation.

A combination of the USM* Harmonic Drive components with a synchronous motor with good acceleration characteristics appears feasible. If a geared system were chosen, the dynamic speed change requirement may necessitate

* United Shoe Machinery - Schaeffer Magnetics Division

TAELE 4.7 - 2

CANDIDATE DRIVE SUBSYSTEMS

Supplier / Characteristic	United Shoe Machinery			Ball Brothers Research Corp.		Syl-vania/ TRW	Philco Ford S.R.S. Div.	Hughes S.S. Div. "OLSCA" (Orientat. Link Solar Cell Array
	Direct		Geared	Solar Array Drive Ass'y (SADA)	Antenna Control & Drive System			
	Pan-cake	Res-pon-syn.	(Flex-spline harmonic)					
Motor	Multi-pole ≤ 82	6 pole step-per, 3 sizes	Any 0-3500 RPM NEMA "C"	Inland 2170-D, 42 slip rings	Inland or Aeroflex DC	128 step 50-100 RPM	8 pole prs. Brush-less DC 72-95rpm	DC Brushless
Gear Ratio	No	≥ 200 per pass		No	No	No	No	No
Size/Weight	Large	Small/Light		3.5d x 9 8.3 lb	10 lbs	Medium	10 lbs	---
Sealed	No	Optional		No	No	No	No	No
Lube	Brng only	Minimum Internal		Vac Kote reservoir	BBRC Vac Kote	Evap. Lube, 50 yrs.	Evap. Lube, 50 yrs.	Dry Lube
Speed Sensor	Pulse Rate	Optional		None	14 Bit Encoder	$\frac{360^{o}}{512}$ deg Encoder	Mag. Pickup	Any
Duty Cycle	0 - 100%			1/24 step 1/2880slew	0-100%	0-100%	0-100%	0-100%
Position Accurary (Backlash)	±.001% 12 sec	≥ 800 steps/ rev	2 to 6 arc min. at motor	Not stated	±.05°	$0.7^{o} = \frac{360}{512}$	---	Servo sun sensors
Power	Hi	Hi	Low	15 w	3 w	21-31v .325 a	<5 w	---
Status/Qualif.	---	200°F Temp. Vib., Shock, Rad., Vacuum 6000 hr life		5 yr. Design, Flt. Units Deliv.	Design Life 7 years	-100° + 120°F 6800 hr. vib. vacuum	5 year design life	Design Study 1968
Application	Open Loop Servo for Space	Tape Dr; Valve	3 Pegasus Bell Stol, Radar, Lox Valve S-V Mech	TRW Classif. Synch. Satellite	OSO I- IV despin, Aerobee 60 units	ATS-III Intel. III despin	U.K. Satellite Despin	A.F. Study
Angular Freedom	360°	360°	360°	360°	± 20°	360°	360°	360°
Max. Speed Output RPM	VARIOUS			VARIOUS	110	150	110	---

use of a differential gear and two motors. This type of drive is used on astronomical telescopes to drive them in right ascension at Earth's rate to follow a star. The fast speed input to the differential is used to slew the telescope to a desired initial setting. However, in geared sys tems, backlash control is only accomplished at the expense of increased friction torque. These considerations make the direct drive motor attractive.

Direct-driven, unsealed, multipole types of drive are also attractive for reasons of simplicity and reliability, but suffer from relatively high power consumption and weight. Geared drives employing relatively high-speed synchronous motors represent low weight and power but suffer because of high load reflected inertia, very high gear ratios (up to 2.59 million for an 1800 rpm motor), as well as lubrication and wear problems. Nevertheless, these problems are minimized in the unique USM Harmonic Drive.

Geared systems, such as the Harmonic Drive giving up to 200/1 per gear pass, would require at least 3 passes in the Earth's rate leg of the drive, and perhaps only 1 in the slewing leg.

The speed change problem appears to be most ea sily sólved by varying the frequency of the multipole motor and using a normally -off electronically actuated brake on the load to save power at the low duty cycle required when driving the array at Earth's rate.

The advantages of USM's direct drive for the array are:

1) No gearing
2) Can be accelerated with high torque
3) Dynamic braking when reverting to low speed.

The multipole **hysteresis** synchronous motor would be driven by two very low frequency sinusoidally varying AC voltages at 90° phase shift. All pole pairs would be energized at once.

A power supply would need development. A design problem is the very low frequency drive requirement.

A promising simulation of such a drive arrangement was conducted at Schaeffer Electronics using a 24 pole motor and 2 DC voltages varied manually in polarity and amplitude. About 3 watts was used, but this would be increased in actual application, depending on maximum torque required.

Schaeffer has delivered to Sylvania for Comsat a motor with the following characteristics:

64 poles

7" diameter bore (clear hole)

Torque: 25 oz-in

Power: 6 watts input

Synchronous speed: 90 rpm

Weight: 3 1/2 pounds

The advanced Nimbus array drive built by Bendix could probably be adapted to meet the Hybrid requirements. However, it is quite heavy, weighing about 22.5 pounds (2 required).

The Ball Brothers array drive system built for TRW for a classified satellite program appears to be an attractive candidate system. Its design operating life is 5 years. It has been qualified and flight units were delivered over a year ago. Test hours on the motor totaled 10^8 hours, on the slip rings 10^5 hours and on the bearings 10^6 hours. A tentative selection of this unit is reflected in the given weight characteristics for the power system.

4.7.7 TELEMETRY MONITORS

The telemetry monitors for the power system listed in Table 4.7-3 will provide the operational data required for the power system, and at the same time will provide sufficient diagnostic data in the event of malfunctions.

4.7.7.1 Overall Functions

The telemetry monitors are needed to perform the following:

- Provide status indications to verify that command functions have been executed.
- Provide measurements of parameters that might directly affect the power subsystem performance.
- Provide data needed for normal, no-failure, mission operations.
- Provide data required during failure modes in order to perform the necessary corrective action.

Typical circuits for the telemetry monitors are shown in Figure 4.7-17 (voltage monitor), 4.7-18 (discrete monitor), and 4.7-19 (temperature monitor). The current monitors listed in Table 4.7-3 will be magnetic amplifier type current sensors such as those manufactured by Magnetic Controls Company for the Pegasus, SERT II, and OAO spacecrafts.

4.7.7.2 Specific Functions

The specific functions performed by the telemetry monitors for the power system components are as follows:

- Solar Array

 a. Measure temperature at two locations on each solar array paddle.
 b. Measure solar array current for solar array bus 1 and bus 2.
 c. Measure the solar array voltage on solar array bus 1 and bus 2.
 d. Indicate the status for the bus tie relay between the solar array bus 1 and bus 2.

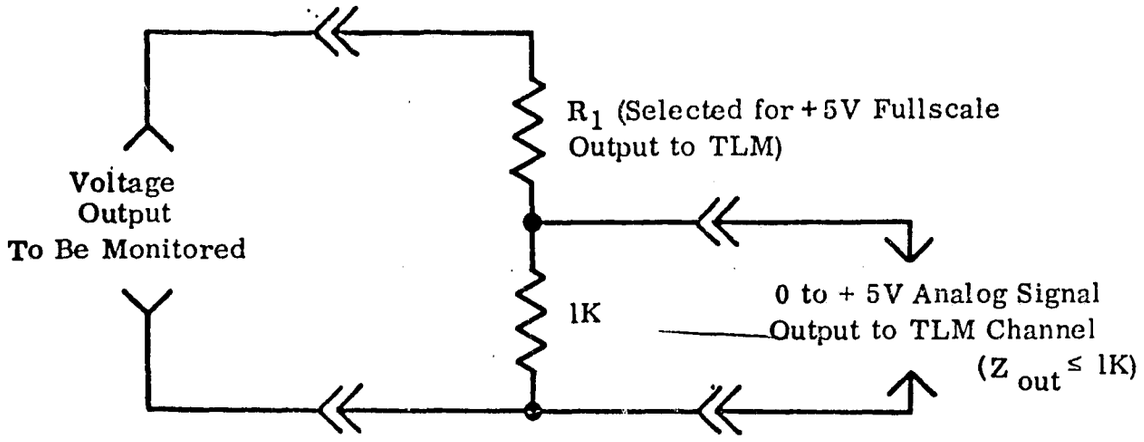


Figure 4.7-17 Typical Analog Voltage Monitor Circuit

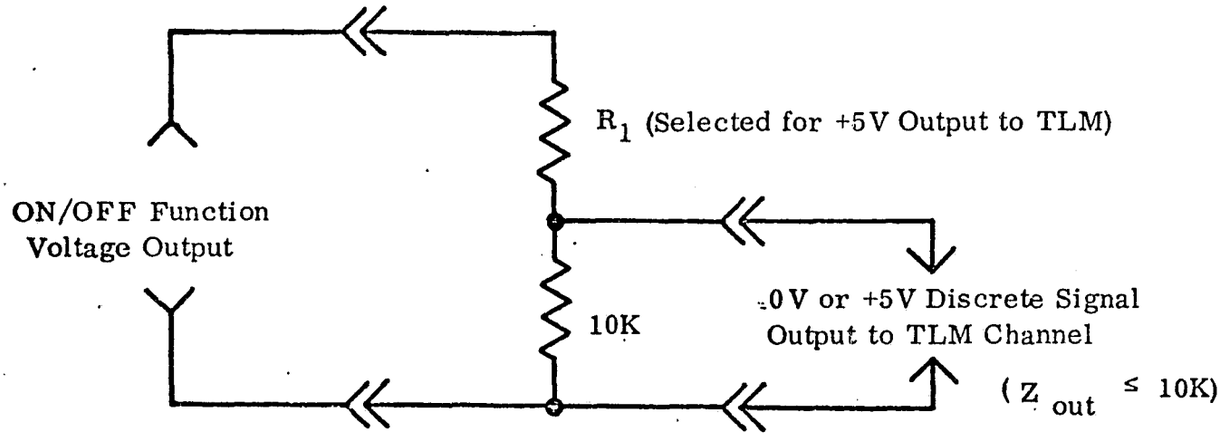


Figure 4.7-18 Typical Discrete Monitor Circuit

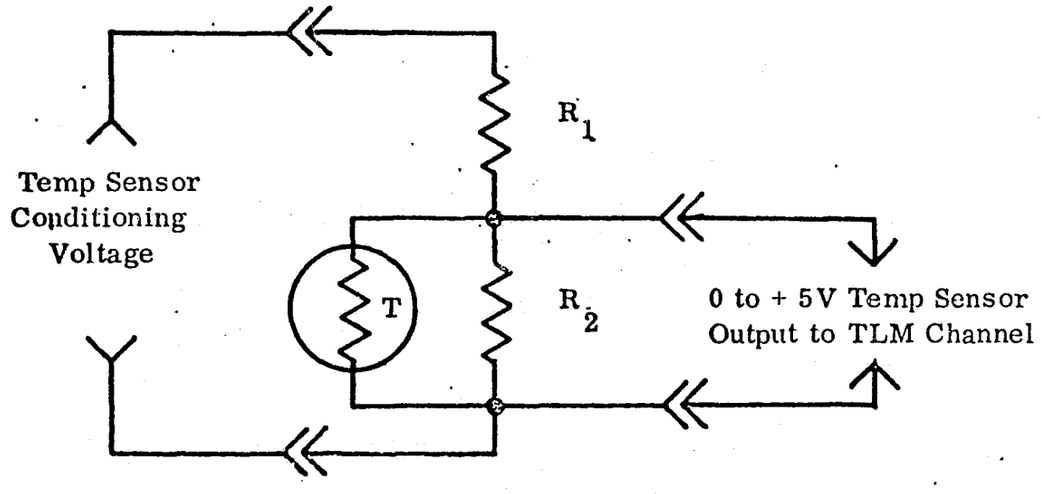


Figure 4.7-19 Typical Temperature Monitor Circuit

Table 4.7-3. Power System Telemetry Monitors

No.	Monitor	Type
1	Solar Array Bus #1 Current	Analog
2	Solar Array Bus #2 Current	Analog
3	Discharge Regulator #1 Output Current	Analog
4	Discharge Regulator #2 Output Current	Analog
5	Battery #1 Charge/Discharge Current	Analog
6	Battery #2 Charge/Discharge Current	Analog
7	Discharge Regulator #1 Temperature	Analog
8	Discharge Regulator #2 Temperature	Analog
9	Solar Panel Temperature #1	Analog
10	Solar Panel Temperature #2	Analog
11	Solar Panel Temperature #3	Analog
12	Solar Panel Temperature #4	Analog
13	Battery #1 Temperature	Analog
14	Battery #2 Temperature	Analog
15	Battery #1 Voltage	Analog
16	Battery #2 Voltage	Analog
17	Solar Array Bus #1 Voltage	Analog
18	Solar Array Bus #2 Voltage	Analog
19	Battery #1 Conditioner Voltage	Analog
20	Battery #2 Conditioner Voltage	Analog
21	Battery #1 Main Charger ON/OFF Status	Discrete
22	Battery #2 Main Charger ON/OFF Status	Discrete
23	Battery #1 Trickle Charger ON/OFF Status	Discrete
24	Battery #2 Trickle Charger ON/OFF Status	Discrete
25	Battery #1 Connect/Disconnect Status	Discrete
26	Battery #2 Connect/Disconnect Status	Discrete
27	Solar Array Paddle #1 Orientation System ON/OFF Status	Discrete
28	Solar Array Paddle #2 Orientation System ON/OFF Status	Discrete
29	Solar Array Bus Tie Relay Connect/Disconnect Status	Discrete
30	Discharge Regulator #1 ON/OFF Status	Discrete
31	Discharge Regulator #2 ON/OFF Status	Discrete

- Discharge Regulators

 a. Indicate ON/OFF status to show that these regulators are connected to th solar array/battery power sources.

 b. Measure the output current to the solar array bus 1 and bus 2.

- Battery

 a. Measure the temperature at the hot spot on each battery.

 b. Measure the battery voltage for each battery.

 c. Measure the battery current for each battery.

 d. Measure the battery reconditioning voltage for each battery.

 e. Indicate the status of the battery connect/disconnect relay for each battery.

- Charger

 a. Indicate the ON/OFF status of the main charge mode for each charger.

 b. Indicate the ON/OFF status of the trickle charge mode for each charger.

The selection of the telemetry monitors have been kept to a minimum level consistent with the parameters that must be monitored for sufficient coverage of the power system functions.

4.7.8 COMMANDS

The commands for the power system listed in Table 4.7-4 will provide the command control required for normal operation of the power system, and at the same time, will provide sufficient command control for back-up control during possible malfunctions. The command signal level for execute is +5 v at 10 milliamperes and in the off state, the command lines will have a -5 v bias level. The duration of an execute command is approximately 50 milliseconds.

Table 4. 7-4. Power System Commands

No.	Command
1	Battery #1 Main Charger ON
2	Battery #1 Main Charger OFF
3	Battery #2 Main Charger ON
4	Battery #2 Main Charger OFF
5	Battery #1 Trickle Charger ON
6	Battery #1 Trickle Charger OFF
7	Battery #2 Trickle Charger ON
8	Battery #2 Trickle Charger OFF
9	Battery #1 Connect
10	Battery #1 Disconnect
11	Battery #2 Connect
12	Battery #2 Disconnect
13	Battery #1 Conditioner ON
14	Battery #1 Conditioner OFF
15	Battery #2 Conditioner ON
15	Battery #2 Conditioner OFF
16	Solar Array Bus Tie Relay Connect
17	Solar Array Bus Tie Relay Disconnect
18	Discharge Regulator #1 ON
19	Discharge Regulator #1 OFF
20	Discharge Regulator #2 ON
21	Discharge Regulator #2 OFF
22	Solar Array Paddle #1 Orientation System ON
23	Solar Array Paddle #1 Orientation System OFF
24	Solar Array Paddle #2 Orientation System ON
25	Solar Array Paddle #2 Orientation System OFF

4.7.9 WEIGHT SUMMARY

The estimated weights for the power system and its components are shown in Table 4.7-5.

4.7.10 LAUNCH PHASE

It has been shown that the power system design fulfills the operational requirements of the satellite under worst-case assumptions. It remains to be shown that the power system supplies the necessary power from launch throughout acquisition.

4.7.11 CONCLUSION

Throughout the analysis, attempts have been made to assume worst-case conditions. The designed power system has been shown to easily meet these conditions. Since worst-case conditions usually do not occur throughout the mission, the resulting margin is a measure of the reliability and the growth potential of the satellite. Obviously, trade-off's can be made with regard to reducing the power system weight, but only with a corresponding reduction of reliability and growth potential. The proposed power system easily supplies a 505-watt daytime load and 130-watt nighttime load when the sun is at the worst sun angle and after five years of radiation damage. Should other than the shunted system be chosen, (further trade-off studies would have to be performed to determine the optimum system for the Hybrid satellite) more power would be available at start of life, but a greater burden would be place on the thermal control system.

Table 4.7-5

Power System Weight Summary

Item	Quantity	Weight (each) lbs.	Weight (total) lbs.
A. Battery	2	25.9	51.8
B. Battery Charge Regulator	1	3.0	3.0
C. Solar Array Paddle	2	51.5	103.0
D. Solar Array Orientation System	2	13.5	27.0
E. Battery Discharge Regulator	2	4.0	8.0
F. Voltage Limiter	2	3.0	6.0
G. Power Control Unit	1	11.0	11.0
Total Weight			209.8

4.8 TELEMETRY AND COMMAND SUBSYSTEM

4.8.1 INTRODUCTION

Telemetry equipment performs the functions of multiplexing and formatting of housekeeping data from all spacecraft systems for transmission to the control ground station. Analysis of this data permits ground monitoring of equipment configuration and major operating parameters. The command system receives, decodes and executes ground commands which control the operating status of spacecraft equipment. Telemetry and Command (T&C) transmitters and receivers operate at VHF utilizing a common omnidirectional antenna; they are independent of the communications repeater. Equipment redundancy is utilized to achieve high reliability in both functions. Command receivers, decoders, and power regulators operate continuously in active redundancy; data multiplexers and transmitters are connected in standby redundancy. A block diagram of the system is shown in Figure 4.8-1. Characteristics are summarized in Tables 4.8-1 through 4.8-4. Power interconnections are illustrated in Figure 4.8-2.

4.8.2 TELEMETRY

The telemetry equipment consists of redundant time-division multiplexers, which also contain the spacecraft clocks, a data switching unit, and redundant transmitters feeding the T&C antenna system.

4.8.2.1 Multiplexer

Both multiplexers sample analog and digital data channels, then format them with calibration and synchronization signals into a single time-division PCM bi-phase channel. Each unit contains its own power supply, clock, and calibration circuits. Only one unit is powered at a given time, with the second in standby; selection is made by transmission of the appropriate command. Functions within the multiplexer are shown in Figure 4.8-3.

The multiplexing FET switches (sampling gates) will accommodate high level inputs without buffer amplifiers. The gates are activated by selection pulses from time-division matrix segments in the programmer block. Commutated

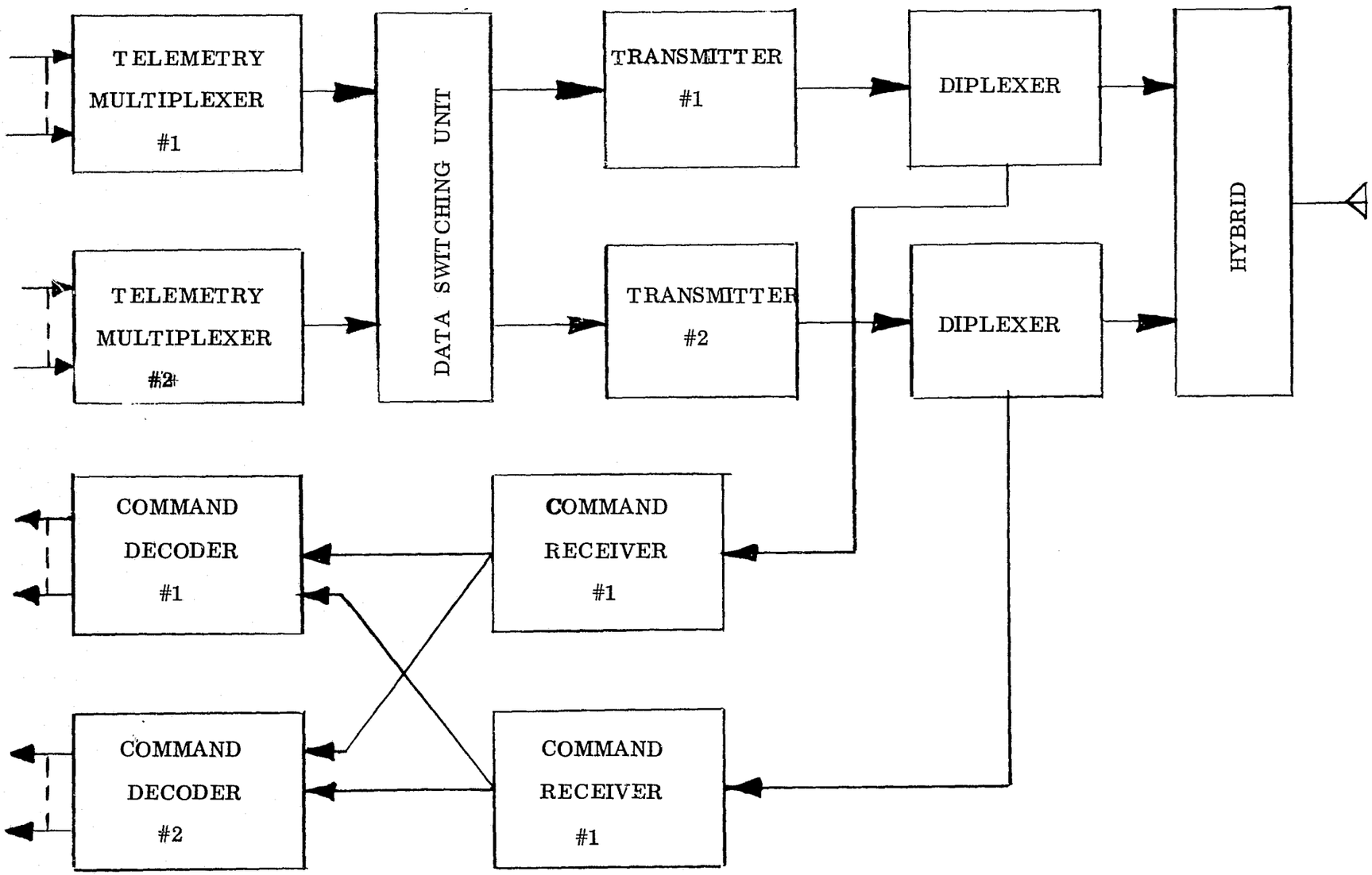


Figure 4.8-1 HYBRID T & C SYSTEM

Table 4.8-1 Telemetry Characteristics

Frequency:	One 30K Hz channel 136 - 137 MHz
R. F. Power:	2 watts
Antenna:	Omnidirectional; circularly polarized
Modulation:	PCM (Bi-ϕL)/PSK
Modulation Index:	$\leq$ 1.5
Multiplex:	Time division
Bit rate:	$\leq$ 400 bps
Format:	Fixed; compatible with GSFC Data Systems Standards
Capacity:	(TBD)
Sampling rates:	(TBD)
Levels:	0-5 vfs analog 0±0.5 v digital "0" 5±0.5 v digital "1"
A/D Conversion Error:	< 1%
Transmission Error Rate:	$< 1 \times 10^{-5}$

Table 4.8-2 Tentative Command Characteristics

Frequency:	One channel 148-154 MHz
Antenna:	Omnidirectional circularly polarized
Modulation:	PCM-FSK/AM/AM
Bit Rate:	128 bps
Format:	64 bit frame compatible with GSFC Data Systems Standards
S/C Addresses:	Two 8 bit words; one for each decoder
Command Capacity:	256
Verification:	Via telemetry; tone execute
Output:	+5.0 volt execute pulse @ 10 mA for 50 ms. ±10%; -5.0 volts standby.
Error Rate:	$< 1 \times 10^{-5}$
Configuration:	Redundant receivers, decoders and regulators.

Table 4.8-3 Power Budget

Command Receivers	2 @ 0.8 watt	1.6 watts
Command Decoders	2 @ 1.5	3.0
Command Regulators	2 @ 1.0	2.0
Multiplexers	1 @ 5.0	5.0
Transmitters	1 @ 5.0	5.0
	Total Average	16.6 watts
	Total Peak*:	19.5 watts

* Includes interrogation increment of 200 mW per receiver, 2.5 watts for addressed decoder.

Table 4.8-4 Weight Budget

Command Receivers	2 @ 1.3 lb.	2.6 lb.
Command Decoder	2 @ 4.0 lb.	8.0
Command Regulator	2 @ 0.5 lb.	1.0
TM Multiplexer	2 @ 4.0 lb.	8.0
TM Switching Unit	1 @ 1.0 lb.	1.0
TM Transmitters	2 @ 0.4 lb.	0.8
Diplexers	2 @ 1.0 lb.	2.0
T & C Antenna Hybrid	1 @ 1.9 lb.	1.9
T & C Antenna Elements	4 @ 0.25 lb.	1.0
	Total Estimated Weight	26.3 lb.

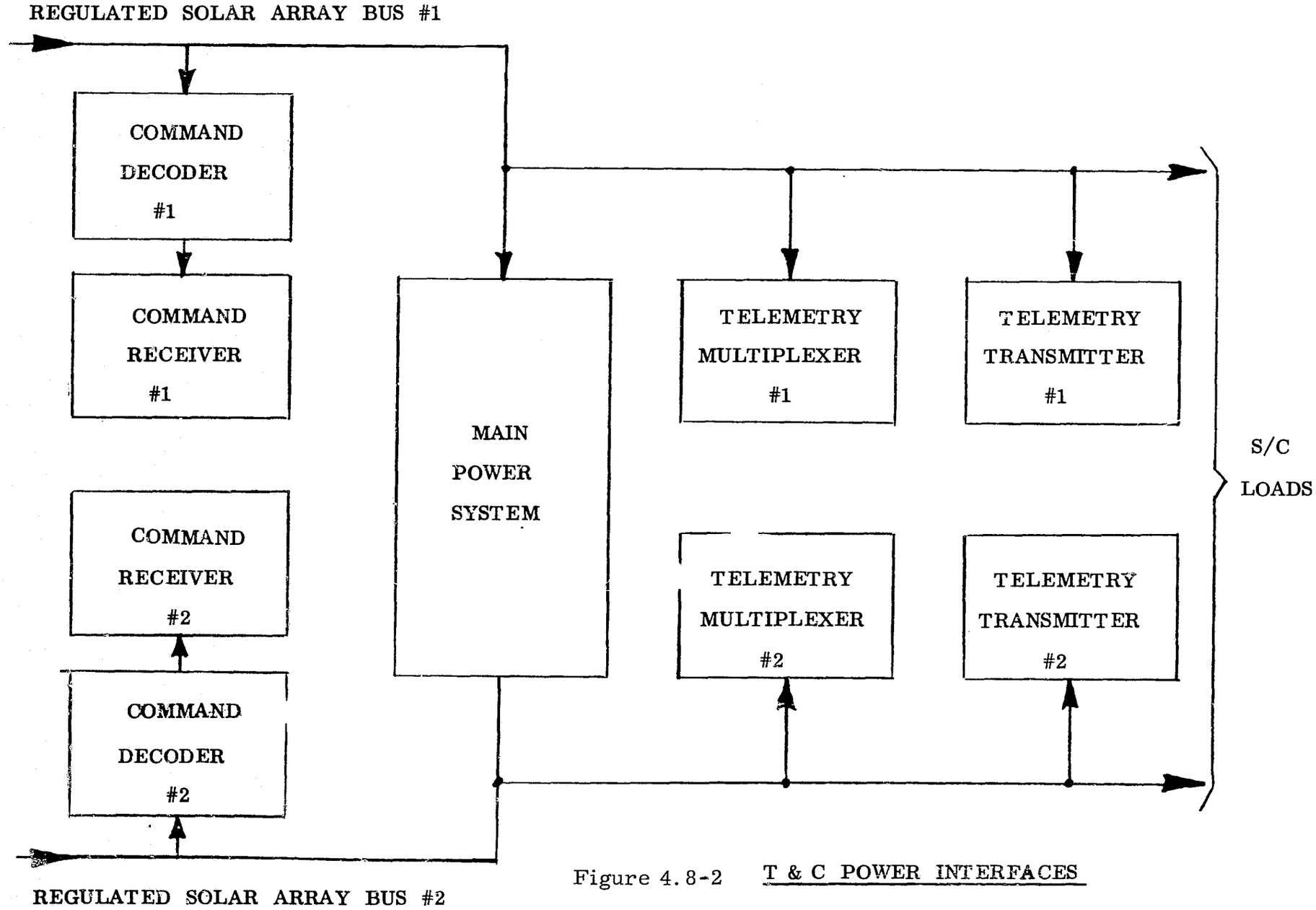


Figure 4.8-2 T & C POWER INTERFACES

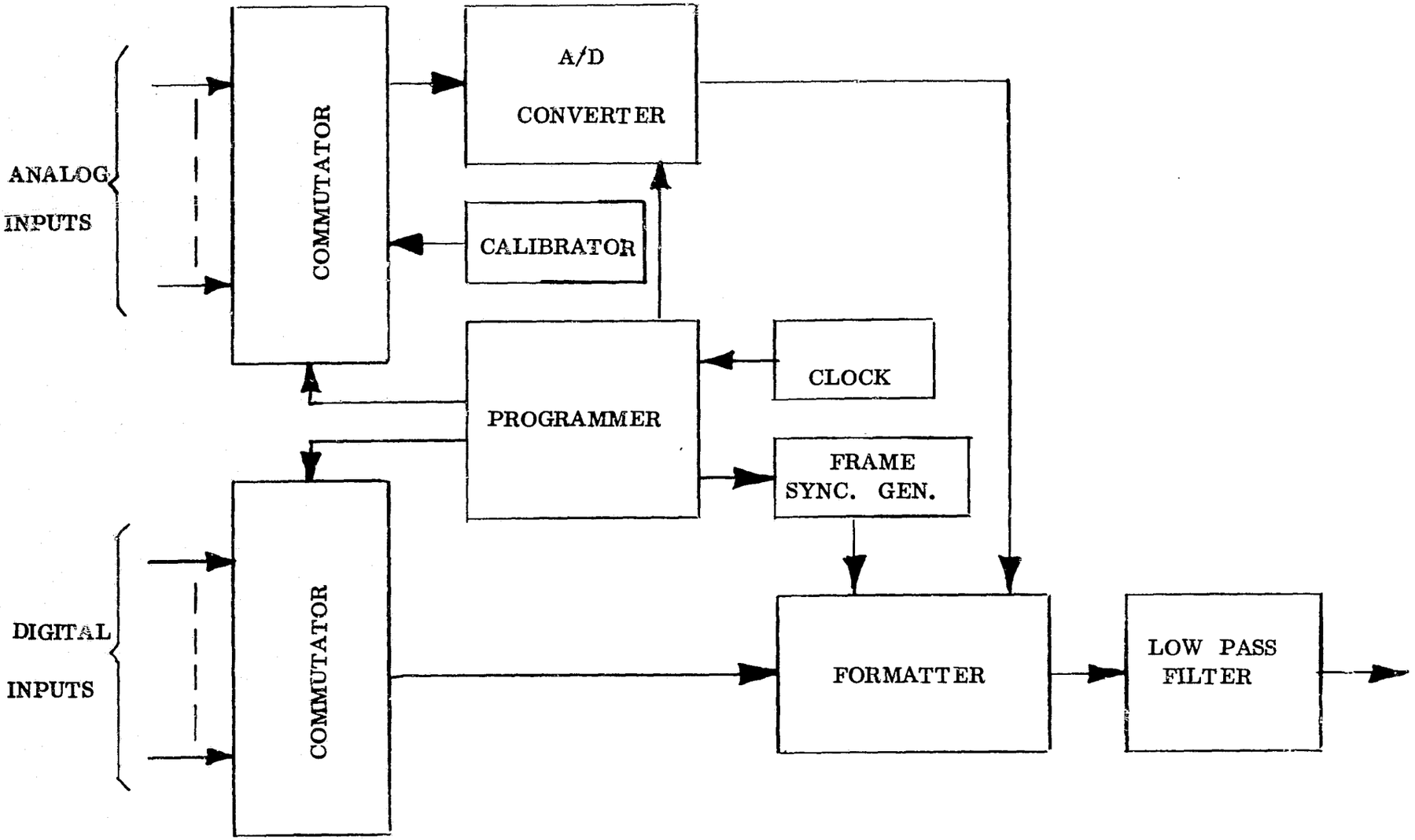


Figure 4.8-3 DATA MULTIPLEXER

digital signals are fed directly to the formatter, whereas output of the analog commutator is a serial PAM wave. This wavetrain is fed into an analog-to-digital converter which encodes each sample into a binary word which is interleaved with the digital commutator data plus calibration and frame synchronization words by the formatter logic. The composite PCM bi-phase signal (illustrated in Figure 4.8-4) is then passed through a constant delay low pass filter to remove unwanted components above the clock frequency. Filter output is applied to the data switching unit.

A five-point calibrator allows correction of the recovered analog data to take variations in spacecraft temperature and supply voltage into account. All switching functions are performed in synchronism with transitions of the self-contained clock. Consisting of a crystal oscillator and binary divider chain, the clock fundamental drives the A/D converter while lower frequency outputs drive the programmer which gates them to the commutators, sync word generator, and formatter.

Conditioned power to operate the multiplexer circuits is derived from the main spacecraft power bus by the internal DC-DC converter. Voltage regulation, isolation from line transients, and overload protection is provided by a conventional series regulator. Power "on" and "off" commands from the command decoder activate transistor switches in the regulator which latch the power supply module "on" or "off". Power, signal, and chassis returns will be isolated.

4.8.2.2 Data Switching Unit

This unit serves two functions:

- TM transmitter selection
- TM transmitter status monitor

Transmitter selection is made via the command system and solid state driver-relay combinations within the unit. Relay position is monitored by providing a conditioned signal to the telemetry digital commutator. Modulation signals from the two multiplexers are OR'd in the switching unit to feed a resistor dividing network which is adjusted to produce equal transmitter modulation indices.

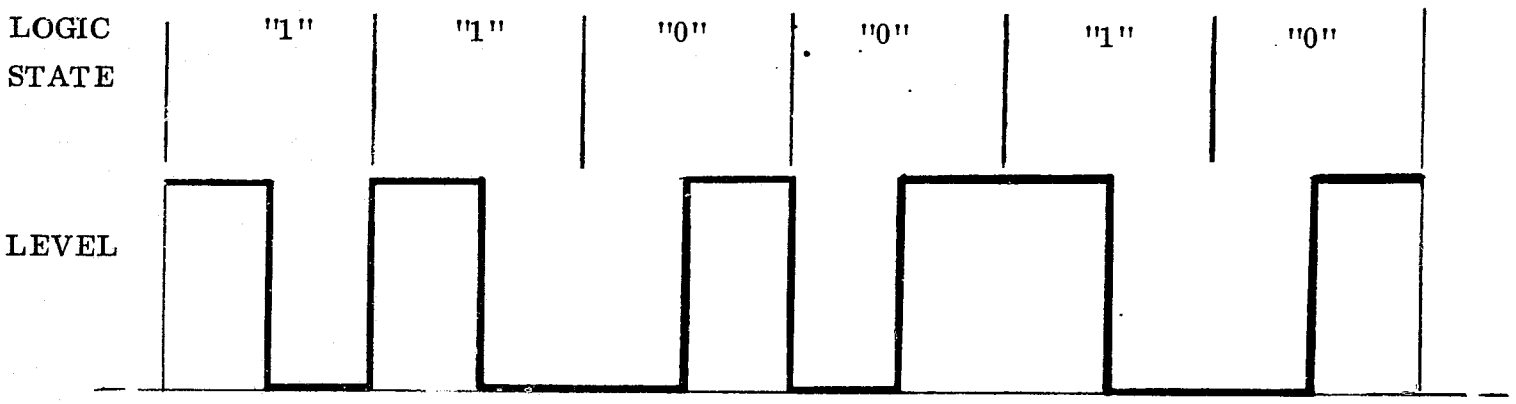


Figure 4.8-4 BI-PHASE SIGNAL

4.8.2.3 TM Transmitters

The VHF telemetry transmitters are qualified solid state, fixed frequency, phase-modulated units. Modulation and power input are applied from the data switching unit as previously described. Power, modulation, and chassis returns will be isolated; r-f output return will be common with the chassis. Output power is 2 watts into 50 ohms at a VSWR of 2:1 or less, any phase. Peak modulation index is 1.57 for a 6V, p-p input into 10,000 ohms. Circuit line-up incorporates temperature compensated crystal oscillator, phase modulator, doubler, driver, and power amplifier. By modulating at one-half the final index, linearity is maintained at 1% or better and distortion products reduced. A low pass filter is inserted between the power amplifier and transmitter output to attenuate spurious output components. Overall dc to rf conversion efficiency is ~40%. Approximate weight is 0.4 lbs.

4.8.2.4 T&C Antenna System

Two diplexers, transmission lines, a hybrid, and turnstile antenna comprise the antenna system. The diplexers isolate associated TM transmitters and command receivers so that both may use the same transmission line and antenna without interference or excessive insertion loss. They contain passive band pass and reject filter elements. Transmission lines are solid dielectric, flexible coaxial cables which interconnect the diplexers to the hybrid. The hybrid unit consists of three 1-1/2 wavelength hybrid rings of stripline construction which combine and power divide the transmitter signals for connection to the antenna feed lines; they also distribute received signals to the command receivers. Feed lines which connect the antenna elements to the hybrid are cut to produce the phase rotation required for launching a circularly polarized wave. Figure 4.8-5 shows the hybrid feed arrangement.

4.8.2.5 T&C Antenna

Maintaining 100% T&C coverage independent of spacecraft attitude is a major requirement placed on the system. Perfectly spherical coverage cannot be achieved for electrically large spacecraft, but can be approached quite closely depending on spacecraft geometry, operating wavelength and antenna complexity. Generally, circular polarization aboard the spacecraft results in the best coverage performance.

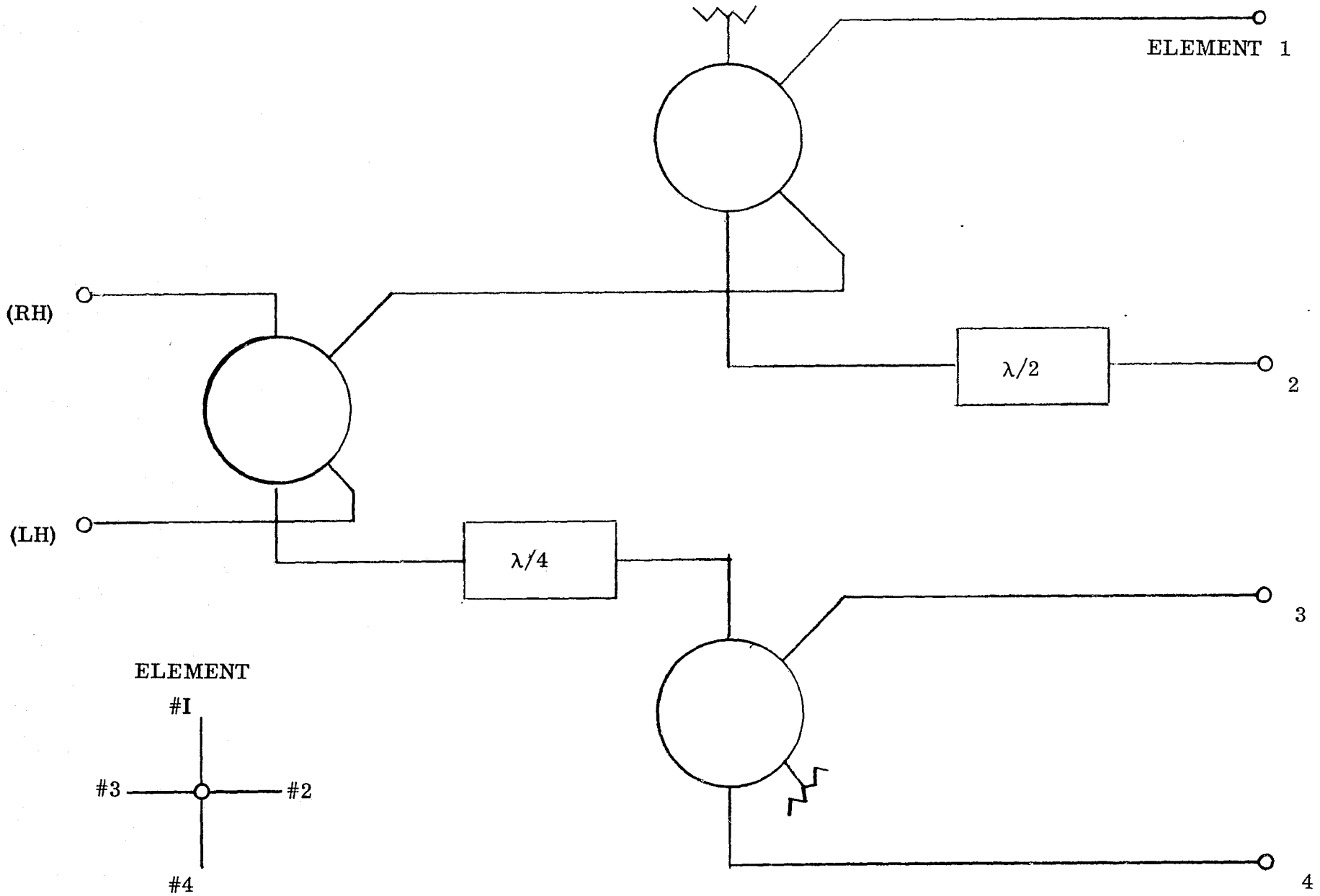


Figure 4.8-5 HYBRID FEED

The relatively small electrical size of the hybrid satellite at VHF suggests a single turnstile antenna mounted to the equipment module will produce quite acceptable results. Model tests on a larger (SERT II) spacecraft indicate composite E_θ, E_ϕ coverage of better than 99% @ -10 dBi. Figure 4.8-6 shows the composite gain distribution for the model illustrated in Figure 4.8-7.

4.8.3 COMMAND

Redundant command receivers, decoders, and regulators make up the command equipment group. PCM-FSK/AM/AM signals on the assigned command frequency are received simultaneously by both receivers which feed both decoders in a "cross-strap" arrangement so that either receiver can operate either decoder. After processing by the address decoder and ground verification via telemetry, the command is executed by transmission of a command-execute tone.

4.8.3.1 Command Receiver

This VHF receiver is a qualified solid state, AM single conversion superheterodyne design incorporating crystal local oscillator and IF filter. It will deliver an output of 5_v rms across 500 ohms at a signal-to-noise ratio of 13 dB or better in a 10kHz band for an input of 1.5 μV @ 50 ohms modulated to a depth of 75%. IF bandwidth is 35kHz minimum at -6dB. Stability is maintained within $\pm$ 2kHz from -10 to +50^{o}C. Power, output, and chassis returns are isolated. Reverse polarity protection and AGC monitoring provisions are incorporated. Both receivers are powered throughout the mission. They cannot be commanded "off" and are powered from dedicated regulators to isolate them from load faults on the main power bus.

4.8.3.2 Command Decoder

The decoder block diagram is shown in Figure 4.8-8. A tentative PCM command format compatible with the NASA/GSFC PCM Command Standard is shown in Figure 4.8-9. A frame length of 64 bits and 128 Hz bit clock is chosen to be compatible with the present ATS/OGO consoles; this fixes the maximum command rate at 2/sec. The logic "0" and "1" states are represented by FSK tones in the 7-12kHz range with clock sidebands which are amplitude modulated onto the command carrier. Each FSK tone is 50% amplitude modulated by the 128Hz sinewave clock.

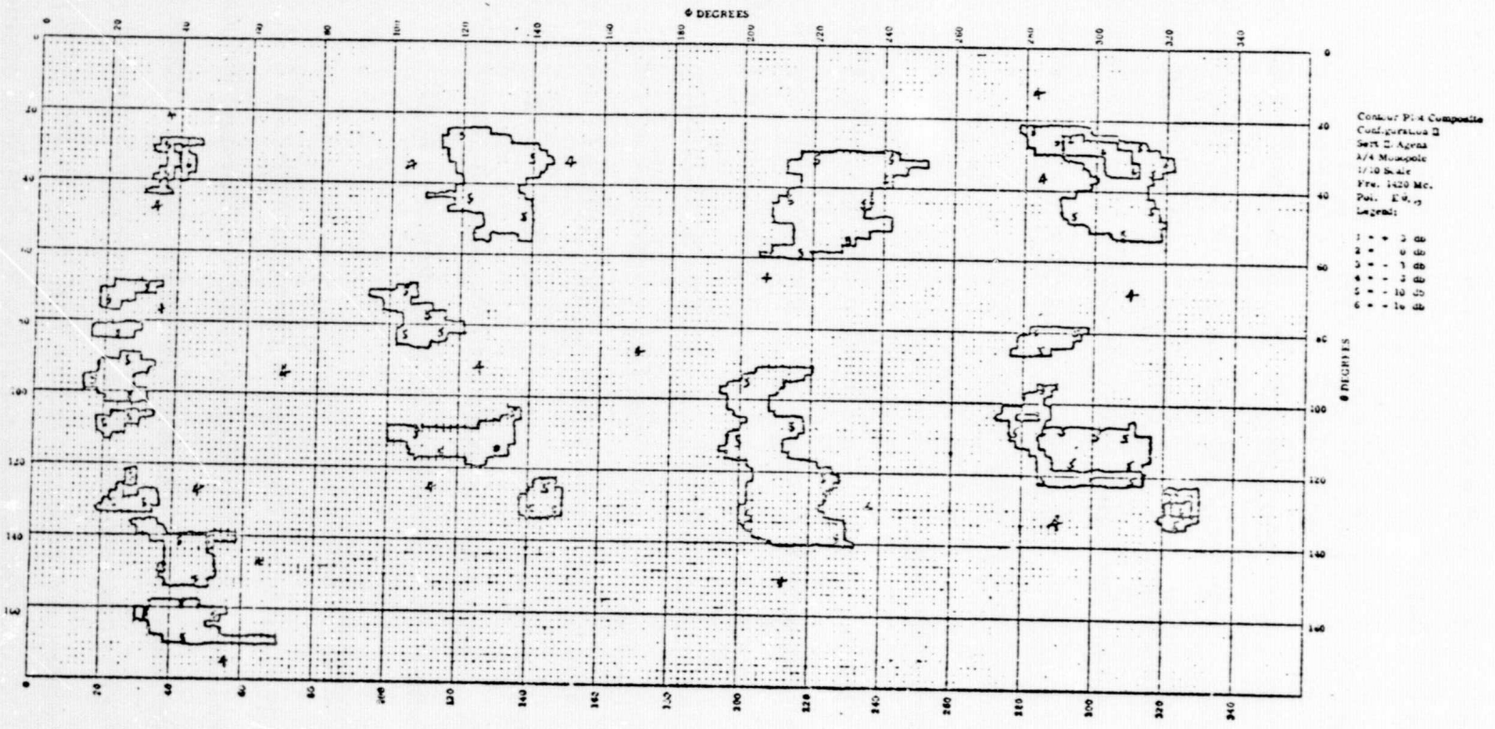


Figure 4.8-6 COMPOSITE ANTENNA GAIN CHART

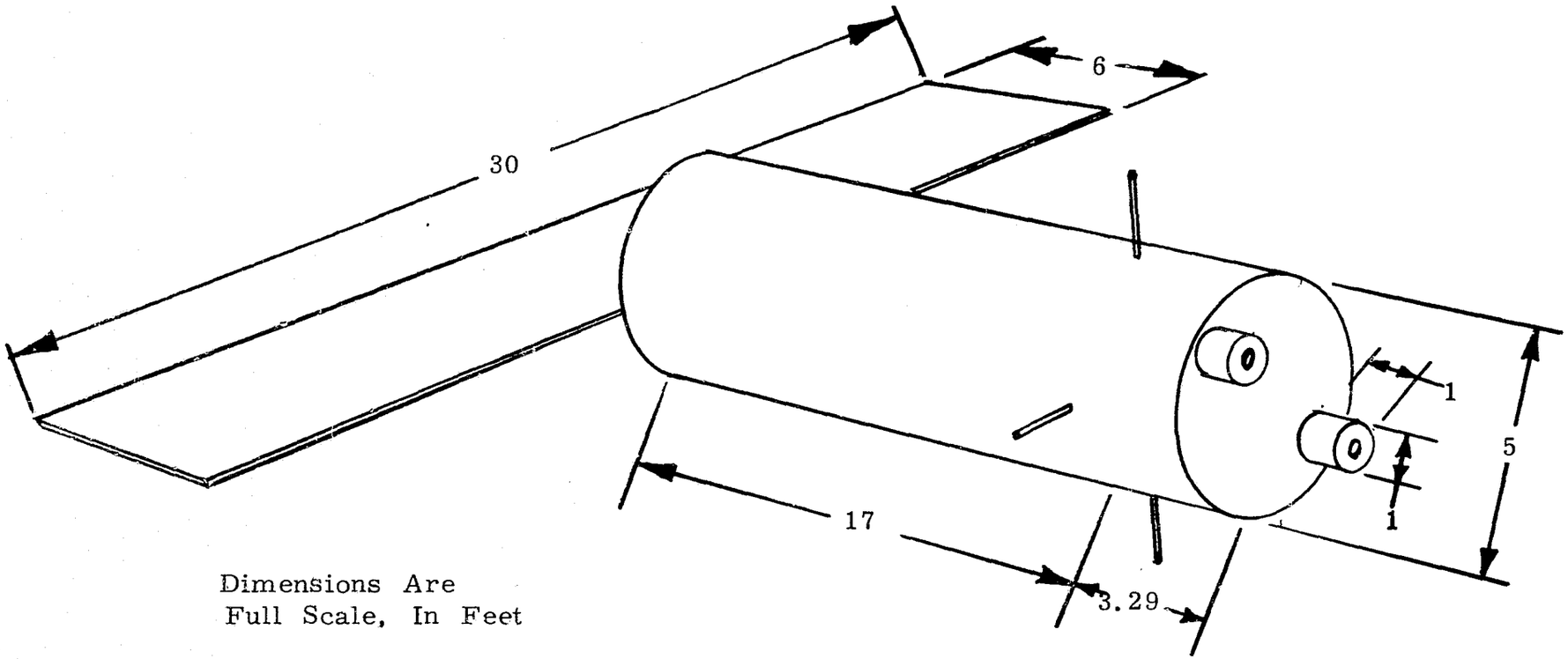


Figure 4.8-7 ANTENNA MODEL

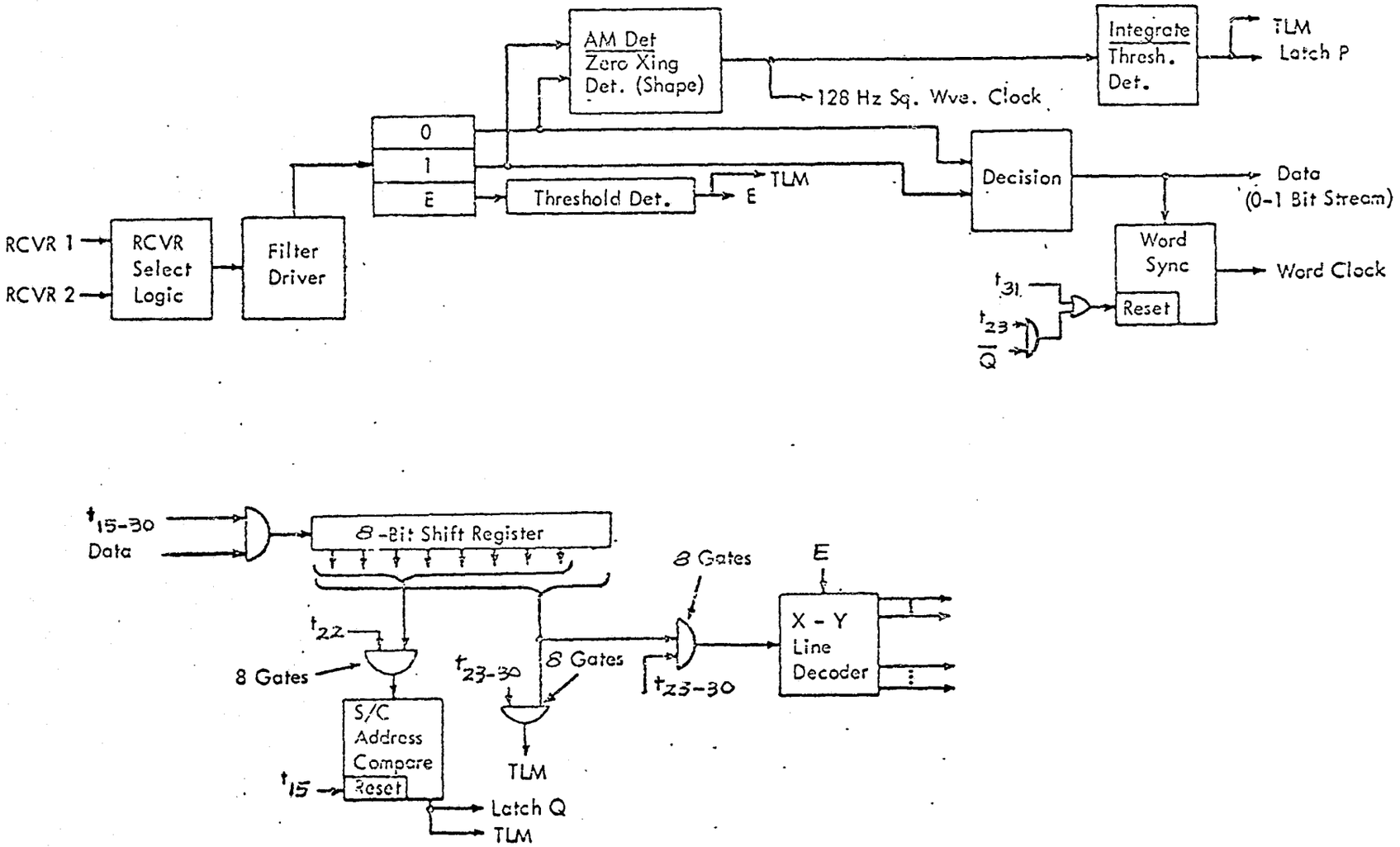


Figure 4.8-8 COMMAND DECODER LOGIC FLOW

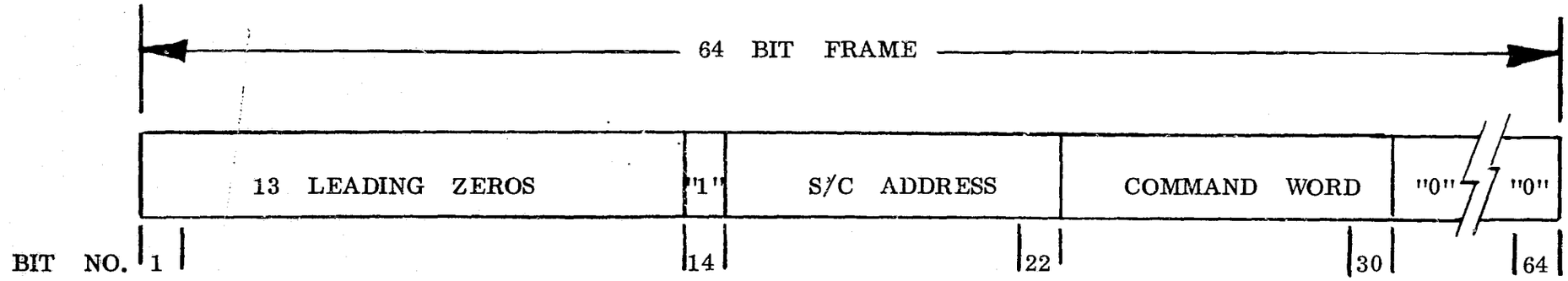


Figure 4.8-9 PCM COMMAND FORMAT

An introductory "0" tone for 13 bit times allows each decoder receiver-select circuit to recognize a valid "0" tone and clock are being received, connect to the active receiver, and set the address-compare latch. The following "1" synchronization bit sets the word clock which gates the following 16 bits into the 8 bit shift register. At bit number 22, the spacecraft address fills the register in each decoder and address compare logic in each determines which decoder is to process the 8 bit command which follows. On no-compare, the power latch and word counter are reset. A valid address results in shifting in the following 8 bit command word which is gated out to the X-Y decoding matrix during bit number 30. Commands are distributed by the output drivers when an execute tone is received, after which the power latch is reset. When the "0" tone and 128Hz clock are removed from the command carrier, all power latches and logic are reset and the decoder returns to the standby condition.

As an alternative to ground verification of commands before execution, command word parity or complement check could be utilized for automatic execute at some small increase in decoder complexity.

Dedicated command regulators are fed from the solar array-battery bus and housed in the command decoders. Accordingly, one command decoder and one receiver are normally powered by each dedicated regulator; in the event one regulator should fail, both receivers and one decoder are powered from the same regulator. Receiver connections are made through a simple current limiter; main and back-up output voltages are staggered by ~2 volts.

The decoders are powered continuously during the mission and cannot be commanded "off".

APPENDIX A

Preliminary Structural Analysis

Presented within are the preliminary stress and dynamic analyses supporting the hybrid spacecraft design.

- Design Criteria

(a) Structural members will be designed so as not to exceed 90% of 0.1% offset yield at design load.

(b) Factors of Safety

1. Prelaunch (1.5) FS

2. Flight Conditions (1.5) FS

3. Random Vibration (1.5) FS

(c) Margins of Safety

MS = R-1 where R = ratio of allowable to design

A minimum MS = +.25 for primary structure and between -0.1 and +0.1 for components and secondary structure.

(d) Loads Calculation

1. Primary Structure: "The static acceleration loads imposed through the SC cg defined in Para. 6.16 of Reference are the structural design loads for primary structural members provided thrust axis first resonance be above 40Hz and lateral first resonance be above 25 Hz for the spacecraft hard mounted at the separation plane. (Preliminary analysis indicates these design goals are readily attainable. Therefore, this criteria will be employed.)

2. Components, Appendages, and Subsystems: To the sinusoidal vibration levels of Para. 6.14 shall be applied the Q's specified in Para. 3.1.1 (Reference). Q = 10 for transverse and Q = 5 for thrust for all non-main body elements. The maximum g level from the spectrum will be utilized.

(e) Material Properties

Assume the usage of 7075-T6 Aluminum Alloy from MIL-Handbook 5A, February 8, 1966, Figure 3.2.7.16. The stress value at .001 and .002 permanent strains are obtained. The $\Delta\sigma$ value between these two strains is then subtracted from design allowables as recorded in Table 3.2.7.0, Mil Handbook 5A (...since the handbook allowables are based upon .002 permanent set.) Ninety percent (90%) of the remaining value is then the design allowable.

$\Delta\sigma$ = 4000 psi

F_{cy} = 67,000 psi

F_{ty} = 66,000

F_{tu} = 76,000

F_{su} = 46,000

$F_{c_{design}}$ = ((67-4) 10^3) (.9)

= 56,700 psi

$F_{t_{design}}$ = (66-4) 10^3) (.9)

= 55,800 psi

$F_{s_{design}} = \frac{F_{su}}{F_{tu}} F_{t_{design}}$

= 33,800 psi

(f) Loading Conditions: For preliminary analysis, the loading environment from first and second stage will be employed.

Primary Structure: Thrust LF design = 15.8

Lateral LF design = 3.0

Components & Appendages:

Thrust LF design = (6.7)(5)

= 33.5

Lateral LF design = 2.3)(10)

=23

For preliminary analysis, the L Band antenna, stowed solar array and VHF band antenna are considered components and appendages.

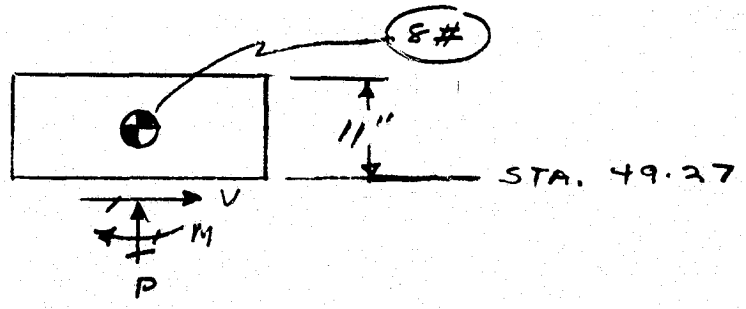
Design Loads To all primary structure, the combined 15.8 ± 3.0 g's are applied. To the L band antenna, VHF antenna and stowed solar array are applied a G of 10 laterally and 5 in the thrust axis, to the vibration spec. of sect. 6,14

Solar array & antennas' thrust $\Delta F = 6.7(5)$
$= 33.5\,g$

solar array & antennas' lateral $\Delta F = 2.3(10)$
$= 23\,g$

All other members are considered primary structure

(a) VHF BAND ANTENNA (STOWED)



$V_{49.27} = 8(23) = 184\#$

$M_{49.27} = 8(23)(5.5) = 1012$ in.-#

$P_{49.27} = 8(33.5) = 268\#$

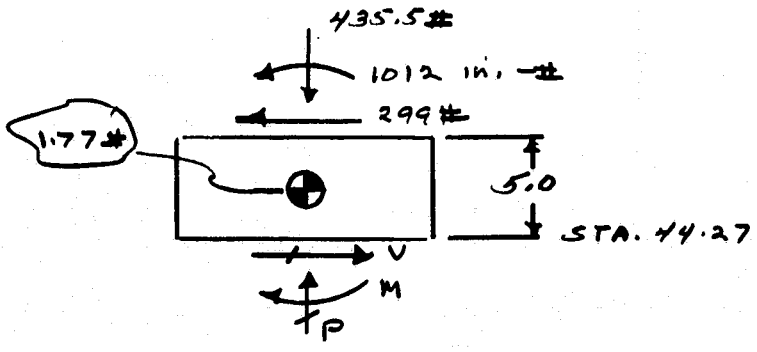
The L band antenna is attached at STA. 49.27, this is applied as a point load at 49.27 Weight of the L band antenna is 5#.

$V_{L\text{-band}} = 5(23) = 115\ \#$

$P_{L\text{-band}} = 5(33.5) = 167.5\ \#$

$V_{49.27}$	=	184 + 115 =	299 #
$M_{49.27}$	=	1012 in.-#	
$P_{49.27}$	=	268 + 167.5 =	435.5 #

(b) UPPER PART OF CYLINDER



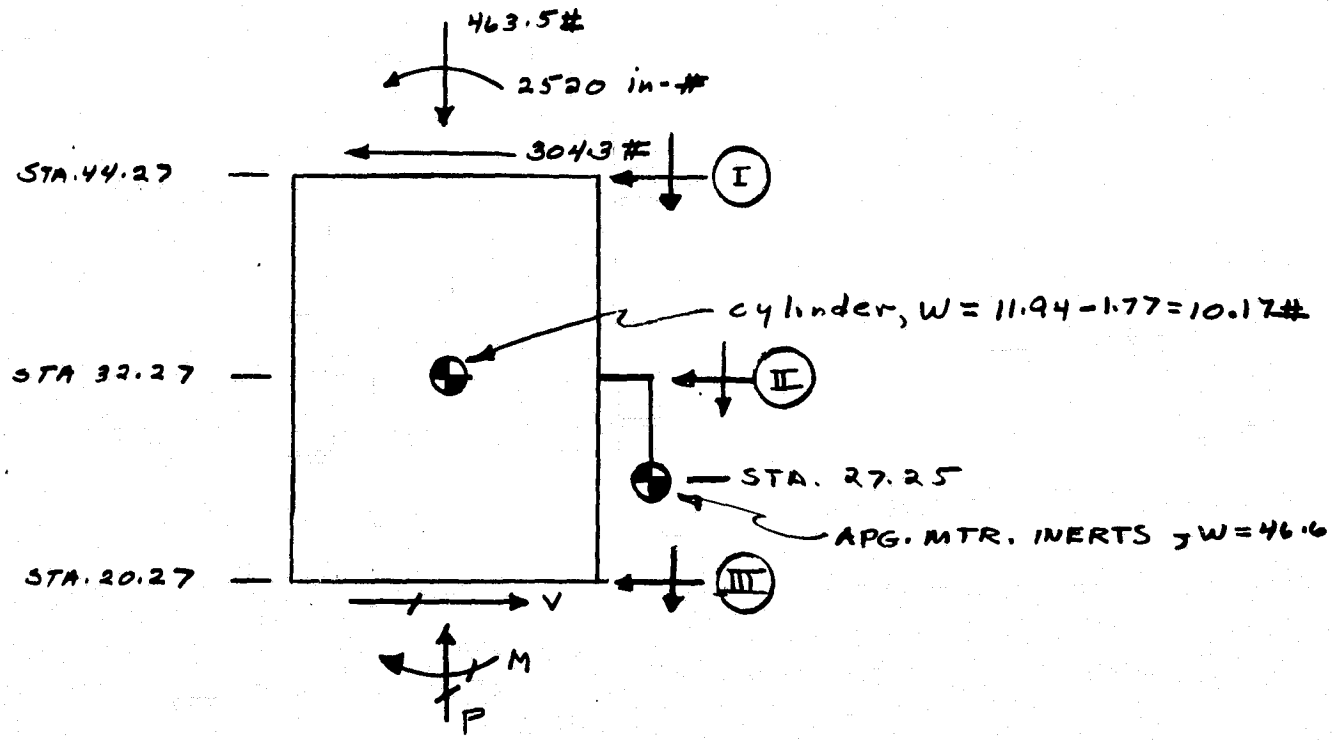
$V_{44.27} = 299 + 3(1.77)$
$= 299 + 5.31$
$= 304.3\ \#$

$M_{44.27} = 1012 + 3(2.5)(1.77) + 299(5)$
$= 1012 + 13.3 + 1495$
$= 2520$ in.-#

$P_{44.27} = 435.5 + 15.8(1.77)$
$= 435.5 + 28$
$= 463.5\ \#$

(c) CYLINDER The application of module and solar array loads to the cylinder is 50% to the top and 50% to the bottom of the cylinder. The weight of the packages within the module is 302.9 lbs. Although a

33.5 g load factor is specified for components, it is not used for simultaneous application to all module components. This results in too severe a load and would assume the unlikely condition that all package resonances were occurring simultaneously



Loading (I):

Wt. = Mod. sup. ring upper + $\frac{1}{2}$(mod. structure + mod. equipment + prop. & tanks + solar array + solar array drive)

= 1.2 + $\frac{1}{2}$(42.4 + 306.9 + 60.5 + 104.8 + 44.0)

= 1.2 + $\frac{1}{2}$(558.6) = 62 + & 79.3

= 280.5 #

Loading (II)

Wt. = cylinder + apg. mtr. inerts + fuel + apg. mtr. ring

$= 10.17 + 46.6 + 614.5 + 2.1$

$= 673.37\#$

LOADING III

WT. = MOD. SUP. RING LOWER + $\frac{1}{2}$ (mod. structure + mod. equipment + prop. & tanks + solar array + solar array drive)

$= 1.9 + \frac{1}{2}(42.4 + 306.9 + 60.5 + 104.8 + 44.0)$

$= 1.9 + \frac{1}{2}(558.6) = 1.9 + 279.3$

$= 281.2\#$

LOADS AT STA. 44.27

·all parts of the loading wt. (loading I) have a 15.8 & 3.0 g load factor, except for the portion of the weight belonging to the solar arrays and solar array drive

$V_{44.27} = 304.3\# + 23(\frac{1}{2})(104.8+44) + 3.0(280.5 - 74.4)$

$= 304.3 + 23(74.4) + 3.0(206.1)$

$= 304.3 + 1710 + 618.3$

$= 2633\#$

$P_{44.27} = 463.5 + 33.5(74.4) + 15.8(206.1)$

$= 463.5 + 2490 + 3260$

$= 6214\#$

$M_{44.27} = 2520$ in.-#

LOADS AT STA. 32.27

$V_{32.27} = 2633 + 3.0(673.37)$

$= 2633 + 2020$

$= \underline{4653\#}$

$P_{32.27} = 6214 + 15.8(673.37)$

$= 6214 + 10610$

$= \underline{16824\#}$

$M_{32.27} = 2520 + 2633(12) - 46.6(3.0)(32.27 - 27.25)$

$= 2520 + 2633(12) - 46.6(3)(5.02)$

$= 2520 + 31600 - 705$

$= \underline{33415\text{ in.-}\#}$

LOADS AT STA. 20.27

The same reasoning applies on loads at STA. 20.27 as applied to loads at STA. 44.27

$V_{20.27} = 4653 + 23(1/2)(104.8 + 44) + 3.0(261.2 - 74.4)$

$= 4653 + 23(74.4) + 3(206.8)$

$= 4653 + 1710 + 620$

$= \underline{6983\#}$

$P_{20.27} = 16824 + 33.5(74.4) + 15.8(206.8)$

$= 16824 + 2490 + 3275$

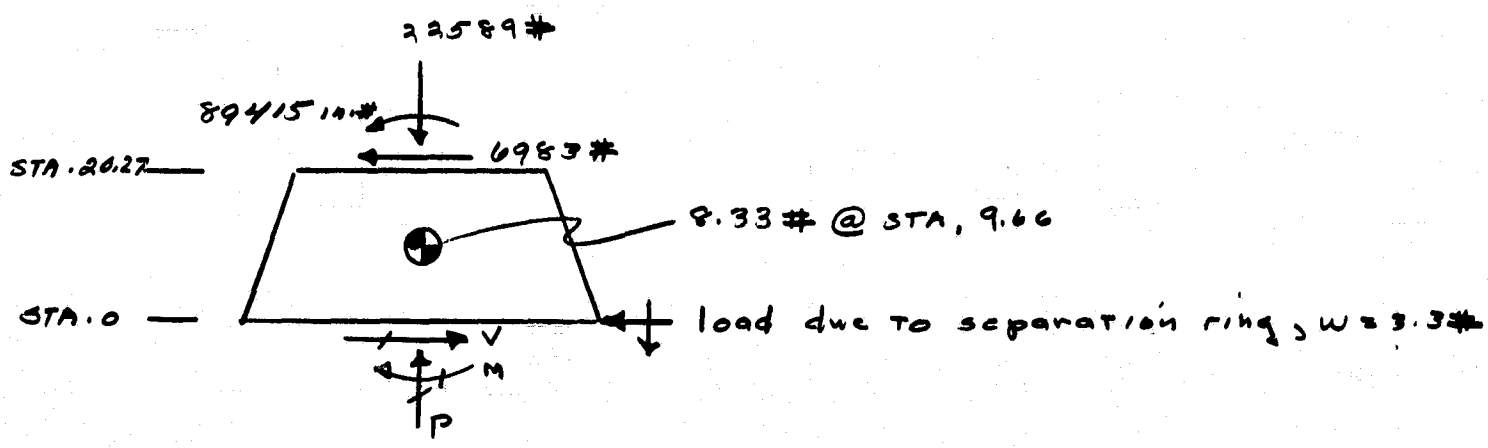
$= \underline{22589\#}$

$M_{20.27} = 33415 + 12(4653)$

$= 33415 + 56000$

$= \underline{89415 \text{ in.-lbs}}$

ⓓ Frustum



$V_0 = 6983 + 3(8.33 + 3.3)$

$= 6983 + 3(11.63)$

$= \underline{7018\#}$

$P_0 = 22589 + 15.8(8.33 + 3.3)$

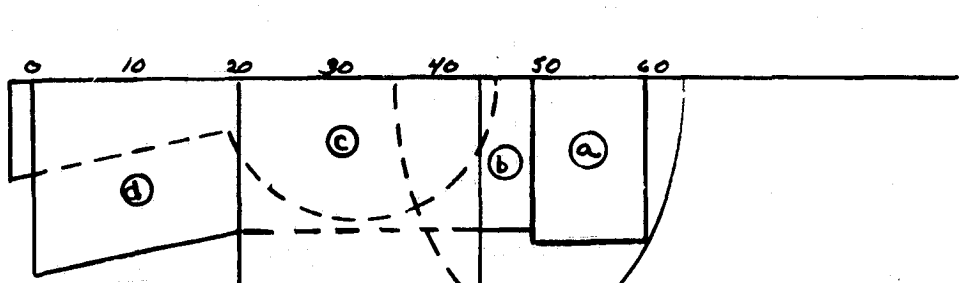
$= 22589 + 15.8(11.63)$

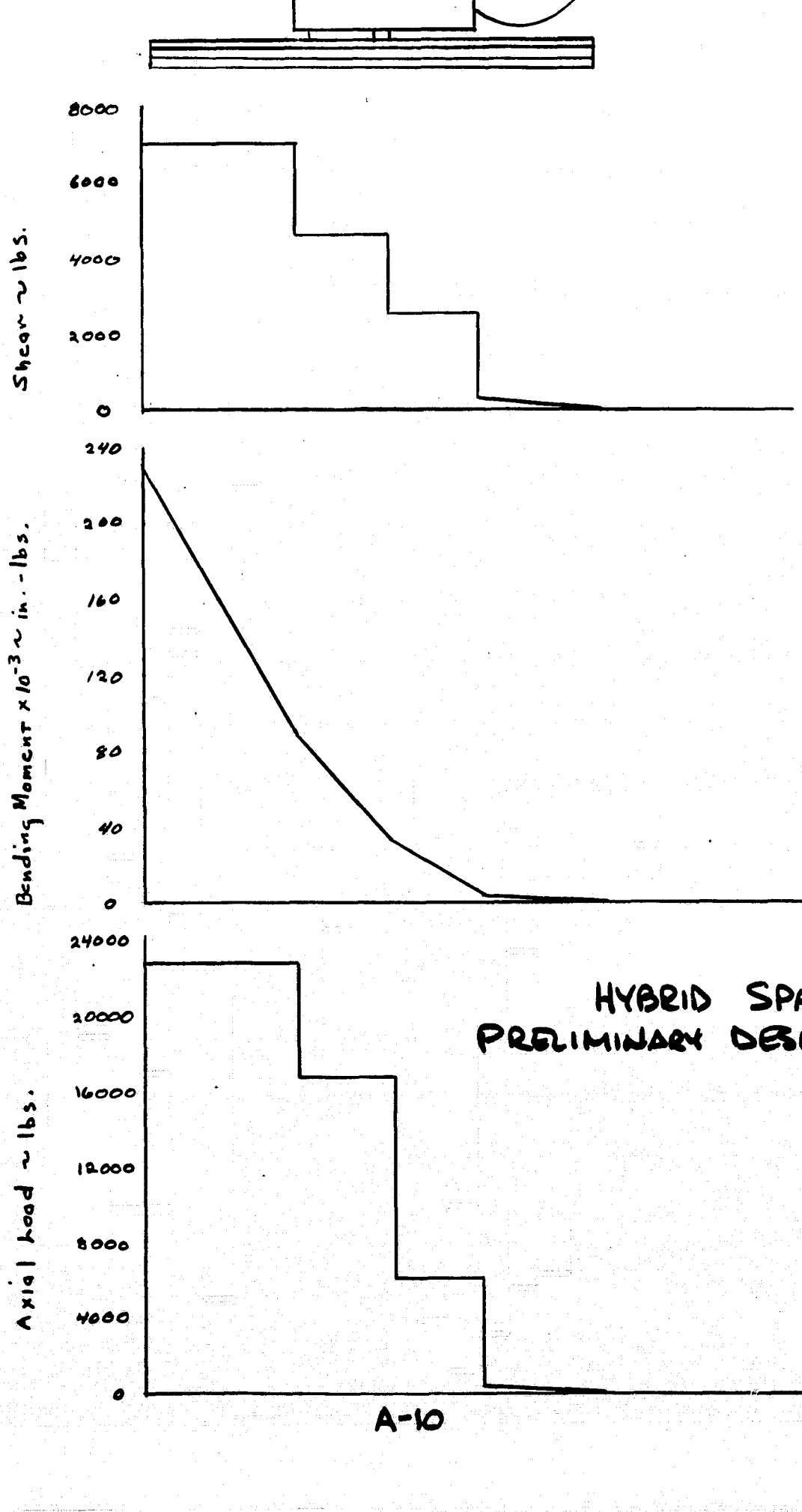
$= \underline{22773\#}$

$M_0 = 89415 + 6983(20.27) + 8.33(9.66)(3)$

$= 89415 + 141,700 + 241$

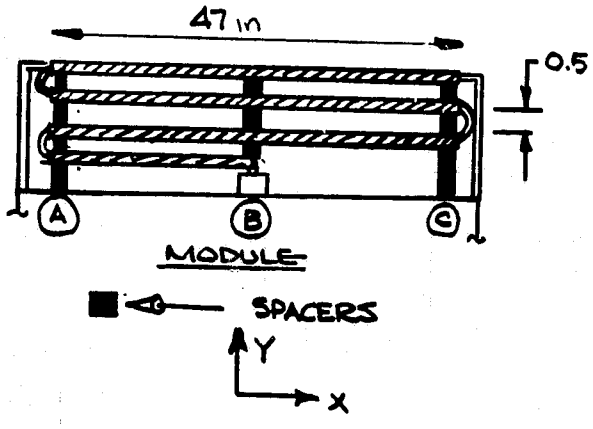
$= \underline{231,356}$





HYBRID SPACECRAFT
PRELIMINARY DESIGN LOADS

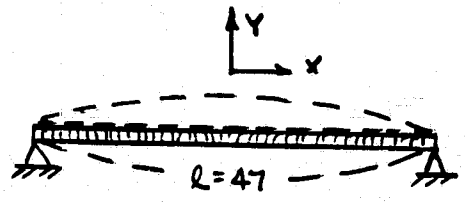
• Solar Array (stowed)



- Stowage envelope limits honeycomb thickness to 3/4 in.
- Thickness between stowed panels approximately 0.5 inch
- Face sheet thickness of 8 mils is required for orbital frequency (see pg)

Between panels at points Ⓐ and Ⓒ are rigid spacers. At point Ⓑ is an elastic spacer designed to preclude slapping of adjacent panels if "out of phase" vibration occurs. The anticipated panel deflections, frequency and elastic spacer characteristics are presented herein

Panel Frequency & Deflection: The panel, 47×55 inches, is assumed simply supported along the 55 inch edge and free along the 47 inch edge. The total weight of the 3 panels is approximately 50 lbs. which is assumed uniformly distributed.



Wt. per panel = W = 50/3 · 16.7 lb

ℓ = 47 in

$$I = \frac{Ah^2}{2} = \frac{(55 \times .008)(.75)^2}{2}$$

$$I = .124 \text{ in}^4$$

$$f_n = 1.57\sqrt{\frac{gEI}{W\ell^3}}$$

$$= 1.57\left(\frac{386 \times 10^7 \times .124}{16.7 \times (47)^3}\right)^{1/2}$$

$$= 1.57\left(\frac{47.86 \times 10^7}{1.734 \times 10^6}\right)^{1/2}$$

$$= 1.57\,(16.6)$$

$$f_n = 26.1 \text{ cps}$$

Stowed Solar Array (cont'd)

The mid span deflection associated with the environment of 23 lateral g's is:

$$\delta_B = \frac{5\,W\ell^3}{384\,EI} \times 23$$

$$= \frac{(5)(16.7)(47)^3}{(384)\times 10^7 \times (.124)} \times 23$$

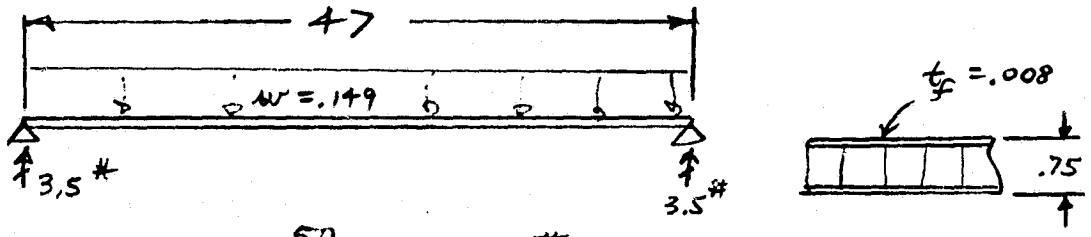
$$= .018 \times 23$$

$$\underline{\delta_B = 0.41 \text{ inches}}$$

Assuming two adjacent panels to "out of phase" during vibration there is interference. Assuming "in phase" vibration there is the problem "can the solar cells withstand the radius of curvature associated with the above deflection?" For the interference problem, assume a mid span spacer. Conservatively assume a beam of $\ell/2$ simply supported and ratio the above δ_B. The deflection, with mid span supports, is $\delta_{max} = .026$ avoiding the slapping of adjacent panels. The design of the elastic mid span spacer is qualitatively discussed herein. The spacer is an elastomeric material possessing high damping capacity. It must be capable of being stowed in 0.5 inches and have sufficient stiffness so as to respond to the 26 cps resonance of the panels (ie -- maintain contact with the vibrating panels). To maintain contact with the panels throughout their excursions the spacer must be compressed when stowed in the 0.5 inch space.

SOLAR CELLS

The cells are checked for panel primary bending and for secondary bending due to panel curvature obtained under load.



Panel wgt. = $\frac{50}{3}$ = 16.7 #

Panel dimensions = 47 x 55

At 23 g's:

$$w = 23\left(\frac{16.7}{47\times55}\right) = .149 \ \#/in/in$$

$$M_{MAX} = \frac{wL^2}{8} = \frac{.149(47)^2}{8} = 41.2 \ in\#$$

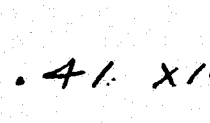
CURVATURE ANALYSIS

Sandwich panel $I = 2(.008)(.371)^2 = .0022 \ in^4$

Elastic curve radius of curvature of panel at point of maximum moment:

$$R = \frac{EI}{M} = \frac{10.5(10)^6(.0022)}{41.2} = 560"$$

Cell configuration:



Cover glass t = .006"
cell t = .011"

$$I = \frac{(.017)^3}{12} = .41 \times 10^{-6}$$

Assume the cell conforms to panel curvature.

$M = EI/R = (10)^7(.41\times10^{-6})/560 = .0073 \ in\#$

$f_b = Mc/I = .0073(.0085)/(.41\times10^{-6}) = 151$ psi Low

SOLAR CELLS (CONT'D)

PRIMARY PANEL BENDING

$M_{MAX} = +1,2$ "*

To obtain the maximum primary axial stress in the cell and coverglass, it is conservatively assumed that these components are fully effective in resisting panel bending. This is not true as the cells are bonded to the substrate (structural panel) with a silastic adhesive. As E for glass is approximately that of aluminum, the glass thicknesses are added to the aluminum face to determine the couple force due to bending.

Couple = $41,2 / .758 = 54,5$ #

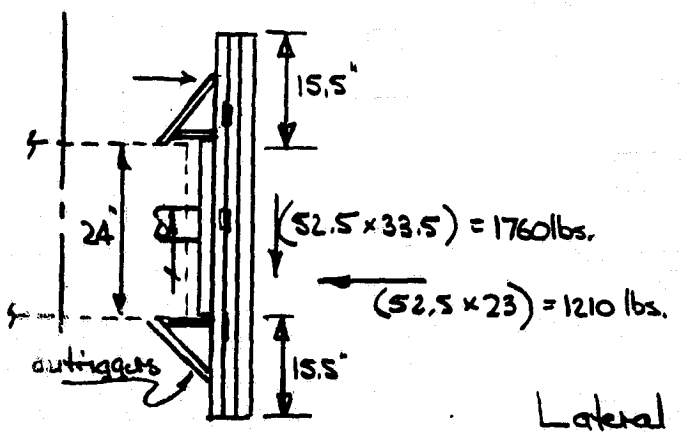
$f_c = 54,5 / (.008 + .017) = 2180$ psi

From MIL-HDBK-17, PART II

$F_c = 6500$ psi (Regular annealed glass)

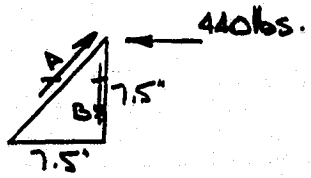
$$\underline{\underline{M.S.}} = \frac{6500}{2180} - 1 = \underline{\underline{2,0}}$$

Solar Array Outriggers



All lateral loads are assumed taken by the 8 outriggers. Thrust axis loads are taken by shear members at the middle of the module. The drive cylinder is assumed to be a 3" diameter member.

Lateral load per outrigger = $\frac{1760}{4}$ = 440 lbs.



$F_A = \frac{440}{.707} = 622$ lbs. $\quad F_B = 440$ lbs.

Assume a 1" diam. tube ($\ell = 10.6$)

Buckling

$$P_{CR} = (1.5)\frac{\pi^2 EI}{\ell^2}$$

$$= \frac{(1.5)(10)^8 A r^2}{2\ell^2}$$

$$= \frac{(.375)(10^8)A}{225}$$

$$P_{CR} = (1.67 \times 10^5)A$$

Crippling

$$P_{CR} = (F_{cy})(A)$$

$$P_{CR} = (55{,}000)A$$

Solar Array Outriggers (cont'd.)

Crippling $\frac{P}{A} = \frac{622}{\pi d t} = 55000 = F_{cy}$

$t_{req'd} = \frac{622}{(3.14)(55000)}$

$t_{req'd} = .004$ in

Use $t = .010$ $P/A = 622/.0314 = 19808$ psi

$\frac{f}{F_{cy}} = \frac{19808}{55000} = .36$

$MS = \frac{1}{.36} - 1$

$MS = 1.78$

Weight: Outriggers $= N(\rho A l)$

$= 8((.1)(.0314)(7.5+10.6)$

$= (.8)(.0314)(18.1)$

$= (.025)(18.1)$

Wt. = 0.45 lb

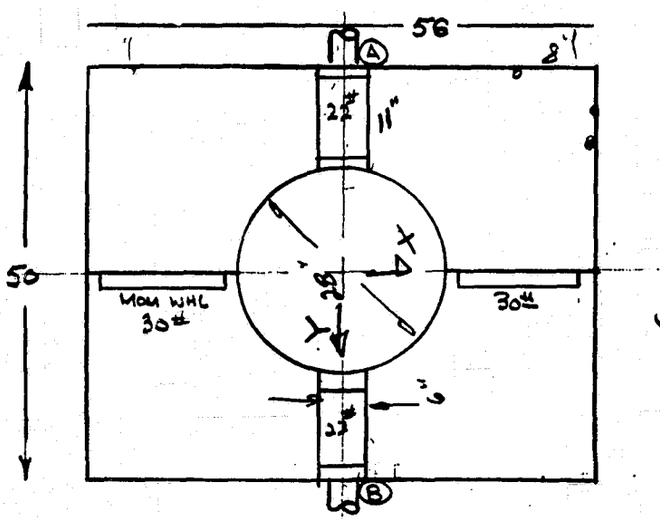
NOTE 6 lb. has been allocated in the weight summary for retention & deployment mechanisms

PRELIMINARY STRUCT. ANAL.

MODULE STRUCTURE

For preliminary analysis the following items of the module structure are investigated:

- Sides
- Top & Bottom surfaces
- Bulkheads



. In considering the loads on primary structure due to the components the 15.8 → 3.0 Load factors are applied, not the 33.5 → 23 normally applied to components, Reference pgs 3... of the loads section of this report. All packages are assumed mounted on the sides of the module with the exception of the following:

- Mom Wheel (30#) (bulkhead)
- 30# Misc (bulkhead)
- Prop. Tanks (60.5 lb) (cylinder)

leaving 247 lbs assumed mounted on the side surfaces. This weight is assumed uniformly distributed along the sides

Side Components:

$$\frac{\text{Thrust Load}}{\text{inch}} = \frac{247(15.8)}{212\text{ in}} = 18.4\text{ lb/in}$$

$$\frac{\text{Lateral Load}}{\text{inch}} = \frac{(247)3}{212} = 3.5\text{ lb/in}$$

Solar Array

Thrust load = (52.4)(33.5)
= 1755 lb. per array

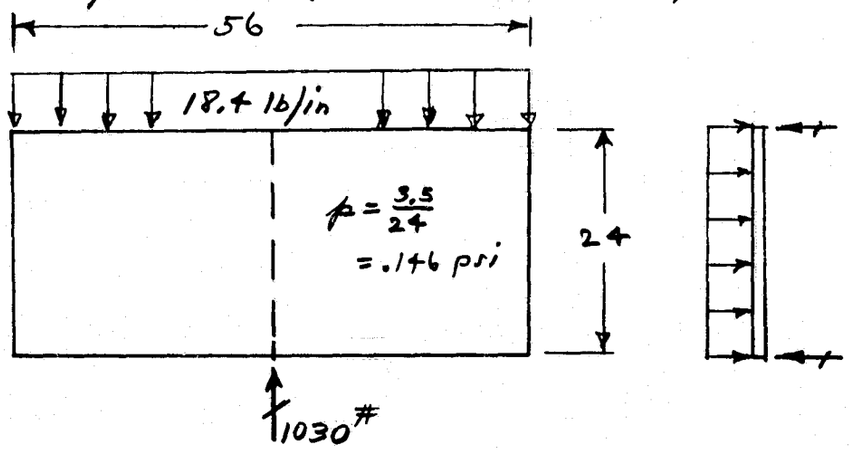
Lateral load = (52.4)(23)
= 1205 lb. per array

7

MODULE STRESS ANALYSIS

LONG SIDE PANEL

The side panel is designed for a distributed load of 18.4 lb/in in the z direction and a 3.5 lb/in loading normal to the panel.



Bulkhead reaction = $18.4(56) = 1030^{\#}$

Maximum shear = $515^{\#}$

Maximum bending moment = $14(515) = 7200$ in lb

The 1/2" thick sandwich panel will be analyzed for the combined effects of the shear and normal loads.

Shear Buckling Allowable

From Goodyear Bondolite Design curves:

$a/b = 28/24 = 1.17 \qquad \sqrt{K} = 2.74$

$b/d\sqrt{K} = \frac{24}{.5(2.74)} = 17.5$

$F_{S_{CR}} = 35000$ psi

Applied shear stress $= \frac{515}{24(.012)(2)} = 900$ psi

Normal Load Analysis

From MIL-HDBK-23A, Chapter 9:

$$V = \frac{\pi^2 t_c E t}{2\lambda b^2 G_c} = \frac{\pi^2 (.476)(10)^7 (.012)}{2(.91)(24)^2 (16000)} = .033$$

$b/a = 24/28 = .86$

$K_2 = .06$

$$\text{Face stress} = K_2 \frac{\lambda b^2}{h t_f} = \frac{.06(.146)(24)^2}{.488(.012)} = 860 \text{ psi}$$

Combined Shear and Normal Loading

From MIL-HDBK-23A, Chapter 8:

$$\text{Face stress, } f = \frac{f'}{1 - \frac{f_s}{F_{s_{CR}}}}$$

f' due to normal load modified to consider effects of shear.

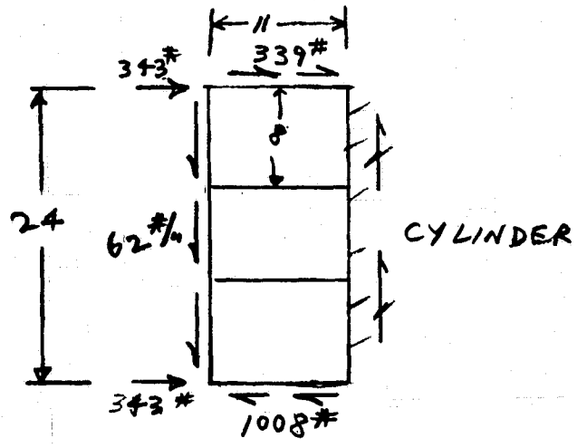
where f' = Face stress due to normal load

$$f = \frac{860}{1 - \frac{900}{35000}} = \frac{860}{1 - .026} = 885 \text{ psi}$$

M.S. = HIGH

MODULE

SOLAR ARRAY DRIVE (SAD) BULKHEAD



P_z from side panel = 1030# Page ___

P_z from SAD = 15.8(22)/2 = 174#

P_z from solar array = 1755# Page ___

q per bulkhead = $\frac{1030+1755+174}{2(24)}$ = 62 #/in

P_y from pressure on side skin = ~~p~~ A/2 per bulk'd

= .146(28)(24)/2 = 49# assuming 1/4 of panel load is reacted at each corner

P_y from SAD = 3(22)/2 = 33#

P_y from solar array = 1205/2 = 603# P. ___

Cap load = $\frac{49+603+33}{2}$ 343#

Top R_y reaction = -343 + 11(62) = 339#

Bottom reaction = -343 - 11(62) = -1008#

SAD BULKHEAD

Bulkheads are 1/4" thick sandwiches with .005 faces.

From Goodyear Bondolite design curves:

$a/b = 11/8 = 1.4$

$\sqrt{K} = 2.6$

$b/d\sqrt{K} = 8/(.25)(2.6) = 12.3$

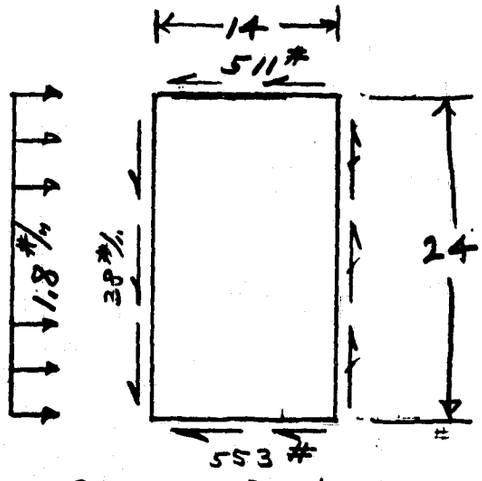
$F_{SCR} = 37000$ psi

$f_s = q/2t_f = 62/(2)(.005) = 6200$ psi

$M.S. = \frac{37000}{6200} - 1 = HIGH$

MODULE

X AXIS BULKHEADS



Sandwich, $t = .25$
$t_f = .005$

Compression load from side panel $= \frac{3.5(25)(2)}{4(24)} = 1.8$ #/"

P_z from side panel $= 18.4(50) = 920$ #

$q = 920/24 = 38$ #/"

From Goodyear Bondolite Design Curves:

For Shear

$a/b = 50/14 = 3.6$ $\qquad \sqrt{K_s} = 2.27$

$b/d\sqrt{K_s} = 14/(.25)(2.27) = 25$

$F_{S_{CR}} = 31{,}000$ psi

$f_s = 38/(2)(.005) = 3800$ psi $\qquad M.S. = \frac{31000}{3800} - 1 = $ HIGH

For Compression

$a/b = 14/24 = .6$ $\qquad \sqrt{K_c} = 2.2$

$\frac{b}{1.732\, d\sqrt{K_c}} = \frac{24}{1.732(.25)(2.2)} = 25$

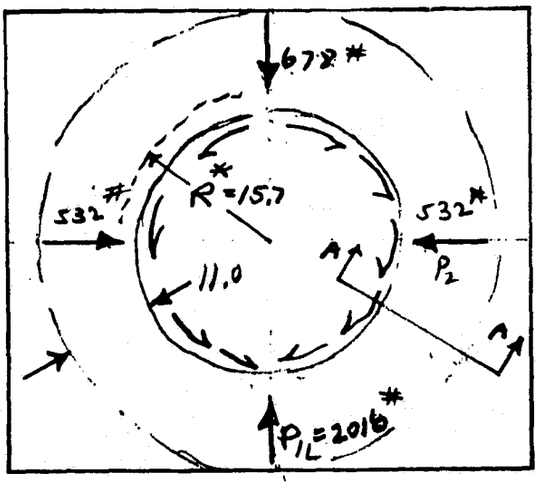
$F_{c_{CR}} = 16000$ psi

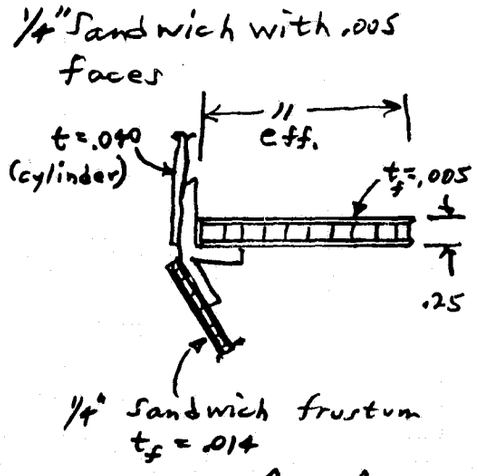
$f_c = 1.8/(2)(.005) = 180$ psi negligible

MODULE

LOWER SKIN

Idealize the skin as a curved ring.





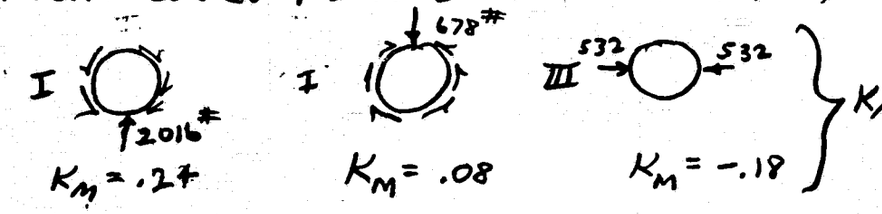
A-A

$R = 14 + 5.5 = 19.5"$

P_1 from SAD bulkhead analysis = 2016# on one side and 678# on the other side (two bulkheads per side)

P_2 from X axis bulkhead = $14(38) = 532$#

From Cases 1 and 3 of Table 8.2.1-1, FAC-SESDSM:



$K_M = .24$ $K_M = .08$ $K_M = -.18$ } K_M's at P_{1_L}

$$M = R\,\Sigma(K_M P) = (14+1.7)\,\Sigma(K_M P)$$
$$M = 15.7\left[.24(2016) + .08(678) - .18(532)\right] = 6950\ \text{"\#}$$

f_{b_t} (at cyl.) $= 6950(1.7)/3.38 = 3500$ psi

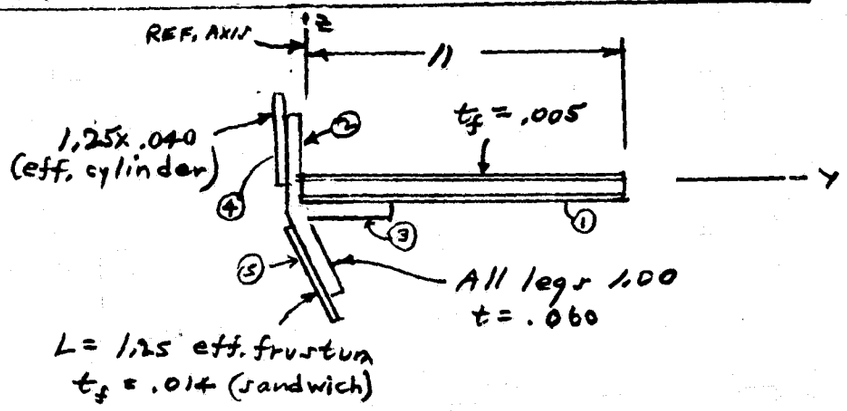
f_{b_c} (at outer edge) $= 6950(11-1.7)/3.38 = 19100$ psi

M.S. = HIGH

* See next page for "ring" section properties.

MODULE LOWER SKIN (CONT'D)

SECTION A-A SECTION PROPERTIES

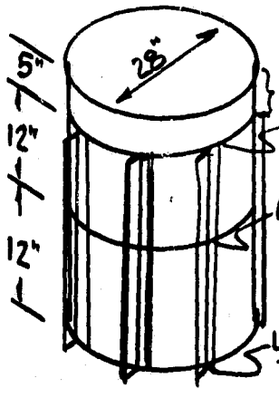


ELE	A	Y	Ay	Ay^2	I_{oz}
1	.11	5.5	.605	3.33	1.11
2	.12	0	0	0	0
3	.06	.5	.030	.015	.005
4	.05	0	0	0	0
5	.035	0	0	0	0
Σ	.375	1.7	.635	3.345	1.115

$$I = 3.345 + 1.115 - 1.7(.635) = 3.38 \text{"}^4$$

PREL. STRUCT. ANALYSIS (CONT'D.)

• CYLINDER



UPPER CYLINDER (TO BE ANALYZED SEPARATELY)

UPPER MODULE RING

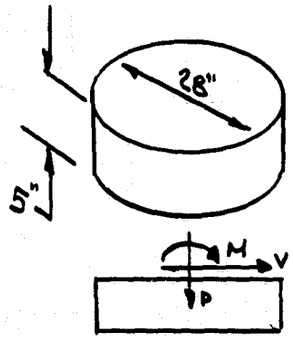
APOGEE MTR RING

LOWER MODULE RING

CONSTRUCTION

STIFFENED SKIN ~.040 7075-T6 ALUM ALLOY ~ 8 STIFFENERS

• UPPER CYLINDER



$\begin{cases} V = 299\,lb \\ M = 1012\ in\ lb \\ P = 436\,lb \end{cases}$

a) Bending (Ref: Roark Third Ed. pg 316)

$$M_{cr} = \frac{k(E)rt^2}{(1-\nu)^2} \qquad (k_{TEST} = .72)$$

$$= \frac{(.72)(10^7)(14)t^2}{(.9)}$$

Solving for thickness reqd.

$$t^2 = \frac{(.9)M}{(.72)(14)(10^7)}$$

$$t^2 = (9\times10^{-9})(1012)$$

$$t^2 = 9.1\times10^{-6}$$

$$t = .003 \text{ for MS} = 0$$

b) Thrust Load (Ref: Roark Third Ed pg 316)

$$\sigma' = (.3)E(t/r) \rightarrow \text{(critical stress level)}$$

(I) $$= (214\times10^3)t$$

Solving for t_{reqd} $\quad P/A = 436/\pi dt$ (II)

$$\frac{436}{\pi dt} = (214\times10^3)t$$

$$t^2 = \frac{436}{214\times10^3(\pi d)} = \frac{2.037\times10^{-3}}{88} = .023\times10^{-3} = 23\times10^{-6}$$

$t_{reqd} = .005$ (MS=0)

CYLINDER (CONT'D)

Assume a 10 mil wall on upper cylinder for functional reasons such as fasteners

Bending

$$M_{CR} = \frac{.72 \times 10^7 \times 14 \times (.010)^2}{.8} = 11200 \text{ in lb}$$

$M_{APPLIED} = 1012$ in lb

$R_B = 1012/11200 = .09$

Thrust

$$S' = (.3)E(t/r) = (3 \times 10^6)(.01/14)$$
$$= 2140 \text{ psi}$$

$$S_{APPLIED} = P/A = 436/\pi dt = 436/.879$$
$$= 496 \text{ psi}$$

$R_C = 496/2140 = 0.23$

INTERACTION FORMULA

$$R_B + R_C = 1.0$$

$$MS = \frac{1}{R_B + R_C} - 1$$
$$= \frac{1}{.32} - 1$$
$$MS = 2.125$$

Weight $= \rho \pi dt l$
$= (.1)(3.14)(28)(.01)(5)$
$= (.314)(.28)(5)$
$= .44$ lb

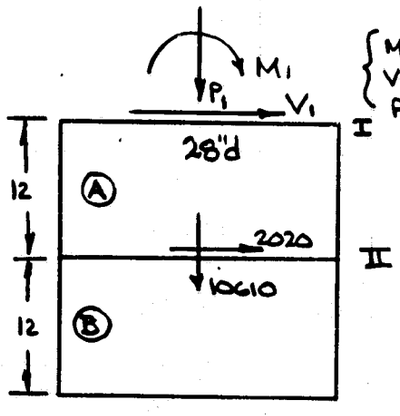
NOTE: Assuming the main cylinder within the module to be ~.040, stiffened, it may prove lighter weight construction to continue the .040 for the 5 inches of the upper cylinder and save the weight of an interface ring with the main cylinder

Weight .040 Upper Cylinder = $.44 \times 4$
$= 1.76$
$\Delta = 1.32$

CYLINDER (CONT'D)

- Main Cylinder

Construction: .040 skin - 7075-T6
8 - 3/4 × 3/4 × .063 stiffeners



$M_1 = 2520$ in lb
$V_1 = 26331$ lb
$P_1 = 6214$ lb

APPLIED LOADS

1. Assume the rings are capable of introducing all loads uniformly
2. The primary purpose of the B stiffeners is due to the eccentricity of the apogee motor loads. Therefore for the applied shown at left the stringer area is not considered
3. The cylinder is analyzed in two segments (A) (B) as shown above

Segment (A)

1. Thrust Load

$\sigma_1 = P_1/A = 6214/\pi dt = 6214/3.52$

$\sigma_1 = 1765$ psi

(Roark Third Ed pg 316) $\sigma_{ce} = .3E(t/r)$

$= 3\times10^6(.04/14)$

$\sigma_{ce} = 8571$ psi

$R_{1C} = \sigma_1/\sigma_{ce} = .206$

2. Bending

$M_{APPLIED} = 2520$ in lb

(Roark Third Ed pg 316) $M_{ce} = \dfrac{kE\,rt^2}{(1-\nu^2)}$

$= \dfrac{(.72)(10^7)(14)(16\times10^{-4})}{(.9)}$

$M_{ce} = 179200$ in lb

$R_{1B} = .014$

3. Transverse Shear

$\tau_{APPLIED} = V/A$

$= (2633)/(3.52)$

$\tau_{APP.} = 748$ psi

{NACA TN 3783 Figs 48b & 49c}

$Z_b = \dfrac{b^2(1-\nu^2)^{1/2}}{rt} = \dfrac{(12)^2(.945)}{(14)(.04)}$

$Z_b = 244$

CYLINDER (CONT'D)

Entering curve 49c $k_s = 40$

$$\tau_{cr} = \frac{k_s \pi^2 E (t/b)^2}{12(1-\nu^2)} = \frac{(40)(9.9)(10^7)\left(\frac{.040}{12}\right)^2}{(12)(.9)}$$

$$= \frac{396 \times 10^7 \times 16 \times 10^{-4}}{(10.8)(144)}$$

$$= (2.75)(1.48) \times 10^3$$

$$\tau_{cr} = 4070 \text{ psi}$$

$$R_{T_1} = 748/4070$$

$$R_{T_1} = .184$$

Segment (A) Margin of Safety

Interaction formula:

$$R_T^2 + R_B + R_C = 1$$

(MilHdbk5A) $$MS = \frac{2}{(R_B+R_C)+\sqrt{(R_B+R_C)^2+4R_T^2}} - 1$$

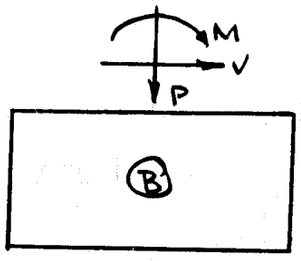
$$= \frac{2}{(.206+.014)+\left((.220)^2+4(.034)\right)^{1/2}} - 1$$

$$= \frac{2}{(.220)+(.184)^{1/2}} - 1$$

$$\boxed{MS = 2.07}$$

CYLINDER

Segment (B)



$M = 2520 + 2633(12) = 34116$ in lb

$V = 2633 + 2020 = 4653$ lb

$P = 6214 + 10610 = 16824$ lb

1. Thrust Load

$S_B = P/A = 16824/3.52$

$S_B = 4779$ psi

$S_{cr} = .3E(t/r)$

$= (3\times10^6)(.040/14)$

$S_{cr} = 8571$ psi

$R_c = .558$

2. Bending

$M_{APPLIED} = 34116$ in lb

$M_{cr} = 179200$ in lb

$R_B = .19$

3. Shear

$\tau_{APPLIED} = V/A = (4653/3.52)$

$= 1320$ psi

$\tau_{cr} = 4070$ psi

$R_T = .324$

Segment (B) Margin of Safety

$$MS = \frac{2}{(.748) + \left[.56 + .42\ _\right]^{1/2}} - 1$$

$$MS = \frac{2}{1.74} - 1 = +.15$$ (see next page)

Section (B) Revising the section B analysis to include the stringer as a for bending and thrust loads to alleviate the small margin on segment (B):

1. Thrust* ΔArea = .76 sq in $A^* = 4.28$ sq in.

$$S_B^* = 16824/4.28$$
$$= 3960 \text{ psi}$$

(See M_{cr}^* below) → $S_{cr}^* = S_{cr}(.048/.040) = 10285$

$$R_c^* = .385$$

2. Bending* $M_{APPLIED} = 34116$ in lb

M_{cr}^*: The critical bending assumes the ΔA to be uniformly distributed as a teff.

$$t_{eff} = \frac{4.28}{\pi d} = .048$$

$$M_{cr}^* = (M_{cr})(.048/.040)^2$$
$$= (179200)(1.44)$$
$$= 258048 \text{ in lb}$$

$$R_B^* = .13$$

3. Shear Stiffeners are not included in shear area

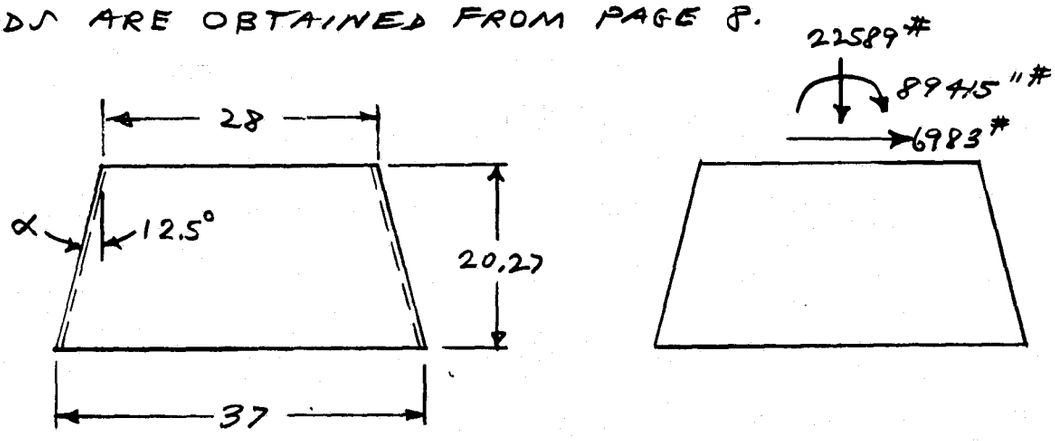
$$R_T = .325$$

$$MS^* = \frac{2}{.52 + \sqrt{(.27) + 0.42}} - 1$$

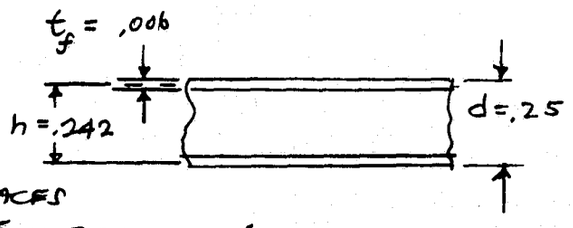
$$MS = \frac{2}{1.35} - 1 = +0.48$$

LOWER FRUSTUM ANALYSIS

LOADS ARE OBTAINED FROM PAGE 8.



SANDWICH DATA



$d = 0.25"$
$t_f = 0.006$
7075-T6 ALUMINUM FACES
$F_c = 56{,}700$ psi $F_s = 33800$ psi
5052 ALUM. HONEYCOMB CORE, 3/16 X.001, 3.1 lb/ft^3

The frustum will be analyzed using methods from NASA Report CR-1457, "Manual for Structural Stability Analysis of Sandwich Plates and Shells", Dec. 1969.

$$R_e = R_{SMALL} / \cos\alpha = 13.9/.976 = 14.25"$$

$$L_e = 20.27/\cos\alpha = 20.8"$$

COMPRESSION

$$P_{cr} = 4\pi R t_f \sigma_{cr} \qquad (4.2\text{-}31)$$

where

$$\sigma_{cr} = \gamma_c K_c \sigma_0$$

Using Fig. 4.2-8 ; (CR-1457)

$R_e/\rho = 14.25/.122 = 117$

$\nu = .54$

$$C_o = \frac{h}{R_e\sqrt{1-\nu^2}} = \frac{.244}{14.25(.95)} = .0180 \qquad \text{(Simplified 4.2-21)}$$

$$\sigma_o = \eta E C_o = 1.0(10)^7(.0180) = 18.0 \times 10^4 \qquad (4.2\text{-}19)$$

$$\sigma_{crimp} = \frac{h}{2t_f} G_{xz} = \frac{.244}{2(.006)}(32000) = 65.0 \times 10^4 \qquad (4.2\text{-}22)$$

$$V_c = \frac{\sigma_o}{\sigma_{crimp}} = \frac{18.0 \times 10^4}{65.0 \times 10^4} = .28$$

From Fig. 4.2-7 :

$$\Theta = \frac{32000}{16000} = 2.0 \qquad K_c = 0.92$$

$$\sigma_{cr} = \nu_c K_c \sigma_o = .54(.92)(18.0 \times 10^4) = 89500 \text{ psi}$$

Use allowable F_c of 56,700 psi (material strength)

$$P_{ALL} = 4\pi R_e t_f F_c \cos^2\alpha \qquad (5.1\text{-}1)$$

$$= 4\pi(14.25)(.006)(56700)(.951) = 58,000 \text{ lb.}$$

BENDING

From Fig. 4.3-1, $\nu_b = .58$

$$\sigma_{crb} = \nu_b K_c \sigma_o = .58(.92)(18.0 \times 10^4) = 96,000 \text{ psi}$$

Use allowable F_c of 56,700 psi

$$M_{ALL} = 2\pi R_e^2 F_c t_f \cos^3\alpha = 2\pi(14.25)^2(56700)(.006)(.976)^3 \qquad (5.2\text{-}1)$$
$$= 403,000 \text{ in. lb.}$$

SHEAR

Critical shear stress, $\tau_{cr} = 1.25 (\tau_{cr})_{\substack{\text{Torsion} \\ \gamma_s = 1.0}}$ (5.5-2)

where

$(\tau_{cr})_{\substack{\text{Torsion} \\ \gamma_s = 1.0}}$ = critical torsional shear stress obtained for $\gamma_s = 1.0$ throughout methods in section 5.4

$$R_e = (R_{small} \cos\alpha)\left\{1+\left[\tfrac{1}{2}\left(1+\frac{R_{Large}}{R_{small}}\right)\right]^{1/2} - \left[\tfrac{1}{2}\left(1+\frac{R_{Large}}{R_{small}}\right)\right]^{-1/2}\right\} \quad (5.4\text{-}3)$$

$$= 13.9(.976)\left\{1+\left[.5(1+1.32)\right]^{1/2} - \left[.5(1+1.32)\right]^{-1/2}\right\}$$

$$= 13.55\left\{1+\left[1.08\right] - \left[.925\right]\right\} = 13.55\left\{1.155\right\} = 15.65''$$

$$T_{cr} = 4\pi R_e^2 t_f \tau'_{cr}$$

τ'_{cr} = Critical stress for equivalent cylinder.

$$= \gamma_s K_s \eta E_f \frac{d}{R_e}$$

From Fig. 4.5-5:

$$Z_s = \frac{L^2}{d R_e} = \frac{(20.27)^2}{.25(15.65)} = 105$$

$$V_s = \frac{16 t_c t_f E}{30 R_e d G_{xz}} = \frac{16(.234)(.006)(10)^7}{30(15.65)(.25)(32000)} = .06$$

$$K_s = .47$$

$$\tau'_{cr} = 1.0(.47)(1.0)(10)^7\left(\frac{.25}{15.65}\right) = 75\,000 \text{ psi}$$

$$T_{cr} = 4\pi R_e^2 t_f \tau'_{cr} = 4\pi (15.65)^2 (.006)(75000) = 1{,}389{,}000 \text{ in.lb.}$$

$$(\tau_{cr})_{Torsion} = \frac{T_{cr}}{4\pi R_{small}^2 t_f} \qquad (5.4\text{-}4)$$

$$= \frac{1380000}{4(\pi)(13.9)^2(.006)} = 95{,}000 \text{ psi}$$

$$\tau_{cr} = 1.25 (\tau_{cr})_{Torsion} = 1.25 (95000) = 119{,}000 \text{ psi}$$

Use 33,800 psi for τ_{cr}

Applied maximum shear stress

$$= \frac{V}{2\pi R t_f} = \frac{6983}{2\pi (13.9)(.006)} = 13300 \text{ psi}$$

MARGIN OF SAFETY

USING THE INTERACTION EQUATION

$$R_c + R_b + R_s^2 = 1$$

$$R_c = 22{,}589/58000 = .39$$

$$R_b = 89{,}415/403{,}000 = .222$$

$$R_s = 13{,}300/33800 = .394$$

$$M.S. = \frac{2}{R_c + R_b + \sqrt{(R_c + R_b)^2 + 4R_s^2}} - 1 = 0.24$$

See Launch Dynamics Section - Frustum was designed by dynamics criteria

VHF Antenna

Although not considered structure the antenna was investigated for the feasibility of stowing the 92 inch antenna in minimum envelope

Diameter = 30 in.

Number of turns = 45

Extended height = 92 in.

Compressed height for 0.5 in tube

$= .5(45) = 22.5$ in.

Torsion stress, $f_s = \frac{PRr}{J}$

r = Tube radius

J = Polar moment of inertia $= 2\pi r^3 t$ for thin-walled tubes

$$f_s = \frac{PR}{2\pi r^2 t} \qquad (1)$$

$$\text{Deflection, } \delta = \int \frac{T_o T_i}{GJ}\, da = \frac{PR^2}{G(2\pi r^3 t)} \times 2\pi R N$$

$$\delta = \frac{PR^3 N}{G r^3 t} \qquad (2)$$

Rearranging Eq. (1) and (2) to solve for P, equating them and solving for f_s:

$$f_s = \frac{\delta r G}{2\pi R^2 N} \qquad (3)$$

Solving for P from Eq. (1) and (3) for one variation

$$P = \frac{\delta G t}{N}\left(\frac{r}{R}\right)^3$$

VHF ANTENNA (cont'd)

For Aluminum:

F_s working $= 20000$ psi
$G = 4 \times 10^6$

For a deflection of 8.25 in.:

$$f_s = \frac{8.25\,(.25)(4\times10^6)}{2\pi\,(15)^2\,(4.5)} = 13800 \text{ psi} \qquad (3)$$

$$M.S. = \frac{20000}{13800} - 1 = +0.45$$

Solving Eq. (1) for P and using t of .020:

$$P = \frac{f_s\, 2\pi n^2 t}{R} = \frac{13800\,(2)\,\pi\,(.25)^2(.020)}{15} = 7.25 \#$$

$$\text{Weight} = \pi^2 D N d t \rho = \pi^2(30)(4.5)(.5)(.020)(.10)$$

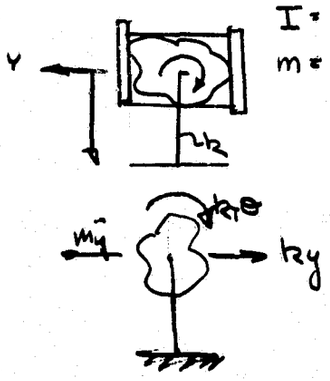
$$= 1.33 \text{ lb.}$$

PRELIMINARY LAUNCH DYNAMICS

Design Goal minimum natural frequencies of 25 cps laterally and 40 cps longitudinally have been established so as to minimize the vibratory response of the spacecraft during the launch phase. At this time preliminary analyses will serve as an indication of the feasibility of these goals.

ⓐ Lateral Frequency

Approximate the lower frustum and cylinder as an effective 29" diam cylinder. Assume the total mass of spacecraft acting at the cg, 32" above separation plane and the inertia of the module and solar arrays also are considered



$I = 829$
$m = 3.26$

$I \approx 320\,000 \text{ lb in}^2 = 829 \text{ lb in sec}^2$

$m \approx \frac{1260 \text{ lbs sec}^2}{386 \text{ in}} = 3.26 \frac{\text{lb sec}^2}{\text{in}}$

$\Sigma F_y = m\ddot{y} = -ky$ Ⓘ $\quad k = EI/\ell^3$

$\Sigma M = I\ddot{\theta} = -k_T\theta$ Ⓘ$\quad \frac{M}{\theta} = \frac{EI}{\ell} = k_T$

$-m\omega^2 y + ky = 0$

$-I\omega^2\theta + k_T\theta = 0$

$(k - m\omega^2)\bar{y} = 0$

$(k_T - I\omega^2)\theta = 0$

$(k - m\omega^2)(k_T - I\omega^2) = 0$

$kk_T - k_T m\omega^2 - kI\omega^2 + mI\omega^4 = 0$

$kk_T + (-k_T m - kI)\omega^2 + mI\omega^4 = 0$

$0 = kk_T + (-k_T m - kI)\alpha + mI\alpha^2$ Ⓘⅈ $\quad$ let $\alpha = \omega^2$

Elastic Properties Assume the effective cylinder to be constructed as the frustum $t = .028$, conservative approach.

$$I \sim \frac{\Delta r^2}{2} = \frac{\pi dt}{2} r^2 = \frac{(91.06)(.028)(14.5)^2}{2} = 268 \text{ in}^4$$

$A = 2.55 \text{ m}^2$

PREL. LAUNCH DYN (CONTD.)

$k = \frac{EI}{\ell^3}$ $\quad \ell = 32 \quad \ell^3 = 32768$

$\underline{k = 8.18 \times 10^4 \text{ lb/in}}$

$k_T = \frac{EI}{\ell} = \underline{8.375 \times 10^7 \text{ in lb/rad}}$

$m = \underline{3.26} \frac{\text{lb sec}^2}{\text{in}} \qquad I = \underline{829 \text{ lb sec}^2 \text{ in}}$

III $\quad 0 = kk_T + (-k_T m - kI)\alpha + mI\alpha^2$

$= 68.5 \times 10^{11} + (-34.08 \times 10^7)\alpha + (2703)\alpha^2$

$$\alpha = \frac{(34.08 \times 10^7) \pm \left[\left(1161.4 \times 10^{14}\right) - \left(740.6 \times 10^{14}\right)\right]^{1/2}}{5406}$$

$$= \frac{34.08 \times 10^7 \pm [20.5 \times 10^7]}{5406}$$

$$= \frac{13.58 \times 10^7}{5.406 \times 10^3} = 2.512 \times 10^4 = \alpha$$

$\omega = 158 \text{ rad/sec}$

$\underline{f_n = 25.2 \text{ cps}}$

(b) Thrust Frequency — Longitudinally, for preliminary purposes, the entire spacecraft is assumed concentrated at the cg (32" above separation plane. The flexibility of the effective cylinder, 29" diam, used previously is again utilized



$m = 3.26 \text{ lb sec}^2/\text{in}$

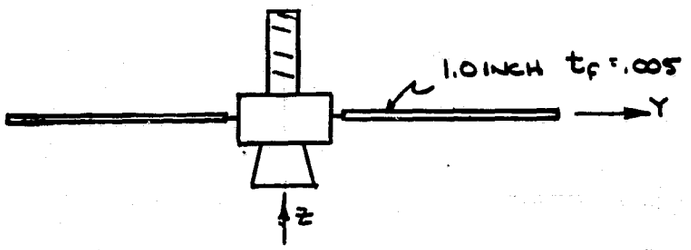
$k = \frac{AE}{\ell} = \frac{(2.55)\,10^7}{32} = .0797 \times 10^7 = 8 \times 10^5$

$$f_n = .159 \sqrt{\frac{8. \times 10^5}{3.26}} = .159 \left(24.5 \times 10^4\right)^{1/2}$$

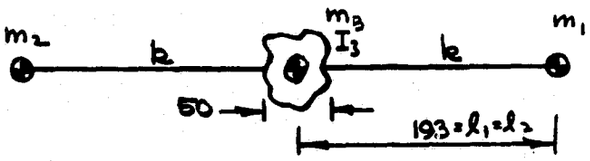
$\underline{f_n = 78.6 \text{ cps}}$

ORBITAL FREQUENCY

A RIGID MODULE IS COUPLED WITH THE FLEXIBLE SOLAR ARRAYS.



W_T = 687.5 LBS
W_{ARRAY} = 51.5 LBS PER SIDE
$W_{RIGID\ BODY}$ = 664.3 LBS



4 DEGREES OF FREEDOM z_1, z_2, z_3, θ_3

$m_1 = m_2$ = 23% OF SOLAR ARRAY MASS = .23 × 52.4 / 386

$m_1 = m_2$ = .03 LB SEC²/IN

m_3 = REMAINDER OF SC MASS = 1.514 LB SEC²/IN (1.72)

I_3 = INERTIA OF SC MAINBODY = 38.2 slug ft² = 458 lb in sec²

k = BENDING STIFFNESS OF ARRAY $\left\{\frac{3EI}{l^3}\right\}$ $(l = 168)$

$= \frac{3(10^7)(.1325)}{(4.74 \times 10^6)} = \frac{(1.325)3}{4.74}$

= 840 LB/IN

FROM PREVIOUS WORK THE CHARACTERISTIC EQUATION IS AS FOLLOWS

$$0 = \left(I_3 m_3 m_1^2\right)\omega^8 - 2m_1 k\left(m_1 I_3 + m_1 l^2 m_3 + I_3 m_3\right)\omega^6 + k^2\left(I_3 + 2m_1 l^2\right)\left(m_3 + 2m_1\right)\omega^4$$

$$= A\omega^8 - B\omega^6 + C\omega^4$$

$$\boxed{0 = A\omega^4 - B\omega^2 + C}$$

$C = (.707)(458 + .06(28224))(1.453 + .06)$

$= (.707)(458 + 693)(1.513)$

$= (.707)(2151)(1.513)$

$C = 2285$

$A = (458)(1.453)(.03)^2$

$= (458)(.0013)$

$A = .595$ ✓

$B = (2)(.03)(.840)\left[(.03)(458) + (.03)(28224)(1.453) \cdots + (458)(1.453)\right]$

$= (.0504)\left[13.74 + 1230.3 + 665.5\right]$

$= (.0504)(1909.5)$

$B = 96.24$ ✓

Orbital Frequency

$$0 = A\alpha^2 - B\alpha + C$$

$$= .595\alpha^2 - 96.24 + 2285$$

$$\alpha = \frac{96.24 - (9260 - 5450)^{1/2}}{1.19}$$

$$\alpha = \frac{96.24 - 61.6}{1.19} = 29.2$$

$$\omega = 5.4$$

$$f_n = 0,86$$

APPENDIX B

Solar Torque Calculations

(Nominal Case)

The actual configuration of the Hybrid as seen in Fig 4.5-2 was simplified for the solar torque calculations. For example, the adaptor structure which is a conical frustrum is modeled as a cylinder, the VHF antenna housing which consists of a shallow conical section surmounting two cylindrical sections of slightly different diameter has been reduced to a flat ended cylinder and the complex reflecting surfaces which are seen viewing the interior of the apogee motor nozzle and the surrounding interior of the adaptor structure have been simplified to a flat circle in the middle of a flat aluminum hollow circle. The VHF antenna, concentrated as a short cylinder having the actual antenna diameter was located at the deployed antenna CG, while the wire mesh L-Band antenna was treated as an equivalent area of small cylinders when viewed head-on or as a narrow flat surface when viewed edgewise. The rest of the spacecraft is flat surfaces with varying properties. Figures B-1 and B-2 illustrate the model while Table B-1 lists the properties of the various surfaces as well as the force equation coefficients at different incident angles for the normal and tangential forces generated by solar pressure (i.e. Force $= KP_fA$, where A= area, P_f = solar pressure and K = force coefficient).

Force vector diagrams were constructed for equinox, and winter and summer solstice sun locations for each of the eight orbit positions shown in Fig 4.5-6. Shadowing and particular questions involving the point of application of the forces and special surface effects were solved for each position. Figures B-3 and B-4 are two examples of the vector diagrams and the summation of torques. The resulting torques are summarized in Table 4.5-1.

Some additional comments follow on the modeling process for calculating solar pressure torques. As previously noted, the satellite physical model for the solar torque calculations consisted of a collection of cylinderial and flat surfaces.

All complex surfaces on the proposed satellite including the apogee motor nozzle, the interior of the conical adaptor, the L-Band and VHF antennas as well as the thermal louvers were reduced to either a cylinder or flat surface having an appropriate exposed surface and in some instances were assigned adjusted reflectance properties.

The application of the given force equations to these surfaces involved engineering judgements in some cases in that the effective point of reaction was adjusted depending on shadowing. In addition, a reasoned selection of which force was normal and which force was tangential had to be made in some cases.

The selection of surface reflective properties used in the equations was made based on nominal accepted values. A study was made of the sensitivity of the calculated solar torques to these values. Thus, variations were introduced in the values for reflectivity, ρ , and specularity, s , in a direction which would nominally increase the resulting forces. That is, for normal incident radiation ρ and s were increased. However, the resulting net solar torques decreased in many cases. In particular the integrated Z axis angular momentum which is of greatest concern, was thereby decreased.

The net solar disturbance torques about any axis represent a complex summation of normal and tangential forces and their associated lever arms about the CG. In the case of incident radiation at off-normal angles to a highly specular surface, the tangential forces are reduced to small values. For near normal radiation the complex interaction of increased reflectance and specularity may increase or decrease the normal force.

Thus, considering the complex interaction of uncertainties in the physical model, point of application of forces and surface characteristics, it would appear more rational to simply increase the total integrated angular momentum about any axis in attempting to add a margin of safety for determining the momentum wheel and propellant requirements. This approach has been followed in the design of the ACS and APS and in the development of the ground command/control concept for attitude stabilization.

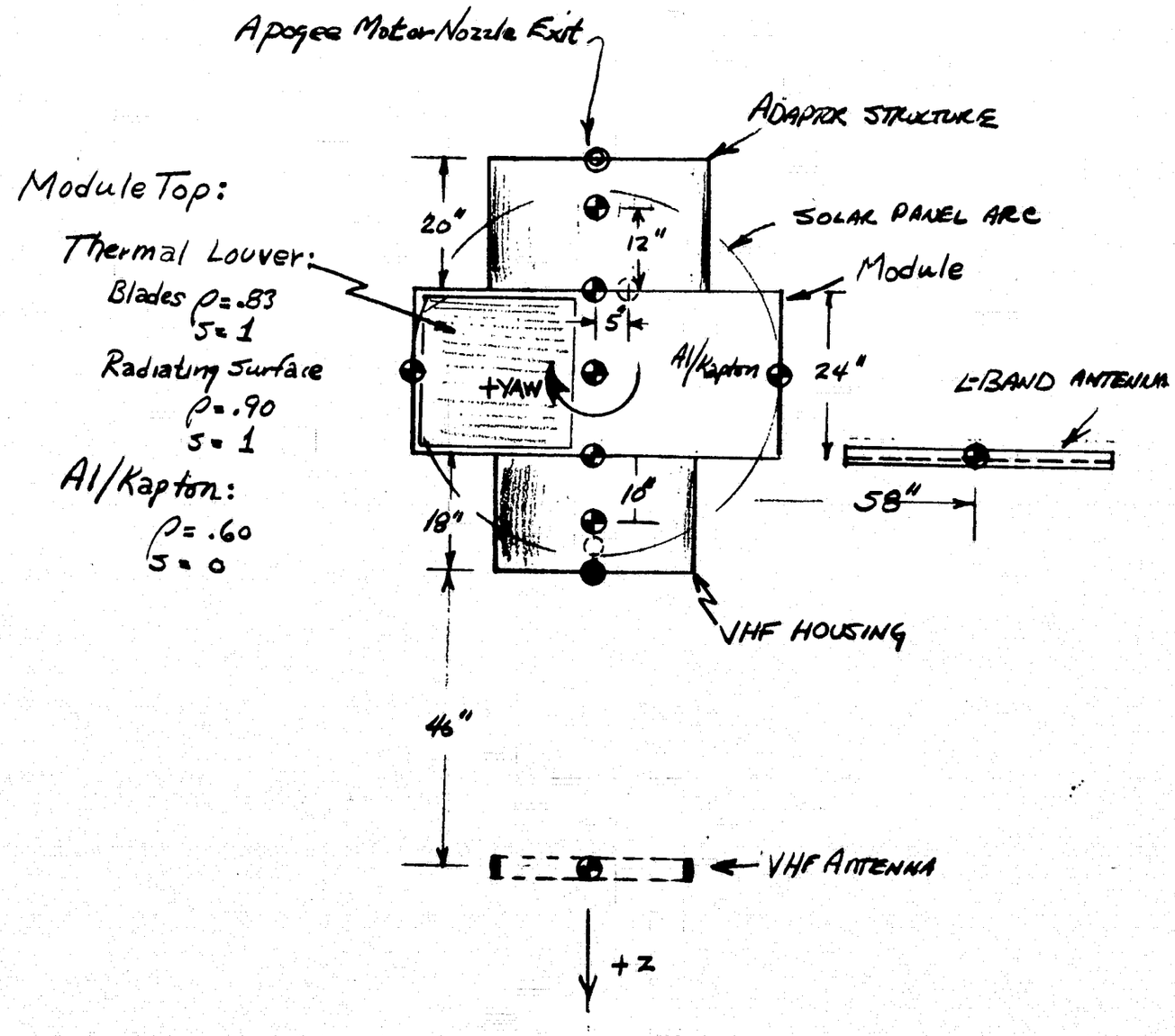


FIGURE B-1 SOLAR TORQUE MODEL

(Top View)

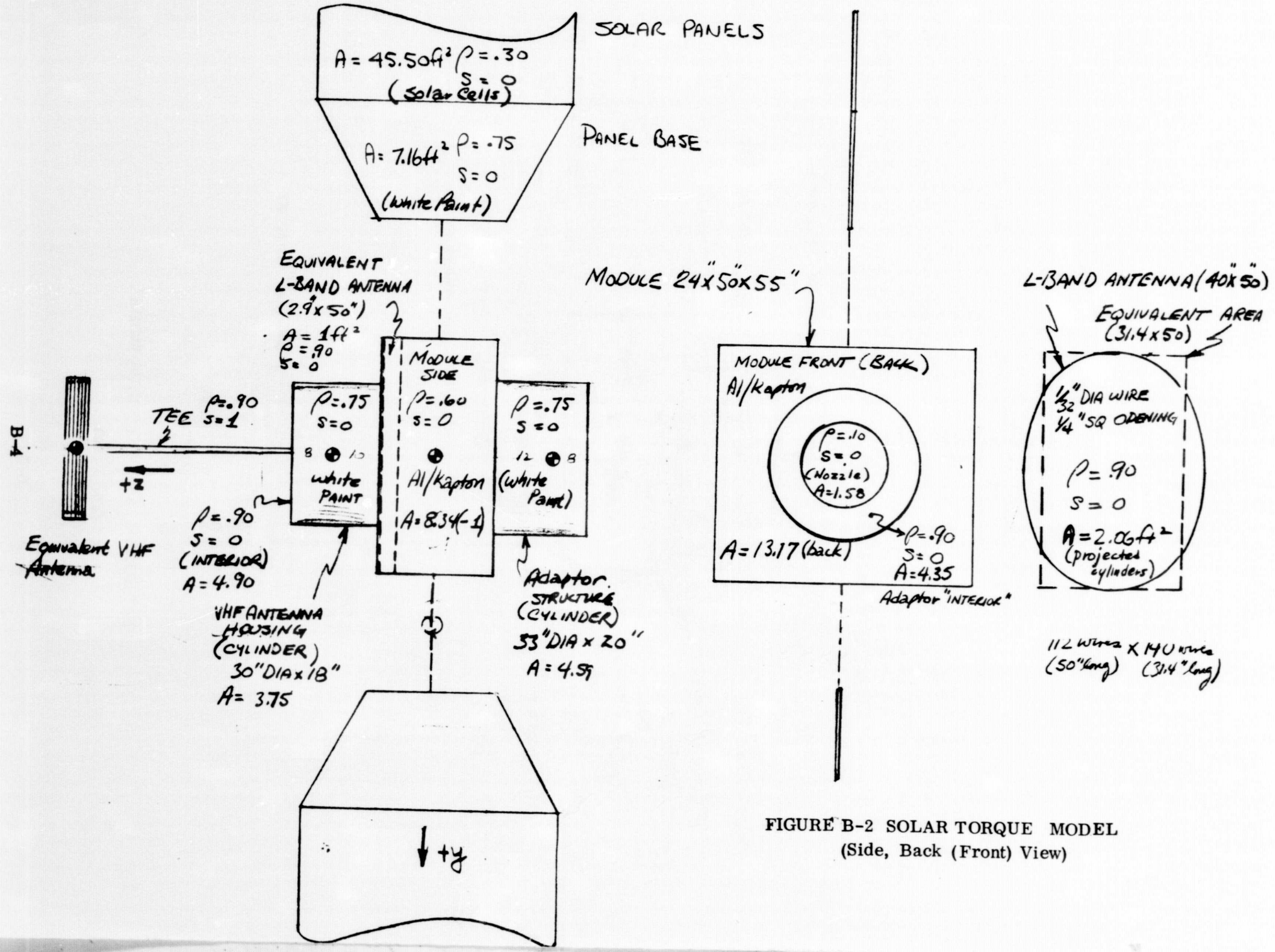
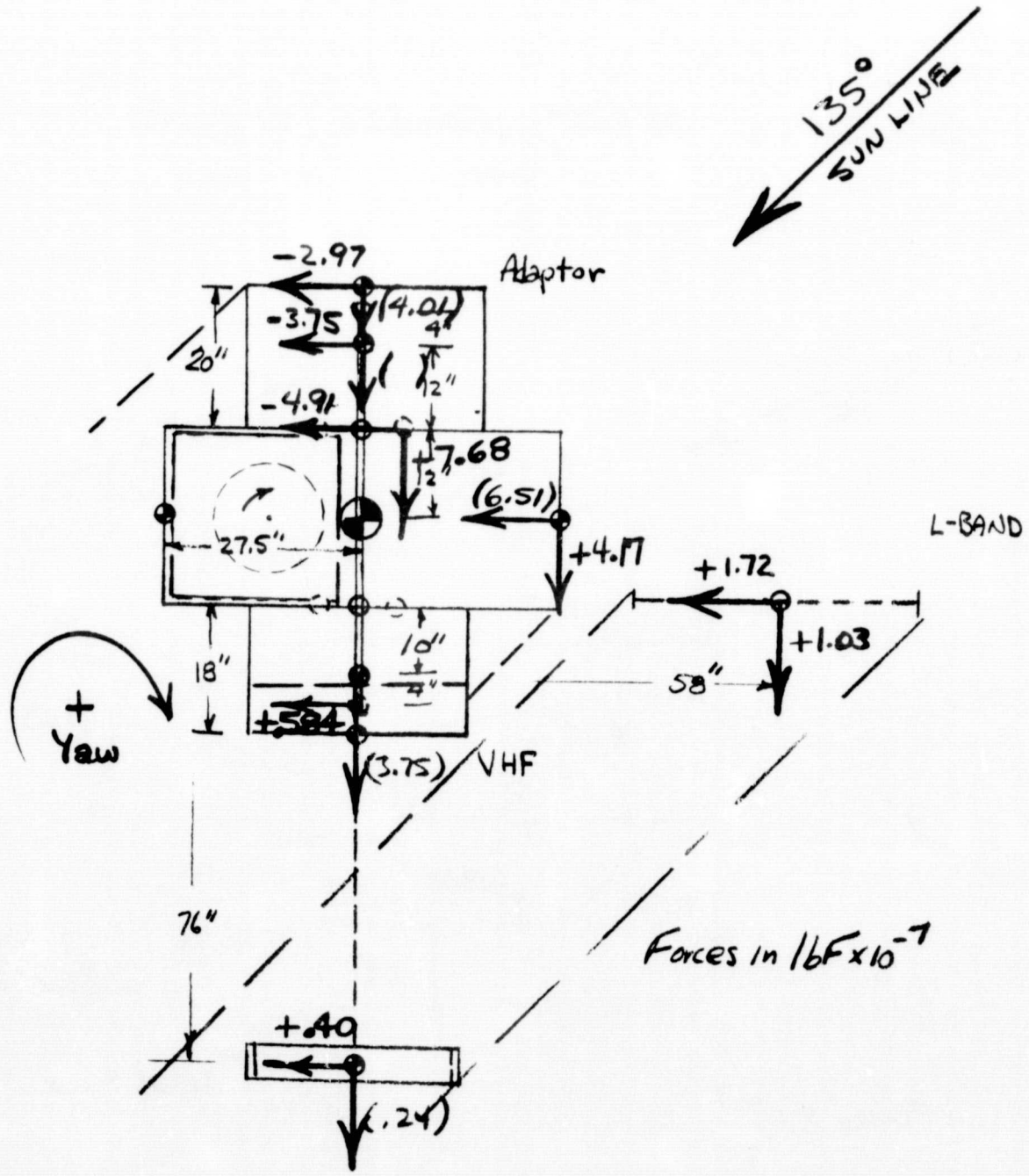


FIGURE B-2 SOLAR TORQUE MODEL
(Side, Back (Front) View)

EQUINOX ORBIT POSITION = 135°

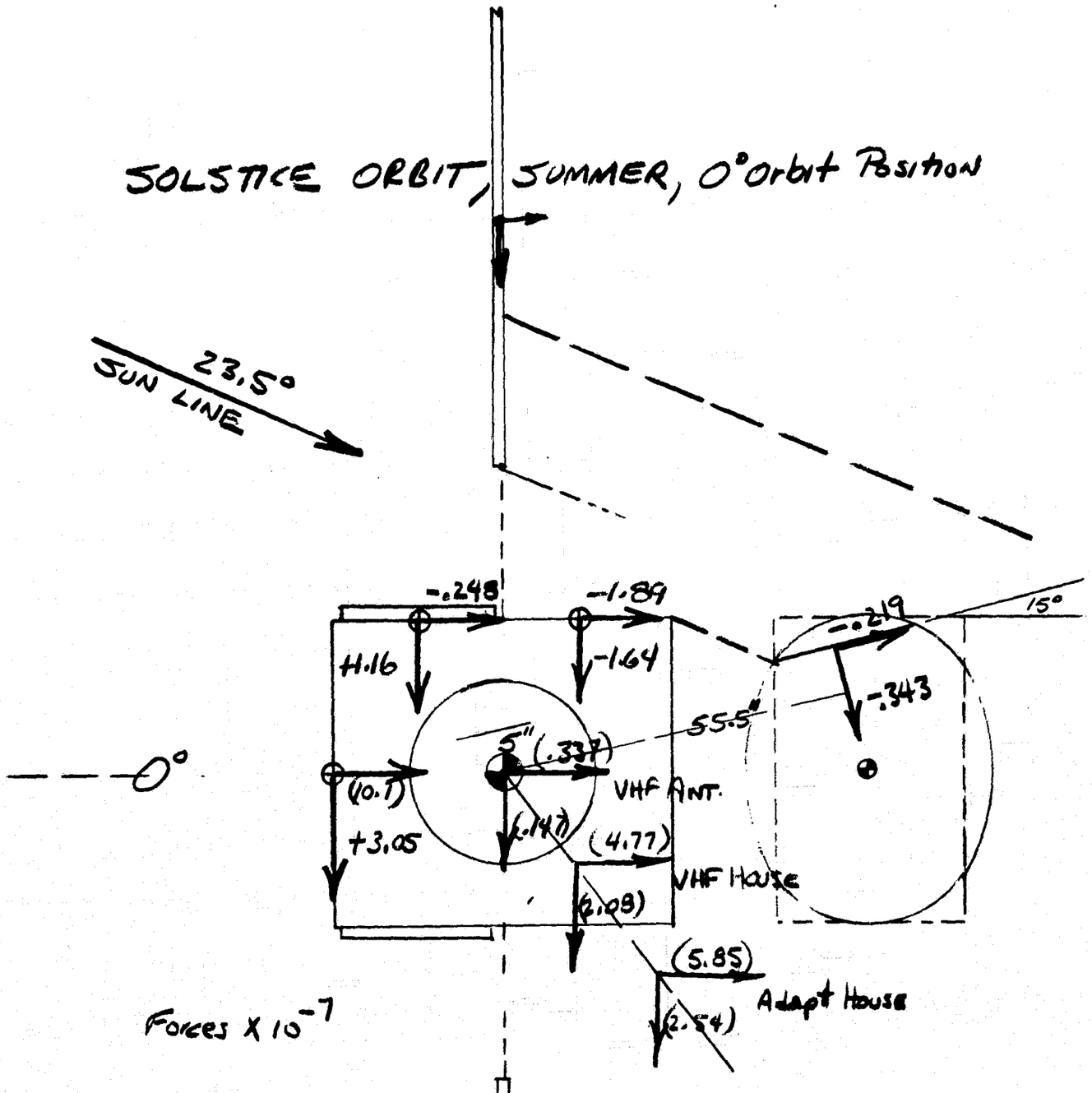


$$\Sigma \tau_y = +(1.03 \times 58) + (1.72 \times 12) + (.40 \times 76) + (4.17 \times 27.5) + (584 \times 14) + (7.68 \times 5) - (2.97 \times 32) - (3.57 \times 24) - (4.91 \times 12)$$

$$= 59.7 + 20.6 + 30.4 + 114.7 + 8.17 + 38.4 - 95.0 - 85.7 - 58.9$$

$$= +272.0 - 239.6 = +32.4 \times 10^{-7} \text{ lbF in} = +2.70 \times 10^{-7} \text{ ft lbF}$$

FIGURE B-3 TORQUE CALCULATION SUMMARY - EQUINOX EXAMPLE



$$\Sigma \tau_z = +(1.16 \times 15.5) + (3.05 \times 27.5) - (.248 \times 25) - (1.89 \times 25) - (1.64 \times 12) - (.343 \times 55.5) - (.219 \times 5)$$

(Body Axis)

$$= 18.0 + 83.9 - 6.2 - 47.2 - 19.68 - 19.02 - 1.10$$

$$= 101.9 - 93.20$$

$$= +8.7 \text{ in-lbF} \times 10^{-7} = .725 \times 10^{-7} \text{ ft-lbF}$$

FIGURE B-4 TORQUE CALCULATION SUMMARY - SOLSTICE EXAMPLE

Table B-1 Solar Torque Data Summary

Item	Part	Surface	Model Max. Area (ft^2)	Shape	ρ	s	Force Equation Coefficients: $F = KP_tA$ ψ or ϕ	0^o	45^o		66.5^o	23.5^o	66.5^o or 23.5^o
1	Solar Panel	Solar Cells	2x45.5	Flat	.30	.95	K_n=1.485	K_t=0	K_n=NA	K_t=NA	K_t=NA	K_t=1.09	K_n= .470
2	Solar Panel Base	White Paint	2x7.16	Flat	.75	0	1.50		NA	NA	NA	1.30	.366
3	VHF Housing Exter.	White Paint	3.75	Cyl.	.75	0	1.39		.778	.500	.316	1.20	.366
4	Adaptor Exterior	"	4.59	Cyl.	.75	0							
5	VHF Housing "Inter."	Aluminum	4.90	Flat	.90	0	1.60		.924	.500	.398	1.39	.366
6	Adaptor "Interior"	"	4.35	Flat	.90	0							
7	Module Sides	Al-Kapton	8.34 ea.	Flat	.60	0	1.40		.782	.500	.318	1.21	.366
8	Module Front (VHF)	"	14.20	Flat	.60	0							
9	Module Back (Adapt)	"	13.17	Flat	.60n	0							
9a	Module Top & Bot (<1/2)	"	5.16	Flat	.60	0							
10	Thermal Louvers	Aluminum	4.00	Flat	.83	1	1.83		.915	.085	.291	1.54	.062
11	Radiator Surface	Second Surface Mirror	<4.0	Flat	.90	1	1.90		.950	.050	.302	1.60	.037
12.	L-Band Antenna	Al Wire Mesh	2.06*	Cyl.	.90	0	1.47		.833	.500	.347	1.27	.366
13	VHF Antenna	Al Rod (compressed)	.52	Cyl.	.90	0							
14	Apogee Motor Exit	Carbon Black	1.58	Flat	.10	0	1.07		.547	.500	.180	.90	.366

* Front Area;
Approx. Side Area = 1 ft^2
Approx. Top Area = .8 ft^2

K_n = Normal force coeff.

K_t = Tangential force coeff.

Appendix C

Incremental Tolerance and Solar Torque Analyses

In this Appendix the results of a worst case tolerance study are presented, dealing with associated CG - CP deviations from the nominal case and the resulting incremental solar pressure torques. The four tolerance effects relating to these solar pressure torques, which are to be added to the solar torques for the nominal case, are:

Item	
1.	Spacecraft CG location in 3 axes.
2.	Solar panel array size tolerances, affecting both CP and CG in 3 axes.
3.	Reflectivity differences between solar arrays.
4.	Bearing and hinge pin clearances in the solar array deployment and orientation mechanisms.

The incremental solar pressure torques resulting from these effects as analyzed herein are summarized in Table 4.5-3 of Section 4.5.3.2, while the associated deviations in CG (β) and CP (γ) are listed in Table 4.5-2 of that section.

Item 1 Spacecraft CG-CP Tolerance Analysis

CG location of spacecraft is measurable within the following tolerance:

GSFC Spec. on a 2000 lb s/c (ATS F&G) ± 0.25 in.

Capability 2000 lb s/c (ATS F&G) ± 0.10 in.

Capability 1300 lb . Hybrid ± 0.06 in stowed

± 0.10 in deploy'd

Applies to x, y, and z directions

β_x = .005 ft (3σ) stowed
= .0083 ft (3σ) deployed

β_y = .005 ft (3σ) stowed
= .0083 ft (3σ) deployed

β_z = .005 ft (3σ) stowed
= .0083 ft (3σ) deployed

These uncertainties are tabulated in Table 4.5-2 for the deployed case. The associated disturbance torques given there are obtained by multiplying the total solar pressure force on the satellite by the indicated CG offsets.

Item 2 Solar Panel Array Size Tolerances

- Tolerance study - CG-CP offset along y axis (longitudinal direction of extended solar array) due to panel size variations.

Y axis tolerances		3σ value
Panel length, (worst case) of		
3 sections hinge pin to hinge pin = 3 (.010)	=	.030 inch
Overall length (tol. on 119 in)	=	.040 inch
RSS	=	.050

Moment Arm

Average CP location (array area only)

= (193 - 119) + 1/2 (119) inches

= 74 + 59.5 = $\frac{133.5}{12}$ = 11.1 ft

Assume worst case: One side all on the small side of the tolerance, other side all on the high side of the tolerance. Also assume no y axis difference in the honeycomb base sections next to the bearings since this can be machined to close tolerances. γ_y = uncertainty in CP = 2(.050) = 0.100 in = .0083 ft. Torque due to the above unbalance is found from $T_z = F_n (\gamma_y - \beta_y)$ where F_n is determined from equation (1) of section 4.5.3.2 and average nominal values of ρ & s are used. See Table C-2 in item 3 for values for ρ & s. Thus:

β_y = .0006 ft, the spacecraft CG deviation

ρ = .300

s = .953

1-s = .047

ψ = 0 $\therefore$ cos ψ = 1

A = 91 sq. ft. panels

F_n = 1.18×10^{-5} lb, total force on the solar panels

The value for $\gamma_y - \beta_y$ is found in Table 4.5-3, and the torque is $T_z = .907 \times 10^{-8}$ ft. lb. This is a bias torque about inertial Z axis.

- Uncertainty of CP along spacecraft x and z axes due to size variation of panels in x and z directions.

Panel width = 55.0 inches ± .03 (est)

= 4.58 ± .0025 ft.

Allowing all high tolerances on 1 side and all low tolerances on same side of the other panel, tolerance is additive, i.e., CP offset is on 1 side of y axis.

$T_Y = F_n (\gamma_z - \beta_z)$ where γ_z = .0025 ft. (above), β_z = .00016 ft

and F_n is due to total (panel + base) area.

$T_Y = 139.36 \times 10^{-7} \times (2.5 - .16)\, 10^{-3}$ ft-lb {see item 4 for source of F_n value of 139.36×10^{-7}

$T_Y = .326 \times 10^{-7}$ ft-lb

This is a bias torque about the inertial Y axis, or equivalently the spacecraft y axis.

Item 3 Reflectance Variations

General

In the solar force equation, values of ρ and s are determined as follows:

Total fraction of reflected sunlight = $\rho = 1$ - absorptance

Fraction of total reflected specularly = s
Fraction of total reflected diffusely = $(1-s)\rho$ } $[s + (1-s)]\rho$

Fraction of total absorbed = $\alpha = 1-\rho$

Thus, $\overbrace{\alpha}^{\text{absorbed}} + \overbrace{\underbrace{\rho s}_{\text{specular}} + \underbrace{\rho(1-s)}_{\text{diffuse}}}^{\text{reflected}} = 1$ (1)

Nominal values of α, ρ, and ϵ (emissivity) for solar cells are given below from reference C-1, p 3-92:

NOMINAL OPTICAL PROPERTIES

	α	ρ	ϵ	
Front surface cells	.70	.30	.85	
Rear surface Thermatrol	.20	.80	.85	Start of life
Rear surface Thermatrol	.43	.57	.85	End of life

We are only concerned with the front surface of the panels since only these surfaces will be facing the sun. Therefore for solar pressure calculation purposes the rear surface material and emissivity are irrelevant.

A nominal value for the diffusely reflected portion of sunlight from solar cells is $\rho(1-s) = .014$. Therefore, the remaining specular portion of the total is, using equation (1):

$$\rho s = 1 - .014 - \alpha$$

and thus,

$$s = \frac{.986 - \alpha}{\rho}$$

Solar array power "losses", compared to their predicted power output based on the characteristics of single cells, that are caused by manufacturing effects are given in reference C-2 page 3-32 as 7%. This is made up of the following factors:

Cover glass and adhesive	< 5%
Soldering	< 1%
Mismatch & Interconnection	< 2%
Total	~ 7%

Of these effects, those contributing to reflectivity deviations are the first two, amounting to less than 6%, say 5%. However, the associated differential reflectivity between two otherwise identical arrays at start of life can be assumed to be much less than this value. Only this differential reflectivity contributes to solar torques.

The deviations of concern are smaller than the capability of a spectrophotometer which measures optical density and thereby, indirectly, reflectivity. Density measurements can be made to a resolution of about 0.02, and in the range of interest, this amounts to reflectivity differences of ±.015 about a nominal value of 0.3, or ±5%.

Statistically, of a population of 20,000 solar cells comprising two identical arrays of 10,000 cells each, the probability of a differential overall reflectivity, i.e. ρ higher in one array than in the other, is determined from the following considerations.

Assuming that reflectivity variations among cells follows a normal distribution, the worst difference between two panel (mean) reflectivities would occur if all the cells above the mean were put on one panel and all below the mean on the other. This difference would be $2 \times 0.675 \times \sigma_o$, where σ_o is the standard reflectance deviation of the original 20,000 solar cells. However, the probability of this single worst event ever occurring is $[(N/2)!]^2/N!$, where N = 20,000. This probability has a vanishingly small value.

In view of the difficulty of obtaining quantitative statistical data on the integrated reflectivity deviations of one solar array relative to another, the relative panel per cent deviation was conservatively assumed to be ±1/100 times the worst case reflectivity degradation due to manufacturing effects, i.e. (±1/100) x 5 percent. This gave rise to a differential force of 0.0097×10^{-7} pounds, an equivalent CP offset (γ_y) of 0.00066 ft., and a bias disturbance torque of 0.108×10^{-7} ft-lb.

Item 4 Bearing and Hinge Pin Clearances

In Figure C-1 the following clearances for ABEC 5 bearings for the array drive were assumed. The shaft diameter is 3 inches and typical high quality bearings were postulated.

Inner diameter clearance	.0003 in
Outer diameter clearance	.0003 in
Eccentricity inner race	.0001 in
Eccentricity outer race	.0002 in
	.0009 in, 3σ value

Worst case cant angle A.

$$A = 2 \times \frac{.0009}{10} = 1.8 \times 10^{-4} \text{ rad} = 37.2 \text{ arc-sec.}$$

In Figure C-2a

$$a = 55 \times A = 55 \times 1.8 \times 10^{-4} = .0099 \text{ in}$$

$A = 1.8 \times 10^{-4}$ rad from Figure B-1

$$b = 79 \times A = 79 \times 1.8 \times 10^{-4} = .0142 \text{ in}$$

$$c = b + (103-79)B$$

where $B = .0004/55 = 7.27 \times 10^{-6}$ rad = 1.5 arc sec

$$c = .0142 + (103-79)\ 7.27 \times 10^{-6} = .01437 \text{ in}$$

$$d = b + (48\,B) = .0142 + (48)\ (7.27 \times 10^{-6}) = .0145 \text{ in.}$$

$$e = d + (150 - 127)B = .0145 + (23)\ (7.27 \times 10^{-6}) = .0146 \text{ in.}$$

$\Gamma \cong B = 7.27 \times 10^{-6}$ rad = 1.5 arc sec

Angle $\partial = A + B + \Gamma = (108 + 7.27 + 7.27)\ 10^{-6}$

$$\partial = 194.5 \times 10^{-6} \text{ rad} = 40 \text{ arc sec}$$

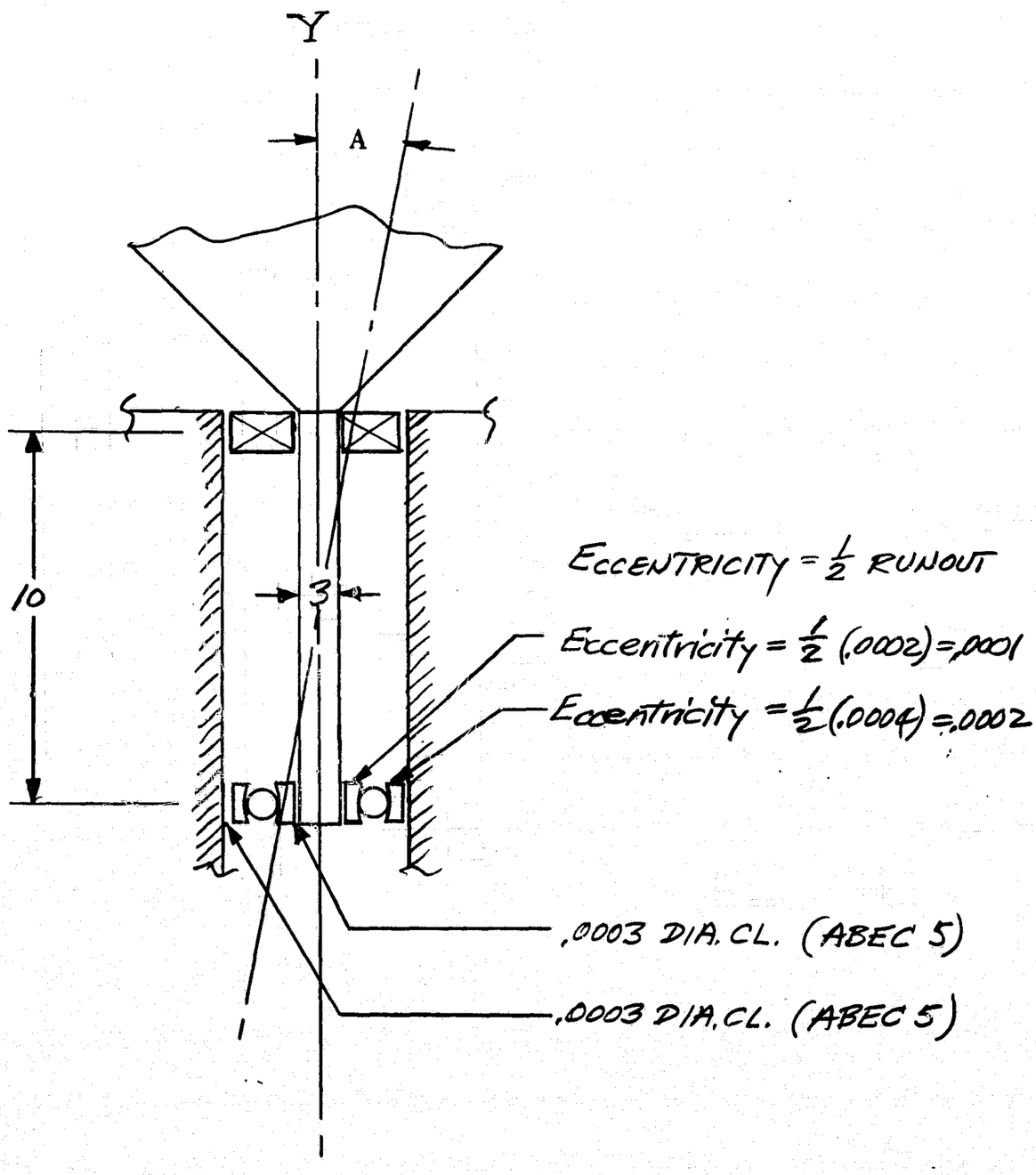


FIGURE C-1 BEARING CLEARANCES, SOLAR ARRAY DRIVE

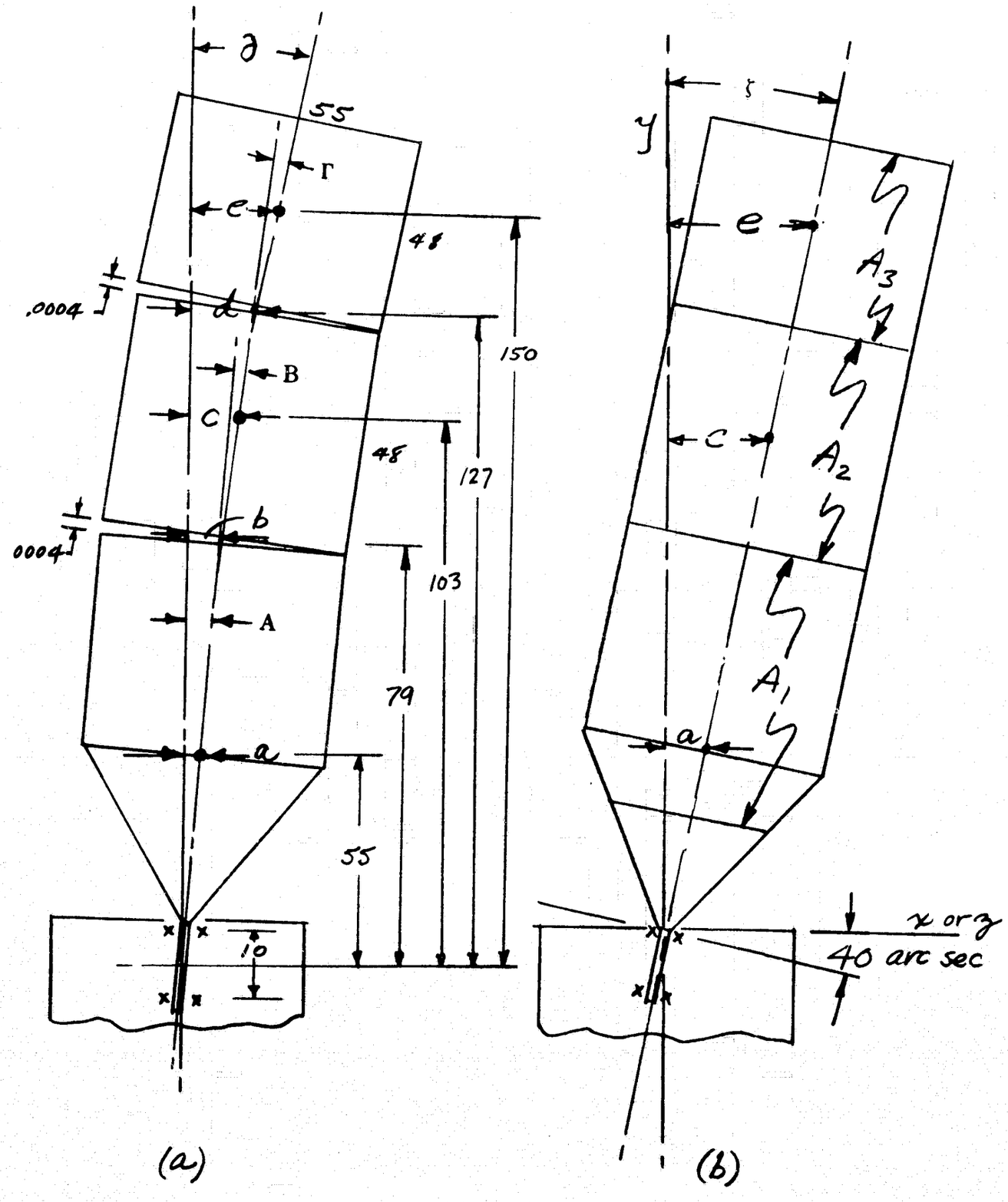


FIGURE C-2 SOLAR PANEL HINGE PIN CLEARANCES

Assume additional mounting surface tilt of 40 arc sec = .0002 in/in runout of MS of bearings, see Figure C-2. Then:

$$\zeta = \partial + 40'' = 80 \text{ arc sec}$$

The resulting CP offset (due to tilt of both panels), γ_z, and CG shift, β_z, are:

$$\beta_z = .00045 \text{ ft}$$

$$\gamma_z = .00622 \text{ ft}$$

Torque about Y axis due to CG-CP offset due to bearing and hinge pin tolerances is:

$$T_Y = F_n (\gamma_z - \beta_z)$$

where F_n is determined from equation (1) section 4.5.3.2 using nominal values of ρ and s for the panels from Item 3 , and for the honeycomb base of panels, white painted,

$$\rho = 0.75$$

$$s = 0$$

$$1\text{-}s = 1.0$$

The total area = A_1 (cells) + A_2 (bases)

$$A_1 = 91 \text{ ft}^2 \text{ solar cells}$$

$$A_2 = 14.24 \text{ ft}^2 \text{ bases}$$

The calculated force on the panels is 117.9×10^{-7} lb and on the panel bases is 21.5×10^{-7} lb. Hence, the torque T_Y is given by:

$$T_Y = (139.4 \times 10^{-7})(.00622 - .00045)$$

$$= .804 \times 10^{-7} \text{ ft-lb}$$

Total Solar Force (Including Cell Reflectivity Degredation Effects

The following solar pressure forces have been calculated for the Hybrid satellite module and solar arrays:

Orbit Position	Solar Force, lb F Module, less panels
0° Sunrise	44.74×10^{-7}
90° Noon	51.49×10^{-7}
180° Sunset	39.90×10^{-7}
270° Midnight	52.14×10^{-7}
Subtotal Module Avg.	47.10×10^{-7}
	Solar Panels + Bases
Solar Panels Only	117.87×10^{-7}
Solar Panel Bases	21.49×10^{-7}
Subtotal Panels + Bases	139.36×10^{-7}
Total Solar Force, Satellite	186.5×10^{-7}

The force on the solar panels given above represents start-of-life conditions. Due to reflectivity changes, mostly caused by mechanical effects, this force will change during the lifetime of the array.

Reference C-2, page 3-20, gives lifetime degradation percentages applied to the power output (related to absorptivity) of solar arrays:

Coverslide browning under proton & UV bombardment	< 1.0%
Mechanical Micrometeoroid erosion loss	< 1.0%
Transmission loss due to 1 MEV Electrons	2.3%
.006" Fused Silica #7940 w/blue filter (.977) from Figure 3.1-14 of Ref. C-2.	
Total	<4.3%

Values of ρ, s are thus found to change during the life of the solar array as given below:

Absorptance α	0.700	0.730 = +4.3%
Reflectance ρ	0.300	0.270 = -4.3%
Specular fraction of ρ, = s	0.953	0.947
Diffuse fraction of ρ, = 1-s	.047	.053

The total solar force on both arrays at start of life and end of life is calculated using the above figures:

F_n at start of life = 117.87 $\times 10^{-7}$ lbs.

F_n at end of life = 115.12 $\times 10^{-7}$ lbs.

References:

C-1. ATS 990-035 EP 69-503, Vol. I-B, Para. 3.3, Pg. 3-92, "Orbital Temperature Analysis for Solar Arrays."

C-2. ATS 990-035 EP 69-503, Vol. I-E, Section III, "Power Subsystem Components".

C-3. ATS 990-035 EP 69-503, Vol. I-B, Para. 3.1.3, pg. 3-43, "Thermal Control Coatings".